Proceedings of the Special Session on

Structural Health Monitoring and Earthquake Engineering

6th International Conference on

Structural Engineering and Construction Management 2015

Kandy, Sri Lanka

11th to 13th December 2015

Abstracts of 6th International Conference on Structural Engineering and Construction Management 2015

Vision

Promoting innovative research for tomorrow's development

Mission

To meet experts, colleagues and friends in the field and to exchange findings, concepts and ideas on research for the development of a sustainable world

ISBN: 978–955–589–210-0

Printed at: Nethwin Printers (Pvt) Ltd.,
Gampola Road, Peradeniya, Sri Lanka
E-mail: nethwin@yahoo.com

Preface

It is with great pleasure that we present the Proceedings of the 6th International Conference on Structural Engineering and Construction Management (ICSECM 2015). This is the sixth conference consecutively organized following the 1st International Conference on Sustainable Built Environment in 2010, 2nd International Conference on Structural Engineering and Construction Management in 2011, 3rd International Conference on Sustainable Built Environment in 2012, 4th International Conference on Structural Engineering and Construction Management in 2013 and the 5th International Conference on Sustainable Built Environment in 2014, keeping its tradition of adhering to engineering excellence.

Taking a step forward from the last four events, the coverage of specialty areas of this conference has been diversified. This book contains the abstracts of research papers from ten different sub specialties in Construction Management, Construction Materials and Systems, Structural Health Monitoring, Structural and Solid Mechanics, Earthquake Engineering, Fatigue Damage of Materials, Water Safety, Hydraulic Structures, Tall Building and Urban Habitat and MSW and Landfill Management. We expect that all these abstracts will be presented in parallel sessions from 11th to 13th December 2015.

We would like to express our appreciation to all keynote lecturers for their invaluable contribution. We are very much grateful to the authors for contributing research papers of high quality. The research papers of these abstracts in the publication have been peer-reviewed. The enormous work carried out by the reviewers is gratefully appreciated. We are also pleased to acknowledge the advice and assistance provided by the members of the international advisory committee, members of the editorial committee along with many others who volunteered to assist to make this very significant event a success. Finally, we acknowledge the financial sponsorship provided by many organizations that has been extremely helpful in successfully organizing this international conference.

It is the earnest wish of the editors that this book of abstracts and volumes of proceedings would be used by the research community and practicing engineers who are directly or indirectly involved in studies related to Construction Management.

Editorial Committee

6th International Conference on Structural Engineering and Construction Management 2015

11th December 2015.

Message from
Conference Chairmen

It is a pleasure for us to welcome all the participants to the 6th International Conference on Structural Engineering and Construction Management 2015 in Kandy, Sri Lanka. We, the co-chairs would gratefully like to mention the previous successful conferences, the 1st International Conference on Sustainable Built Environment 2010, 2nd International Conference on Structural Engineering and Construction Management 2011, 3rd International Conference on Sustainable Built Environment 2012, 4th International Conference on Structural Engineering and Construction Management 2013 and the 5th International Conference on Sustainable Built Environment in 2014, all held in Kandy, Sri Lanka.

The theme selected for the conference - Structural Engineering and Construction Management- is extremely relevant for today's world. With the vision of promoting innovative research for tomorrow's development, we organize this conference as a meeting place of talents, knowledge and dedication. Therefore, we trust that the conference will produce great ideas from a variety of Research and exchange the knowledge of experts, colleagues and friends who are working for the world's sustainable development.

The conference focuses on different sub topics in Structural Engineering and Construction Management, Construction Materials and Systems, Structural Health Monitoring, Structural and Solid Mechanics, Earthquake Engineering, Fatigue Damage of Materials, Water Safety, Hydraulic Structures, Construction Management, Tall Buildings and Urban Habitat and MSW and Landfill Management. The proceedings of the conference are peer reviewed. The full papers are published in volumes in paper format with a book of abstracts.

The host city of the conference, Kandy, is a world heritage city famous for its unique architecture, culture, natural beauty and climate. We hope that you will enjoy your time in Kandy during the conference.

We, the conference co-chairs express our sincere thanks to our guests, keynote speakers, authors, members of the international advisory committee, members of the editorial committee financial sponsors and many others who volunteered to assist to make this very significant event a success.

Prof. Ranjith Dissanayake
Prof. S.M.A. Nanayakkara
Prof. Priyan Mendis
Prof. Janaka Ruwanpura
Dr. G.S.Y De Silva
Eng. Shiromal Fernando

Co-chairs

6th International Conference on Structural Engineering and Construction Management 2015
11th December 2015.

Message from
Dean, Faculty of Engineering, University of Peradeniya

I am glad to submit this message for the Sixth International Conference on Structural Engineering and Construction Management (ICSECM-2015), which is a continuation of the efforts of the organizers to share knowledge and research in the sectors. This time too, the conference is held in historic city of Kandy, in Sri Lanka.

The ICSECM - 2015 is organized as a joint effort of a number of professionals, and a number of institutions; including Engineering Faculties of Peradeniya, Moratuwa and Ruhuna Universities in Sri Lanka. The topic covered and the keynotes delivered by professionals in the field add more depth to the objectives and outcomes of the conference.

I take this opportunity to thank the organizers for their commitment and persistent effort to make the conference a success. These events facilitate a forum for many young undergraduate and postgraduate students to receive a good initial exposure to present their work, and for some few, to get a flavor of organizing events of global importance.

I believe that the organizers of ICSECM-2015 will continue their dialog of bringing concerned professionals from diverse fields, from different parts of the worlds, into the discussion forum of ICSECM.

I wish the conference a great success.

Prof. Leelananda Rajapaksha

Dean,
Faculty of Engineering,
University of Peradeniya,
Peradeniya,
Sri Lanka.

Table of Contents

SECM/15/010

Clustering Techniques and Artificial Neural Network for Acoustic Emission Data Analysis

U. B. Attanayake [1*], H. M. Aktan[2], J. Mejia[3], and R. Hay[4]

[1]Western Michigan University, Kalamazoo, United States
[2]Western Michigan University, Kalamazoo, United States
[3]TISEC Inc., Morin Heights, QC J0R 1H0, Canada
[4]TISEC Inc., Morin Heights, QC J0R 1H0, Canada
E-Mail: upul.attanayake@wmich.edu, TP: +1 269 276 3217

Abstract: Acoustic emission (AE) sensor technology is commonly used for real-time monitoring of fatigue sensitive details. This is mainly due to its ability to detect fatigue events (crack initiation and opening) by mounting sensors in the vicinity of potential crack location. Also, AE data can be used for damage location detection. Even though AE provides many capabilities with regard to fatigue monitoring, many implementation challenges exist. A majority of the challenges is associated with noise elimination, AE signal analysis, and interpretation of the results. This article describes AE implementation for monitoring a fatigue-sensitive detail and use of data analysis techniques such as cluster analysis, non-linear mapping (NLM), and three-class classifiers to identify the relationship of each cluster to the characteristics of crack opening signals, background noise, and structural resonance.

Keywords: Acoustic Emission, Artificial Neural Network, Cluster Analysis, Data Analysis, Fatigue Monitoring.

1. Introduction

Fatigue is one of the most critical problems for steel bridges as well as for any steel structures that needs to be considered during design and operation. Irrespective of the causes of cracking, fatigue events (i.e., crack initiation or crack growth) need to be identified to and monitored to assure safety. An acoustic emission (AE) monitoring system with strain gages is one of the most effective technologies for fatigue event detection. AE has been successfully implemented in the field and evaluated for continuous monitoring of fatigue-sensitive details. At this time, AE is the only technology that is capable of real-time monitoring of fatigue events and providing data for damage location detection. The reasons for widespread use of the technology are;

- AE can be used as a local as well as a global crack growth monitoring tool [1-3].
- AE is capable of locating the source of failure [2, 4].
- AE is capable of detecting and locating defects in areas obscured from view or in areas that are difficult to inspect (e.g. weld defects, material imperfections, etc.) [2, 5].
- The data from an AE monitoring system can be used to track the history of crack growth activity [1].
- Parametric data (strain, displacement, temperature, etc.) can be used to correlate AE events in order to improve the accuracy of data analysis results [2].
- Very minimal surface preparation is required to mount AE sensors [1].
- Frequent access to a detail is not required once the sensors are installed [1, 2].
- Technology has been used for decades in many disciplines and the experience is well documented.

With any technology there are advantages as well as implementation challenges. This is no different for AE technology implementation and data interpretation. The following is an abbreviated list of challenges associated with AE monitoring, data analysis, and results interpretation [1, 2, 4-7]:

- AE monitoring requires extensive expertise to plan, set up the sensors, test, and interpret results.
- The service environment contributes extraneous noise to the signals.

- Challenging to implement standard noise reduction methods because the signals are transient and random in time.
- A large amount of data is recorded during monitoring; hence, effective data analysis and management are necessary, especially for long-term monitoring.
- Complicated geometries and low strength signals make tasks more difficult.
- Unable to detect dormant cracks using AE monitoring.
- Unable to quantify the extent of damage using AE data.
- Unable to repeat AE measurements.

A majority of the challenges is associated with noise elimination, AE signal analysis, and interpretation of results. This article describes AE implementation for monitoring a fatigue sensitive detail (local monitoring) and use of data analysis techniques such as cluster analysis, non-linear mapping (NLM), and three-class classifiers to identify the relationship of each cluster to the characteristics of crack opening signals, background noise, and structural resonance; thus, eliminating a majority of challenges associated with noise elimination, AE signal analysis, and interpretation of the results.

2. AE Monitoring System Implementation

2.1 System Configuration

The monitoring system selected for this project has a low-power computer. The operating system and essential software are installed in a 2 GB hard drive. The supplemental software and sensor data are stored in a 110 GB drive. The monitoring system components are shown in Figure 1. The monitoring system consists of only one AE board (PCI/DSP-4) with four-channels. The system capability can be extended to accommodate 4 AE boards with a total of 16 AE sensors. The monitoring system included 4 PK30I narrow band sensors (Figure 2a). Each AE sensor has an integral, ultra-low noise, low power preamplifier with a 26 dB voltage gain. The frequency range for the sensor is 200 – 450 kHz with a resonance frequency of 300 kHz. The data acquisition settings included a 40 dB preamplifier voltage gain, 45 dB threshold, 1 kHz to 1 MHz analog filter range, and waveform settings of 1MSPS sample rate, 256 µs pre-trigger, and 1k waveform length. Magnetic holders were used to mount the AE sensors (Figure 2b and c).

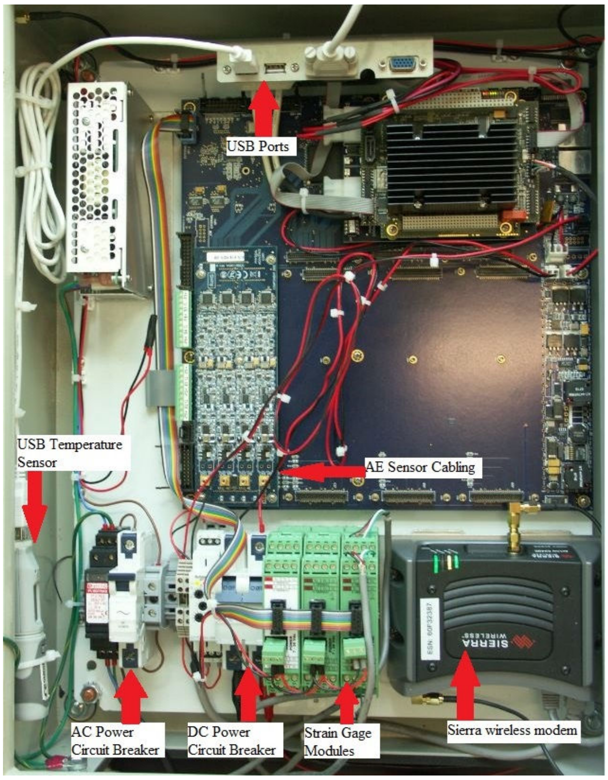

Figure 1: Monitoring system components in the enclosure

(a) An acoustic emission sensor

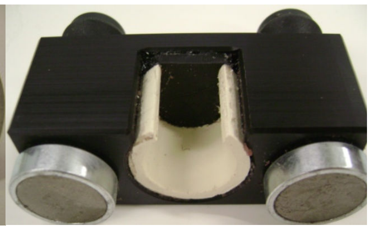

(b) A spring-loaded magnetic holder

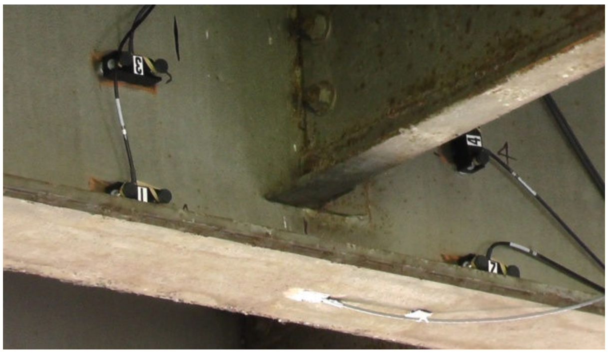

(c) AE sensors mounted on a steel girder

Figure 2: (a) An acoustic emission sensor, (b) a spring –loaded magnetic holder, and (c) AE sensors mounted on a steel girder

2.2 System Implementation

The bridge (S16 of 11015) is located in Stevensville, Michigan, and carries I-94 over Puetz Road. After reviewing biennial inspection reports and conducting a field visit to document the bridge superstructure and substructure condition, the I-94 EB bridge was selected. The longest span of the EB Bridge is 56 ft - 6 in. and has a 54.5^{o} skew. The span is supported on an integral abutment and a pier with expansion bearings. The superstructure consists of 12 steel I-girders (10-W30×108 and 2-W30×99) and a 9 in. thick cast-in-place concrete deck. The girders are connected transversely using intermediate and end diaphragms. The partial depth diaphragm connection detail is classified as a category C' fatigue-sensitive detail [8].

Once the AE sensors were mounted and the data acquisition started, AE source locations appeared on a source location page. Pencil lead break (PLB) signals are used to demarcate the area of interest as well as to fine-tune the data acquisition settings: preamplifier voltage gain and the signal threshold. Pencil lead breaks were performed and the waveforms were recorded. Figure 3 shows the source locations calculated based on the PLB signal arrival time. These source locations mark the boundaries of the area of interest for continuous monitoring.

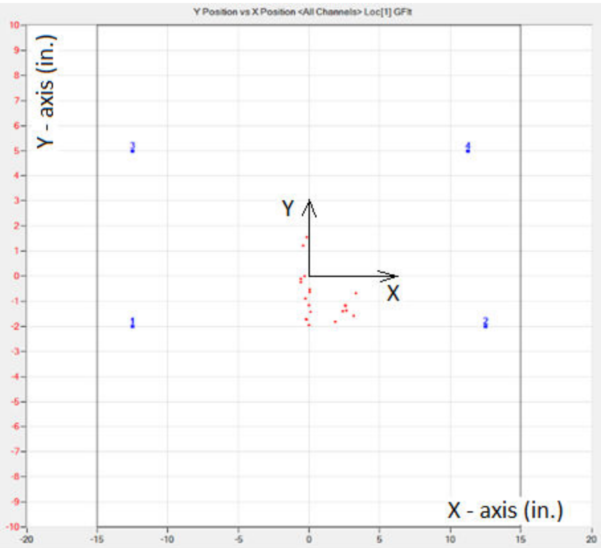

Figure 3: AE source locations generated through pencil lead breaks

3. AE Data Analysis and Results Interpretation

The ICEPAK^{TM} software developed by TISEC Inc. was used to classify data via pre-trained classifiers designed by the software package [9].

3.1 Unsupervised Learning via Clustering

The data collected from the bridge was examined directly to identify any significant similar AE activity formations using non-linear mapping (NLM) and clustering analysis available in ICEPAK^{TM}. NLM can be performed in time, power, phase, cepstral, and auto-correlation domains. The data set used for NLM and clustering analysis included little more than 11,000 AE signals that were above the set threshold of 45dB. NLM was performed using one feature domain at a time to visually detect significant naturally forming concentrations. Out of the 5 domains, the spectral power domain produced three significant concentrations as shown in Figure 4a. Clustering was performed using the same spectral power domain features, and produced three significant concentrations as presented in Figure 4b. The clusters are aligned with the visual presentation of the NLM result.

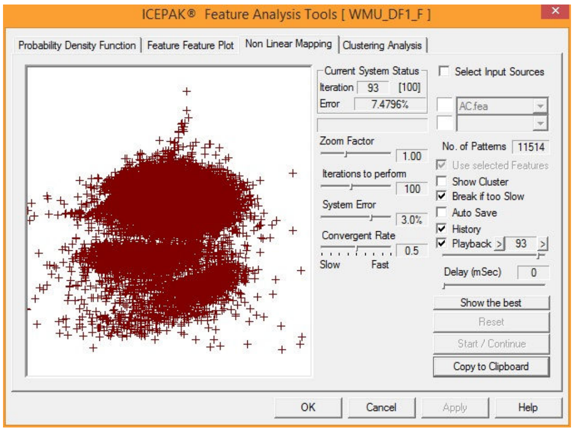

(a) NLM in power domain

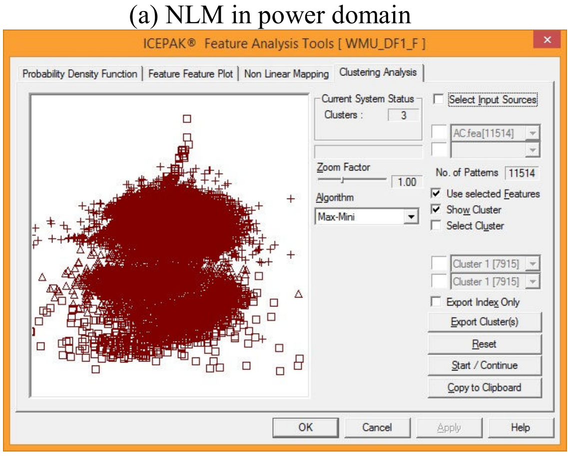

(b) Clustering in power domain

Figure 4: NLM and clustering in power domain

The individual data clusters were exported and labelled as [cl1], [cl2], and [cl3]. Then, each cluster was used to train a three-class classifier. Four statistical classifiers (i.e., linear discriminant, K-nearest neighbour, empirical Bayesian, and minimum distance classifiers) and a neural network classifier were tested. The design of the classifiers included optimizing the feature sets. The design procedure included separating available data into two groups; one was used to train the classifiers and the other to test the performance of the classifiers. As an example, results of the linear discriminant three-class classifier is shown in Figure 5. Cluster [cl1] had a total of 7,915 data points. This set was separated into two groups of 3,957 and 3,958 data points for training and testing, respectively. When the linear discriminant three-class classifier was trained with 3,957 data points, the data was classified into three classes with rejections. As shown in Figure 5, classes 1, 2, and 3 contain 3777, 2, and 0 data points with 178 rejections. The classification rate is 95.45%. In other words, 95.45% of the data in [cl1] falls into class 1. A similar process was employed for [cl2] and [cl3] data sets, and yielded classification rates of 94.99% and 95.95%, respectively. When all three data sets were considered, the linear discriminant three-class classifier yielded a weighted average classification rate of 95.43% for training (Figure 5). Overall, all the classification methods yielded very high classification rates for training as well as for testing.

Linear Discriminant Classification Results

	Class	1	2	3	Reject	Total	Percent
cl1.cxf	1	3777	2	0	178	3957	95.45%
cl2.cxf	2	0	1005	5	48	1058	94.99%
cl3.cxf	3	0	3	711	27	741	95.95%

Training : 95.43%

	Class	1	2	3	Reject	Total	Percent
cl1.cxf	1	3822	2	0	134	3958	96.56%
cl2.cxf	2	0	995	6	57	1058	94.05%
cl3.cxf	3	0	7	715	20	742	96.36%

Testing : 96.08%

Figure 5: Linear discriminant three-class classifier training and testing results

Next, the PLB data was tested against this three-class classifier with a rejection option. The rejection option is triggered when an incoming signal cannot be classified with an acceptable level of confidence. The PLB data file contained 100 data points. The PLB data fell into class 1 and 2 but not class 3, with a lot of rejections. The type of waveforms in the class 1 and 2 along with the rejected ones are shown in Figure 6.

The analysis of waveform characteristics of signals in each class and the rejected group yielded the following observations:

- The waveforms classified as class 1 usually have very fast rise times, relatively quiet pre-trigger portion, and a broad spectral content spanning from 100 to 400 kHz (Figure 7).
- The waveforms classified as class 2 usually have very fast rise times; however, the pre-trigger portion may show some small structure, and the main pocket contains multiple ringing peaks. The spectral content mainly centers around 150 kHz with very little or nothing above 250 kHz, and nothing below 100 kHz (Figure 8).
- The waveforms classified as class 3 usually have a slower rise time, and the spectral content is mainly located below 100 kHz and centered around 50 to 75 kHz. Moreover, there is absolutely nothing above 200 kHz (Figure 9).
- The waveforms classified as “rejected” are mostly associated with over-saturated clipped waveforms, and some have slow changing, somewhat smooth, waveform centered around 50 kHz (Figure 10).
- The number of waveforms being classified as class 1 is 4 to 6 times more than those of class 2 and class 3 while the sizes of class 2 and class 3 are relatively comparable. In general, there are about 5% of waveforms being rejected.

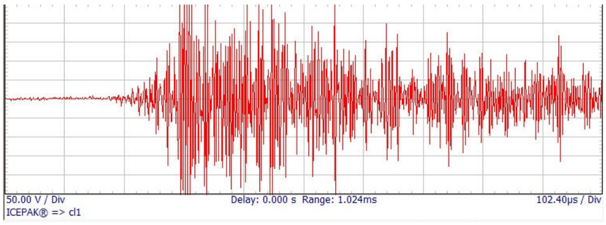

Note: X-axis: Time (102.4 µs/Div);
Y-axis: Voltage (50 V/Div)
(a) A sample PLB waveform in class 1

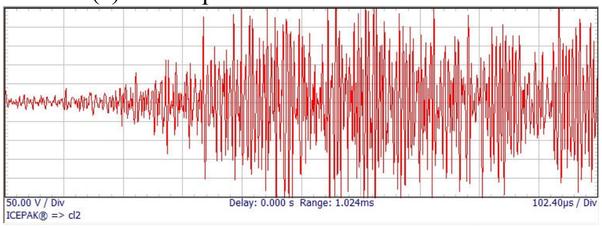

Note: X-axis: Time (102.4 µs/Div);
Y-axis: Voltage (50 V/Div)
(b) A sample PLB waveform in class 2

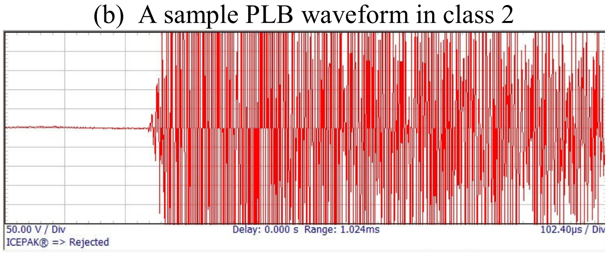

Note: X-axis: Time (102.4 µs/Div);
Y-axis: Voltage (50 V/Div)
(c) A sample rejected PLB waveform

Figure 6: Sample waveforms in class 1, class 2, and the rejected group

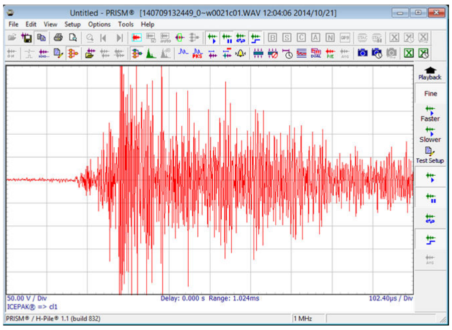

(a) Time domain
X-axis: Time (102.4 µs/Div)
Y-axis: Voltage (50 V/Div)

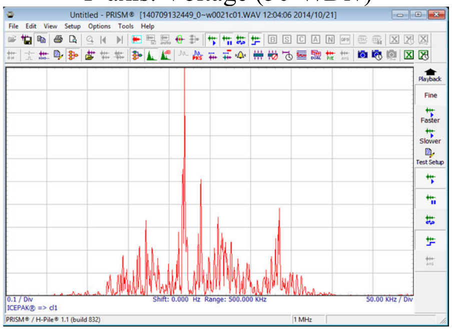

(b) Frequency domain
X-axis: Frequency (50 kHz/Div)
Y-axis: Amplitude (0.1/Div)

Figure 7: A sample class 1 waveform and its power spectrum

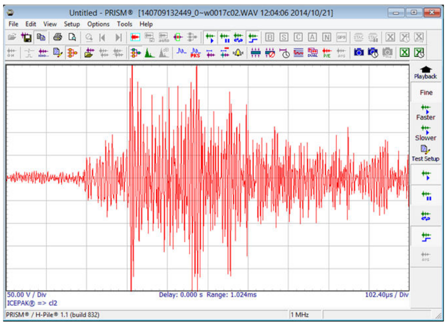

(a) Time domain
X-axis: Time (102.4 µs/Div)
Y-axis: Voltage (50 V/Div)

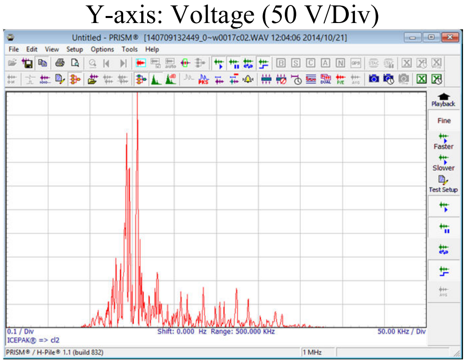

(b) Frequency domain
X-axis: Frequency (50 kHz/Div)
Y-axis: Amplitude (0.1/Div)

Figure 8: A sample class 2 waveform and its power spectrum

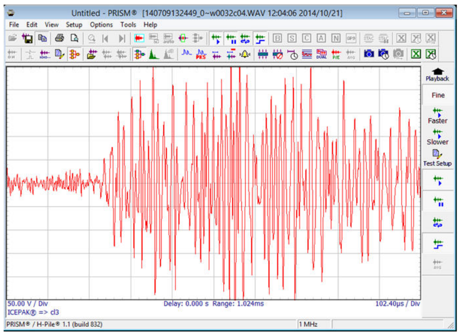

(a) Time domain
X-axis: Time (102.4 µs/Div)
Y-axis: Voltage (50 V/Div)

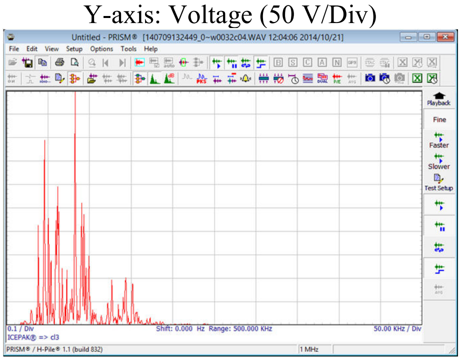

(b) Frequency domain
X-axis: Frequency (50 kHz/Div)
Y-axis: Amplitude (0.1/Div)

Figure 9: A sample class 3 waveform and its power spectrum

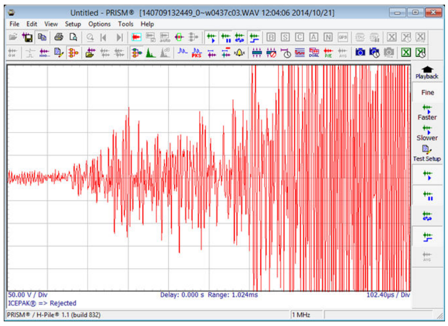

(a) Time domain
X-axis: Time (102.4 µs/Div)
Y-axis: Voltage (50 V/Div)

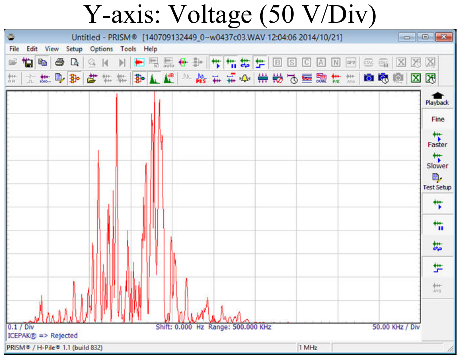

(b) Frequency domain
X-axis: Frequency (50 kHz/Div)
Y-axis: Amplitude (0.1/Div)

Figure 10: A sample “rejected” waveform and its power spectrum

3.2 Results Interpretation

There are two general types of fracture-related AE activities observed under cyclic loading conditions: crack tip opening during increasing load (upward load cycle) and crack face rubbing during decreasing load (downward cycle).

The observations of sample data analysis show that both class 1 and class 2 waveforms are more structured with a faster rise time at the beginning of the waveform. Thus, they are associated with the AE signals from the crack opening. Even though class 1 and class 2 waveforms represent characteristics of crack opening signals, more accurate characterization requires having access to AE signals that represent properties of steel used in the bridge, component dimensions, exposure conditions, etc. Class 3 waveforms are more slowly rising, and their spectral content is more inline with common background transient noise. The rejected waveforms are more likely due to saturation and clipping of the signal, and the non-saturated ones, centered around 50 kHz are more likely results from structural resonance.

Since class 1 and 2 waveform characteristics closely represented AE signals from the crack opening, the source location plots were analysed. However, during this particular implementation there were no active sources documented within the zone of interest. Therefore, further analysis was not performed. Yet, the data analysis procedures presented in this article demonstrated the possibility of identifying crack type signals from common background transient noise and structural resonance.

4.0 Summary, Conclusions, and Recommendations

Regardless of the causes of cracking, fatigue events (i.e., crack initiation or crack growth) need to be identified to and monitored to assure safety of structures. AE has been successfully implemented in the field and evaluated for continuous monitoring of fatigue-sensitive details.

This article described AE implementation for monitoring a fatigue sensitive detail (local monitoring) and use of cluster analysis, non-linear mapping (NLM), and three-class classifiers to identify the relationship of each cluster to the characteristics of crack opening signals, background noise, and structural resonance. The following are the specific conclusions and recommendations that are derived from this study:

- Cluster analysis and NLM of data can be performed in the time, power, phase, cepstral, and auto-correlation domains independently. The AE data collected from the bridge was examined directly to identify any significant similar AE activity formations. NLM with the spectral power domain produced three significant concentrations. Clustering was performed using the same spectral power domain features, and the clusters were well aligned with the visual presentation of the NLM result. NLM and cluster analysis demonstrated the usefulness of such techniques for understanding AE data.

- Waveform characteristics of pencil lead break (PLB) data and the AE data in three clusters were evaluated. Then, the dominant frequency ranges of each cluster were calculated. The results were used to identify the relationship of each cluster to the characteristics of crack opening signals, background noise, and structural resonance.

- Developing a fatigue cracking signal characteristic database of typical steel and welds used in a specific bridge, and using that database instead of PLB data would allow further refining of the AE data interpretation and more accurately detecting the critical events.

- The signal analysis process presented during this study, further refined with a database of fatigue cracking signals, can be integrated into remote monitoring to minimize receiving false alarms.

Acknowledgements

This project is funded by the Michigan Department of Transportation. The authors would like to acknowledge the support extended by Mr. Steve Kahl and the research advisory panel members for successful completion of the project. Further, the continuous technical support provided by Mr. Roger Chan, TISEC Inc., is greatly appreciated.

Research publication liability disclaimer

This publication is disseminated in the interest of information exchange. The Michigan Department of Transportation (hereinafter referred to as MDOT) expressly disclaims any liability, of any kind, or for any reason, that might otherwise arise out of any use of this publication or the information or data provided in the publication. MDOT further disclaims any responsibility for typographical errors or accuracy of the information provided or contained within this information. MDOT makes no warranties or representations whatsoever regarding the quality, content, completeness, suitability, adequacy, sequence, accuracy or timeliness of the information and data provided, or that the contents represent standards, specifications, or regulations.

References

[1] Federal Highway Administration (FHWA). Feasibility of Nondestructive Crack Detection and Monitoring for Steel Bridges, *Report No. FHWA-HRT-12-060*, Final Report, NDE Center, McLean, VA 22101, 2012.

[2] Department for Transport (DFT). Design Manual for roads and bridges, *Report No. BA 86/06,* UK, 2006.

[3] Nair, A., Cai, C.S. "Acoustic emission monitoring of bridges: Review and case studies", Engineering Structures, Vol. 32, No. 6, pp. 1704-1714, 2010.

[4] McCrea, A., Chamberlain, D., and Navon, R., "Automated inspection and restoration of steel bridges—a critical review of methods and enabling technologies*",* Journal of Automation in Construction, Vol. 11, No. 4, pp. 351 – 373, 2002.

[5] Kaphle, M., Tan, A. C. C., Thambiratnam, D. P., and Chan, T. H. T., "A Study on the Use of Acoustic Emission Technique as a Structural Health Monitoring Tool", Journal of Engineering Asset Management and Infrastructure Sustainability, pp. 459 – 469, 2012.

[6] Huang, M., Jiang, L., Liaw, P.K., Brooks, C.R., Seeley, R., and Klarstrom, D.L., "Using Acoustic Emission in Fatigue and Fracture Materials Research", JOM-e, Member Journal of TMS, Vol. 50, No. 11, 1998.

[7] Shield, C., McKeefry, J. "Acoustic Emission Monitoring of Fatigue Cracks in Steel Bridge Girders", *MN/RC – 1999-36*, Minnesota Department of Transportation, St. Paul, MN 55155, 1999.

[8] AASHTO *LRFD* Bridge Design Specifications, Customary U.S. Units, 7th ed., American Association of State Highway and Transportation Officials, Washington, DC, 2014.

[9] TISEC. "ICEPAK – Pattern Analysis Software." TISEC Inc. 601 Route 364, Morin Heights, Quebec, Canada J0R 1H0. http://www.tisec.com/shop/enter.html,Visited, (Date)2010.

SECM/15/57

Preliminary investigation of changes in damping mechanism caused by corrosion in reinforced concrete beams.

D. C. Hettiarachchi[1*], Y.Matsumoto[1] and R. Takanami [1]

[1]Saitama University, Saitama, Japan
*E-Mail: dileepa1@gmail.com, TP: +818066950883

Abstract: Corrosion induced damages are one of the major durability issues that reinforced and pre-stressed concrete structures face, during their service life span. Vibration - based test methods have gained great attention in the structural health monitoring field during the last decades as, they are non-destructive and easy of conducting, compared to the other test methods. Dynamic characteristics of undamaged and damaged materials vary from each other and reflected through the modal parameters, like natural frequency, damping ratio and mode shapes, etc. In an RC member, along with the initiation of corrosion process, generation and propagation of corrosion products through the voids in concrete, initiate tensile cracks. Further to that, reinforcement will lose its effective diameter and at a later stage, the bond between reinforcement and concrete is reduced. These internal activities can cause changes in the damping mechanism of that member. Finally, failure will occurs due to loss of bearing capacity of the member. This study is focused on the vibration behaviour of reinforced concrete beam specimens, by performing modal tests under free vibration condition. The accelerated corrosion technique is used to induce artificial corrosion at different degrees. The damping ratio, evaluated by half-power bandwidth method and Eigen system Realization Algorithm was used to investigate changes expected in the damping mechanism.

Keywords: corrosion, non-destructive, vibration, damping mechanism

1. Introduction

Vibration based structural health monitoring (SHM) has been investigated in the field of non-destructive SHM in order to identify the premature deteriorations of Reinforced Concrete (RC) bridges or Pre-stressed Concrete (PC) bridges, among other available test methods. These deteriorations have been attributed mainly to corrosion of reinforcement during the service life of the structure due to various reasons [1]. Previous researches carried out in this area have shown that corrosion of reinforcement or tendons can cause a complete breakdown of the bond between concrete and reinforcements along with extensive cracks developed up to spalling of cover concrete. This phenomenon can cause catastrophic failures, resulting in injuries or severe fatal damages. Therefore, it is important to identify these types of damages in a structure at its early stage, so that necessary remedial actions can be taken to prevent or minimize the damages.

Physical properties of a structure like mass, stiffness and damping are related to modal parameters (natural frequencies, modal damping and mode shapes etc.) of the same. Damages of the structure alter the physical properties so that it will be reflected through changes in modal parameters. This phenomenon is the platform for the concept of vibration based SHM.

Corrosion of reinforcement bars or tendons in a reinforced concrete or pre-stressed concrete element is an electro-chemical process that causes ultimately loss of effective diameter and mass of rebar and induces internal cracks in concrete and finally spalling of cover and reduce the bond between reinforcement and concrete [2]. These deteriorations can directly alter the physical properties of that element and, consequently, the modal properties. The investigation of changes in modal parameters can be used to develop a structural health monitoring paradigm of structures, due to corrosion induced damages.

The natural frequency is a global property of a structure directly related to the stiffness properties. Maas et al [3] has shown that the natural frequency is a reliable indicator of structural damages in concrete structures, but mostly efficient after the

first crack has occurred. The damping ratio also shows significant response to damages or changes to the structural integrity [4]. Damping changes in an RC member along with the increase of corrosion induced damages, may be used as a tool to identify those damages, even if those are not visible to human inspections.
It can be hypothesized that there should be certain effect of structural damages on the mechanisms of damping. For example, when the crack width increases, damping could be affected due to friction between both faces of the crack. Further, if slippage of rebar takes place, again, there could be a significant change occur in damping due to variation of friction between rebar and concrete. These changes may be observed by investigating the changes in the modal damping values with the increase of corrosion level.

According to Maas et al. [3], linear and nonlinear dynamic properties can be used as damage indicators. A lot of researches have been done in this area by using linear dynamic damage indicators. They performed dynamic vibration test on 6 meters long concrete beams and damaged them with three point bending experiment, by increasing the cracking load. At each load step, those beams dynamically tested in a free-free setup under a swept sine excitation. According to them, damping is sensitive to the damage level and excitation force amplitude.

Razak, and Choi [5] conducted an experimental investigation to study the effect of corrosion on the modal parameters of reinforced concrete beams. Here an appreciable amount of steel corrosion damage was introduced by considering the crack width and spalling of cover concrete. The modal parameters were obtained by performing modal tests, both on damaged beams and control specimen. They concluded that both natural frequency and damping ratio are damage sensitive. But natural frequency is more damage sensitive and the variation of damping ratio is inconsistent with that of natural frequency.

Shahzad et al. [6] conducted laboratory tests to examine the possibility of using damping ratio to detect corrosion damages in RC beams. Uniform and local corrosion pattern were induced using accelerated corrosion technique and modal parameters were examined and compared with increasing in corrosion damage levels. According to the results obtained in this research, modal damping increased with damage level and more sensitive to corrosion damages when compared with natural frequency.
This paper describes a preliminary experiment in order to investigate changes in modal properties of RC beam due to corrosion of reinforcing bars. The experiment focuses on possible changes in damping mechanism along with development of corrosion of reinforcing bars and associated damages in concrete. The degree of corrosion was controlled by a series of accelerated corrosion tests (ACT). Impact testing was conducted at different corrosion levels to identify relevant modal parameters like damping ratio and natural frequency.

A better understanding in this area as a non-destructive test method, can be utilized to develop a SHM paradigm to investigate the health status of RC members in civil engineering structures effectively and efficiently.

2. Methods

2.1 Specimens
Three identical reinforced concrete beams, named Tr-1, 2 and 3 were cast for the following purposes.
a) Tr-1: to study a suitable experiment setup and instrumentation for ACT and impact testings.
b) Tr-2: to study the effect of corrosion, on natural frequency and damping ratio of an RC member under three stages of ACT
c) Tr-3: to conduct a series of ACTs and modal tests based on the understanding from Tr-1 and Tr-2 above.

The dimensions of the specimens were 100 x 70 x 880 mm and 10 mm diameter two reinforcing bars were embedded in each specimen that provided a reinforcement ratio of 4.4%. Two reinforcing bars were used in order to facilitate development of cracks. Cover to reinforcement was 30mm and grade of concrete was 40 MPa. See Figure 1 for more detail.

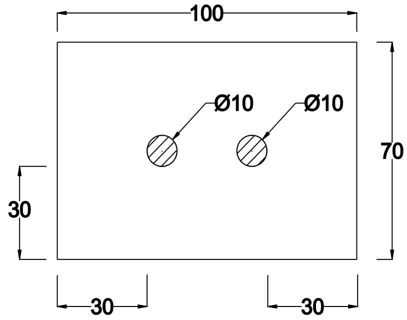

Figure 1: Dimensions of the specimens

2.2 Accelerated corrosion test
Localized corrosion pattern at the centre of the specimen of 100mm wide was subjected to ACT,

since localized corrosion may be realistic when considering the actual structures. Specimens were subjected to an electro-chemical ACT with a constant current supply of 200mA equivalent to a current density of 3000 μA/cm^2. A constant power output unit was used to provide a constant current. The current was applied between the steel reinforcement and a copper sheet of 200 x 100 x 5 mm placed under a sponge sheet that was used to facilitate the electric flow between concrete and copper sheet as the specimen was not submerged in the solution (Figure 2). Here, the copper sheet acts as the cathode and the reinforcement acts as the anode. Sodium chloride solution of 3% by weight was used as the electrolyte to provide electrical contact between anode and cathode.

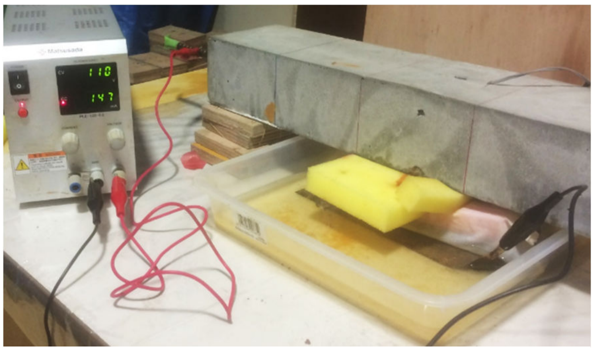

Figure 2: Accelerated corrosion Test

2.3 Impact testing

Impact testings were performed after each ACT by subjecting the specimens to hammer excitation under free-free support condition. Five piezoelectric accelerometers were mounted on the bottom surface of the specimen and strain gauges installed on top of the embedded reinforcing bars. The accelerometers were connected to charge amplifiers and strain gauges were connected to dynamic strain meters to obtain dynamic responses. Plastic hammer was used to give an impact to the top surface of the specimen from 270 mm away from one end, which can excite first three bending vibration modes (See Figure 3 & 4). First bending vibration mode was considered in this analysis hereafter.

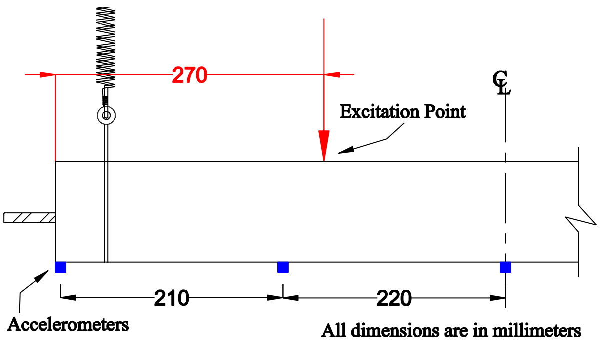

Figure 3: Accelerometer locations and point of hammer excitation in impact test

Modal properties were identified by both time and frequency domain methods: natural frequencies and damping ratios were identified from Fourier transform (FT) and half-power bandwidth method (HBW) and Eigensystem Realization Algorithm (ERA).

Figure 4: Impact testing

2.4 Static strain measurement

There will be an internal expansion due to pressure applied by the corrosion products which, finally exceed the tensile capacity of the concrete and initiate a crack [7]. This internal pressure can be reflected through the internal expansion of the concrete and can be identified by static strain measurement at the location of local corrosion during the ACT. For this purpose, strain gauges were embedded in concrete in the direction perpendicular to the longitudinal axis of the beam in the localized corrosion area and near to an end of the Tr-1 specimen.

3. Results and Discussions

3.1 Modal properties

According to the findings from the trial tests did on the Tr-1 specimen, for proper establishment of a constant current in the ACT, it was required to wet the local corrosion area of the specimen and maintain a sufficient level of electrolyte solution.

The time history responses were processed using both FT and ERA to estimate the natural frequency and damping ratios of the specimens at the end of each ACT. It was observed that, along with increases in the degree of corrosion, the natural frequency tended to decrease and the damping ratio tended to increase. Figure 5 shows examples of the acceleration time histories and the corresponding spectra before and after an ACT. As observed in the figure, relative spectrum amplitude at first natural frequency was reduced after the ACT.

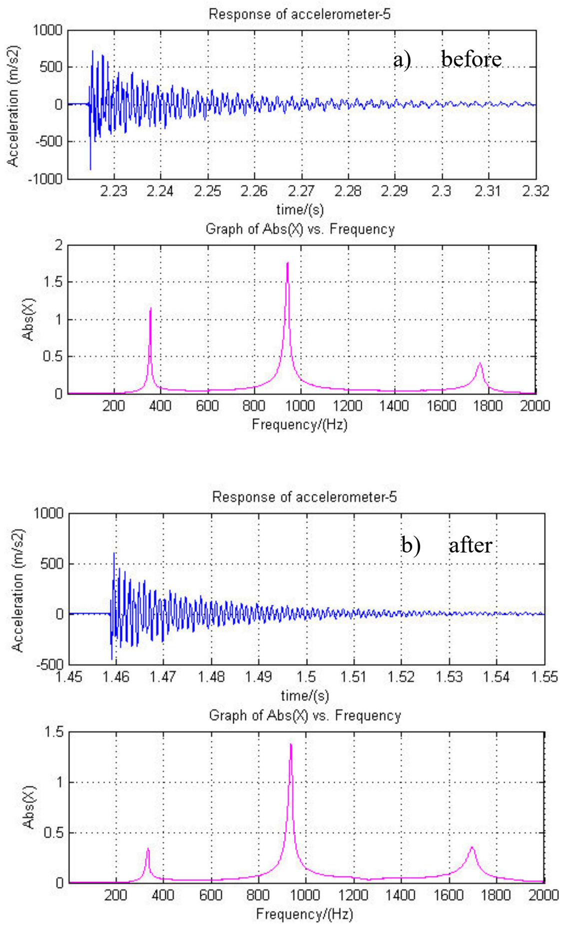

Figure 5: Responses before and after a corrosion process of Tr-3 specimen

Table 1 shows a summary of results obtained from impact testing for Tr-2 specimen. In addition to, the natural frequencies (f_1) and damping ratios (DR_1) obtained for the first mode, normalized values of both of those modal parameters (normalized by the corresponding healthy state at level-0) are also included in the table for comparison purpose. Accordingly, decreases in the normalized natural frequency (R_f) were observed when corrosion level increased, and increases in the normalized damping ratio (R_{DR}) can be observed after each level of the corrosion process.

Table 1: Natural frequencies and damping ratios obtained with increased of corrosion- Tr-2 specimen

Corrosion Level	f_1 /(Hz)	R_f	DR_1	R_{DR}
L-0	357.0	1.000	0.0104	1.000
L-1	289.5	0.811	0.0521	4.988
L-2	264.2	0.740	0.0626	5.987
L-3	238.6	0.668	0.0799	7.644

HBW method incorporated with FT and ERA were used to identify natural frequencies and damping ratios in Tr-3 specimen. The results of HBW method and ERA showed agreement at a certain degree, although some differences were observed in the damping ratio, in particular.

Table 2 shows a summary of results obtained from impact testing for Tr-3 specimen, as an example. The degree of corrosion here is expressed by multiplying the amount of current provided in milliamperes during the mentioned time in seconds for each ACT interval. Before starting the ACT, the specimen was subjected to a modal test to study the initial status of modal properties mentioned as "control" in Table 2. Figures 6 and 7 shows the natural frequencies (f_1) and damping ratios (DR_1), respectively, at different corrosion levels presented in Table 2.

Table 2: Natural frequency and damping ratio identified by ERA with increased level of corrosion- Tr-3 specimen

Modal test No.	Duration of ACT / (h)	Degree of corrosion / (A*s)	f_1 / (Hz)	DR_1
control	-	-	352.66	0.0068
1	0.5	360	353.46	0.0077
2	0.5	720	355.41	0.0068
3	0.5	1080	354.23	0.0075
4	1.0	1800	354.16	0.0068
5	1.0	2520	353.73	0.0070
6	1.0	3240	355.12	0.0063
7	1.0	3960	354.82	0.0066
8	2.0	5400	354.49	0.0067
9	2.0	6840	353.54	0.0072
10	*4.0*	*9720*	*340.79*	*0.0109*
11	2.0	11160	334.40	0.0123
12	4.0	14040	331.72	0.0161
13	0.0	14040	332.65	0.0123
14	15.0	24840	332.70	0.0151
15	4.0	27720	332.16	0.0148

The first sign of a longitudinal crack observed at the bottom of the specimen before the 10th modal test. The crack propagated up to two sides before the 14th modal test. It should be noted that for the understanding purpose of the continuation of corrosion process even with different current supply, the current supplying interval was reduced to two hours between 10th and 11th modal tests and four hours between 14th and 15th modal tests. Zero current passed between 12th and 13th modal tests for 24 hours.

According to Figures 6 and 7, at initial stages of corrosion both natural frequency and damping ratio show mild fluctuations. After the 9th modal test (the level of corrosion in between 7000-10,000 A*s), a significant change of modal parameters can be observed. This stage is directly related to the occurrence of the first crack. The crack was further developed through either side of the specimen due to increased level of corrosion.

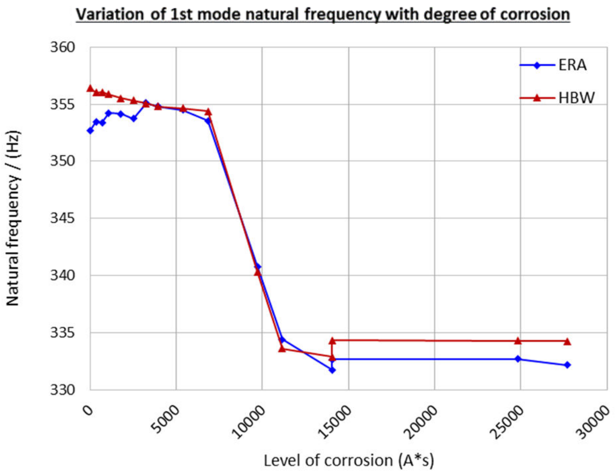

Figure 6: Variation of 1st mode natural frequency with level of corrosion

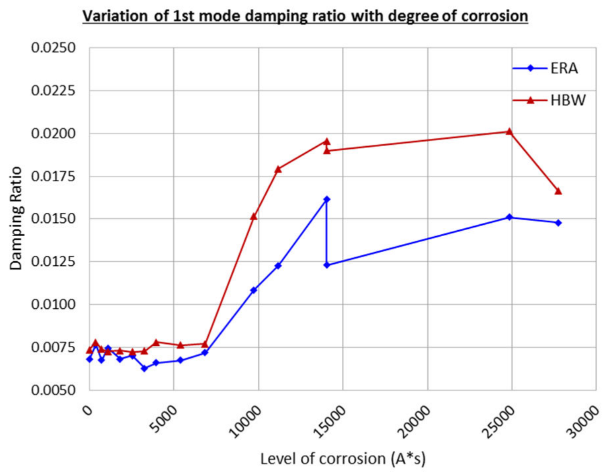

Figure 7: Variation of damping ratio obtained from 1st mode with level of corrosion

The sudden increase in natural frequency and drop in damping ratio values around the corrosion level of 14,000 A*s is due to stop of the current supply as mentioned above. Corrosion leaks were observed even in this state, but in very slow rate and later, those leaks were solidified, which may be the reason to increase the natural frequency around 0.3% and reduce the damping ratio by 24% in the immediate next modal test. At the end of the series of ACT, it was found that there was a 5.8% reduction of natural frequency and 117% increase of damping ratio with respect to the control stage of Tr-3 specimen.

3.2 interpretation of results of modal properties

These observations could be explained as follows. Before starting and up to a certain limit of continuation of the corrosion process, the stiffness of the specimen will not be changed significantly. Once the stress due to accumulation of corrosion products around the interface of reinforcement and concrete inside exceeded the tensile capacity of concrete, an internal crack will be developed. With further increase of corrosion level, these cracks develop over the cover depth and surface crack will appear [7]. At this stage, the damage can be clearly identified from outside of the specimen (corresponding to the 10th modal test). After appearing the crack, the stiffness of the specimen is reduced and the effective diameter of rebar also reduced further. Therefore, the natural frequency reduces with further increase of the corrosion level (See Figure 6).

In parallel, the damping mechanism may also be subjected to following changes. At the beginning, the damping mechanism is dominated by the material damping. After developing the cracks, friction damping due to the opening and widening of the cracks and due to abrasion of loose particles trapped inside the cracks (See Figure 8) can add additional friction damping component, while there is a contribution from material damping from the non-cracked areas in the same cross sections. Further, there can be a slippage or relative displacement in between reinforcement and concrete at the interface that contribute friction damping to the system. At this stage, the contribution from material damping reduces.

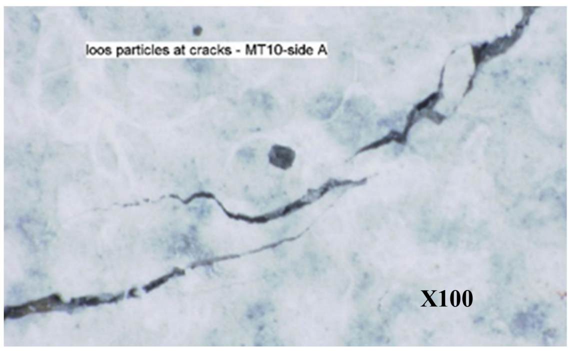

Figure 8: Loose particle trapped inside

In the later part of corrosion process due to more extension of the cracks cause to reduce the contribution from material damping further. Widening of the cracks and removing of the fine loose particles affect to abrasion of cracked surfaces and reduce the friction damping also at the later stages of corrosion.

3.3 Static strain measurement

From the static strain measurements obtained from Tr-1 specimen, it is understood that the results may be consistent with the phenomena that there is an internal stress due to corrosion products generated and internal strain around that area increases accordingly. Once the crack developed, the strain increases steeply as the crack is widened. (See "Detail -A" between 1500s – 2000s in Figure 9).

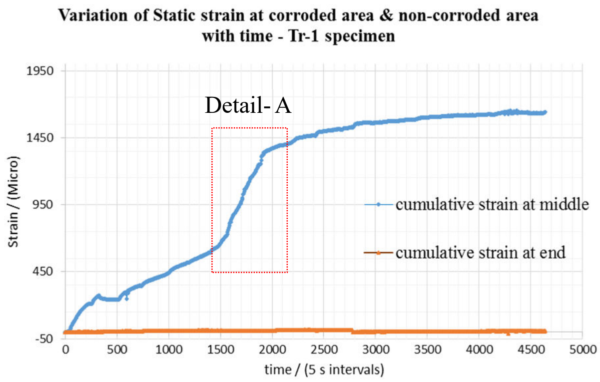

Figure 9: Variation of static strain with increase of corrosion of Tr-1 specimen

3.4 Accelerated corrosion test

The ACT on specimens took over around 20 hours, which continue over 3 days along with intermediate modal tests under stipulated conditions in Section 2.2 above. The examination of corroded reinforcing bars revealed significant loss of steel in the localized corrosion area. Out of two reinforcing bars, one showed higher loss of steel area compared to the other (See Figure 10). Possible reasons for this may be include inhomogeneous material properties of concrete, presence of aggregate around the reinforcing bars that acting as barriers to flow of corrosion products and development of crack across and deviations in cover to reinforcement.

Figure 10: Corrosion of reinforcement - specimen Tr-3

Crack development during ACT was monitored. At early stage, fine leaks of light yellow colour were observed from side walls and, then, a hair crack developed around that place. After that, due to increase in crack width, corrosion process accelerated and greenish and dark brownish colour corrosion products tended to leak from the cracks.

4. Conclusions

Findings obtained from this preliminary experimental study are summarized as follows:

(a) The damping ratio showed higher sensitivity to corrosion induced damage than the natural frequency in the results described in this paper. In order to ensure this result, further investigations are in progress.

(b) The results of this study may have shown an evidence of damping mechanism changes along with deteriorations due to corrosion of reinforcing bars in an RC beam. Further experiments are being conducted to investigate this.

References

[1]. Wallbank R.J., The performance of concrete in bridges- A survey of 200 highway bridges, Department of Transportation, London. (1989).

[2]. S.Ahmad, Reinforcement corrosion in concrete structures, its monitoring and service life prediction-a review, Elsevier-Cement & concrete composites 25, 2003, pp 459-471.

[3]. Stefan Maas, Arno Zürbesa, Danièle Waldmanna, Markus Walteringa, Volker Bungarda, and G. De Roeckb. Damage assessment of concrete structures through dynamic testing methods. Part 1 – Laboratory tests, Elsevier- Engineering Structures Vol. 34, 2012, pp 351–362.

[4]. R.O.Curadellia, J.D.Rierab, D. Abrosinia, M.G. Amania, Damage detection by means of structural damping identification, Elsevier -Engineering Structures 30, 2008, pp 3497-3504.

[5]. H.Abdul Razak, F.C Choi, The effect of corrosion on the natural frequency and modal damping of reinforced concrete beams , Elsevier -Engineering Structures 23, 2001, pp 1126-1133.

[6]. S.Shahzad, H.Yamaguchi, R.T.Takanami and S.Asamoto, Detection of corrosion induced damage in reinforced concrete beams based on structural damping identification, Proceeding - Hokkaido University Collection of Scholarly and Accademic Papers (HUSCAP),2013.

[7]. H.S.Wong, Y.X.Zhao, A.R.Karimi, N.R.Buenfeld and W.L.Jin, On the penetration of corrosion products from reinforcing steel in to concrete due to chloride-induced corrosion, Elsevier – Corrosion Science 52 ,2010, pp 2469-2480.

SECM/15/063

Damping properties of existing single-span prestressed concrete girder bridges with different service periods

T. Tanaka[1], S. e Rehmat[1] and Y. Matsumoto[1*] and Abeykoon J. Dammika[2]

[1]Saitama University, Saitama, Japan
[2]University of Peradeniya, Peradeniya, Sri Lanka
*E-Mail: ymatsu@mail.saitama-u.ac.jp, TP: +81-(0)48-858-3557

Abstract: Invisible damages in bridges, such as corrosion of rebar, may not be detected by periodic visual inspection that is the principal method in bridge maintenance. A possible non-destructive technique which has been investigated to assist visual inspection is vibration-based structural health monitoring. The modal properties of bridges, such as the natural frequencies, mode shapes and modal damping ratios, are expected to change due to damages and/or deteriorations. In the present study, damping properties of existing PC girder bridges were identified so as to investigate the possibility of the modal damping ratios as an indicator of damage detection. Vibration measurements were made at ten single-span PC bridges with similar dimensions under normal service conditions by using wireless and wired sensor systems. Eigensystem realization algorithm (ERA) with an improved screening process was applied to extracted free vibration records. Modal properties up to the fourth vibration modes were identified for many bridges. For the third vibration mode that was identified stably in most bridges, there was a trend that the modal damping ratio of old bridges was greater than other newer bridges. Although this result does not necessarily indicate the relationship between the damage and damping property, it may support the possibility of damping in the evaluation of structural state.

Keywords: Damping properties, Eigensystem realization algorithm, Single-span prestressed concrete girder bridge

1. Introduction

There are a lot of bridges in transportation network. These bridges were constructed with about 50 years of design life. There are bridges which have been in service for over 50 years without major accidents by performing appropriate maintenance works. In Japan, more than 40% of the bridges are expected to exceed 50 years in service in 10 years' time [1]. Aging of the bridges have become a problem and appropriate maintenance is needed. Current major inspection is performed by visual inspection. However the visual inspection has some problems. For example, it is impossible to see inside of the concrete; it is difficult to inspect structural parts where sufficient space is not available for an inspector for access [2]. The structural health monitoring based on dynamic characteristics of bridges has been studied as a technique to assist the visual inspection [3]. While it has been reported that the change in damping parameters by damage and deterioration can be relatively large, compared to that in natural frequencies, the identification accuracy of damping from measured vibration data is not high [4]. If factors affecting damping are of wide variety, physical interpretation of damping change is difficult. In addition, understanding of damping of real bridge is not sufficient.
The objectives of this study were to identify damping ratio of existing bridges with high accuracy and to elucidate their damping characteristics. In the present study, damping properties of existing PC girder bridges were identified so as to investigate the possibility of the modal damping ratios as an indicator of damage detection.

2. Target bridges

Ten existing single-span prestressed concrete girder bridges were selected for the present study. In Table 1, a list of selected bridges is shown. Those bridges were selected because they had single-span, different ages of service, and bridge length in a limited range and there was not excessive traffic volume. The ranges of completion year was 1975 to 1994. The bridge length varied

Table 1: Target bridges

Bridge No.	Completion year	Structure format	Length	Width
I (old)	1975	Pretension T beam	16.33	9.50
II (old)	1975	Pretension hollow slab	16.13	9.50
III	1976	Pretension T beam	16.60	18.00
IV	1978	Pretension T beam	19.66	13.95
V	1980	Pretension T beam	20.80	16.80
VI	1985	Pretension T beam	19.30	7.50
I (new)	1991	Pretension T beam	16.33	9.50
II (new)	1991	Pretension hollow slab	16.14	9.50
VII	1991	Pretension T beam	17.36	12.00
VIII	1994	Pretension T beam	15.00	10.00

between 15 m and 20.8 m. The structural format was either pretension T beam or pretension hollow slab. In Bridges I and II, old and new bridges are built alongside each other. The selected bridges have not been reported as damaged or deteriorated by previous visual inspection.

3. Experimental modal analysis

3.1 Vibration measurement

Vibrations of the bridges induced by ordinary road traffic were measured. Vertical acceleration was measured at several locations at each bridge by using a wired or wireless measurement system. If wiring was difficult, the wireless measurement system was used. Sampling rate of the wired measurement system was 250 samples per second, while the sampling rate of wireless measurement system was 100 samples per second.
Vibration sensors were placed at different positions to identify mode shapes of the bridges by experimental modal analysis. In Figure 1, an example of sensor position is shown. Additionally, video recording was taken so as to understand the traffic situation during the vibration measurement

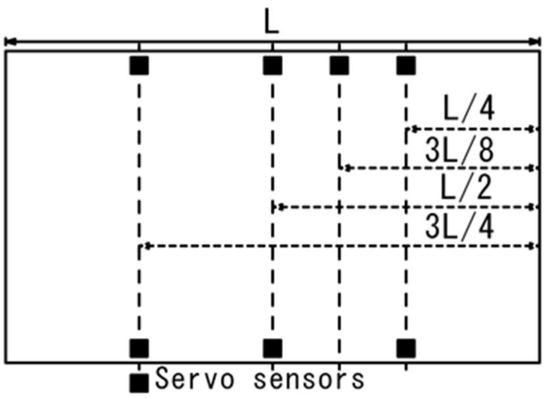

Figure 1: Example of sensor setting

3.2 ERA analysis

In the experimental modal analysis of present study, Eigensystem Realization Algorithm (ERA) [5] was applied to vibrations induced by passing vehicles. ERA needs free vibrations that were extracted from vibration records obtained in the measurement. In Figure 2, an example of extraction of free vibration is shown. Bridge vibration was induced while a vehicle ran over the bridge. After the vehicle passed the bridge, the bridge vibration continued for a while, which was regarded as free vibration in this study. The video recording was used to confirm there was no other vehicle on the bridge during those extracted free vibrations.

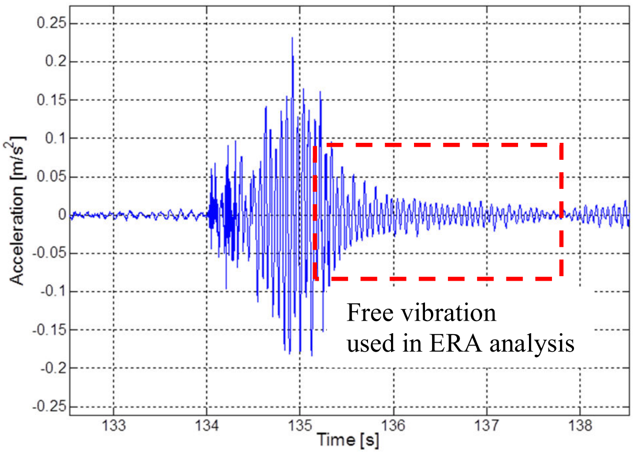

Figure 2: example of extraction of free vibration.

3.3 Screening in ERA

In ERA, physical vibration modes were identified by applying screening process based on several criteria, such as the stability of mode characteristics to the change in system order. In some cases, the damping ratio showed considerable variation with changes in system order, although the natural frequency was identified stably. In this study, the stability of the damping ratio was focused on in the identification of modal properties, as follows.
Firstly, modes corresponding to an assumed system order were identified. There were some modes that did not have a physical meaning were removed by screening in the next step. In the screening process, a stabilization diagram is used to show the stability of identified modes against system order. Figure 3 shows an example of stabilization diagram before screening which displays all the identified modes.

Unstable identified modes were then removed by screening methods. The conditions used for screening are as follows.

Modal Assurance Criterion greater than 0.9 (1)

Removing of negative damping (2)

Removing damping greater than 10 % (3)

Max Frequency difference = 0.1 (4)

Modal amplitude ratio = 0.8~ 1.2 (5)

In Figure 4, the stabilization diagram after screening is shown. Unstable modes shown in Figure 3 were removed and stable modes only were left in Figure 4.

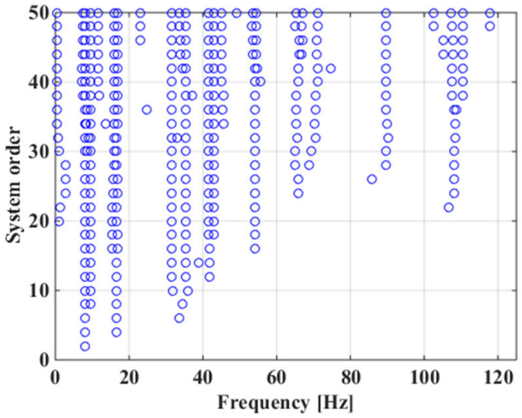

Figure 3: Stabilization diagram before screening

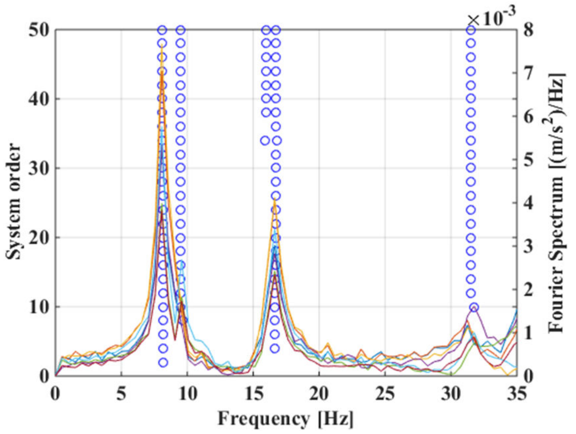

Figure 4: Stabilization diagram after screening

The stability of damping ratio was then examined. Figure 5 shows the stabilization of the damping ratio of first mode (around of 8 Hz) to the change in system order. An appropriate range of system order was then defined as follows. Firstly, the minimum system order was judged by the number of peaks in Fourier spectrum. As in Figure 4, there were three clear peaks in this example, so that the minimum system order can be judged as 6 (the number of peaks times 2). According to Figure 5, the damping ratio became stable when the system order was higher than 8. On the other hand, when system order was over 30, the damping ratio tended to vary significantly, which implied that those system orders were too high. Thus, it was decided that the appropriate range of system order should lie between 8 and 28, in this particular case.

3.4 Identified mode shapes

Examples of mode shapes identified by ERA are shown in Figures 6 and 7. This figure shows a side view of the bridge. Circles at both ends represent support points, and others show normalized displacement at sensor positions. Sensors placed at the upstream side and those at the downstream side edge were represented by circles in different colors. As seen in Figures 6 and 7, it was difficult to understand mode shape, especially the deformation in the transverse axis of the bridge from the result of ERA. The mode shapes shown in Figures 6 and 7 are similar, although their natural frequencies are different, i.e., 8.14 Hz and 16.7 Hz. In order to understand mode shapes, theoretical modal analysis using the finite element method was conducted as described in the next section.

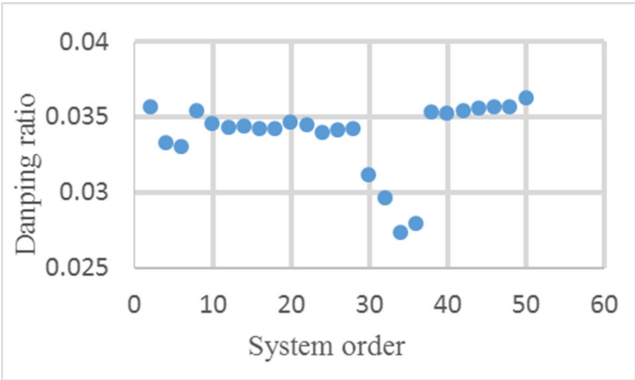

Figure 5 Stabilization of damping ratio

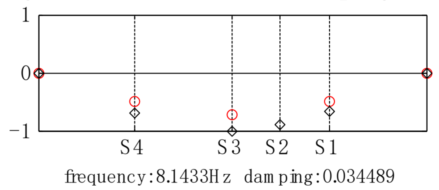

Figure 6: First mode shape identified by ERA

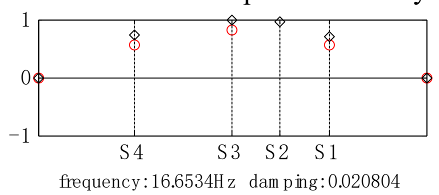

Figure 7: Third mode shape identified by ERA

4. Theoretical modal analysis

In the theoretical modal analysis, NASTRAN NX software was used. Only superstructure of the target bridges with girders and slab was modelled. As for the support conditions, spring elements were used to express rubber pads. The spring

Table 2: List of identified vibration modes

Mode No.	Mode shape name	Range of natural frequency	Mode shape of experimental analysis	Mode shape of theoretical analysis
1	Symmetric vertical bending (SV)	6.39 ~ 9.13 Hz	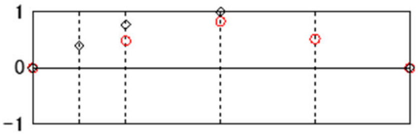	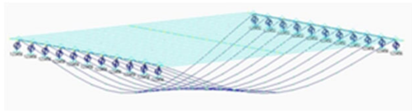
2	Symmetric torsional (ST)	6.66 ~ 11.9 Hz	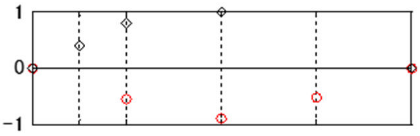	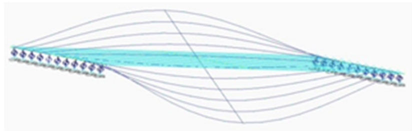
3	Vertical-transverse bending (SVT)	9.76 ~ 20.8 Hz	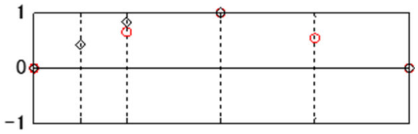	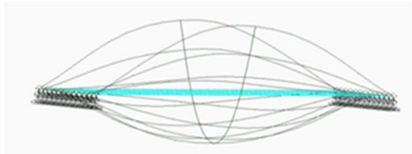
4	Symmetric vertical-transverse bending (AsVT)	15.9 ~ 33.9 Hz	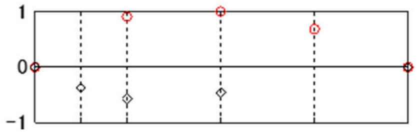	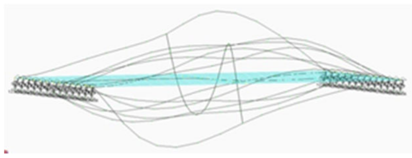

constant was adjusted to obtain natural frequencies close to the experimental identification.
In Table 2, the first four vibration modes identified are summarized. The first four mode shapes identified were named as symmetric vertical bending (SV, Mode 1), symmetric torsional (ST, Mode 2), symmetric vertical-transverse bending (SVT, Mode 3) and asymmetric vertical-transverse bending (AsVT, Mode 4) in this study.

5. Analytical damping evaluation

An analytical energy-based damping evaluation [6] was applied to the modal damping ratios identified. In general, the mechanism of vibration damping in a bridge is complicated and it is difficult to model accurately. However, for single-span bridges investigated in this study, the sources of damping could be limited. In this study, the damping of bridges was modeled to be provided by internal energy losses in main girders, crossbeams and rubber pads at the supports.
The damping ratio of the *n*th-order mode can be expressed by the ratio of the modal damping energy D_n to the modal potential energy U_n in one period (Equation 6).

$$\xi_n = \frac{D_n}{4\pi U_n} \tag{6}$$

The potential energy was assumed to be dominated by the strain energy due to the deformation corresponding to the mode shape. The damping energy was defined as the sum of the damping energy in the main girders, crossbeams and rubber pads. The damping energy D was represented by Equation 7 that was proportional to the strain energy V of the structural components and the equivalent loss factor η.

$$D = 2\pi\eta V \tag{7}$$

The total damping energy D_n of *n*th-order mode was expressed as the sum of the damping energy in the main beams $D_{n,b}$, crossbeams $D_{n,c}$ and supporting part $D_{n,r}$ (Equation 8). The damping ratio of *n*th-order mode was obtained by Equation 8.

$$\xi_n = \frac{D_{n,b} + D_{n,c} + D_{n,r}}{4\pi U_n} \tag{8}$$

Focusing on Bridges I (new) and I (old), which had equivalent structure formats and different damping trend, the damping ratios were estimated by the energy damping evaluation method. The potential energy was calculated using the model created by the theoretical modal analysis. The loss factors were determined initially based on the results by Iino [6] and adjusted manually to obtain the damping ratios estimated close to the average values of the damping ratio identified by the ERA.

6. Results and discussion

6.1 Identified modal damping ratios

Figures 8 to 11 show the damping ratios of the four modes shown in Table 2 for all the bridges. Those four vibration modes were identified in most of the bridges. Modes 2 and 3 were observed to be relatively stable in all the bridge except Bridge 5. The identification results for Mode 2 showed relatively large variation than those for Mode 3. It was expected initially that the identification of Mode 1 was the easiest. However, the results of the actual identification showed that there were many unidentified cases and the variation in identification was relatively large.

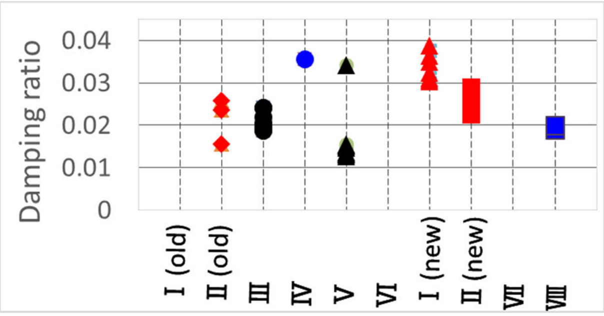

Figure 8: Damping ratio of Mode 1

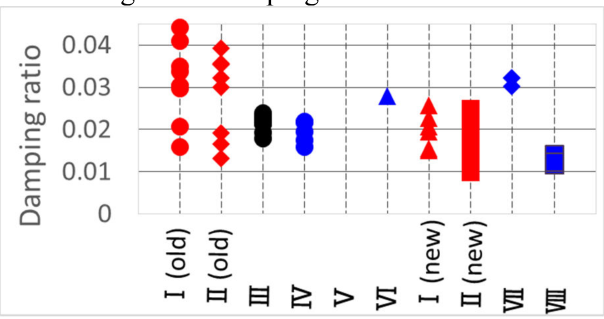

Figure 9: Damping ratio of Mode 2

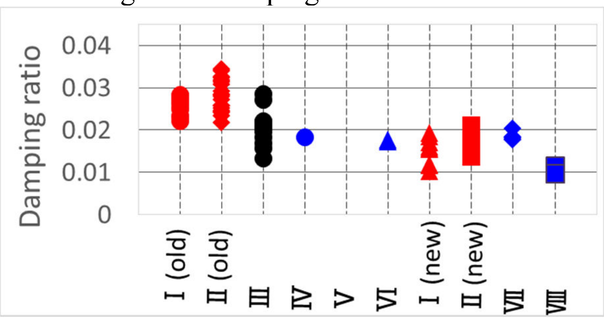

Figure 10: Damping ratio of Mode 3

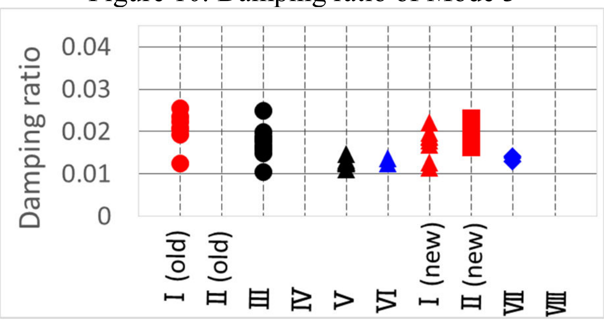

Figure 11: Damping ratio of Mode 4

6.2 Difficulty in lower order mode identification

Figures 12 and 13 show examples of stabilization diagram for the data from which the identification of lower order vibration modes was difficult. In the figures, the red arrows show the natural frequencies up to the third order mode obtained in the theory modal analysis. Those data were obtained at Bridges I and II, which were the oldest among the measured bridges in this study. Fourier spectrum did not show clear peaks corresponding to the first two modes, as shown in Figures 12 and 13.

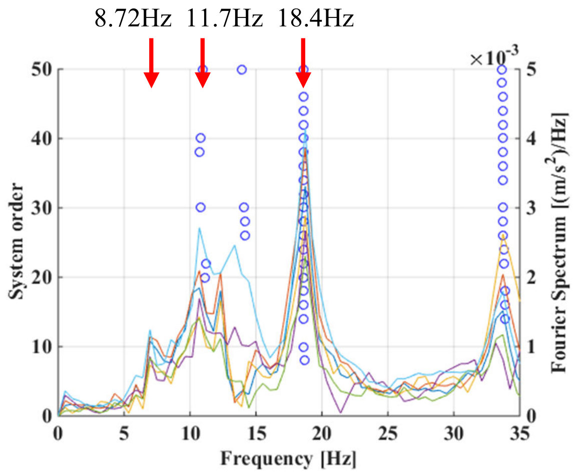

Figure 12: Stabilization diagram showing lowest order modes-Bridge I

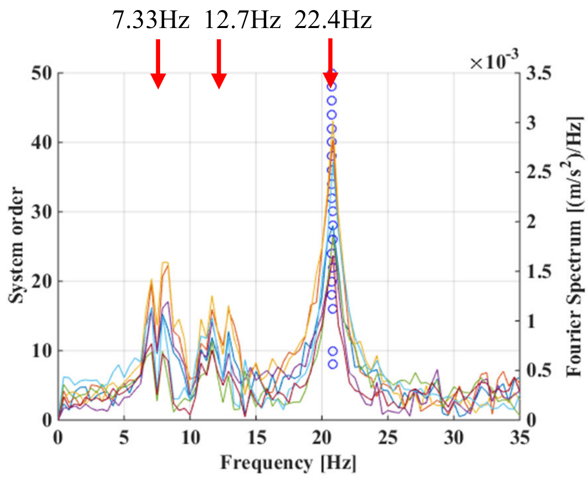

Figure 13: Stabilization diagram showing lowest order modes-Bridge II

6.3 Relationship between damping ratio and age of bridge

Here, the damping ratio of Mode 3 which showed most stable identification results is focused on. In Figure 14, the relationship between the average damping ratio of each bridges and completion year is shown. It was seen that the damping ratio of some of the old bridges were greater than the others. For those other bridges, the damping ratio of Mode 3 ranged from 0.015 to 0.02.

In Figure 15, the locations of Bridges I and II are shown. The structural format of Bridges I (new) and I (old) and Bridges II (new) and II (old) were almost identical (Table 1). The comparison of the damping ratio of Mode 3 for these pairs of bridges also show the trend that the older bridge had greater damping than the newer bridge, as observed in Figures 16 and 17.

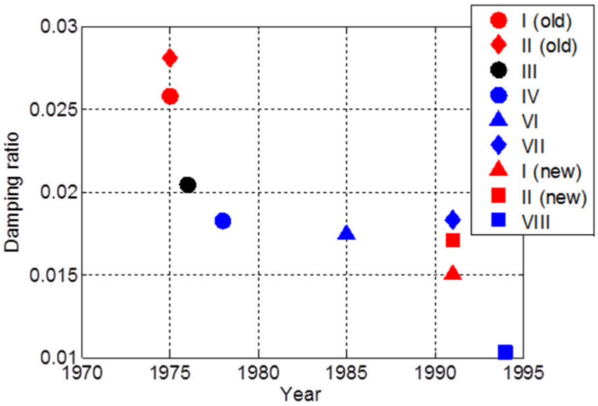

Figure 14: The average of damping ratio vs completion year

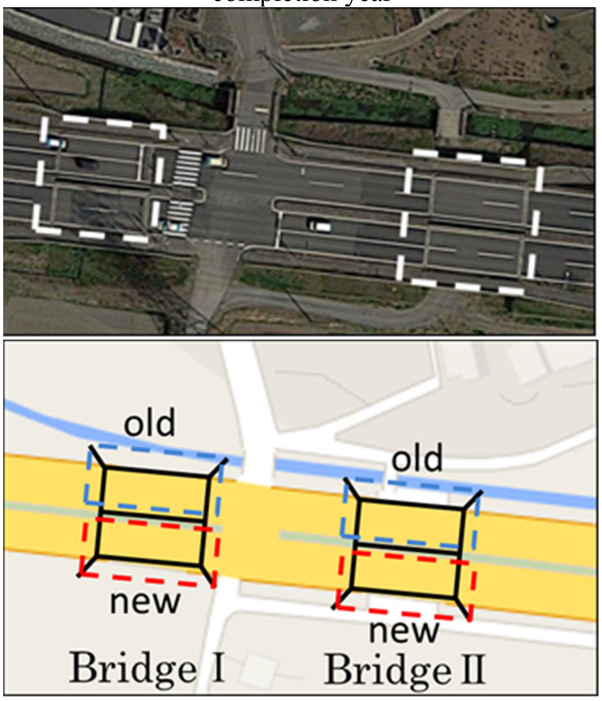

Figure 15: Location of Bridges I and II

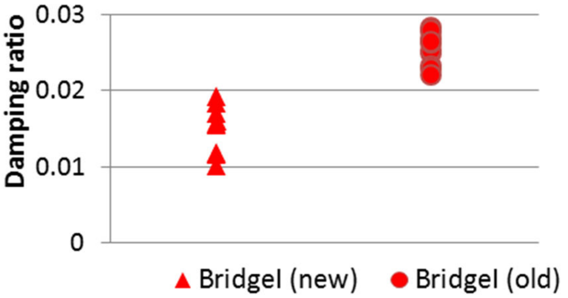

Figure 16: Comparison of damping ratio of Mode 3 for Bridge I

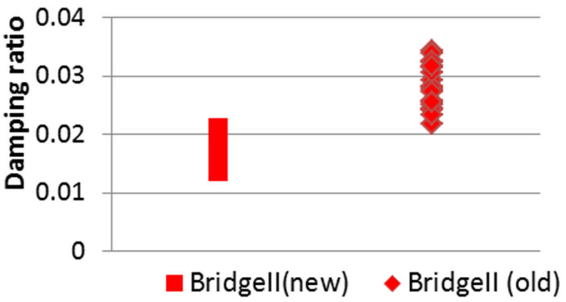

Figure 17: Comparison of damping ratio of Mode 3 for Bridge II

It was found in the previous study that damages in a concrete beam increased the damping [4]. For the selected bridges, any visible damages or deteriorations had been detected by visual inspection, and it cannot be concluded form the results in this study that the bridges with higher damping ratio might have damage or deterioration. Further study is proceeded to investigate possible reasons for the difference in damping ratio observed in the results, including the possibility that invisible damages or deteriorations resulted in different damping ratios.

6.4 Contributions of different structural components to damping

Figures 18 and 19 show the estimated contribution from different components to the damping and the average damping ratios identified by the ERA. Table 3 shows the adjusted loss factors used in the results shown in Figures 18 and 19. As observed in the figures, the contributions from different components to the damping are dependent on the vibration mode. In the lower two modes, the contributions from the main beams and supports to the damping ratios were dominant. In the higher two order modes, the contribution from the crossbeams to the damping ratios was relatively large.

For Bridge I (new) shown in Figure 18, the damping ratio identified for the SV mode was underestimated by the analytical damping evaluation as seen in the figure. Possible causes for this underestimation may include the effect of the other damping sources, such as energy dissipation to the abutment and ground. Figure 18 shows that the damping ratio of Bridge I (new) identified by the ERA decreased with increasing the mode order, with the exception of the AsVT mode. According to the contribution from each structural component shown in Figure 18, it can be understood that only crossbeams can cause an increase in the damping of fourth order mode than the third order mode.

For Bridge I (old) shown in Figure 19, the damping ratio decreased with increases in the mode order. This trend appeared to be represented reasonably by the damping model and equivalent loss factors presented in Table 3.

Figures 18 and 19 show that the damping ratios in Bridge I (old) were higher than the corresponding damping ratios in Bridge I (new). It can be seen in Table 3 that those greater damping ratios in Bridge I (old) than Bridge I (new) could be attributed to the greater equivalent loss factor for the main girders in Bridge I (old) with the loss factors for the crossbeams and supports unchanged. Although further investigation is required, the results shown above implies that, based on analytical damping evaluation, changes in a set of damping ratios can be interpreted as changes in damping in a specific structural component that could be caused by damages or deteriorations.

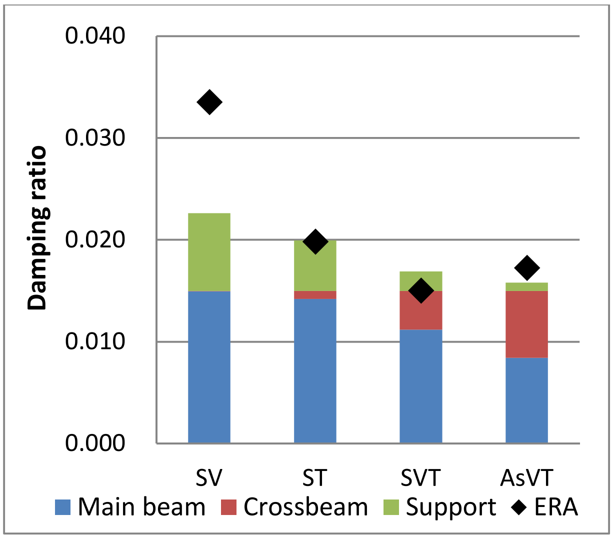

Figure 18: Damping ratio of Bridge I (new) by energy damping evaluation method

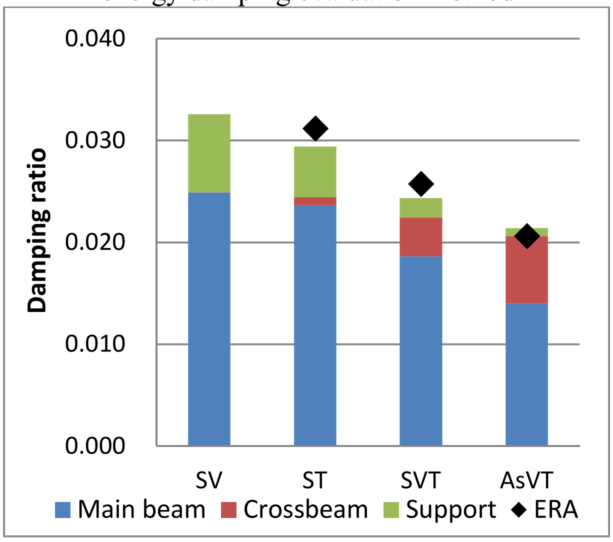

Figure 19: Damping ratio of Bridge I (old) by energy damping evaluation method

Table 3: List of loss factor

	η_b	η_c	η_r
Bridge I (new)	0.03	0.03	10
Bridge I (old)	0.05	0.03	10

7. Conclusions

The following conclusions are drawn from the results of this study.

- Four vibration modes were identified in the frequency range below about 35 Hz for the single-span PC girder bridges with a bridge length between 15 and 21 m.
- The symmetric torsional mode (Mode 2) and the vertical-transverse bending mode (Mode 3) were identified with higher stability than the other vibration modes in most bridges.
- For the third vibration mode, the damping ratios of some old bridges were greater than the damping ratios of the other bridges.
- The energy-based damping assessment described above can be used to explain the changes in damping associated with deteriorations or damages in bridges.

Reference

[1]. Ministry of Land, Infrastructure, Transport and Tourism, "*The future of standards for proper management of road structures*", http://www.mlit.go.jp/common/000986133.pdf [Accessed 9 October 2015] (in Japanese)

[2]. E. Matsumura, "Present aspects on inspection and diagnosis of concrete structures", Concrete Journal, Vol.39, No.6, pp.8-15, 2011. (in Japanese)

[3]. S. Maas, A. Zurbes, D. Waldann, M Waltering, V. Bungard, G. De Roeck, "Damage assessment of concrete structures through dynamic testing methods", Engineering Structure, Vol.34, pp.351-362, 2012.

[4]. R.O.Curadelli, J.D.Riera, D.Ambrosini, M.G.Amani, "*Damage detection by means of structural damping identification*", Engineering Structure, Vol.30, pp.3497-3504, 2008.

[5]. J. N. Juang, Applied System Identification, Prentice Hall PTR, Upper Suddle River, 1994, pp.133-147.

[6]. A. J. Dammika, K. Kawarai, H. Yamaguchi, Y. Matsumoto, T. Yoshioka, "Analytical damping evaluation complementary to experimental structural health monitoring of bridges", J. of Bridge Engineering, ASCE, Vol.20, No.7, 04014095, 2015.

[7]. H. Iino, "*Experimental identification of damping capacity of composite two-girder bridge and discussion based on the energy evaluation method*", Master's thesis, Graduate School of Science and Engineering, Saitama University, 2003. (in Japanese)

SECM/15/70

Numerical analysis of the backfilling sequence effect on gravity retaining wall behaviour

C. Sanjei[1*] and L.I.N. De Silva[1]

[1]University of Moratuwa, Katubedda, Sri Lanka
*E-Mail: sanjeic@gmail.com, TP: +94770569867

Abstract: Gravity retaining walls derive their capacity to resist lateral movement through the dead weight of the wall. The design methodologies proposed by standards do not take into account the construction sequences that simulate the process by which the soil and retaining wall are brought together. However, in reality, at least during the backfilling process, the retaining wall undergoes many displacements that are not so far considered in the design. In this investigation, effect of construction sequences in the gravity retaining walls with different shapes is investigated with the help of finite element method. Two different construction sequences, namely the backfilling after wall construction and the backfilling parallel to wall construction, are compared for different wall shape models. Lateral displacement of the bottom and the top of the wall is plotted for each model and construction sequence with construction stages. Bearing pressure distribution, lateral earth pressure and failure wedge angle are summarized and compared with design values. Each wall showed different behaviours for each of the construction sequences. Back filling after wall construction minimizes the sliding failure and bearing pressure. Overturning failure could be reduced by backfilling parallel to wall construction. However, it was observed that, comparatively, backfilling after wall construction is effective than backfilling parallel to wall construction, suggesting that proper selection of construction method also may reduce negative effects on the wall stability.

Keywords: gravity retaining wall, construction sequence, numerical modelling, backfilling, lateral displacement

1. Introduction

To ensure stability of retaining structures, they shall be designed to withstand lateral pressures due to soil and water, the effects of surcharge loads, self-weight of the wall, and earthquake loads. In addition, earth-retaining systems shall be designed to provide adequate structural capacity with acceptable movements, adequate foundation capacity with acceptable settlements, and acceptable overall stability of slopes adjacent to walls. These are the serviceability requirements. The tolerable levels of lateral and vertical deformations are controlled by type and location of wall structure and surrounding facilities.

Gravity retaining walls derive their capacity to resist lateral loads through the dead weight of the wall. The gravity retaining wall types include rigid gravity walls, mechanically stabilized earth (MSE) walls, and prefabricated modular gravity walls.

In the construction process of retaining walls, back fill is done after the construction. This is the traditional method we usually use. However, often construction sequence is not taken in to account in the design methodology of the retaining walls. In overall the stability design is believed to be reliable and accurate, because the safety factors have been allowed in design calculations. However, would the design calculations be adequate against the disturbances during the construction sequence? Would different construction sequences determine the stability of gravity retaining walls? With respect to construction sequence, which is the most suitable shape for gravity retaining wall? These are the main questions that would be addressed in this research.

Research on influence of compaction behind the retaining walls were carried out by Broms (1971), Transport and Road Laboratory-UK (1977, 1980, 1989), Ducan and See (1986), and Kulathilaka (1990). Ahmed (2012) explored the effect of construction sequences on the behaviour of a backfilled retaining wall. In his investigation, the influence of the construction sequences on the behaviour of an L shaped stiff retaining wall was investigated with a numerical model. He had

obtained the same observations and results by the experimental tests as well. These observations highlighted the fact that rotations and translations of the wall occur simultaneously during the staged backfilling process, which better simulate the real construction process.
However, the design methodology does not take into account the construction sequences that simulate the process by which the soil and the gravity retaining wall are brought together. There is little research which addresses the effect of construction sequences of gravity type retaining walls. Possible construction sequences are backfilling after wall construction and backfilling parallel to wall construction. This research will compare both construction sequences for different shapes of gravity retaining walls.

2. Objectives

The objectives of the study were, (i) to carry out a through literature survey on the area of investigation, (ii) to carry out numerical analysis on the effects of construction sequence on different shapes of gravity retaining walls, and (iii) to investigate the effects of construction sequences on bearing pressure distribution and failure wedge of gravity retaining walls.

3. Methodology

An extensive literature review was conducted to identify the research need and to gain necessary knowledge on the topic. By preliminary calculations different shapes and the dimensions of the retaining walls were determined. A finite element analysis using PLAXIS was conducted for the two construction sequences (backfilling after wall construction and backfilling parallel to wall construction). The results were illustrated using appropriate graphs and diagrams (for bearing pressure distribution, failure surface, wall deformation shape etc). By further analysis of the results the conclusions and suggestions were made.

4. Retaining Wall Design

In order to construct the finite element model for this study, retaining walls were designed based on BS 8002 design guide. Three different shapes with constant height and cross sectional area were selected and trial method was used to get proper stable retaining wall based on BS 8002.
In the design procedure, first force exerted on the retaining wall was estimated by considering the statical equilibrium on the soil wedge bounded by the wall, the failure surface and the surface profile. Calculations were based on Coulomb's method of analyse and wedge method.
The soil properties used in design are the dry density γ_{bulk}=18 kN/m^3, the angle of shearing resistance ϕ=32°, and the coefficient of cohesion C=0. The retaining wall was designed as mass concrete wall with concrete Grade 40 N/mm^2, young's modulus E=26MN/m^2, and density γ=24kN/m^3.
Optimal base sizes were calculated for three walls by considering overturning, sliding, and bearing capacity. Cross section area and height are maintained as constant. The dimensions were calculated considering the safety against self-weight failure.

5. Format of Reference Lists

Performance of an earth retaining system depends on many factors, in particular, successive stages of construction. The conventional design methods using design guidelines are not capable of evaluating the yield information on likely displacements in the system. The finite element analysis, which is widely used in design practices today, can be used to model complex soil-wall interaction problems.
Numerical analyse was carried out in plane strain and 15-nodes triangular elements. Movement of the wall is the major consideration in determining the wall deflection. Hence fine mesh was used in the model. Soil was modelled using Mohr-Coulomb model and concrete wall model as linear elastic model. The utilized soil modelling parameters and concrete retaining wall modelling parameters are presented in Table 1 and Table 2.

Table 1: Concrete properties

Parameters	Name	Concrete	Unit
Material model	model	Linear elastic	-
Type of material behaviour	type	Non-porous	-
concrete unit weight-Grade 40	γ_{bulk}	24	kN/m^3
Permeability in hori,vert.dirn	k_x, k_y	0	m/day
Young's modulus	E_{ref}	26,000,000	kN/m^2
Poisson's ratio	v	0.15	-
Strength reduction factor	R_{inter}	-	-

Table 2: Dense sand properties

Parameters	Name	Dense sand	Unit
Material model	model	M-C model	-
material behavior	type	drained	-
Soil unit weight	γ_{bulk}	18	kN/m^3
Permeability in hori.& vert.dirn	k_x, k_y	0.36	m/day
Young's modulus	E_{ref}	20,000	kN/m^2
Poisson's ratio	v	0.3	-
Cohesion	C_{ref}	0.1	kN/m^2
Friction angle	φ	32	°
Dilatancy angle		2	°
Strength reduction factor	R_{inter}	1	-

6. Construction Sequences

In order to investigate the effect of the construction sequences, the backfill soil was divided into 6 layers of 0.5m thick each that yield the total initial height of 3m. The general layouts of the geometry configuration of numerical model are as shown in figure 1, 2, and 3.

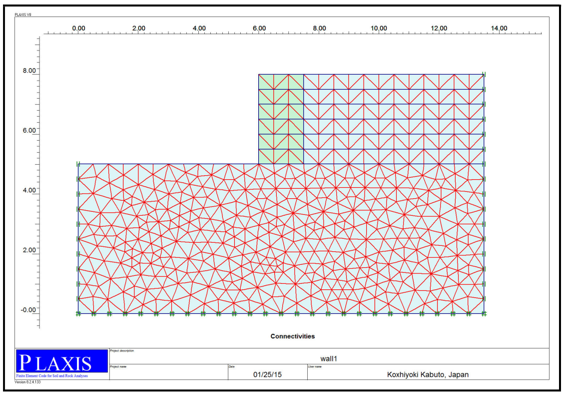

Figure 1: Finite element model-1

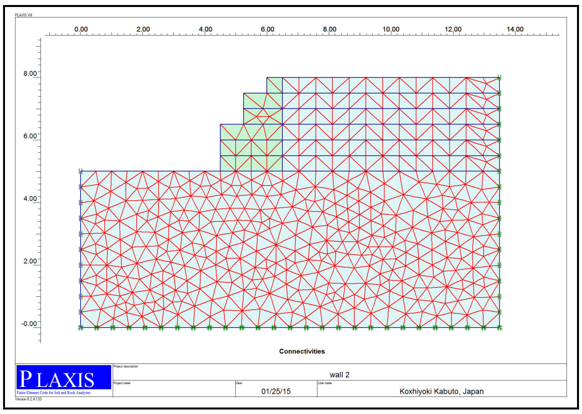

Figure 2: Finite element model-2

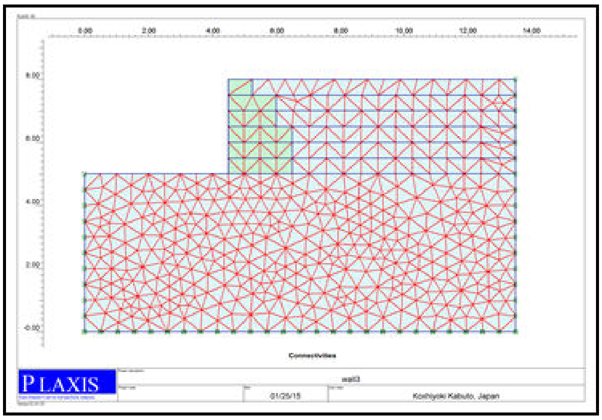

Figure 3: Finite element model-3

Suggested construction sequences are, (i) backfilling after wall construction (construction method 1) (ii) backfilling parallel to wall construction (construction method 2).

In backfilling after wall construction (construction method 1), calculations for the multi-phases numerical analysis were performed using the stage construction procedure. The calculations were executed in 8 phases including the wall construction and surcharge loading, starting from the initial state where the wall is constructed, each phase corresponding to a single loading of 0.5m of backfilling, yielding a total of 6 layers (phases), and ending with the state where all finite element model components, including surcharge loading, were activated. For each stage the calculation progress until the prescribed ultimate state is fully reached.

In backfilling parallel to wall construction (construction method 2), calculations for the multi-phases numerical analysis were performed using the stage construction procedure. The calculations were executed in 7 phases including the surcharge loading, starting from the initial state where the wall is constructed parallel to each phase corresponding to a single loading of 0.5m of backfilling, yielding a total of 6 layers (phases), and ending with the state where all finite element model components, including surcharge loading were activated. For each stage the calculation progress until the prescribed ultimate state is fully reached.

7. Fem Analysis and Results

7.1 Total displacement (movement) comparison

Model	Construction method	Construction stage's movement	
		Clock wise	Anti-clockwise
Model 1 (0, 3, 1, 2)	1	0-1-2-3	3-4-5-6-7-8
	2	0-1	1-2-3-4-5-6-7
Model 2	1	0-1-2-3-4-5	5-6-7-8
	2	0-1,3-4,6-7	1-2-3,4-5-6
Model 3	1	1-2-3-4-5	0-1,5-6-7-8
	2	0-1,3-4	1-2-3,5-6-7

7.2 Horizontal displacement plots

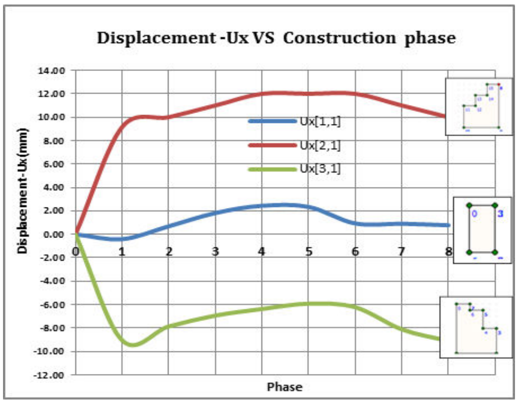

Figure 3: Construction method 1 - backfilling after wall construction (reference to top edge)

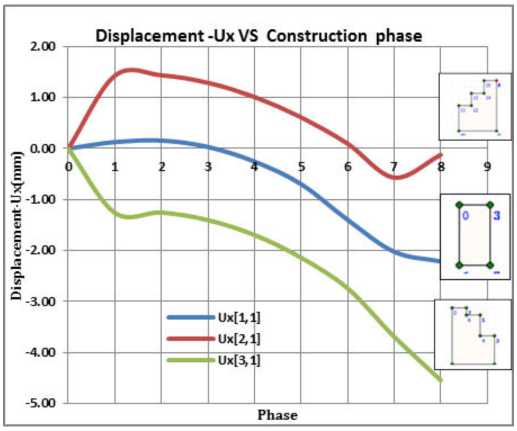

Figure 5. Construction method 1 - backfilling after wall construction (reference to bottom base)

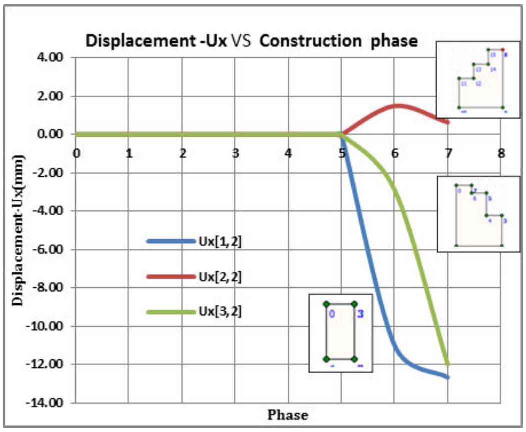

Figure 6: Construction method 2 - backfilling parallel to wall construction (reference to top edge)

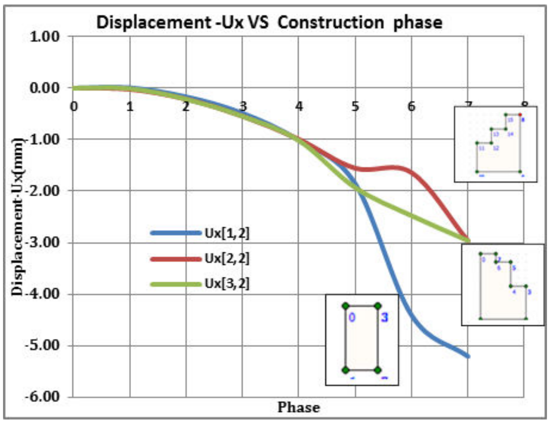

Figure 7: Construction method 2 - backfilling parallel to wall construction (reference to bottom base)

7.2.1 Final displacement analysis in a view

Model	Construction sequence	Horizontal Displacement diagram (backfilling right hand side)	Vertical displacement	Comments
Model 1	1	0.77mm; 2.21mm	14.8mm	Ux=+2.98mm
	2	12.67mm; 5.21mm	10.7mm	Ux= -7.46mm
Model 2	1	10mm; 0.12mm	15.2mm	Ux=+10.12mm
	2	0.64mm; 2.96mm	10.7mm	Ux=+3.6mm
Model 3	1	9.106mm; 4.544mm	15.2mm	Ux=-4.544mm
	2	12mm; 2.96mm	14.8mm	Ux=-9.04mm

7.3 Sliding and overturning analysis

Model	Construction sequences	Dominating factors		Overall dominating factor
		Overturning	Sliding	
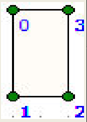	1	1-5	5-8	Overturning - toward backfilling side
	2	3-7	1-7	Overturning and sliding - outward the backfilling
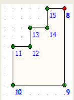	1	1-8	-	Overturning - toward the backfilling
	2	3-6	1-7	Sliding - out ward the backfilling
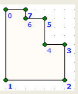	1	1-8 anti clockwise	1-8	Overturning - outward the backfilling
	2	4-7	1-7	Sliding - outward the back filling (high value)

7.4 Bearing pressure distribution

Model	Construction sequences	Maximum bearing pressure(kN/m^2)		Pressure distribution	Comments
		FEM	MANUAL		
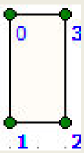	1	93.87	195.84	**Non uniform**	Safe against bearing
	2	103.32		**Non uniform**	Safe against bearing
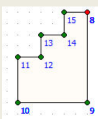	1	81.68	100.01	**Non uniform**	Safe against bearing
	2	81.76		**Non uniform**	Safe against bearing
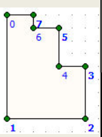	1	104.46	201.64	**Non uniform**	Safe against bearing
	2	123.3		**Non uniform**	Safe against bearing

7.4.1 Indication of Shadings

(red)	**Reject**
(yellow)	**Neutral limit**
(green)	**Acceptable limit**

7.5 Wedge failure angle

Model	Failure wedge angle-Theoretical	Wedge failure angle-FEM	Comments
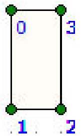	58.75°	55°-construction 1 52°-construction 2	**Approximately equal. safer construction**
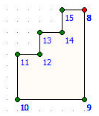	58.75°	68°-construction 1 65°-construction 2	**Both safer constructions**
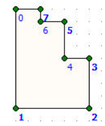	66°	38°-construction 1 45°- construction 2	**Both show critical conditions**

8. Discussion and Conclusion

Often the design methodology of retaining walls does not take into account the construction sequences, which simulate the process by which the soil and the retaining wall are brought together. In the present investigation, the influence of the construction sequences on the behaviour of mass concrete retaining wall is investigated with three different gravity retaining wall models using FEM. Two different construction sequences were used to evaluate the affect of the construction methods. Out of the three types of walls considered, the third type is found to have the lowest stability. It shows high bottom and top displacement outward the backfilling. Both sliding and overturning are in the same direction. Bearing pressure is 201.64kN/m^2 (BS 8002). When considering wedge failure, the wedge starts from under the base. The wall is likely to fail due to above critical reasons. In addition, the centre of gravity of the wall is toward the outward face of wall. This is the reason for high rotation in anticlockwise direction, which is negative in this instance. **For these reasons, wall type-3 is not preferable in stable construction of high walls.**

Other two gravity walls show stability against backfilling. When we consider the wall type-1, it shows unfavourable horizontal displacement in top and bottom of wall for construction method 1. Both sliding and overturning are outward the backfilling.

Construction method-1 shows smaller top and bottom displacement in opposite directions,

however in clockwise direction, which is positive in this instance. Bearing pressure is within the limit. Significant (2.21mm) sliding has increased the stability of the wall. **For these reasons, the construction sequence of method 1, i.e., backfilling after wall construction, is preferable for wall type 1.**
The wall type 2 appears to be the most preferable among all three types of walls. Both construction sequences are preferable for this wall type. In construction method 1, even though overturning is significantly high, it is toward the backfilling, which is a desirable direction. Centre of gravity of wall is toward the backfilling face, resulting in increased stability. Construction method 2 shows a small sliding and overturning tendency. However, its failure wedge angle is smaller than construction method 1. **Therefore, both construction sequences are preferable for wall type 2.**

Finally with this examination, we could conclude that the construction sequence is a critical factor to be considered in the design stage of gravity type walls as our observations clearly demonstrate that the construction sequences influence the stability of the wall both during and after wall construction.

Acknowledgement

Authors acknowledge the University of Moratuwa, Sri Lanka for the providing the foundation and technical support for the study.

References

[1]. Ahmed, R., “Effect of Construction Sequences on the Behaviour of a Backfilled Retaining Wall”. *IACSIT International Journal of Engineering and Technology*, 2012, 4(6), 844-846p

[2]. Kulathilaka, S. A. S., “Different forms of Earth retaining systems, their mechanisms, methods of Design and construction”, *Colombo, Sri Lankan Geotechnical Society*, 1998, 1-34 p.

[3]. Shamsabadi A., Shi-YuXu, Taciroglu E., “*Development of Improved Guidelines for Analysis and Design of Earth Retaining Structures*”, California: California Departmentof Transportation Caltrans, 2013.

[4]. Huggins, E. L., “*Numerical And Reliability Analysis Of Gravity Cantilever Retaining Walls Backfilled With Shredded Tires Subjected To Seismic Loads*”, Clemson: Clemson University, 2012.

[5]. Ramli, M., Karasu, T. J. R., Dawood, E.T., “The stability of gabion walls for earth retaining structures”, *Alexandria Engineering Journal*, 2013, Issue 52, 705-7010 p.

[6]. Chen, R. H., Chiu, Y. M., “Model test of geocell retaining structures”, *Geotextile and Geomembranes*, 2008, Volume 26, 56-70 p.

SECM/15/83

Deriving Damage Indices for Concrete Girder Bridges subjected to Flood Loading

F.Kalendher[1*], S.Setunge[1], H.Mohseni[1] and W.Lokuge[2]

[1] RMIT University, Australia
[2] University of South Queensland, Australia
*Email-farook.kalendher@rmit.edu.au

Abstract: It is noted that the intensity and frequency of disasters have increased over the past few decades and the damage to infrastructure after a natural hazard has consequently increased. The recent flood events in Queensland, Australia had an adverse effect on the country's social and economic growth. Due to climate change impacts, it is reported that the frequency and intensity of flood events have increased noticeably in recent years. Failure of transport infrastructure after a flood event significantly affects the community, road authorities and wider stakeholders. Bridge structures are often vulnerable to flood events due to their proximity to water ways and the resultant direct impact of flood on structures. In identifying strengthening needs for vulnerable bridge structures, damage, flood intensity relationship is required.

The paper has reviewed different bridge design codes used over several years in Australia for designing the bridges and the method of design for flood loading is identified. Various failure mechanisms of bridges due to flood events have been investigated through analysis of case studies and the most common failure mechanisms of the bridges in Queensland as the result of the 2011 and 2013 flood events have been identified. A case study bridge has been modelled using the general purpose finite element software, ANSYS. The damage to bridges due to impact of floating items under different flood scenarios has been investigated. Damage curves have been generated for the case study bridge under different flood intensities.

Key Words: Bridge, Flood, ANSYS, Damage Curves

1.0 Introduction

Natural disasters such as Flooding and Bush Fire have caused significant damage to road infrastructure in Australia. The recent 2010 and 2013 flood events in Queensland impacted the country socially and economically. Frequency of flood events in Queensland appears to have increased during past decades. IBISWORLD [1] reports that the flood in March 2009 inundated 62% of the state costing $234 million damage to infrastructure in Queensland. Theodore in Queensland was flooded three times within 12 months in 2010 and it was the first town, which had to be completely evacuated in Queensland. StateOfQueensland [2] reports that 9170 road network and 4748 rail network were damaged while 411 schools, 138 national parks and 89 bridges and culverts were destroyed during 2010-2011 floods in Queensland. Approximately 18000 residential and commercial properties were significantly affected in Brisbane and Ipswich IBISWORLD [1] during this time. The State government of Queensland and the Federal Government of Australia have incurred $6.8 billion to rebuilding Queensland. They have paid more than $12Million for individual, family and households while more than $121 Million in grants for small business, primary producers and non-profit organizations. They have also paid more than $12 Million as concessional loans to small businesses and primary produces (Rebuilding a stronger, more resilient Queensland 2012). Bridge infrastructure is vital in post disaster activities such as search and rescue operations because bridges help access to the disaster affected area Ellingwood [3]

2.0 Significance of the work

Bridge could damage in many ways when it is under an extreme flood event. Farook, Lokuge [4]. If the bridge is completely inundated during the flood, the damage to the bridge depends on the length of time it was submerged as well as the types of debris collected around or passing the bridge components. Extra care should be taken to inspect the supports of the bridges, even after the flood water recedes. Approaches of a bridge could be damaged due to debris impact, settlement or depressions. Debris against substructure and superstructure, bank erosion and damage to scour protection will damage the waterways. Bridge substructure could fail due to movement of abutments, wing walls, piers, rotation of piers and missing, damaged dislodged or poorly seating of the bearings while the superstructure could fail due to the debris on deck, rotation of deck, dipping of deck over piers or damage of girders. Pritchard [5] identified that urban debris such as cars; containers etc. and the insufficient bridge span to through that debris were the main cause for damaging bridges aftermath of 2011/2012 extreme flood events in Queensland. Figure 1 depicts some the damaged bridges from Lockyer Valley Region in Queensland.

Figure 1: Damaged Bridges in Lockyer Valley Region in Queensland

Analysis on the performance of bridges under 2011/2013 flood in Lockyer Valley Region, Queensland Farook, Lokuge [4] indicates that the bridge deck is the most commonly affected component followed by the bridge approach, pier/abutment scouring, cracks in the abutment wing walls and misalignment of abutment headstock connections to piles. Reinforced or prestressed concrete girder bridges are a common design configuration used in Australia. During the Lockyer Valley floods in 2013, vulnerability of girder bridges was observed by significant damage to these structures.

Bridge structures have a major impact on resilience of road infrastructure and the damage to bridges could increase the vulnerability of the community served by the road infrastructure significantly. A systematic method of quantifying vulnerability of bridge structures under varying flood loading is currently a significant gap in knowledge.

Using the concrete girder bridges as case studies, the methodology to derive structural vulnerability models for bridge structures and determine vulnerable structures in the road network have been proposed.

3.0 Review of design standards

The service level of a bridge depends mainly in its load carrying capacity that is controlled by the design standards used at the time when the bridge was designed. This has resulted in bridges on the same road having different design standards and hence having different load capacities. The design

standard used to build a bridge is a good indication of the age and strength of the bridge. The design standards used in Australia can be grouped into three categories. These design standards are denoted by the descriptions of the actual design loads that were used as standard design loads such as T44, MS18 (which is a metric equivalent of ASHTO HS20) and pre-MS18 where the design standards frequently changed depending on developments in other parts of the world. All three categories that have been described above are summarised in Table 1 Different bridges in Lockyer valley region are constructed at different times ranging from 1899 until 2010. Construction date and the possible Bridge design codes used are given in Table 2 for some of the bridges in the case study area.

Table 1: Bridge Design Standards used in (NSW) Australia. Muhunthan [6]

Design Standards - Pre-1948			
(i)	PWD	Pre-1927	Traction Engine Standard
(ii)	PWD	Pre-1927	Standard UDL
(iii)	DMR	1927	Standard UDL + Pt. Loads
(iv)	DMR	1938	Standard UDL + Pt. Loads
Design Standards - MS18			
(i)	DMR	1948	Standard Truck (MS18)
Design Standards - Post-1976			
(i)	NAASRA BDS	1976	Standard Truck
(ii)	NAASRA BDS	1976	Abnormal Vehicle Standard
(iii)	Ordinance 30C	1982	Articulated Vehicle
(iv)	AUSTROADS '92	1992	Standard T44 Truck & HLP
(v)	AUSTROADS '92	1992	HLP 320 & HLP 400 (abn.)
(vi)	AS 5100	2004	SM1600

Table 2: Bridge Design standards used for Bridges in Lockyer Valley Region. Farook, Lokuge [4]

Bridge Name	Construction Date	Codes Used
Evans Bridge	19540101	DMR'48
Weigels Crossing	19980101	NAASRA
Knopkes Crossing	19890101	NAASRA
Maincamp creek	20010101	92 AUSTROADS
Moon Bridge	19990101	92 AUSTROADS
Dodt Road Bridge	20040101	AS 5100
Main green swamp	19840101	NAASRA
Forestry Road Bridge	19660101	DMR'48
Kirsop Bridge	18991230	PWD-Pre-1927
Frankie Steinhardt's Bridge	20100701	AS 5100

3.1 AS 5100 Bridge Design Code

The AS 5100 Bridge Design Code requires that bridge over waterways be designed for flood loadings. Equations Kirkcaldie and Wood [7] are provided for determining the drag and lift forces on the superstructure for serviceability limit state and ultimate limit state. The serviceability design flood is to be associated with a 20 year return interval. The ultimate limit state design flood is to be associated with a 2000 year return interval.

The code recommends Equation (1) and Equation (2) for calculating the drag force on the superstructure for the serviceability state (F^*_{ds}) and the ultimate limit state (F^*_{du}).

$$(F^*_{ds}) = 0.5\, C_D {V_S}^2 A_S \qquad (1)$$

$$(F^*_{du}) = 0.5\, C_D {V_U}^2 A_S \qquad (2)$$

Where V_S is the mean velocity of water flow at superstructure level for serviceability limit state (m/s); V_U is the mean velocity of water flow at superstructure level for ultimate limit state (m/s); C_D is the drag coefficient; A_S is the projected area of the superstructure (including any rails or parapets) normal to flow (m^2); and F^*_{ds} and F^*_{du} have the units of kN.

In the absence of more exact analysis, the code recommends a drag coefficient of 2.2. This is based on the research undertaken up to the time of publication of the code. The previous code, the 1976 NAASRA Bridge Design Specification, recommended a C_D of 1.4.

The code suggests that lift force may act on the superstructure when the flood stage height is significantly higher than the superstructure and the deck is inclined by superelevation. Equation (3) and Equation (4) are recommended for calculating the serviceability design lift force (F^*_{LS}) and the ultimate design lift force (F^*_{LU}) on the superstructure respectively. The equations are adapted from the equations for lift on piers.

$$(F^*_{LS}) = 0.5\, C_L {V_S}^2 A_L \qquad (3)$$

$$(F^*_{LU}) = 0.5\, C_L {V_U}^2 A_L \qquad (4)$$

Where C_L is lift coefficient depending on the angle between flow direction and the plane containing the deck (values for varying angles are quoted in code); A_L is the plan deck area (m^2).

Forces due to debris shall be calculated using Equation (5) as follows:

$F_{deb}= \quad 0.5\ C_d\ V_u^2\ A_{deb}$ (5)

Where

A_{deb} = projected area of debris

Forces due to log impact shall be calculated as follows:

Where floating logs are possible, the ultimate and serviceability design drag forces exerted by such logs directly hitting piers or superstructure shall be calculated on the assumptions that a log with a minimum mass of 2t will be stopped in a distance of 300mm for timber piers, 150mm for hollow concrete piers, and 75mm for solid concrete piers.

Hence for the problem in question, F_{log} shall be given by the following equation (6)

F_{log} = $\text{m}V^2/2\text{d}$ where m= 2000kg, d= 0.075m and V= flood velocity (6)

4.0 Behaviour of Concrete Girder Bridges under flood loading – Numerical modelling

For the purpose of modelling the bridge, a bridge that carries a state route of Ipswich-Toowoomba road over Tenthill Creek in Gatton, Queensland, Australia has been selected. This is a simple span reinforced concrete, prestressed I-girder bridge built in 1970's. The bridge is 82.15m long and about 8.6m wide and is supported by a total of 12 pre-stressed 27.38m long beams over three spans of 27.38m. The beams are supported by two abutments and two headstocks.

General purpose finite element software, ANSYS has been used to model the bridge deck and to analyse the flood loading effect on to it. The middle span of bridge deck was analysed. All four girders were assumed simply supported and rest on the headstock of the piers. Self-weight of the bridge and the flood loads acting laterally to one of the end girder were considered in the analysis. The flood load was fed as a pressure on the face of the end girder. The bridge deck (I-girder) has been analysed using ANSYS. Figure 2 illustrates the Tenthill Creek bridge configuration. Section details of the bridge deck and the girder is given in Figure 3.

Figure 2: Tent hill Creek Bridge Configuration

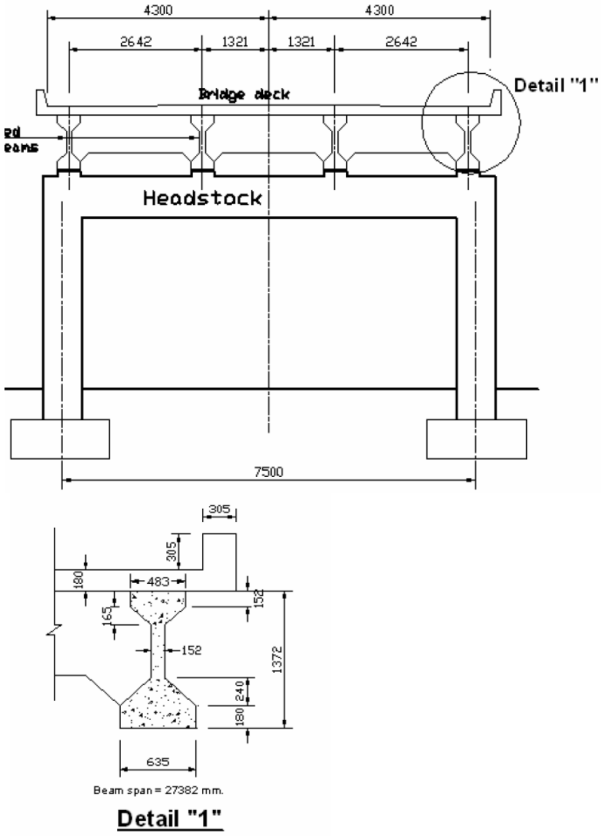

Figure 3: section details of a longitudinal prestressed I-girder beam. Nezamian and Setunge [8]

5.0 Deriving Damage Indices

Damage Indices can be derived using two methods. These indices are then used to derive damage curves for bridges under flood for various exposure conditions.

Method 1: Damage Index using structural capacity of the bridge/girder
In this method, the Damage Index (DI) is measured as the ratio between the moment capacity of the bridge girder (ϕMu) and the moment induced by flood loading on the bridge girder (M^*) .

$$\text{Damage Index (DI)} = (\phi Mu)/M^* \qquad (6)$$

This method requires analysis of bridge structure under the following different exposure conditions

- Bridge Elevation
- Flood Velocity
- Flood Water Level

Method 2: Damage Index using cost estimates of bridge under flood
In this method, Nishijima, Faber [9] define the Damage Index as the ratio between the repair cost and the replacement cost of the bridge under flood. Replacement cost is calculated based on the assumption that the bridge is completely damaged.

$$\text{Damage Index(DI)}= \frac{Repair\ Cost}{Replaceemnt\ Cost} \qquad (7)$$

Latter method has not been discussed in this paper.

5.1 Calculation of the existing capacity of the girder

In accordance with the Australian codes of practice for structural design, the capacity analysis methods contained in this section are based on ultimate limit-state philosophy. This ensures that a member will not become unfit for its intended use. The capacity analysis results would be compared with structural analysis results to identify the deficiencies. This approach sets acceptable levels of safety against the occurrence of all possible failure situations. The nominal strength of a member is assessed based on the possible failure modes and subsequent strains and stresses in each material.

A typical beam section of the headstock is shown in Figure 3. The positive and negative flexural and shear capacities of the section were calculated in accordance with Australian standards (AS3600, 1988). The nominal steel rebars areas; nominal steel yield strength of 400 MPa for longitudinal reinforcement and 240 MPa for shear reinforcement and nominal concrete compressive strength of 20 MPa were used in the section capacity analysis. The degradation due to corrosion of the steel and creep and shrinkage of the concrete were ignored. Using an excel sheet, the existing moment capacity of the concrete girder section was found to be 600kNm.

ANSYS model was run for different flood velocities ranging from 0.5m/s to 5.0m/s in steps of 0.50m/s increment. Figure 4 depicts the bridge deck model used in the analysis.

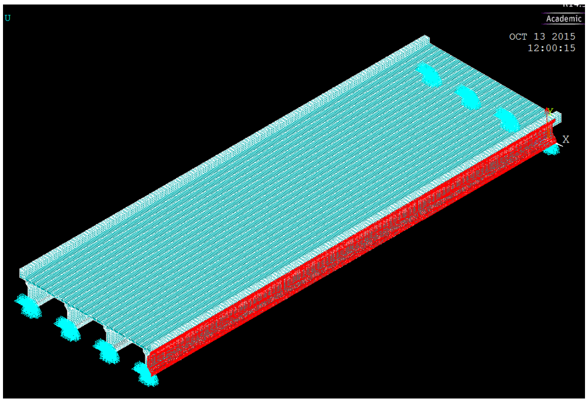

Figure 4: ANSYS bridge Deck Model

Horizontal support reaction of the end girder was obtained each time from the ANSYS Postprocessor. Using these reaction values flood induced bending moment of the end girder was calculated with the help of an excel sheet as shown in table 3

Table 3: Calculation of Flood induced bending moment (M^*)

Velocity (m/s)	Pressure (kNm^{-2})	Reaction (kN)	W(kN/m)	M*	ØMu/M*
0.50	0.275	1.276	0.0932	8.544	56.18
1.0	1.1	7.223	0.527	48.355	9.93
1.5	2.475	17.133	1.252	114.71	4.18
2.0	4.4	31.001	2.265	207.61	2.31
2.5	6.875	48.848	3.568	327.04	1.47
3.0	9.9	70.652	5.161	473.02	1.01
3.5	13.474	96.42	7.043	645.53	0.74
4.0	17.6	126.15	9.215	844.57	0.57
4.5	22.275	159.85	11.676	1070.2	0.45
5.0	27.5	197.8	14.448	1324.3	0.36

F_d= 0.5 $C_D {V_S}^2 A_S$ where F_d = kN, V_s= m, $A_s = m^2$

Flood Pressure = F/A=0.5$C_D {V_S}^2$ where C_D = 2.2

M_y^* (Maximum girder bending moment about minor axis) = R_{x1} - Wx^2/2

Where x1= distance between the resultant support reaction and the half span of the girder; x= the length of the girder (=27.38m in this case)

Mu = 600kNm (Existing capacity of the girder as calculated from the section analysis of the reinforced concrete girder)

Ø = 0.8 (Safety factor for the moment capacity as per AS 5100)

Structural Vulnerability curve for this girder bridge is drawn as shown in figure 5.

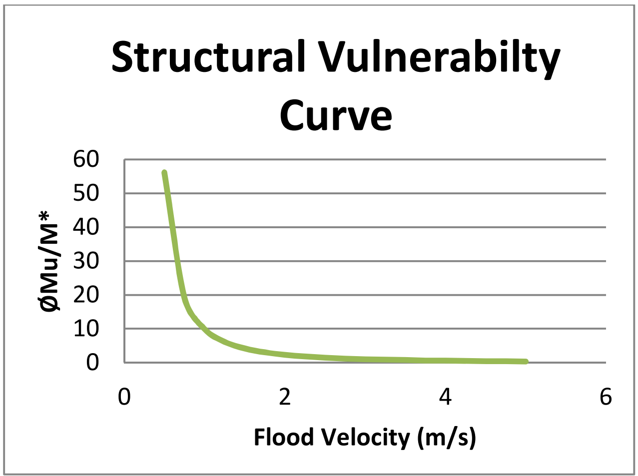

Figure 5: Structural vulnerability Curve for Tent hill Creek Concrete Girder Bridge

6.0 Conclusion

Reinforced or prestressed concrete girder bridges are a common design configuration used in Australia. During the Lockyer Valley floods in 2013, vulnerability of girder bridges was observed by significant damage to these structures. Structural performance of Tenthill Creek Concrete Girder Bridge has been studied in this paper. For the girder not to fail under flood loading, the existing moment capacity of the girder (ØMu) must be greater than the moment induced by the flood force (M*). In other words ØMu/M*>1. The critical flood velocity to satisfy this condition could be read from the above structural vulnerability curve. For the bridge considered in this case study, the critical flood velocity is read as 2.75 m/s. Outcomes will enable identification of the vulnerable girder bridges in the road networks and will assist road authorities to make optimised hardening decisions. On the other hand, emergency management services will be able to avoid vulnerable structures in determining evacuation routes.

Acknowledgement

The author wishes to tender his gratitude to Professor Sujeeva Setunge for providing guidance on his PhD research degree at RMIT University and organizing a full scholarship from RMIT University and a top up scholarship from Bushfire & Natural Hazards Cooperative Research Centre, Melbourne, Australia

References

[1]. IBISWORLD. *Queensland floods: The economic impact Special Report*. 2011 [cited 2015 10 April]; Available from: http://www.ibisworld.com.au/404.aspx?404;http://www.ibisworld.com.au:80/common/pdf/QLD%20floods%20special%20report.pdf.

[2]. StateOfQueensland. *Rebuilding a stronger, more resilient Queensland*. 2012 [cited 2014 10 December]; Available from: http://www.qldreconstruction.org.au/u/lib/cms2/rebuilding-resilient-qld-full.pdf.

[3]. Ellingwood, B.R., *Assessment and mitigation of risk from low-probability, high-consequence hazards.* Australian Journal of Structural Engineering, 2009. **9**(1): p. 1.

[4]. Farook, K., et al. *Failure mechanisms of bridge infrastructure in an extreme flood event*. in *Proceedings of the 1st International Conference on Infrastructure Failures and Consequences (ICFC 2014)*. 2014. RMIT Publishing.

[5]. Pritchard, R., *2011 to 2012 Queensland floods and cyclone events: Lessons learnt for bridge transport infrastructure.* Australian Journal of Structural Engineering, 2013. **14**(2): p. 167.

[6]. Muhunthan, B., *A PROPOSED STRATEGY FOR UPGRADING BRIDGE*

INFRASTRUCTURE NETWORK, 2008, GRIFFITH UNIVERSITY GOLD COAST.

[7]. Kirkcaldie, D.K. and J.H. Wood, *Review of Australian standard AS 5100 Bridge Design with a view to adoption: volume 1*. 2008.

[8]. Nezamian, A. and S. Setunge, *Case study of application of FRP composites in Strengthening the Reinforced Concrete Headstock of a Bridge Structure.* Journal of Composites for Construction, 2007. **11**(5): p. 531-544.

[9]. Nishijima, K., M.H. Faber, and M.A. Maes. *Probabilistic assessment of extreme events subject to epistemic uncertainties*. in *ASME 2008 27th International Conference on Offshore Mechanics and Arctic Engineering*. 2008. American Society of Mechanical Engineers.

SECM/15/116

Development of optimal bridge management system considering practical usefulness

K. Taniwaki [1*] and H. Oonishi [2]

[1] Professor, Department of Architecture and Environmental Eng., Fukui University of Technology, Gakuen 3-6-1,Fukui 910-8505, Japan
[2] Graduate student, Department of Social System Engineering, Civil Engineering Course Fukui University of Technology
*E-Mail: taniwaki@fukui-ut.ac.jp TP: +81776292701

Abstract: Several bridge management systems (BMS) have been developed to estimate the future expenditure for bridge management, but those have not been sufficiently applied to the practical bridge management for the reason of complex problem that the damaged bridge members should be repaired at one time as much as possible considering the whole bridge system. In this study, a useful BMS for practical bridge management is developed without special techniques. The deterioration transfer curves for slab, girder and abutment are introduced for three classifications of rapid deterioration, standard deterioration and no degradation members. The most economical repair plan is determined by comparing the life cycle costs for nine cases considering the annual budget limit. The effectiveness and practical usefulness of the system are illustrated by applying it to the bridge management of 1381 bridges in Fukui city, Japan.

Keywords: Bridge management system (BMS), deterioration transfer curve, optimum repair plan

1. Introduction

Each Japanese local government has developed the own bridge management system (BMS) for the bridge maintenance management according to the guideline established in the local government. It has been mainly used to estimate the future expenditure for bridge management, but it has not been sufficiently applied to the practical bridge management. On the other hand, the guideline for periodic bridge inspection was re-established for bridge maintenance management by the ministry of Land, Infrastructure, Transport and Tourism (MLIT) in Japan [1] in 2014. The local governments are requested to develop the BMS according the guideline established by the MLIT.

In the past researches, some papers proposed to use optimization techniques such as mathematical programming and GA for determination of optimum repair plan for each member element in the bridge. Kaito et al. [2] studied optimal maintenance strategies of bridge components based on an average cost minimizing principle presented by Haward [3]. One of author proposed to determine the optimum repair plan by using the mathematical programming and 2 stage optimization process [4,5]. Many contributions have been made to development of expert systems for bridge management by using the genetic algorithm [6-9].

However, those contributions have not been applied to the practical bridge maintenance for the reason that the system dealt with the management of a member element without considering the repair of whole bridge system. In the practical bridge repair, the damaged bridge members should be repaired at one time as much as possible for the reduction of cost for scaffolding and shortening period of closing traffic. Therefore, development of effective bridge management system according to the guideline by MLIT is awaited for the complex problem in the practical bridge management expectantly. In this study, a useful BMS for practical bridge management is developed without special techniques. The deterioration transfer curves for slab, girder and abutment are introduced for estimation of future deterioration. The distributions of condition ratings are characterized with three deterioration transfer curves for rapid deterioration, standard deterioration and no degradation members in this study. The most economical repair plan is determined by comparing the life cycle costs for nine cases considering the annual budget limit, in which the damage degree is introduced to determine the priority of repair. The effectiveness and practical usefulness of the system are illustrated by applying it to the bridge management of 1381 bridges in Fukui city, Japan.

2. Introduction of deterioration transfer curves

According to the Fukui prefectural policy the maintenances of special bridges such as truss, arch and cable-stayed bridges are managed in the post maintenance. The normal bridges such as slab, PC, RC and steel plate girder bridges are managed in the preventive maintenance. The defects in member elements of slab, girder and abutment influence the life span of a bridge, and the deterioration transfer curves of those member elements are introduced for estimation of future defects using the inspection data of 284 bridges(Lv.1 bridge and Lv.2 bridge) in Fukui city, Japan shown in table 1. The number of bridges that the ages are unknown(unknown bridge) is 1097 bridges in total 1381 bridges. The inspection was executed in the simplified manner established in Fukui prefecture. According to the guideline by Fukui Prefecture the result of inspection is classified into the three stages of no defects, minor defects and serious defects. Lv.1 bridges indicate that no defects were founds for main members and Lv.2 bridges indicate that minor or serious defects were found. On the other hand, the 4 stages of rating condition established by the MLIT in 2014 is shown in table 2. In this study the result in inspection, no defects, minor defects and serious defects, are assigned to the stages I (1.0), II (2.0) and III (3.0) respectively. The real number from 1.0 to 4.0 is used to express the transition of condition rating hereafter.

In this study, the cubic equation $y = at^3 + 1$ is applied to express the deterioration transfer curves for all member elements. The coefficient *a* is calculated by the equation (1) using the least squares method.

$$a = \frac{\sum_{i=1}^{n} \left(\bar{y}_i \cdot t_i^3 - t_i^3 \right)}{\sum_{i=1}^{n} t_i^6} \qquad (1)$$

where $\bar{y}_i$ is the condition rating of the member element in the *i*th bridge. *n* is the number of bridge. t_i is the age of the *i*th bridge at the time of the inspection.

Figure 1 shows the deterioration transfer curves for concrete slab. The standard equation indicates the deterioration transfer curve obtained by eq. (1) using the condition ratings for concrete slab in all bridges that their ages are known. The condition ratings are widely distributed, and it is not suitable to express the characteristics of deterioration with the standard equation only. Therefore, in this study the following border equations are introduced to determine the allowable range for the standard equation.

$$y^f(a) = \beta a t^3 + 1 \qquad (2)$$

$$y^S(a) = \frac{1}{\beta} a t^3 + 1 \qquad (3)$$

y^f, y^S are respectively the faster and slower deterioration limit equations in the allowable range. β is set at 1.8 in this study. The allowable range is drawn in a pattern of slanted lines in figure 1. The characteristics of rapid deterioration, which shows that the deterioration is faster than the deterioration limit y^f, are expressed with the rapid equation calculated by using the condition ratings for concrete slabs in the bridges out of the deterioration limit y^f. The rapid deterioration curve shows that the concrete slab will deteriorate up to the condition rating 4.0 in about 55 years. The characteristics of slow deterioration, which shows that the deterioration is slower than the deterioration limit y^S, indicate that the concrete slab will not deteriorate. In this study, the no degradation equation is applied to the concrete slabs which have not deteriorated for more than 30 years.

Figure 2 shows the deterioration transfer curve for steel floor slab. In this case, the number of steel floor plate girder bridge is not so many and the characteristics of deterioration are expressed with the standard deterioration curve only. This curve shows that the steel floor slab will deteriorate up to the condition rating 4.0 in about 40 years for the cause of corrosion.

The deterioration transfer curves for slabs, girders and abutments are summarized in table 3. The deterioration transfer curve for RC girder is also expressed with the standard equation only for the reason that the number of bridge with RC girder is not many. The deterioration transfer curves for PC girder, steel girder and abutment are characterized

Table 1 : Configuration of the bridges considered in this study

Bridge type	Lv.1 bridge	Lv.2 bridge	Bridge which the ages are unknown	Unknown bridge
RC slab bridge	9	23	964	996
RC girder bridge	0	3	46	49
PC bridge	55	128	58	241
Steel plate girder bridge	10	35	28	73
Steel floor plate girder bridge	0	21	1	22
Total	74	210	1097	1381

Table 2 : 4 stages in the condition rating

Condition rating		Maintenance immediacy of action
Ⅰ (1.0)	Good condition	No structural defects
Ⅱ (2.0)	Preventive maintenance	Minor structural defects without failure of function of structure, but special attention from viewpoint of preventive maintenance
Ⅲ(3.0)	Early repair	Structural defects with need of early repair in order to prevent failure of function of structure
Ⅳ(4.0)	Urgent repair	Serious structural damage with need of urgent repair in order to restore function of structure

Table 3 : Coefficient of deterioration transfer curves for member elements

Member element	Kind	Deterioration speed	Equation	Coefficient a
Slab	Concrete slab	Slow	$y = at^3+1$	0 (In the case that the condition rating has been 1.0 for more than 30 years)
		Standard	$y = at^3+1$	4.40521E-06
		Rapid	$y = at^3+1$	1.65922E-05
	Steel floor plate girder bridge	Standard	$y = at^3+1$	4.34201E-05
Girder	RC girder	Standard	$y = at^3+1$	2.87650E-06
	PC girder	Slow	$y = at^3+1$	0 (In the case that the condition rating has been 1.0 for more than 30 years)
		Standard	$y = at^3+1$	7.14042E-06
		Rapid	$y = at^3+1$	2.16099E-05
	Steel plate girder bridge	Slow	$y = at^3+1$	0 (In the case that the condition rating has been 1.0 for more than 30 years)
		Standard	$y = at^3+1$	1.53946E-05
		Rapid	$y = at^3+1$	4.49396E-05
Abutment	Concrete	Slow	$y = at^3+1$	0 (In the case that the condition rating has been 1.0 for more than 30 years)
		Standard	$y = at^3+1$	6.40834E-06
		Rapid	$y = at^3+1$	2.13383E-05

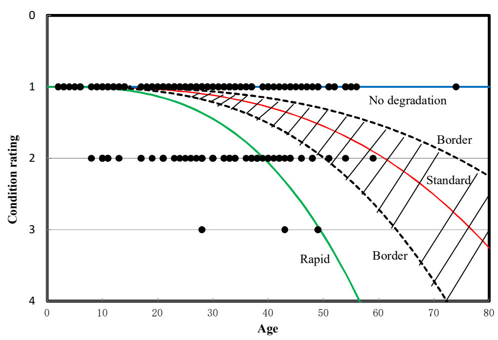

Figure 1: Deterioration transfer curves for concrete slab

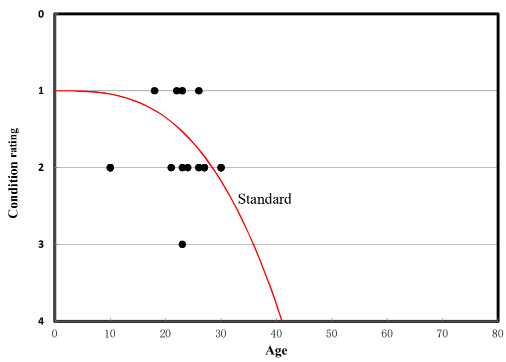

Figure 2: Deterioration transfer curve for steel floor slab

in three equations for no degradation, standard and rapid deteriorations.

In the inspection data the ages for 1097 bridges are unknown. In this study the ages of those bridges are estimated by investigating the age of each member element. The age for each member element is derived from the deterioration transfer curve for each member element. The bridge age is taken the youngest age among the ages for slab, girder and abutment considering the lower and upper limits of the ages

3. Assumptions for determination of optimum repair plan

For determination of optimum repair plan we assume the repair works and their unit prices, extension of bridge life span due to the preventive maintenance, and inspection, repair and rebuilding costs.

3.1 Repair method for slab

The repair methods, repair areas and unit prices for the condition rating 2.0 are shown in table 4. The crack injection method or section repair method is selected for the repair work of concrete slab. The area of repair is assumed at 25 % of area of concrete slab. The painting method is set for corrosion of steel floor slab and the area of repair is the whole area of steel floor slab. The efflorescence in filling concrete between PC girders is observed for the main defect of concrete slab in PC bridge. Therefore, the filling processing method is selected and the repair area is assumed at 50% of the length of filling concrete.

The repair methods, repair areas and unit prices for the condition rating 3.0 are shown in table 5. The crack injection method or section repair method is selected for the repair at 50% of area of concrete slab. The repair area of painting method for steel floor slab is the whole of steel floor slab. The area of filling processing method is set at the full length of filling concrete in PC bridge. The steel sheet adhesion method is also the alternative of repair methods for future progress of deterioration.

In case of the condition rating 4.0, the concrete slab needs reinforcement across the whole slab. The replacing method or steel sheet adhesion method is chosen as shown in table 6. The painting method is also applied to the repair of corroded steel floor. The filling processing method is also applied to the repair for whole of filling concrete in PC bridges.

3.2 Repair method for girder

It is clear from the inspection data that the cause of deteriorations for steel girders in steel plate girder bridges is corrosion. The painting method is chosen for repair of steel girders at the condition ratings 2.0, 3.0 and 4.0 as shown in tables 4-6. The average circumference length for painting in the steel girder is assumed at 2m. The crack injection method and section repair method are applied to the repair of girders in RC and PC bridges. The average circumference lengths in the cross sections of RC and PC bridges are assumed at 2m. The areas of repair are assumed at 25 % and 50% of girders in RC and PC bridges for the condition ratings 2.0 and 3.0 respectively. The section repair method is applied to the repair of whole girders at the condition rating 4.0.

3.3 Repair method for abutment

The crack injection method and section repair method are applied to the repair of abutments in all bridges at the condition ratings 2.0 and 3.0 as shown in tables 4 and 5. It is assumed that the height of repair area in the abutment is 2.0 m at the condition ratings 2.0 and 3.0. The wide of repair area is the half of the bridge wide at the condition rating 2.0 and the bridge wide at the condition rating 3.0 respectively. The section repair method is applied to the repair of abutment at the condition rating 4.0 and the repair area is the same as that at the condition rating 3.0.

3.4 Assumptions in the repair plan

Repair cost for the condition rating at the middle from 2.0 to 3.0 is calculated by the linear interpolation method using the repair costs for the condition ratings 2 and 3. The inspection cost is set at 50000 yen per bridge. Bridges are inspected once in 5 years. The bridges shall be inspected at the same time when the bridges are repaired. The rebuilding cost is the sum of new construction cost and removal cost, in which the new construction costs for superstructure, abutment and pier in each bridge type are assumed as shown in table 7. The removal cost is assumed at 40% of the new construction cost. The bridge life span shall be extended from 10 to 50 years for each bridge type considering the preventive maintenance as shown in table 8 following the policy of bridge management in Fukui prefecture, Japan. In the repair plan, the bridge shall be rebuilt when the bridge age reaches at the extended life span.

4. Determination of optimum repair plan

Table 4 : Repair works and unit prices in the condition rating Ⅱ(2.0)

Member element	Bridge type	Condition rating Ⅱ(2.0)		
		Repair method	Assumption of area of repair	Unitprice
Slab	Concrete slab	Crack injection method	25% of area of slab	1.7(10^4 yen/m²)
		Section repair method	25% of area of slab	5(10^4 yen/m²)
		Filling processing method	50% of {bridge length×(number of girder＋1)}	0.5(10^4 yen/m)
	Steel floor plate girder bridge	Painting method	Area of slab	0.3735(10^4 yen/m²)
Girder	RC girder	Crack injection method	25% of (2m×bridge length×number of girder)	1.7(10^4 yen/m²)
		Section repair method	25% of (2m×bridge length×number of girder)	5(10^4 yen/m²)
	PC girder	Crack injection method	25% of (2m×bridge length×number of girder)	1.7(10^4 yen/m²)
		Section repair method	25% of (2m×bridge length×number of girder)	5(10^4 yen/m²)
	Steel plate girder bridge	Painting method	2m×bridge length×number of girder	0.3735(10^4 yen/m²)
Abutment	All bridges	Crack injection method	50% of (2m×Width)	1.7(10^4 yen/m²)
		Section repair method	50% of (2m×Width)	5(10^4 yen/m²)

Table 5 : Repair works and unit prices in the condition rating Ⅲ(3.0)

Member element	Bridge type	Condition rating Ⅲ(3.0)		
		Repair method	Assumption of area of repair	Unitprice
Slab	Concrete slab	Crack injection method	50% of area of slab	1.7(10^4 yen/m²)
		Section repair method	50% of area of slab	5(10^4 yen/m²)
		Filling processing method	Bridge length×(number of girder＋1)	0.5(10^4 yen/m)
		Steel sheet adhesion method	Area of slab	8(10^4 yen/m²)
	Steel floor plate girder bridge	Painting method	Area of slab	0.3735(10^4 yen/m²)
Girder	RC girder	Crack injection method	50% of (2m×bridge length×number of girder)	1.7(10^4 yen/m²)
		Section repair method	50% of (2m×bridge length×number of girder)	5(10^4 yen/m²)
	PC girder	Crack injection method	50% of (2m×bridge length×number of girder)	1.7(10^4 yen/m²)
		Section repair method	50% of (2m×bridge length×number of girder)	5(10^4 yen/m²)
	Steel plate girder bridge	Painting method	2m×bridge length×number of girder	0.3735(10^4 yen/m²)
Abutment	All bridges	Crack injection method	2m×Width	1.7(10^4 yen/m²)
		Section repair method	2m×Width	5(10^4 yen/m²)

Table 6 : Repair works and unit prices in the condition rating Ⅳ(4.0)

Member element	Bridge type	Condition rating Ⅳ(4.0)		
		Repair method	Assumption of area of repair	Unitprice
Slab	Concrete slab	Replacing method	Area of slab	13.5(10^4 yen/m)
		Steel sheet adhesion method	Area of slab	8(10^4 yen/m²)
		Filling processing method	Bridge length×(number of girder＋1)	0.5(10^4 yen/m)
	Steel floor plate girder bridge	Painting method	Area of slab	0.3735(10^4 yen/m²)
Girder	RC girder	Section repair method	2m×bridge length×number of girder	5(10^4 yen/m²)
	PC girder	Section repair method	2m×bridge length×number of girder	5(10^4 yen/m²)
	Steel plate girder bridge	Painting method	2m×bridge length×number of girder	0.3735(10^4 yen/m²)
Abutment	All bridges	Section repair method	2m×Width	5(10^4 yen/m²)

Table 7 : Unit cost for rebuilding of bridge

Bridge type	Super structure(unit cost)	Abutment (unit cost)	Pier (unit cost)
RC slab bridge	8 (10^4 yen/m^2)	45 (10^4 yen/m)	0 (yen/m)
Steel plate girder bridge	15 (10^4 yen/m^2)	100 (10^4 yen/m)	100 (10^4 yen/m)
RC girder bridge	10 (10^4 yen/m^2)	60 (10^4 yen/m)	0 (yen/m)
PC girder bridge	13 (10^4 yen/m^2)	100 (10^4 yen/m)	100 (10^4 yen/m)

Table 8: Extension of bridge life span due to the preventive maintenance

Bridge type and conditions of construction site	Year of preventive repair after bridge construction	Period remained before rebuilding	Extension of bridge life span
Steel plate girder bridge	In case of no preventive repair	60 years	―
	In case of preventive repair in 41 to 59 years after bridge construction	70 years	+10 years
	In case of preventive repair within 40 years after bridge construction	100 years	+40 years
Concrete bridge locate in the salt damage region	In case of no preventive repair	50 years	―
	In case of preventive repair in 31 to 49 years after bridge construction	60 years	+10 years
	In case of preventive repair within 30 years after bridge construction	100 years	+50 years
Concrete bridge locate out of the salt damage region	In case of no preventive repair	75 years	―
	In case of preventive repair in 41 to 74 years after bridge construction	85 years	+10 years
	In case of preventive repair within 40 years after bridge construction	100 years	+25 years

The preventive repair is executed at the condition rating from 2.0 to 3.0. The repair at 3.0 is recognized as the post maintenance and the condition rating at more than 3.0 is not allowed. The optimum repair plan is the most economical case obtained by comparing the life cycle costs for the following nine cases.

① Repair is executed at the condition that the condition rating of slab is 2.0 or more, or one of other element is 3.0 or more.

② Repair is executed at the condition that the condition rating of girder is 2.0 or more, or one of other element is 3.0 or more.

③ Repair is executed at the condition that the condition rating of abutment A1 is 2.0 or more, or one of other element is 3.0 or more.

④ Repair is executed at the condition that the condition rating of abutment A2 is 2.0 or more, or one of other element is 3.0 or more.

⑤ Repair is executed at the condition that the condition rating of slab is 2.5 or more, or one of other element is 3.0 or more.

⑥ Repair is executed at the condition that the condition rating of girder is 2.5 or more, or one of other element is 3.0 or more.

⑦ Repair is executed at the condition that the condition rating of abutment A1 is 2.5 or more, or one of other element is 3.0 or more.

⑧ Repair is executed at the condition that the condition rating of abutment A2 is 2.5 or more, or one of other element is 3.0 or more.

⑨ Repair is executed at the condition that the condition rating of one of member element is 3.0 or more.

In the above nine cases all member elements that the condition rating is 2.0 or more shall be repaired at the same time considering the repair of whole bridge system. The condition rating for a member element in the multi-span bridge takes the maximum value among those for the element in each span. In the case that the bridge is rebuilt within 5 years later from the nearest repair time, the nearest repair shall be replaced by the rebuilding.

The annual budget limit must be taken into account for the determination of optimum repair plan. In this study, the flow chart shown in figure 3 is proposed for the determination of optimum repair plan considering the annual budget limit. At first the optimum repair cases in nine cases are determined for all bridges without considering the annual budget limit. After then, focusing on the youngest year where the annual budget limit is violated, the repairs in this year are postponed to the next year. To determine the turn of bridge that the repairs are postponed, the following defect degree, D_f, is calculated and the bridges are arranged in ascending order of D_f.

$$D_f = \sum_{i=1}^{n} \left\{ (D_G^i - 1.0) + (D_S^i - 1.0) + (D_{A1}^i - 1.0) + (D_{A2}^i - 1.0) \right\} + W \tag{4}$$

where $D_G^i, D_S^i, D_{A1}^i, D_{A2}^i$ are, respectively, the condition ratings of the girder, slab, abutments A1 and A2 in the ith span. W is the weight of the bridge and n is the number of span.

The smaller value of D_f indicates that the bridge has less defects, so that the repairs are postponed to the next year in turn in the ascending order of D_f until the annual budget limit is satisfied. In the case that the corresponding repair time t is the first time of repairs, the first repair time is fixed at t+1 years, and then, the following repair times are determined again while keeping the condition of the optimal case without considering the annual budget limit. In the case that the corresponding repair time t is after the first time, the corresponding repair time is fixed at t+1 years and the following repair times are also postponed to the next year. This process is repeated until the annual budget limit is satisfied during the management period

5. Numerical examples

The bridge inspections were executed in the years from 2004 to 2014 and the repair plan is implemented in 2015. The initial condition ratings are revised considering the progress of deterioration after the inspections. The maintenance management period is set at 75 years. The annual budget limit for maintenance and management of bridges is set at 1.3×10^8 yen.

Figure 4 shows the repair cost in each year during the management period (75 years). During the first 11 years the number of repair bridge is limited so as to satisfy the annual budget limit. After then, the repair cost required in a year is less than the half of annual budget limit.

Figure 5 shows the comparison of the cumulative repair costs for the optimum repair plan and the post maintenance plan (the repair case ⑨). The optimum repair plan requires the larger repair cost than that for the post maintenance plan during the first 11 years. Then, the repair cost for the optimum maintenance plan is smaller than that for the post maintenance plan from 12 to 39 years. In 40 years both the repair costs are almost the same for the reason that many bridges have to repair again for the optimum repair plan. In 75 years 7.6 % reduction can be observed in the cumulative repair cost for the optimum repair plan compared with that for the post maintenance plan.

The repair history of PC bridge (No.75) is shown in figure 6. The optimum repair case for PC bridge is the repair case ②. The initial bridge repair is postponed to 7 years later considering the repair priority, and both the girder and slab are repaired in the initial repair. The second repair of girder is executed in 43 years for the reason that its condition rating reaches at 2.0. The repairs in three members of slab, abutments A1 and A2 are executed for the third repair simultaneously in 56 years. The bridge is rebuilt in 71 years for the reason of the maximum life span of PC bridge (100 years old).

The repair history of steel floor plate girder bridge (No.171) is shown in figure 7. The optimum repair case is the repair case ③. The initial bridge repair is executed for the abutment A1 in 10 years. The second bridge repair is executed for the slab in 31 years. The third repair is executed for both the girder and abutment A2 in 40 years. The forth repair is executed for the abutment A1 in 45 years. The bridge is rebuilt in 66 years for the reason that the fifth repair is so close to the rebuilding within 5 years and the repair is replaced by the rebuilding.

6. Conclusions

In this paper, a useful BMS is developed for the practical bridge management. The BMS can determine the most economical repair plan considering the repair of whole bridge system. The proposed system can repair the members that the condition ratings are 2.0 or more simultaneously so as to satisfy the annual budget limit, in which the defect degree is introduced to determine the priority of repair. The cumulative repair cost for the optimum repair plan is reduced by 7.6 % of that in the post maintenance plan. The final optimal bridge repair plan can be determined by comparing the optimum repair plans for several annual budget limits and management periods.

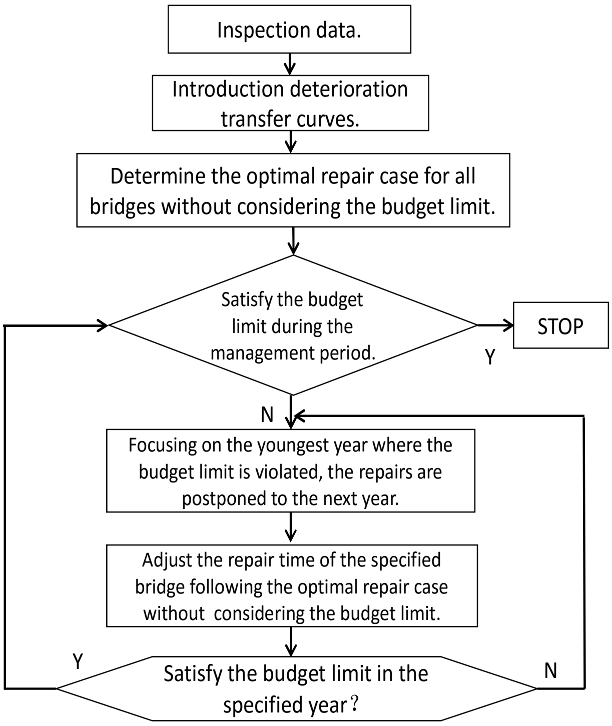

Figure 3: Decision process of the optimal repair time considering the annual budget limit

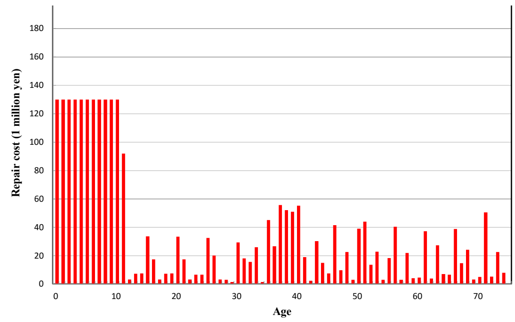

Figure 4: Repair cost in each year

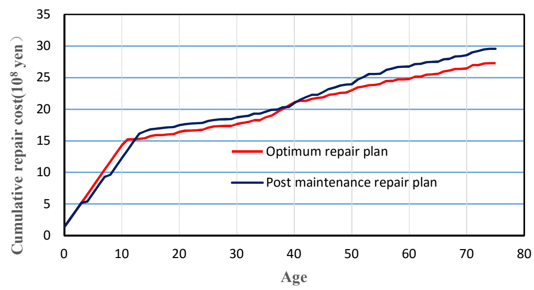

Figure 5: Comparison of cumulative repair costs for optimal repair plan and post maintenance repair plan

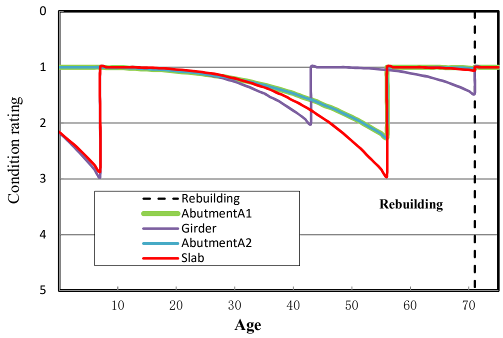

Figure 6: Repair history of pc bridge (no.75)

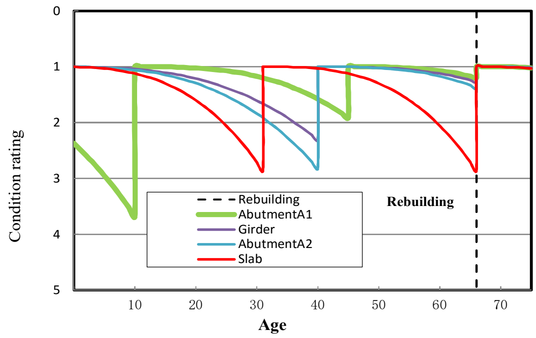

Figure 7: Repair history of steel floor plate girder (no.171)

References

[1]. The ministry of Land, Infrastructure, Transport and Tourism, guideline for periodic bridge inspection (in Japanease) , http: //www.mlit.go. Jp/ report/press/road01_hh_000429.html

[2]. Kaito,K., Yasuda,K., Kobayashi,K. and Owada,K., Optimal Maintenance Strategies of Bridge Components with an Average Cost Minimizing Principles", J. of Structural Mechanics and Earthquake Engineering, No.801/I-73, pp.83-96, 2005 (in Japanese).

[3]. Howard,R.A., Dynamic programming and Markov processes, M.I.T. Press, 1964.

[4]. Taniwaki,K and Ohga,M., An efficient optimal selection method for repairing components of damaged bridges using two stage branch-and bound method, Journal of applied mechanics, Vol.9, 2006, pp.239-250 (in Japanese).

[5]. Taniwaki,K., Ohga,M. and Karunananda,K., Optimal Bridge Maintenance Strategy determined by The Markov Process and Two Stage Optimization Technique, Internet J. of Social Management system (Qualified paper in SSMS2009), 2009, 10 pages.

[6]. Nakamura,H., Kawamura,K., Onimaru,H. and Miyamoto,A., Optimization of Bridge Maintenance Strategies by Using GA and IA Techniques, J. of Structural Engineering, Vol.47A, pp.201-210, 2001 (in Japanese).

[7]. Chikata,Y., Shimizu,H. and Hirose,A., A Study on GA Applied Bridge Repair Planning with the Virus Theory of Evolution, J. of Structural Engineering, Vol.47A, pp.211-219, 2001 (in Japanese).

[8]. Furuta,H., Yokota,T. and Dogaki,M., Application of Fuzzy Learning and Classifier to Bridge Maintenance Management System, J. of Structural Engineering, Vol.49A, pp.233-243, 2003 (in Japanese).

[9]. Jha,M.K. and Abdullah,J., A Markovian approach for optimizing highway life-cycle with genetic algorithms by considering maintenance of roadside appurtenances, J. of the Franklin Institute, Vol.343, pp.404-419, 2006.

SECM/15/130

RC Jacketing on RCC frame of Overhead water tank using results of Non Destructive Testing - A case study.

A. Mishra[1*], M. Singh[2*], A. Srivastava[3*]

[1] Post-Graduate Student, Department of Civil Engineering, BITS-PILANI, Pilani, India
[2] Research Scholar, Department of Civil Engineering, BITS-PILANI, Pilani, India
[3] Associate Professor, Department of Civil Engineering, BITS-PILANI, Pilani, India
*Email: manpreet_singh04@yahoo.com TP: +919780508420

Abstract – A three storey RCC frame of an old overhead water tank in BITS Pilani campus had developed wide visible cracks, rusting of steel reinforcement and concrete spalling conditions at many locations. The condition of these structures was assessed by visual inspection, non-destructive testing (NDT) like rebound hammer, ultrasonic pulse velocities, rebar locator etc. and laboratory tests, to ascertain their suitability for further use. Based on the results of the tests conducted RC jacketing technique using anti corrosive agent, micro concrete and polymer modified mortar for retrofitting was suggested and implemented. The NDT was conducted again after the completion of retrofitting of the structure. This case study presents the use of standard and innovative repair materials, appropriate technology, workmanship, and quality control for successful repair, strengthening and restoration of damaged structures.

Key words – Retrofitting, Non-destructive testing, Rebound Hammer, UPV, rebar locator, micro-concrete, RC Jacketing

1. Introduction

Structures have a variety of performance requirements. Retrofitting of structures is done to improve these requirements like safety, serviceability and restorability. In retrofitting, the structure must be designed so that it serves its purpose of use and is both safe and durable. Consideration is given to the ease of retrofitting and post-retrofitting maintenance, as well as overall economy and environment-friendliness.

Of all the retrofitting processes, RC jacketing provides a better solution to avoid buckling problems. Retrofitting is a technical addition to the system of the building, which improves the load carrying capacity and the strength. It also increases the structural life span, with high serviceability.

To evaluate the performance of a structure and verify that it fulfills its performance requirements, it is necessary to express it in terms of quantifiable physical quantities that represent performance. This can be done using various tests. Ideally such tests should be done without damaging the concrete. The tests available for testing concrete range from completely non-destructive, where there is no damage to the concrete, to those where the concrete surface is slightly damaged i.e. partially destructive tests, such as core tests and pull out and pull off tests, where the surface has to be repaired after the test.

The condition can be assessed by various Non Destructive Tests (NDT) like rebound hammer test, Ultrasonic pulse velocity (UPV) test, rebar locator test, half-cell potential test, carbonation test and lab tests. The Rebound hammer test is used to access concrete compressive strength at several locations. When testing, “Rebound Number” is measured which depends upon the strength of concrete/mortar close to the surface and a site specific correlation is been developed to correlate compressive strength with likely compressive strength. To obtain information about Concrete quality i.e. voids, flows, cracks etc. the Ultrasonic Pulse Velocity test is done. The results help in identifying the areas required to be strengthened or retrofitted. The interpretation is done using the IS: 13311-Part 1, which characterizes the quality of concrete in terms of the ultrasonic velocity.

At the site for the determination of cover, for locating reinforcement bars and for finding the probable reinforcement bar diameter, Rebar Locator is used. For assessing the percentage risk of corrosion of reinforcement bars, Half-cell potential test is done. The interpretation is done using the ASTM Standard No. ASTM C 876:1991 (Re-approved 1999).

For repairing of the concrete structures, micro concrete which is a dry ready mix cementetious based composition formulated for use in repairs of areas where the concrete is damaged & the area is restricted in movement making the placement of conventional concrete difficult can be used.

2. Case Study

The Birla Institute of Technology & Science (BITS), Pilani is an all-India Institute for higher education. BITS is located in the Vidya Vihar campus adjacent to the town of Pilani in Rajasthan (India).

BITS has a vast campus and there are numerous structures which have been standing for the past many years. Over the years, due to ageing effect or other causes some signs of distress have appeared on these structures which need to be addressed.

A three storey RCC frame of an old overhead water tank in BITS Pilani campus, whose age would be around 40 years had developed wide visible cracks, rusting of steel reinforcement and concrete spalling conditions. The condition of some elements of RCC frames/stages carrying the water tank was critical including the bottom of tank. No Design Details and Architectural drawings were available.

The condition was assessed by various NDT test like Visual inspection, Rebound hammer test, Ultrasonic pulse velocity test, Rebar locator test, Half-cell potential test, Carbonation test and Lab test. And on the basis of results, design & recommendations for the retrofitting were determined.

3. Scope of Work

The scope of work includes following:
a) Visual inspection with photographs to assess physical condition of structural elements.
b) Carrying out various types of Non-destructive tests on structural elements.

The proposed non-destructive tests for RCC are broadly classified as:

• **Tests for strength and quality of concrete**
Schmidt's Rebound Hammer test, Core Sample testing and Ultrasonic Pulse Velocity testing on representative elements/samples. Determination of cement content in the laboratory.

• **Tests for assessing the risk of corrosion**
Determination of depth of concrete cover, depth Carbonation, half-cell Potential meter tests.

Below mentioned scope of work includes conducting various tests as suggested:

Table 1: Test and Instruments used

Sr. No.	Description of tests	Equipment used
A	Visual Inspection	
B	NDT of RCC Elements	
1	Schmidt's rebound hammer test	Concrete test hammer type N manufactured and supplied by PROCEQ SA ZURICH
2	Ultrasound Pulse velocity test	Ultrasonic Instrument TICO manufactured and supplied by PROCEQ SA ZURICH

3	Cover meter tests	Instrument PROFOSCOPE by PROCECQ
4	Carbonation test	PHENOLPHTHALEIN
5	Half-cell potential test	Instrument Contained copper sulphate electrode, sponger for electrode, case for connecting reinforcement with crocodile carrying case.
6	Taking out concrete cores (70mm/50mm dia.)	Core Drilling machine of make TYROLIT
C	Laboratory test	Compressive strength and density tests.

4. Test and Observations

4.1 Visual Inspection details:

Table 2: Details of Visual Inspection: Water tank

Sr. No	Location	Name of Distress	Photos
01	Outer wall of water tank C-3 & C-4, Outer wall of water tank C-5 & C-6, Outer Slab near C-1,C-2,C-3,C-4,C-5	Patch of dampness	 Figure 1
02	Outer wall of water tank above C-1, C-2	Water Seepage	 Figure 2

03	Vertical Cracks in bottom and middle parts of Column No. C-1. Horizontal cracks from bottom to top in Column No. C-2, C-3, C-4, C-5, C-6. Vertical cracks in bottom and middle parts of Column No. C-3, Beam No. B-2, B-4, B-5, B-6, B-7, B-8, B-9, B-10, B-11	Moderate Cracks (5mm to 10mm)	 Figure 3
04	Bottom Part of Column C-1, Middle part of Column C-1, Bottom Part of Column C-2, Inner side of Beam B-2, Soffit of Beam B-8, B-3, B-1, Patches in outer slab	Corroded Reinforcement	 Figure 4

4.2 Rebound Hammer Test Results

Table 3: Details of Rebound Hammer Test Results: Water tank

Interpretation: As Per IS:13311-Part II

→ *Denotes Rebound hammer Test Conducted in Horizontal Direction*
↓ *Denotes Rebound hammer Test Conducted in Vertically Downward Direction*
↑ *Denotes Rebound hammer Test Conducted in Vertically Upward Direction*

S.No.	**Test Locations**	***Impact Direction**	**Rebound No.**						**Average Rebound No.**	**Corrected Rebound No.**	**Observed Compressive Strength**
			1	**2**	**3**	**4**	**5**	**6**			
	Ground										
	Columns										
1	C	→	22	24	21	20	18	20	21	21	7
2	C	→	38	40	38	42	42	38	40	40	17
3	C-3 (Core	→	36	40	35	38	39	37	38	38	16
5	B	→	28	24	26	28	24	28	26	26	10
6	B	→	22	20	18	20	18	20	20	20	6

7	B-4 (Core	→	43	44	39	43	40	41	42	42	18
8	B-5 (Core	→	30	32	33	29	32	31	31	31	13

Laboratory Test Results For Compressive Strength

Table 4: Details of Laboratory Test Results: Water tank

S. No.	**Sample ID**	**Diameter**	**Length (mm**	**L/D**	**Correction**	**Max. Load**	**Cylindrical Compressi**	**Corrected Cylindrical**	**Equivalent**	**Natural**	**Saturated**
	Ground										
	Columns										
1	C-3 (Core	67.47	134.3	1.991	0.999	39.18	11.0	10.9	**13.7**	2257	2311
2	C-4 (Core	67.56	119.1	1.763	0.974	39.20	10.9	10.6	**13.3**	2228	2292
	Be										
3	B-4 (Core	67.62	118.2	1.749	0.972	42.82	11.9	11.5	**14.5**	2187	2274
4	B-5 (Core	67.51	124.4	1.902	0.989	38.52	10.8	10.6	**13.3**	2231	2316

Density

4.4 Test Results of Ultrasonic Velocity Tests

Table 5: Details of Ultrasonic Velocity Tests: Water tank

Interpretation: As Per IS:13311-Part I

** 'Direct': Probes Kept on Opposite Faces*
** 'Semi-direct': Probes Kept on Perpendicular Faces*
** Indirect': Probes Kept on Same Face*

S.No	**Test Location**	*** Method of Probing**	**Observed UPV**	**Corrected UPV (m/sec)**	**Inference** (IS : 13311-I)
	Ground Level				
	Colum				
1	C-	Dire	46	46	Doubtful
2	C-	Dire	37	39	Doubtful
5	C-3 (Core WT-1)	Dire	347	347	Medium
7	C-4 (Core WT-2)	Dire	356	356	Good
	Beam				
13	B-	Dire	45	65	Doubtful
14	B-	Dire	22	22	Doubtful
19	B-4 (Core WT-5)	Dire	344	344	Medium
20	B-5 (Core WT-6)	Dire	346	346	Medium

4.5 Rebar locator Test Results

Table 6: Details of Rebar locator Test Results: Water tank

Interpretation : As Per IS:456 – 2000						
Note: Only 'Clear' Concrete Cover is Measured. Approximate dia. will be calculated. *Accuracy of results depends on Depth, Diameter, Spacing & Positioning of Reinforcement Bars.*						
S.No.	**Test Location**	**Face**	**Size**	**Reinforcement**		
				Main	**Stirrups (mm)**	**Cover (mm)**
	Ground					
	Columns		**(Diameter)**			
1	C-		53	8X18 mmø	6 mm ø @ 220	35-
2	C-		53	8 X 20 mm ø	6 mm ø @ 225	55-
3	C-		53	8 X 20 mm ø	6 mm ø @ 220	28-
	Beam					
4	B-1(MID.)	I.Side(5	550X250	3 X 25 mm ø	10mm ø @ 325	30-
5	B-1(MID.)	Soffit(2	550X250	2 X 25 mm ø	10mm ø @ 325	20-
6	B-2(SUPP.)	OSide(5	550X250	4 X 25 mm ø	10mm ø @ 235	38-

4.6 Test Results of Carbonation Tests

Table 7: Details of Carbonation Test Results: Water tank

Interpretation:				
Indicator Color: Deep Purple				
Sl. N	**Test Location**	**Depth of Carbonation**	**Minimum Concrete Cover Measured**	**Minimum Concrete Cover IS -456**
	Ground Level			
	Columns			
1	C-	49	35	40
2	C-	56	55	40
3	C-3 (Core WT-1)	37	28	40
4	C-4 (Core WT-2)	51	62	40
	Beam			
5	B-	41	30	20
6	B-	49	30	20
7	B-4 (Core WT-5)	42	26	20
8	B-5 (Core WT-6)	36	28	20

4.7 Test Results of Half-Cell Potential Tests

Table 8: Details of Half-Cell Potential Tests Results: Water tank

Interpretation: As Per ASTM:C876-1991			
By convention, potentials are considered negative when measuring the steel with respect to the electrode. The interpretation of measurements is in terms of the likelihood of corrosion.			
Sl. N	**Test Location**	**Half-cell Reading**	**Risk of corrosion**
	Ground		
	Columns		
1	C-	0.46	90
2	C-	0.42	90
3	C-	0.38	90
	Beam		
4	B-	0.32	90
5	B-	0.40	90
6	B-	0.46	90

4.8 Conclusions from the results

To assess the damages, Visit was made. Following points noted:

a. There are visible signs of rusting of steel reinforcement in columns, beams & roof slabs. This has caused the Spalling/ deterioration of concrete.

b. There are serious cracks and damages in the columns, beams and slabs.

c. As per NDT test report, the concrete has deteriorated at many places.

d. During the visit, many places were found to have severe structural cracks, corrosion of reinforcement. Proper rehabilitation measures need to be taken to rectify the damages.

5. Methodology

5.1 Repair Scheme for Column

The following repairs scheme is adopted for the correction of column:

1. Propping the beams on all the sides of the columns for full vertical height. The props shall be able to take the total load coming on to the column.
2. Chipping open the cover concrete until all the corroded steel rods are and cleaning of rods with brush
3. Chipping the spelled surface of concrete to remove all loose materials. Then brushing it with steel wire brush to remove all loose particles.Washing the surface with potable water.
4. Applying a coat of anticorrosive coating like NITO-ZINCPRIMER manufactured by M/s FOSROC or approved equivalent to all the existing reinforcement.
5. Anchoring new bars by drilling holes in the tie beams for a length of 10 times the diameter of bar.(10XDia of bar)or into the pedestal. Additional bars thus introduced are bonded with the concrete using Hilti chemicals for re-barring. Tie new longitudinal bars using new column ties. The ties have to be anchored into the concrete by drilling holes in the concrete and inserting the ends of the ties into the holes. The depth of drilling shall be such that length of the ties from the center of

new longitudinal bar is 8 times the diameter of tie.

6. Leak proof formwork which should not deform or leak due to pressure of concrete shall be fabricated and erected in position. The formwork should be coated with mould release agent prior to the final fixing in position. Making proper supporting arrangements for keeping the shutter in correct line and length.
7. Encasement using high slump concrete of grade M25 (minimum).It shall be ensured that clear cover to the new steel is 50mm. Curing compound is to used for curing purposes.

5.2 Repair Scheme for Beams

Basic steps involved in the repair of beams are same as that for columns except for the following point.

1. Encasement is done using micro concrete of SIKA/ FOSROC or equivalent approved material with 25% aggregate (washed/cleaned) by weight of size 6.4 mm and down size. The curing has to be done immediately after stripping the formwork.

5.3 Repair Scheme for Slabs

The repair of slabs is also almost the same as that of columns and beams except for the following points:

1. Propping the slab at intervals of say about 1.5 m.
2. Additional bars introduced are anchored to the beam. Additional steel shall be tied to the existing steel or anchored using anchors drilled into the slab.
3. The micro concrete, with 25% aggregate of size 6.4 mm and down is poured by funnels by drilling holes of about 50 mm dia. at 2 m intervals in both directions. The curing has to be done immediately after stripping the formwork. It shall been ensured that clear cover to the new steel is 25 mm.

5.4 Repair Scheme for Tank Dome

1. Cracked or any surface of concrete which is prone to cracks are repaired with polymer modified mortar.

5.5 After the completion of the project the NDT tests will be conducted again to ascertain the quality and strength of aspects improved in the structure.

6 Conclusions

This paper deals with strengthening and enhancement of performance of existing structure. The use of NDT for functional and structural evaluation of a structure is shown. The study of design method of reinforced concrete jacketing for strengthening of structure including design of beams and columns and use of innovative construction materials i.e micro concrete, epoxy grouting and polymer modified mortar is done.

Further scope of work –

1. Detailed economic analysis of the work.
2. Cost- benefit study for the selection of RC jacketing over demolishing and reconstructing a new structure.
3. Studying performance of structure after retrofitting.

7 References

1. Bhavar Dadasaheb O, Dhake Pravinchandra D, Ogale ramesh A,“ Retrofitting of existing R.C.C building by method of jacketing”, International journal of research in modern engineering and emerging technology Vol 1, Issue:5-2013

2. Dr. Gopal L. Rai, “Different strenghtening techniques for R.C columns”, R and M international Pvt. Ltd.

3. Mahdi shariati, Nor Hafizah ramli-sulong, Mohammad Mehdi Arabnejad k.h, Payam shafigh and Hamid Sinaei, “Assessing the strength of reinforced concrete structures through ultrasonic pulse velocity and Schmidt rebound hammer tests”, Scientific research and essays Vol 1, Issue:1-2011.

4. IS 13311(1992), “Code of practice for Non Destructive Testing of concrete – methods of test part: 1 Ultrasonic pulse test”, Bureau of Indian standards (BIS), New Delhi.

5. 13311(1992), “Code of practice for Non Destructive Testing of concrete – methods of test part: 2 Rebound Hammer test”, Bureau of Indian standards (BIS), New Delhi.

6. IS 1893 (2002). “Indian Standard criteria for Earthquake Resistant Design of structures part 1: General Provisions and Buildings”, Bureau of Indian standards (BIS), New Delhi.

SECM/15/154

Development of an integrated software tool for whole of life management of concrete storm water pipe assets.

S.Setunge[1*] and H. Tran[1]

[1]RMIT University, Australia
*E-Mail: sujeeva.setunge@rmit.edu.au

Abstract: In Australia, there are 500 local councils, each managing 300-1000 km of storm water drainage systems. Majority of the storm water pipes are concrete and are built in 1960's. Currently the councils use CCTV inspections to assess around 10% of the network and make maintenance decisions for the whole asset stock. This creates a major challenge for asset managers since the decisions are made based on assumed levels of deterioration. Catastrophic failure of pipes due to inefficient management will lead to flooding, which can be a major hazard to the community and infrastructure. The paper presents the outcomes of a study conducted to assess the whole of life performance of concrete storm water pipes. Data from CCTV inspections are converted to a discrete rating and are used to derive Markov chain based deterioration models for the network. Based on these, optimized inspection strategy is developed for the pipe assets combined with a life cycle costing module, tree root invasion model and hydraulic and structural failure modules. The proposed integrated management model is suitable for capturing the whole of life performance of any infrastructure asset.

1. Introduction

Storm water pipelines are essential infrastructure that plays a pivotal role in Australia's economy, prosperity, social well-being, quality of life and the health of its population. If the catastrophic failures of these pipes can be prevented, the economic, environmental and social significance of this prevention is far-reaching and cannot be assessed by a single measure. In Australia, there is approximately 300,000 km of concrete pipes with an estimated total asset value of $45 billion (Concrete Pipe Association of Australasia). Most stakeholders of pipe infrastructure have recognized the severe consequences of pipe failures. As such there is on-going research funded by industry, e.g., the Water Service Association of Australia and the Water Research Foundation (US).

The life expectancy of buried concrete storm water pipes can exceed 100 years, but the age of failed pipes, e.g., cracked or collapsed, is much shorter. In Australia, the 2010 infrastructure report card for Victoria (Engineer Australia, 2010) rated storm water pipes at C-, meaning that major changes are required to be fit for the current and future purposes. Most recent collapses of concrete pipes that can be classified as catastrophic to the public are related to pipe deterioration: (i) the collapse of the Cunningham Pier main drain in Geelong in 2014 resulting in discomfort of road users; (ii) the collapse of a trunk drain in Southern England causing disruption and diversions near the railway station in 2010; and (iii) the collapse of storm drain in South Carolina in 2014 causing a day-long road closure.

Various attempts have been made to develop a practically useable technique for failure prediction of buried pipes. Moore et al.(2004) investigated the soil–pipe interaction of buried concrete pipes. Busba and Sagues (2013) conducted experiments to study the effect of cracked surfaces on the corrosion behaviour of reinforcing steel in concrete pipes. Mahmoodian and Alani (2013) studied the reliability of concrete pipes subjected to thickness reduction due to sulphide attack. In Australia, limited research into buried concrete pipes has been carried out. Sharma et al (Sharma et al., 2008) developed a dynamic model to predict sulphide production in a concrete storm water system. Tran et al (2010) applied Markov theory to model the deterioration of storm water pipes by using CCTV data.

The reoccurrence of unexpected pipe failures has demanded a better and implementable asset management framework for buried drainage pipes. This study proposes an effective asset management framework (AMF) and describes a software tool developed to implement the AMF for storm water pipes.

2. Asset management framework

The asset management framework (AMF) of drainage pipe assets is developed in this study based on:

- The general view of asset management policy set out by asset owners and operators (i.e. Local Councils)
- The requirement of Australian Accounting Standard (ASSB 116), which states that the useful life of asset be reviewed at least at the end of each annual reporting period so that adequate depreciation is applied.
- The suggested management method described in the Practice Note 5 issued by Institute of Public Works Engineering Australasia (IPWEA) for storm water drainage pipes (IPWEA, 2015).

The AMF consists of 6-step as described in the following:

1. Assign criticality rating (or failure consequence) to each drainage pipe asset
2. Collect condition data of pipe asset
3. Estimate time-based failure probability
4. Conduct risk analysis
5. Monitor and control risk
6. Conduct annual review

Assigning criticality rating

With a large network of buried drainage pipes, it is not affordable to inspect and perform repair on all pipe assets at the same time. Therefore, it is recommended that the criticality rating is assigned to each pipe asset based on some criteria such as social-economic consequences (if the asset fails unexpectedly) for prioritized maintenance program. The social consequence is discomfort of community, traffic disruption and bad reputation and so on, which can be quantified by some penalty value. The economic consequence is the business loss, accident compensation and litigation cost.

Collecting condition data

The CCTV inspection method can be used to collect condition data in terms of structural condition (e.g. 1-5 condition grading) and structural defects (e.g. cracks and corrosion of reinforcing steel), which focuses on structural failure or pipe collapse. On the other hand, hydraulic (or serviceability) condition (e.g. 1-5 condition grading), and hydraulic defects (tree roots and deposits) are dependent on pipe overflow and flooding.

A condition grading scheme can be applied to pipe defects to produce a qualitative assessment of overall structural and hydraulic condition (called snapshot condition) at the current time. The snapshot condition appears to be suitable for drainage pipe assets because CCTV data shows that pipes often have different defects caused by various mechanisms including random attack. Currently, available Australian grading schemes are the IPWEA Practice Note 5-2007 and Water Services Association of Australia (WSAA)'s Inspection Code 2013 (WSAA, 2013).

For analysis of condition data, Tran (2015) recommended to collect at least 600 data points of condition data from a random sampling strategy, which can be applied to the cohort of critical pipes (at least) or the whole network (at best). For each data point, at least the construction year and inspection years must be known. It is well known that reliability of data will enhance the predictions.

Estimating failure probability

A failure must be defined. For example of a structural failure, it can be defined as load on pipes exceed the pipe strength at crack (called proof strength) or pipe strength at collapse (called ultimate strength) as per Australia Standard (AS 3725, 2007). For example of a hydraulic failure, it can be defined as peak flow load exceed pipe's flow capacity.

When information is not sufficient to conclude a failure, the probabilistic approach is recommended to estimate the likelihood of failure (or failure probability) over time.

Conducting risk analysis

Risk is generally quantified as the product of quantitative consequence and the failure probability, which are described in Step 1 and 3. Risk analysis is conducted to provide risk ranking of assets, which can be used for prioritized repair and replacement programs on high risk assets. The risk analysis also helps to identify environmental factors (e.g. inspection information, corrosion of steel, concrete cracking tree root) that most affect risk.

Monitoring and Controlling risk

Risk can be monitored through regular inspection program and can be controlled by taking maintenance actions and adopting best management practices in design, installation and operation.

For the regular inspection program, it is essential to determine optimal inspection frequency and adequate inspection method that can minimizes cost and maximizes benefit. Some experience-based recommendations are available as described in IPWEA's Practice Note 5. A better alternative is based on predictive modeling.

For risk control, it is imperative to determine when, where and how maintenance actions should be carried out to minimize risk and cost. This can be achieved through combining experience and predictive modeling.

Conducting annual review

The annual review is conducted to provide:

- Report of current status and performance of assets
- Update of remaining life of assets
- Annual budget for inspection and maintenance program.

OVERVIEW OF SIMS

The Stormwater-Pipe Inspection Management System (SIMS) is a software tool, which is run on web based platform hosted in cloud. http://www.assethub.com.au/sims_v1/Home.aspx

SIMS is developed by RMIT University in collaboration with Melbourne Water and 6 City Councils (Brimbank City, City of Darebin, City of Greater Dandenong, City of Monash, City of Port Phillip and City of Whittlesea) through a research project "Whole Life Care for Asset Management of Stormwater Drainage Pipe Assets" from 2013-2015.

SIMS is aimed to help managing stormwater pipe assets to achieve the following objectives:

1. Implementing of a comprehensive risk-cost effective asset management program for stormwater drainage pipe assets;

2. Focusing on structural safety and hydraulic serviceability

3. Complying with IPWEA guidelines (Practice Note 5, 2007), asset accounting Policy of Accounting Standards for Statutory Boards (ASSB) and best practice recommendations by the industry.

The current version (2015) of SIMS is applicable to concrete pipes only. One effective feature of SIMS is that a notification email of task completion will be sent to user if it takes long time to process a user-command. SIMS presents results in figures, tables and text files.

3. Demonstration

SIMS implements steps 3 to 6 of AMF. The following steps are explained to use SIMS.

- Import data
- Run Markov deterioration model
- Run Markov inspection model
- Run Markov lifecycle model
- Run Markov reliability model
- View results

Import pipe data

Import pipe data module is aimed to store information on individual pipe assets and related factors (e.g. ID number, construction year, pipe diameter, pipe inspection, pipe maintenance and so on) for analysis and modeling. Figure 1 shows the menu for import of pipe data and pipe inspection. A template can be downloaded for filling data and then uploading.

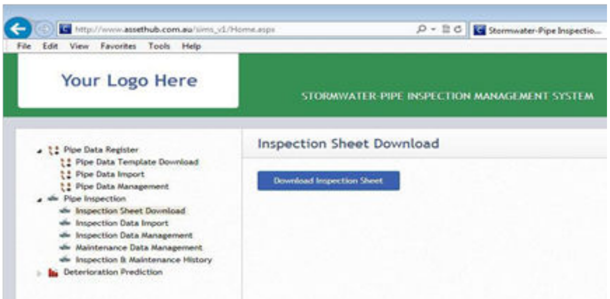

Figure 1 Importing data into SIMS

Run 'Markov Model Analysis'

Utilizing the CCTV condition data, a Markov deterioration model is derived based on the Markov chain theory, which predict the probability of condition change over a unit time. For example, with a typical 5-condition status as described above, if a pipe is in current condition 1, there will be 5 predictive transition probabilities that the pipe will stay in the same condition or move to another 4 possible condition next year. The calculation of predictive transition probabilities is shown in Equation 1 (Tran et al., 2010):

$$[p_1^t\ p_2^t\ p_3^t\ p_4^t\ p_5^t\ ] = [1\ 0\ 0\ 0\ 0] * \begin{bmatrix} P11 & \cdots & P15 \\ \vdots & \ddots & \vdots \\ 0 & \cdots & P55 \end{bmatrix}^t$$

Where p_1^t is predictive probability in condition 1 at time t, [1 0 0 0 0] represents for current condition, p12 is transition probability from condition 1 to condition 2,

The model is used to provide condition change over time for the whole network or pipe cohorts, which can be used for preparation of annual budget and asset valuation of the whole network over time. The model can also be used for an individual pipe that is considered to belong to the relevant pipe cohort or pipe network. Detailed description and calibration of the Markov model are described in (Tran et al., 2008, Tran et al., 2010).

Figure 2s shows that a user can apply the Markov model for structural or hydraulic condition. Figure 2b shows that pipe cohort can be selected for analysis by applying filtering on related factors. Figure 2c shows various options for running Markov model.

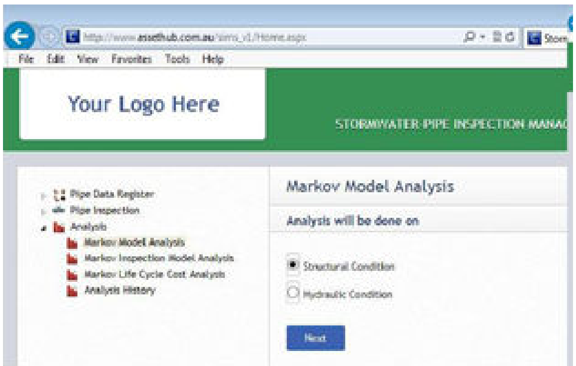

Figure 2a Running Markov model

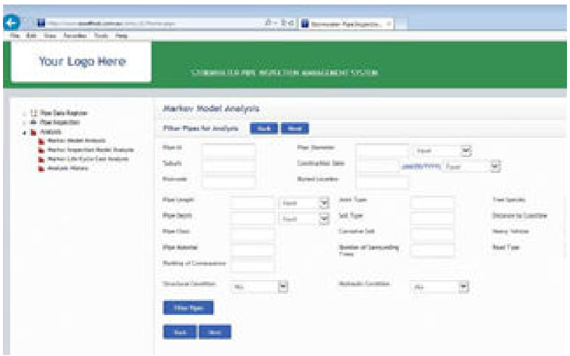

Figure 2b Pipe filtering

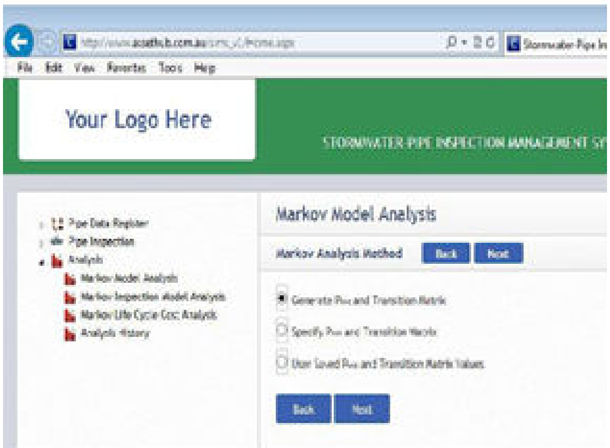

Figure 2c Options for Markov model

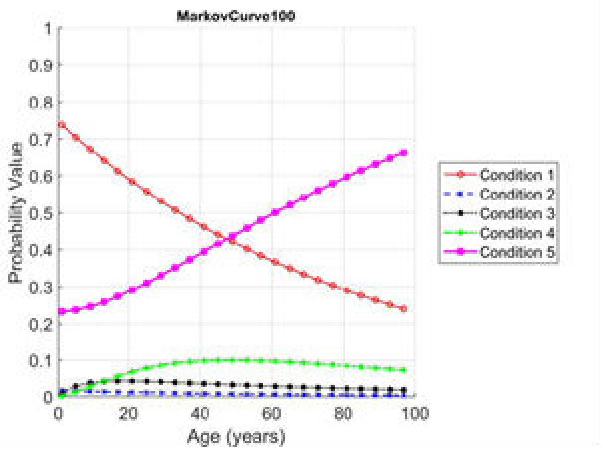

Figure 2d Result of Markov model

Figure 2d shows an example of a Markov model for structural deterioration of whole network. The interpretation is that if the average age of network is assumed 40 years as of 2015 (although individual pipes were installed in different past years), there are 45% of pipes in condition 1, 2% in condition 2, 5% in condition 3, 10% in condition 4 and 40% in condition 5. If pipe in condition 5 is valued as $1 unit and condition 1 as $5 unit, then the current valuation of pipe network can be estimated. Annual change of pipe condition and values and annual budget for maintenance can also be estimated for future years from the Figure 2d.

Run ‘Markov Inspection Model Analysis’

The Markov Inspection Model is developed to estimate the next inspection time of a pipe with known current condition over a short planning horizon, which can be typically 10-20 years. The purpose of inspection is to detect pipes in poor condition for timing repair in order to avoid unexpected failure and to minimize annual cost. For this purpose, a penalty will be incurred if the inspection time is too long and thus fails to detect the poor condition. The optimal inspection time is estimated by using Monte Carlo simulation approach. In this approach, samplings of condition changes over the planning horizon are generated by Markov deterioration model. For each sampling, various inspection times are tried and associated cost are calculated in a process that stops when a poor condition is detected. Then average cost for each inspection time is taken over all samplings. The inspection time with minimal average cost is selected.

To run Markov Inspection Model Analysis for a pipe or a cohort, the selection of structural or hydraulic condition and then pipe filtering are first carried out in the same step as shown in Figure 2a and 2b of the Markov model. Figure 3a shows the required parameters. Figure 3b shows how annual cost rate varies with different inspection time and from there the optimal inspection time with minimal cost can be identified. Figure 3c shows that the longer the inspection time, the lower the cost but the higher the number of undetected poor conditions, which might require a compromise for risk-cost management.

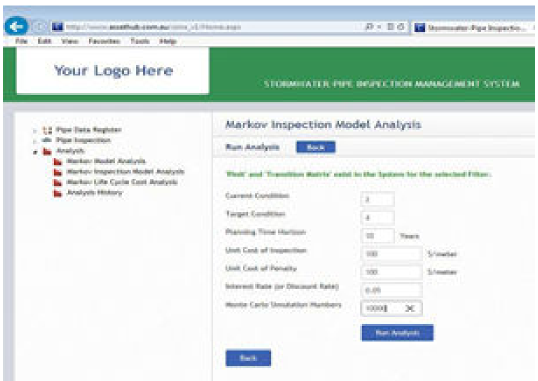

Figure 3a Required parameters of Markov inspection

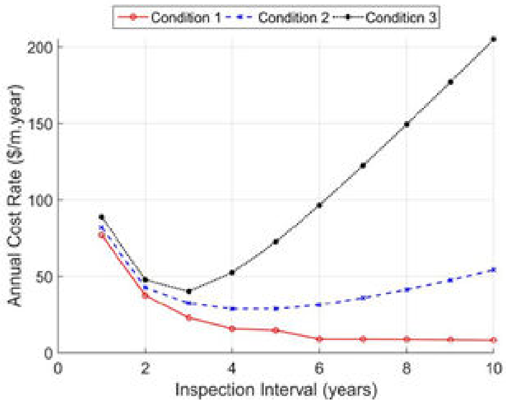

Figure 3b Optimal inspection time

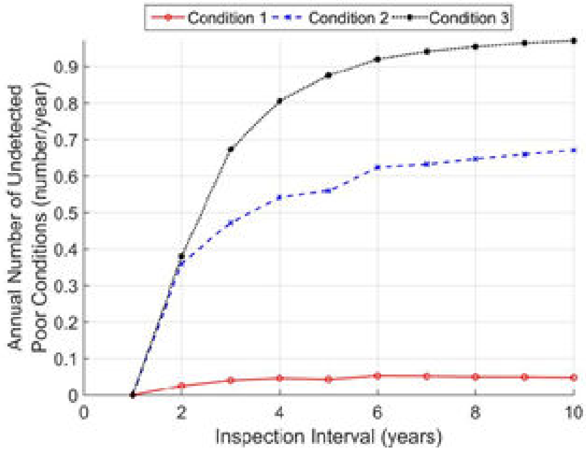

Figure 3c Number of undetected poor conditions

Run ‘Markov LifeCycle Model Analysis’

The Markov LifeCycle Model is developed to estimate the lifecycle cost of inspection and repair for a pipe with known current condition over its expected service life time of typically 100 years. The lifecycle cost can be useful for budgeting and risk-cost mitigation.

For an inspection-based asset management strategy for stormwater pipes, the cost rate function (Hong et al., 2014) as shown in Equation 2 is utilized to determine the average cost per year over a planning horizon of T years.

$$CR(TI) = \{\sum_{i=1}^{ni} CI * e^{-\epsilon*i*TI} + \sum_{i=1}^{nm} CM * e^{-\epsilon*tMi} + \sum_{i=1}^{nf} CF * e^{-\epsilon*tFi}\}/T$$

where CR is cost rate (dollar/year), CI is unit inspection cost (dollar/unit length), CM is repair cost (dollar/ unit length), CF is replacement cost (dollar/ unit length), is interest rate with typical value of 5%, ni is number of inspection, nm is number of repair, nf is number of replacement, TI is inspection interval, tMi is time at the ith repair, tFi is time at the ith replacement, T is expected service life. The exponent function in Equation 2 transforms cost value in future time into cost value at present time using the concept of present value.

The lifecycle cost is estimated by using Monte Carlo simulation approach. In this approach, samplings of condition changes over the planning horizon are generated by Markov deterioration model. For each sampling, various inspection times are tried and associated costs are calculated in a process that replaces a failed pipe with a new pipe and repairs a poor condition to a better condition. Then average cost for each inspection time is taken over all samplings. The inspection time with minimal average cost is selected.

To run Markov Inspection Model Analysis for a pipe or a cohort, the selection of structural or hydraulic condition and then pipe filtering are first carried out in the same step as shown in Figure 2a and 2b of the Markov model. Figure 4a shows the required parameters.

Figure 4b shows how annual lifecycle cost varies with different inspection time and from there the optimal inspection time with minimal cost can be identified. Figure 4c shows that the longer the inspection time, the lower the cost but the higher the number of undetected poor conditions, which might require a compromise for risk-cost management.

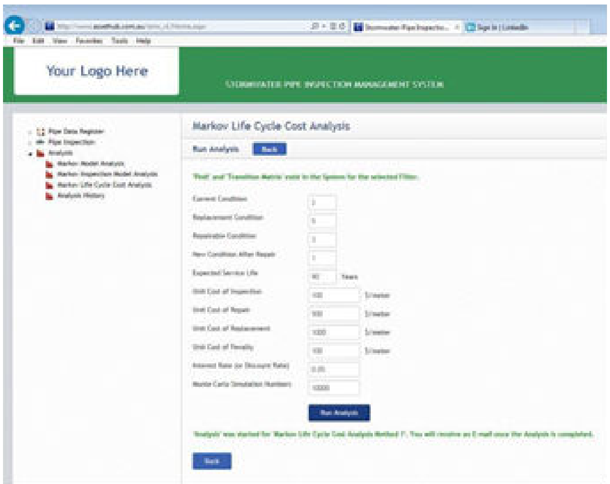

Figure 4a Required parameters of Markov lifecycle model

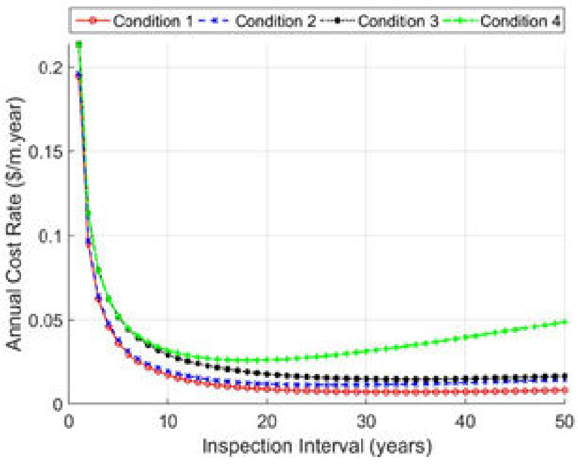

Figure 4b Optimal inspection time

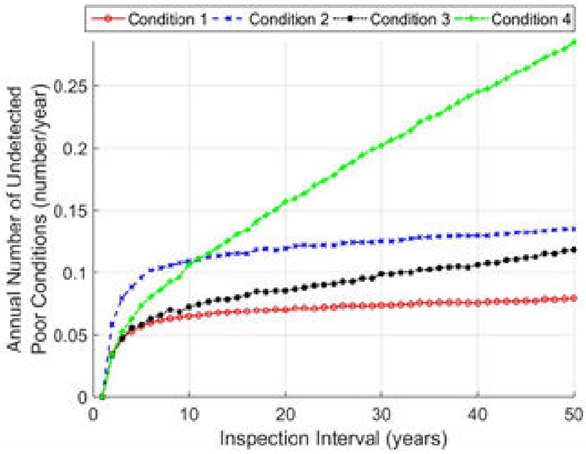

Figure 4c Number of undetected poor conditions

Run ‘Markov Reliability Analysis’

The Markov Reliability Model is developed to estimate the time-dependent likelihood of failure (or failure probability) for both structural and hydraulic failure types and thereby allows estimating the remaining life 7

based on risk concept. The reliability of a structure is often assessed by establishing a limit state function

(G) which consists of the load or load effect (S) on the structure and the resistance of the structure (R) (Melchers, 1999).

$$G(X) = R-S \qquad (3)$$

where X is a vector of random variables that define S and R in the n-dimensional space.

Mathematically, G(X) <0 or R<S indicates a failure domain. The failure probability Pf of the structure is then defined as:

$$Pf = \text{probability}\ [G(X) < 0] \qquad (4)$$

The failure probability is estimated by using Monte Carlo simulation approach. In this approach, samplings of condition changes over the planning horizon are generated by Markov deterioration model. Sadiq et al. (2004) suggested to reduce tensile strength of cast iron pipes in proportion with decreasing pipe wall thickness due to pit corrosion. Based on their proposed idea, pipes with structural conditions from 1 to 5 can be assumed to have load bearing capacity Tp reduced by 0%, 7.5%, 15%, 22.5% and 30% respectively. Similarly, pipes with hydraulic conditions from 1 to 5 can be assumed to have pipe diameter reduced by 0%, 10%, 20%, 30% and 40% respectively. The threshold values of these assumptions for structural and hydraulic conditions can be adjusted with experimental or field testing. Time-dependent reliability assessment is conducted by varying pipe structural strength and hydraulic flow capacity as per the outcome from the Markov model. Values of remaining random variables affecting external structural and hydraulic loads on pipes are generated from their assumed distribution with constant means and coefficient of variation taking values between 0 and 0.4.

Figure 5 shows an example for calculating the probability of hydraulic failure for different variations of influential variables. As can be seen from the Figure, the probability of failure is increased over time due to pipe deterioration and change of influential variables. If the failure probability of 0.1 is considered high risk, then remaining life of pipes is 10 years for hydraulic failure.

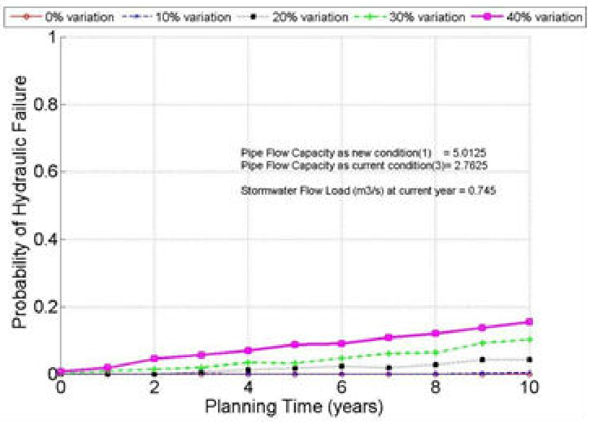

Figure 5 Example of probability of hydraulic failure

4. Discussion

The proposed AMF is considered a hybrid approach in which reactive management (i.e. wait to fail) is applied to non-critical pipes and proactive approach (i.e. regular inspection and repair) is applied to critical pipes. This approach is suitable for network of drainage stormwater pipes, whose failures are not frequent and catastrophic as compared to bridges and water mains and where budget is limited. SIMS provides an effective tool to understand and monitor risks and achieve optimal risk-cost management for the proposed AMF. However, SIMS requires accurate pipe data and sufficient inspection data, which are not always met by asset owners. For effective use of SIMS in the near future, the asset owners need to complete their data acquisition. A guide covering required data collection practices are currently being developed by the RMIT research team.

5. Conclusions

The paper presents an integrated asset management model for concrete storm water assets developed based on data collected by local councils in Victoria, Australia and the decision making practice adopted. The proposed methodology integrates data collected from CCTV inspections and pipe attributes. Whilst the full implementation of the model requires significant input data, the paper demonstrates the complete model with assumed input parameters for change in pipe strength and variability of condition data.

References

[1]. AS 3725 2007. Design for Installation of Buried Concrete Pipes. Australia: Standard Australia.

[2]. BUSBA, E. & SAGÜÉS, A. A. 2013. Localized corrosion of embedded steel in cracked reinforced concrete pipes. Corrosion, 69, 403-416.

[3]. CONCRETE PIPE ASSOCIATION OF AUSTRALASIA. Concrete Pipe Facts [Online]. Available: http://www.cpaa.asn.au/General/concrete-pipe-facts.html [Accessed 12/09/2014.

[4]. ENGINEER AUSTRALIA 2010. Australian Infrastructure Report Card. Canberra: Engineer Australia. HONG, H. P., ZHOU, W., ZHANG, S.

& YE, W. 2014. Optimal condition-based maintenance decisions for systems with dependent stochastic degradation of components. Reliability Engineering and System Safety, 121, 276-288.

[5]. IPWEA 2015. Practice Note 5: Stormwater Drainage. Melbourne: Institute of Public Works Engineering Australasia

[6]. MAHMOODIAN, M. & ALANI, A. M. 2013. Multi-failure mode assessment of buried concrete pipes subjected to time-dependent deterioration, using system reliability analysis. Journal of Failure Analysis and Prevention, 13, 634-642.

[7]. MELCHERS, R. E. 1999. Structural Reliability Analysis and Prediction, Chichester, UK, Wiley.

[8]. MOORE, I. D., LAPOS, B. & MILLS, C. 2004. Biaxial Testing to Investigate Soil–Pipe Interaction of Buried Fiber-Reinforced Cement Pipe. Transportation Research Record: Journal of the Transportation Research Board, 1868, 169–176.

[9]. SADIQ, R., RAJANI, B. & KLEINER, Y. 2004. Probabilistic risk analysis of corrosion associated failures in cast iron water mains. Reliability Engineering and System Safety, 86, 1-10.

[10]. SHARMA, K. R., YUAN, Z., DE HAAS, D., HAMILTON, G., CORRIE, S. & KELLER, J. 2008. Dynamics and dynamic modelling of H2S production in sewer systems. Water Research, 42, 2527-2538.

[11]. TRAN, D. H., NG, A. W. M., MCMANUS, K. J. & BURN, S. 2008. Prediction models for serviceability deterioration of stormwater pipes. Structure and Infrastructure Engineering, 4, 287-295.

[12]. TRAN, D. H., PERERA, B. J. C. & NG, A. W. M. 2010. Markov and neural network models for prediction of structural deterioration of stormwater pipe asset. Journal of Infrastructure System, ASCE, 16, 167-171.

[13]. TRAN, H. 2015. Sensitivity of Markov Model to Different Sampling Sizes of Condition Data. Journal of Performance of Constructed Facilities, 06015005.

[12]. WSAA 2013. Conduit Inspection Reporting Code of Australia Version 3.1. Melbourne.: Water Service Association of Australia (WSAA).

SECM/15/157

Dynamic Response of RC Bridges due to Heavy Vehicles

T.M. Sooriyaarachchi[1], W.A.M.T.C.W. Aththanayaka[2], De Silva Sudhira[3*] and De Silva Subashi[4]

Department of Civil and Environmental Engineering, Faculty of Engineering,
University of Ruhuna, Galle, Sri Lanka
*E-Mail: sudhira@cee.ruh.ac.lk,

Abstract: As a South Asian country, Sri Lanka is having a promising development in infrastructures in the country. Amidst of them, concrete bridges that are constructed in highways and expressways have substantial effect on developing transportation sector. The performance evaluation of bridges starts with the inspection of the bridge to determine the present condition. Currently, Structural Health Monitoring (SHM) in most of the developed countries is characterized by traditional visual inspection along with referencing of old inspection reports to maintain an accurate account of the bridges condition. This paper presents evaluating method for current condition of reinforced concrete bridges by evaluating dynamic characteristics of the bridge. Accelerations of the bridge were measured by imposed in moving vehicles. For the measurements, tri-axial accelerometer was used. Analysing of the acceleration is complex due very large number of readings and acceleration values required to filter from other disturbances. Matlab program was developed to filter and analyse the acceleration readings. In addition, displacements were calculated from the acceleration waveforms to evaluate bridge stiffness for different moving loads. The effect of the loads generated by moving vehicles on the displacement of the bridge is varying with the speed of the vehicle. To simulate that in model of the structure, an appropriate method was applied. By considering both result taken from actual acceleration measurements and the model, current condition state of the bridge was evaluated.

Keywords: Structural Health Monitoring, acceleration, displacement, bridge rating

1. Introduction

Bridges become lifelines of world transportation system during last two century. During the last seventy years a number of reinforced concrete (RC) bridges and pre-stressed concrete (PC) bridges were build all over the country. Maintenance of bridge structures in a transport network is essential in order to ensure safety, in addition to providing cost-effective maintenance operation of the network to save replacement cost by maximum utilization of service period.

Structure health monitoring (SHM) of bridges is essential for reliable structural conditions. Also SHM systems of bridges should be upgrade rather than it's depending on visual inspection and Non-Destructive Testing (NDT) and static load test can be increase the accuracy of test.

Deterioration and overloading become major factors that can happen to reach end of the lifespan of structure. Figure 1 shows collapse of a steel bridge in to Daduru Oya in Meeliyadda, Kurunegala due to deterioration and overloading (News Lanka) [4].

Figure 1: Meeliyadda Bridge collapse, 2015

When a vehicle passes over a bridge movement may generate in bridge girder base on its stiffness. With the Deterioration, stiffness of bridge get lower value and ultimately movement can be increase (Takács, (2002)) [7]. Uneven moment than designer allowed can happen to collapse of bridge. Here, Acceleration sensors can be used to track deck vibrations as well those results can be used to optimize typical visual inspection results or non-destructive test results.

2. Methodology

2.1 Bridge Selection

For the analysis and validations, three numbers of RC bridges in Ginthota, Magalle and Mahamodara were selected (Ref. Figure 2).

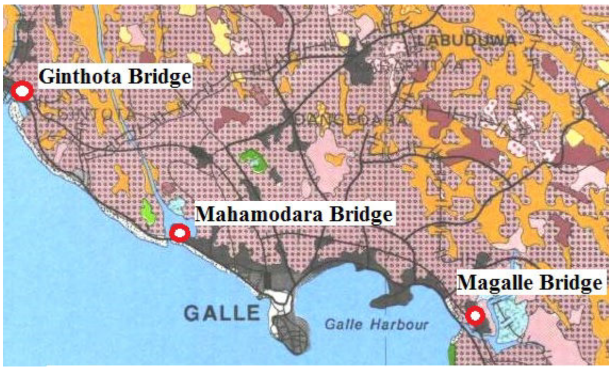

Figure 2: Selected bridges

A newly constructed Magalle bridge was used to validate the final outcome of the results. Also Ginthota Bridge which shown in Figure 3 is one of moderately deteriorated bridge which constructed in 1964 and another bridge at Mahamodara is slightly deteriorated Bridge (Pradeep, et. al, (2013)) [5].

Figure 3: Ginthota Bridge

Those three bridges are existing along the coastal line on Colombo-Galle (A2) main road. Coastal exposure condition can happen to accelerate deteriorate processes severely and effective lifespan of selected three bridges will be shorten than bridges that exposed to normal environmental conditions.

2.2 Instrumentation

Tri-axial accelerometer is used as main instrument to grasp vibration response vs. moving vehicle. Tri dimensional Acceleration of bridge deck was measured at the middle span and end of the bridge deck as well on top of the support. The accelerometer had tightened to the bridge deck via grouted steel plate that can transfer deck vibration to sensor as it is.

Figure 4: Instrument used for test

Figure 4 consequently shows the Tri-axial accelerometer, data reader and data logger which used to measure accelerometer on the middle span of Ginthota Bridge. A high resolution data recorder that can record up to 50,000 data per second was used to capture deck vibrations. Accuracy of data will be critical when final deformation keep it in micro meter range.

2.3 Data Acquisition

Accelerations in the bridge deck were recorded for varies types of vehicles. Although for the further analysis definite load class was selected. Therefore dynamic loads from regularly loaded busses were selected due to its availability. Also own vehicle which having known load can used for receive deck vibrations and it may increase cost of test. With the change of vehicle speeds, there were different in accelerations. Similar accelerations results were selected around 40 kmh^{-1} to ensure the corrected result.

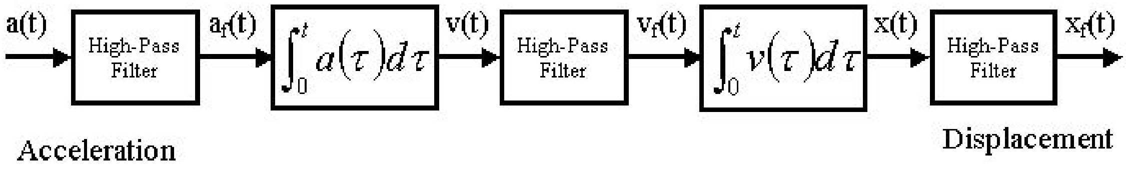

Figure 5: Double Integration with High pass filtering

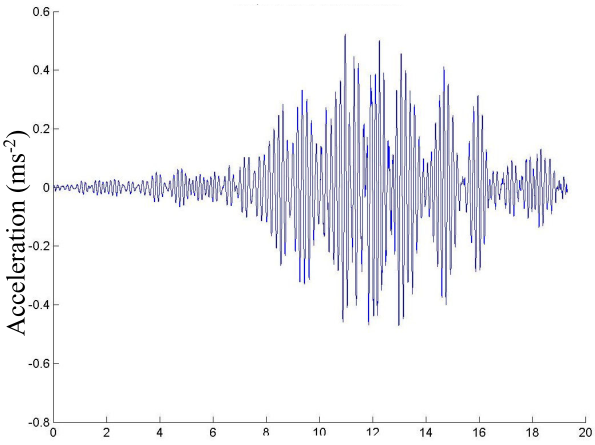

Figure 6: Acceleration graph vs. Time.

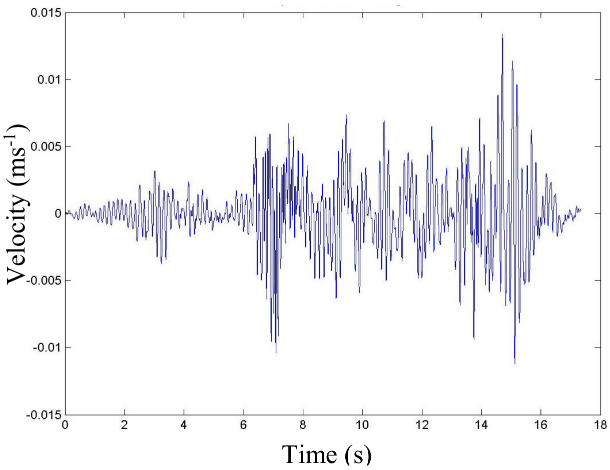

Figure 7: Velocity graph vs. Time

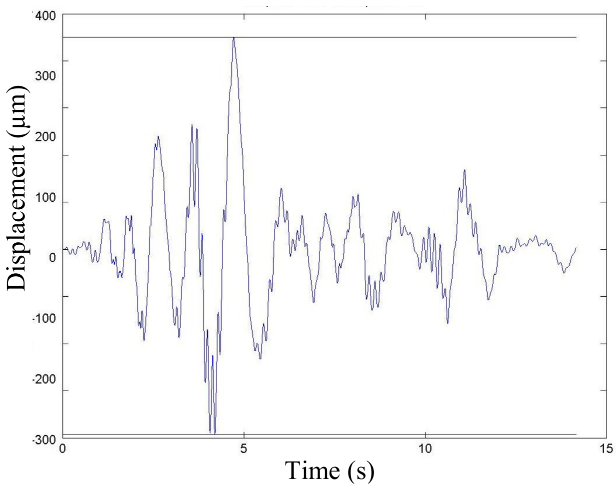

Figure 8: Displacement graph vs. time

Using dynamic test results that can be monitor some deviation with results of accelerations as well as deflections in to tri-axial direction. The relationship of deflection vs. stiffness acts as major reasons for deviation of results in to tri directions. Usual bridge deck has relatively low stiffness along the direction of gravity due to its shape and major gravitational load apply along the low stiffness direction.

Considering those criteria movement of bridge deck along either traveling direction or crossing direction can be neglect. The possibility to fail bride along gravitation direction is too high with normal load condition rather than loading due to natural disaster or motor-vehicle accidents.

The variation of deflection along the bridge deck can predict by acquiring multiple measurement in several locations along the deck. Consider about resultant deflection along the deck vs. moving load, maximum deflection come off at mid span as well deflection on support reaches to neutral region.

2.4 Acceleration Data Analysis

The recorded accelerations were converted into displacements by double integration method (Slifka, (2004)) [6]. Noises that generate with data recording session was led to make some different in deflection results.

High pass filters were used to remove that generated noise signals. All the process was done using a coded matlab script. Compiling procedure inside matlab environment is shown in Figure 5.

Acceleration of mid span of Ginthota Bridge according to moving load is shown in Figure 6.

Corresponding velocity as shown in Figure 7 can be generated by single integration process of filtered acceleration data and deflection as shown in Figure 8 predicted by re-integration of velocity results.

Mechanical condition of vehicle, road surface condition and driving path along the girder can generate slightly different results in repeated tests. That error can repeat off by taking the mean average value of arrived results. Table 1 shows calculated deflection results of Ginthota Bridge at mid span and top of the pier for number of vehicle at same load conditions.

Table 1: Calculated deflections of Ginthota Bridge

Displacement at mid span (μm)	Displacement at the pier (μm)
352.6	52.8
368.2	41.3
333.1	42.6
322.3	46.1
368.2	51.8

The average deflection of Ginthota Bridge is about 348μm in mid span and 46 μm in top of the pier.

2.5 Bridge Model

From referring each structural drawings bridge models were designed based on finite element method (FEM). For each bridge were drawn in the ANSYS work bench as Transient structure. Material properties, reinforcement location and pre-stressed or post stressed load applied on FEM model to fell initial condition of bridge. The load equal to measure the actual deflection (18000 N) was applied as transient load and speed as actual speed of data recording. The characteristic data of model constructed for Ginthota Bridge and FEM model are shown in Table 2 and Figure 9, consequently.

Table 2: model properties of Ginthota Bridge

Dimensions (m)	Material by volume
Length = 25. 162	Concrete = 92.3%
Depth = 04.155	Steel = 3.7 %
Width = 15.25	

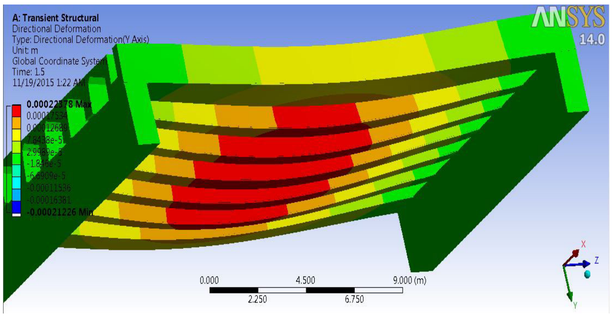

Figure 9: Model of the Ginthota Bridge

Assign material properties for original bridge conditions are shown in Table 3.

Table 3: Material properties assign for Ginthota FEM model

Property	Concrete	Steel
Density (Kg/m^3)	2300	7850
Ultimate Compressive Strength (MPa)	41	450
Ultimate Tensile Strength (MPa)	5	450
Young's Modulus (Pa)	3.e+010	2.e+011
Poisson's Ratio	0.18	0.3

To simulate the deterioration of concrete in the model, compressive strength and young's modulus of the concrete were reduced as a percentage. Change of young modulus that affect to deformation of girder vs. concrete compressive strength is shown in Figure 10 [1] (Carmichael, (2009)). Further, to simulate corrosion of steel, steel volume of the structure change as a percentage.

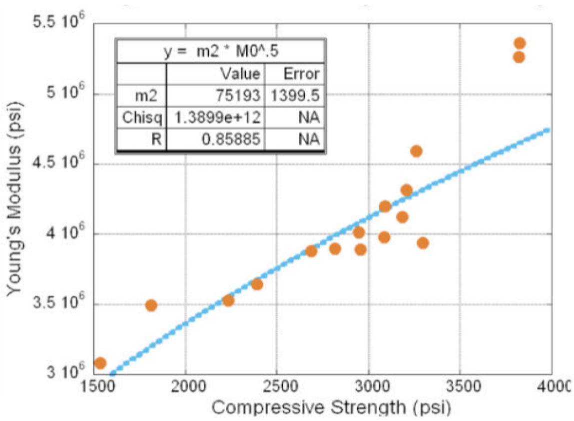

Figure 10: Young's modulus vs. compressive strength of concrete

Deterioration of bride can simulated as deduction of material properties as percentages. The maximum deformations of the bridges for varies level of deteriorations were taken into account and deformation changes against deterioration percentage was drafted. Results generates for original bridge conditions of Ginthota Bridge with standard moving load is shown in Figure 11.

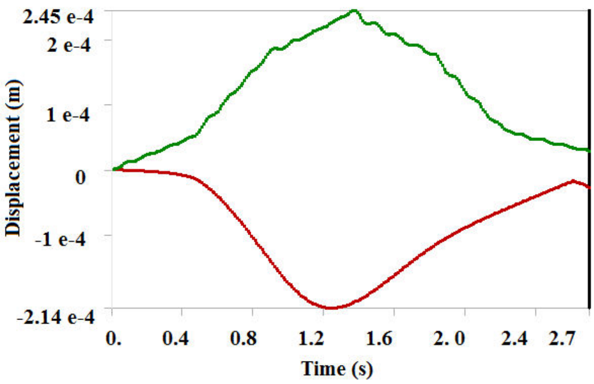

Figure 11: Deformation of deck at centre span

The deformations taken from the accelerations for each bridge were compared with the deformation vs. deterioration percentage curve and percentage of deterioration of the bridge is identified. Condition of the bridge can be predicted by comparing results from FEM model and actual measurements.

2.6 Validations of Results

For the validations of the model displacement derived from FEM model compared with deterioration level of the known bridge. Here newly constructed Magalle bridge was selected and assume that bridge exists its zero deterioration level. This was verified with visual inspection reports available [3, 5]. Measured deflection values and deflection that obtained from FEM model was obtained approximately shows equal distribution.

2.7 Bridge Management System (BMS)

A user friendly and accurate BMS was launched as a part of Dynamic response structure health monitoring. However, in real structures health monitoring system cannot be developed only based on dynamic loads. Visual inspections as well as non-destructive test data acquire major cause of SHM. Therefore another bridge assessment tool that used to predict SHM by using only visual inspection and non-destructive data was used to optimize dynamics load response SHM. Evaluate the current condition state of the bridge using NDT data and visual inspection, available BMS was used. [8](Kariyawasamm et al., (2013))

Table 4: structural health rating system of RC bridges

Number	Condition state	Physical Description
9	Excellent	A new bridge.
8	Very good	No problem noted.
7	Good	Some minor problem.
6	Satisfactory	Structural members show minor some deterioration.
5	Fair	All primary structural element are sound but may have minor section loss, deterioration, spalling, or scour.
4	Poor	Advanced section loss, deterioration, spalling, scour
3	Serious	Loss of section, etc. Has affected primary structural components. Local failures are possible. Fatigue cracks in steel or shear crack in concrete may be present.
2	Critical	Advanced deterioration of primary structural elements. Fatigue cracks in steel or shear crack in concrete may be present or scour may have removed structural support. Unless closely monitored it may necessary to close the bridge until corrective action is taken.
1	Imminent Failure	Major deterioration or loss of section in critical structural component or obvious vertical or horizontal movement affecting structural stability. Bridge is closed to traffic but corrective action may put back in light service.
0	Failed	Out of service. Beyond corrective action.

As a result of compiling all input data, overall rating of the bridge was evaluated. The rating number and conditions state are shown in Table 4 (Chase et al, 1999) [2]. Depend on that rating, decision about the condition state of the bridge can forced to change or user can make sure that structure is further keep its current condition.

5. Conclusions

Management and preservation of existing concrete bridges is a complex engineering concern with public safety and financial implications. Successful treatment to limit the rampant effects of structural defect, deterioration, and damage and control functional decline requires early diagnosis. The high replacement value of structurally deficient bridges justifies the cost of diagnostic evaluation. Instrumentation and monitoring is the only tool that can enable the reliable evaluation required before any intervention.

Bridge structures are evaluated by ordinary techniques cannot predict actual structural rating by itself. Either Static load test or dynamic response test is the way to optimize usual prediction. Structural evaluation of existing bridges is a complex process consisting of a series of integrated system components and procedures. Modern bridge management requires the development of integrated administrative and engineering solutions, which are not only technically and financially feasible, but also practical and rapid.

Acknowledgement

The authors wish to express their gratitude and appreciation to the Department of Civil and Environmental Engineering, University of Ruhuna Hapugala, Galle, Srilanka who financially supported to this research work and Ms. Hasini Vitharana, Mr. Pubudu Jayawardana, Research Students, University of Ruhuna. Also authors wish to thank Chief Engineer and Technical staff of Road Development Authority (RDA), Galle, and Director, Bridge Design Division, RDA, Baththaramulla, Srilanka. Also authors wishes to than Mr. Yasuyaki Kurihara, Steel Research Laboratory, JFE Steel Corporation, Kawasaki, Japan.

References

1. Carmichael, R. P. (2009). Relationships between Young's modulus, compressive strength, Poisson's ratio, and time for early age concrete. *Master, Department of Engineering, Swarthmore College*.

2. Chase, S. B., Small, E. P., & Nutakor, C. H. R. I. S. (1999). An in-depth analysis of the national bridge inventory database utilizing data mining, GIS and advanced statistical methods. *Transportation Research Circular*, *498*, 1-17.

3. Sudhira De Silva, Chandana Nawarathna, and Laksiri Pradeep, Evaluation Criteria for Condition State of Reinforced Concrete and Prestressed Concrete Bridges, Proceedings of the Seventh Academic Sessions, University of Ruhuna, March 2010, pp. 37-45

4. News Lanka, weekly newspaper (25/6/201); page no 4.

5. Laksiri Pradeep, Sudhira De Silva and Chandana Nawarathna, Structural Assessment of Reinforced Concrete Bridge Structures Exposed to Chloride Environment, Proceedings of the International Conference on Sustainable Built Environment (ICSBE-2010) Kandy, Vol. 1, No.1, 13-14 December 2010, pp. 480-487
6. Slifka, L. D. (2004). An Accelerometer based approach to measuring displacement of a vehicle body. *Master of Science in Engineering, Department of Electrical and Computer Engineering, University of Michigan–Dearborn*.

7. Takács, P. F. (2002). Deformations in concrete cantilever bridges: observations and theoretical modeling, PhD Thesis, Department of Structural Engineering The Norwegian University of Science and Technology Trondheim, Norway, March 2002, pp. 184

8. K. K. G. D. D. L Kariyawasam, U.B.H.U Hemapala, G.S.Y. De Silva and G.H.M.J. Subashi De Silva, Development of a Bridge Assessment Tool to identify Current Condition of Reinforced Concrete and Pre-Stressed Concrete Bridges, *Proceedings of International Conference on Structural Engineering and Construction Management*, 13-15 December 2013, paper no. SBE/13/139

SECM/15/9

Seismic Evaluation of a Low-Rise Reinforced Concrete Commercial Building by the Capacity Spectrum Method

U. B. Attanayake [1*]

[1]Western Michigan University, Kalamazoo, United States
E-Mail: upul.attanayake@wmich.edu, TP: +1 269 276 3217

Abstract: This paper presents seismic evaluation of a typical low-rise reinforced concrete commercial building based on the capacity spectrum method (CSM) recommended in ATC-40. A nonlinear three-dimensional finite element (FE) model is developed for assessing the seismic capacity of the structure. To simulate a more realistic behavior of the building during ground motions, effects of foundations, masonry infills, and other site-specific features are integrated into the model. Seismic capacity of the structure is determined using pushover analysis and compared with the demand imposed by predicted ground motions. Results indicate that this building possess the most undesirable brittle failure with low level of seismic capacity. Further, this analysis method reveals several earthquake vulnerable features and the effectiveness of 3D modeling of buildings with strength and stiffness irregularities. Finally, design recommendations for eliminating earthquake vulnerable features are proposed. However, the typical details used at the foundation-superstructure connection limits the structural system seismic capacity.

Keywords: Capacity Spectrum Method, Building, Earthquake Vulnerability, Pushover Analysis, Soft-Story.

1.0 Introduction

Typical low-rise commercial buildings have the first floor taller than the other floors or have relatively less number of infill panels and partition walls. Seismic performances of these buildings are pretty complex. The most common failure mode of these buildings is the weak and/or soft story mechanism. A weak storey is defined as the one in which the storey strength is less than 80 percent of that of the storey above. A soft storey is defined as the one in which the lateral stiffness is less than 70 percent of that in the storey immediately above or less than 80 percent of the average stiffness of the three stories above.

During past earthquakes, many of them collapsed while others survived. Around 280 earthquakes have occurred from 1988 to 1992, about 59,940 persons were killed, and 1769,000 persons became homeless [0]. During the 1990 Iran earthquake, more than 130,000 houses and commercial buildings were damaged. More than 105,000 houses and 320 apartment buildings were damaged by the 1989 Loma Prieta earthquake. Most of the buildings that failed in Turkey, 1992, were modern buildings designed and particularly, constructed without compliance with seismic code regulations. Ruiz et al., [0] has considered the seismic performance of buildings with weak first story during the Mexico City earthquake in 1985. The idea of a soft first story had been formerly proposed as a means to reduce the seismic response of buildings because of its action as a base isolator. But, 8% of the damaged buildings in the Mexico City area had a weak first story. In the same time Miranda and Bertero [0] also have considered the same earthquake and have mentioned that 39% of engineered buildings that collapsed or suffered severe damage were buildings of five or fewer stories. The percentage of this type of building that collapsed or suffered severe damage was significantly smaller than the percentage of 7-to 15-story buildings that were severely damaged. Overstrength is the primary reason for the survival of most of these low-rise buildings. The number of totally collapsed buildings during the 1999 Chi-Chi earthquake was 20,815. The reasons for such serious building damage were due to very high-intensity ground motions, bad construction quality and improper structural system [0]. Among those collapsed and severely damaged buildings, street-front buildings, school buildings, and town halls were dominant. A majority of the damaged buildings had shear walls in only one direction. So, the buildings were very strong on wall direction while their capacities could be just equal to the capacity specified by the code in the direction without wall [0]. In India, reinforced concrete frame buildings with brick masonry infills have shown excellent performances, during past two moderate earthquakes, even though most such buildings were not designed and detailed for seismic response [0]. Further, they have mentioned that the survival of aforementioned buildings was mainly due to the beneficial influence of masonry infill walls. Asymmetric structures, in terms of mass or stiffness distribution, suffer an additional response due to the coupling of lateral and torsional motions. This coupling motion can induce higher demands on resisting elements than lateral motion alone and, unless properly accounted for in the structural design, may result in severe damage or collapse [0].

One of the most effective ways of minimizing potential earthquake related losses is to conduct reliable assessments of the vulnerability of existing structures and to develop and implement effective ways to upgrade structures identified as hazardous. Further, the lessons from such assessments can be used to revise analysis, design, and detailing guidelines. Both elastic (linear) and inelastic (nonlinear) methods are available for analysis of existing structures. They are static lateral force procedure, demand/capacity ratio method, secant method, non-linear time history analysis method, and non-linear static pushover analysis method. Elastic analysis methods cannot predict a realistic behavior of a structure. Therefore, inelastic analysis methods are used to study behavior of structures under earthquake loading. The most direct or realistic inelastic analysis method is the complete time history analysis, which is considered overly complex and impractical for general use. Most promising and simplified analysis is the nonlinear static pushover method. In fact, the pushover analyses can give information on the structural strength capacities and the deformation demands. It can also expose design weaknesses that may remain hidden in an elastic analysis. Such weaknesses include story mechanisms, excessive deformation demands, strength irregularities, and overloads on potentially brittle elements, such as columns and connections.

1.1 Capacity Spectrum Method (CSM)

The CSM had been introduced in several guidelines for seismic evaluations such as the ATC-40 [0] and FEMA-273 [0]. This is an approximate procedure to analyse the seismic response of a structure with a nonlinear static analysis (pushover). By applying nonlinear static pushover method, it is possible to compute the relation between the total lateral force on a structure against the lateral deflection of the roof of the structure. This curve is often referred to as the 'pushover' or capacity curve, which represents the overall behavior of the structure. The transformed capacity curve from shear force versus roof displacement coordinates into spectral acceleration versus spectral displacement coordinates, Acceleration-Displacement Response Spectra (ADRS), the *capacity spectrum* is developed. Performance evaluation of a structure is required to have the response spectrum (or demand spectrum). Demand is the minimum required deformation and strength capacity levels of a structure required to withstand during a considered earthquake ground motion. The plot of estimated displacements in ADRS format is called the *demand spectrum*. The capacity spectrum method, a nonlinear static procedure which provides a graphical representation of the global force-displacement capacity curve of the structure and compare it to the response spectra representations of the earthquake demands, is a very useful tool in the evaluation of existing structures. Results from many applications of this method confirm its robustness and accuracy as a reliable analysis method for evaluating existing structures [0].

2.0 Objective and Scope

The main objective is to examine the seismic performance of a typical, low-rise, reinforced concrete, commercial building by using the *Capacity Spectrum* method. The results is used to propose retrofitting methods and some guidelines, to be considered in designing such buildings, to avoid possible earthquake hazards during future earthquakes.

To achieve the aforementioned objectives, a typical, low-rise, reinforced concrete commercial building is selected and the ATC-40 [0] recommended seismic evaluation procedures are employed.

3.0 Modelling for Evaluation

3.1 Flexural Behavior

In this analysis, it is required to find yield moments of all the flexural members. There is no specific formula suggested in ATC-40 [0] to calculate the yield capacity of concrete members. Hence, a well-accepted and commonly used method documented in literature [0, 0] is used.

3.2 Shear Behavior

Shear is rather complex to handle because so-called "shear failure" is a failure under combined shearing force and bending moments, sometimes, axial load, or torsion, or both may act simultaneously. Design code equations for shear capacity are conservative when compared with test results. The expected component strength needs to be used for structural evaluation. Further, the analysis methodology used for structural evaluation is displacement based. According to ATC-40 [0], the expected strength is defined as the mean maximum resistance expected over the range of deformations to which the component is likely to be subjected. Hence, the equations proposed in the following sections are used in this analysis.

3.2.1 Shear Strength of Columns

Reinforced concrete columns are subjected to axial compression or axial tensile and shear forces due to combined effect of gravity and lateral loads. Axial compression tends to increase the shear capacity while axial tension decreases it.

3.2.1.1 Concrete Shear Capacity (V_c)

ACI design code equations [0] for concrete shear strength of columns under axial compression and axial tension are compared with experimental results as shown in Figure 1. Both the equations provide a safe lower bound to the strength. Eq. 1, proposed by ATC-40 [0], represents average value of test data for columns under axial compression (k=1 and λ=1 are used).

$$V_c = 3.5\lambda\left(k + \frac{N}{2000A_g}\right)\sqrt{f'_c}\,b_w d \;\;\ldots\ldots\ldots(lb) \quad \text{(1a)}$$

$$V_c = 0.29\lambda\left(k + \frac{N}{2000A_g}\right)\sqrt{f'_c}\,b_w d \;\;\ldots\ldots\ldots(N) \quad \text{(1b)}$$

Where k=1 in regions of low ductility and 0 in regions of moderate and high ductility, λ=0.75 for lightweight aggregate concrete and 1 for normal-weight aggregate concrete, N= axial compression force (zero for tension force), and A_g= gross cross sectional area.

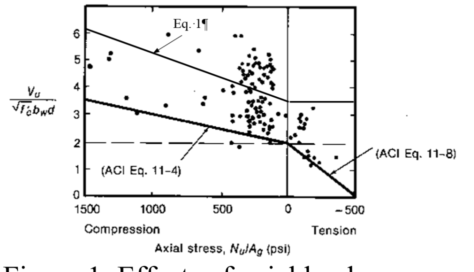

Figure 1: Effects of axial loads on concrete shear strength (Experimental data source [0])

According to Eq. 1a and its conditions, under tensile forces in regions of low ductility, concrete possess constant shear strength and shows contradictory behavior with the test results presented in Figure 1. Priestley et al. [0], presents a model for concrete shear strength without axial force effects. According to that model concrete possesses constant shear capacity under low ductility. Columns in typical low-rise buildings are seldom subjected to tensile forces. Considering the above facts, it is recommended to use Eq. 2 for columns with low ductility or small tensile forces.

$$V_c = k\sqrt{f'_c}\,A_e \qquad (2)$$

where, effective shear area, A_e=0.8A_g.

3.2.1.2 Shear Capacity of Stirrups (V_s)

The equation recommend by ATC-40 [0] is given below.

$$V_s = \frac{A_v f_y d}{0.6s} \qquad (3)$$

Where A_v is the area of the shear reinforcements, s is the spacing of stirrups, and f_y is the yield strength of the shear reinforcements. Eq. 3 is derived from Eq. 4 by assuming that the angle between the compression diagonals and the column axis as 30^0.

$$V_s = \frac{A_v f_y d}{s}\cot\theta \qquad (4)$$

In the presence of axial compression, the diagonal cracks tend to be flatter than 45^0 [0]. Priestley et al. [0] proposed an equation similar to Eq.3 with $\theta = 30^0$ and confirmed its validity after comparing its predictions with experimental data.

Tests have consistently demonstrated that the angle of inclination of the diagonal cracks is not noticeably affected by axial tension and that the shear resisting mechanism of truss action remains operative [0]. Hence, Eq. 5 is suitable for calculating shear capacity of transverse reinforcements of columns under axial tension.

$$V_s = \frac{A_v f_y d}{s} \qquad (5)$$

3.2.2 Shear Strength of Beams

3.2.2.1 Concrete Shear Capacity (V_c)

There is no particular formula suggested in ATC-40 [0] to calculate concrete shear strength of reinforced concrete beams. Eq. 6 is in given in ACI 318 [0] to calculate V_c.

$$V_c = \left(1.9\sqrt{f'_c} + 2500\frac{\rho_w V_u d}{M_u}\right)b_w d \le 3.5\sqrt{f'_c}\,b_w d \;\cdots(lb) \quad \text{(6a)}$$

$$V_c = \frac{1}{6}\left(\sqrt{f'_c} + 100\frac{\rho_w V_u d}{M_u}\right)b_w d \le 0.29\sqrt{f'_c}\,b_w d \;\cdots(N) \quad \text{(6b)}$$

Where $\rho_w = A_s/b_w d$ is the reinforcement ratio, V_u is the factored shear force, and M_u is the factored moment. The application of Eq. 6a for continuous beams has been subjected to disputation. The shear span (a) is equal to M_u/V_u, which shows that there is a support to accommodate a compression strut at zero moment position. But for continuous beams there is no support to carry a compression strut reaction at the zero moment point. Hence, Eq. 7 is recommended for continuous beams [0].

$$2\sqrt{f'_c}\,b_w d \;\cdots\cdots\cdots\cdots\cdots\cdots (lb) \quad (7a)$$

$$0.166\sqrt{f'_c}\,b_w d \;\cdots\cdots\cdots\cdots (N) \quad (7b)$$

Eq. 7 does not incorporate the effects of longitudinal reinforcements on shear strength of concrete. Eq. 8 accounts the shear strength contribution from longitudinal reinforcements through the dowel action [0].

$$v_c = v_b = (0.85 + 120\,\rho_w)\sqrt{f'_c} \le 2.4\sqrt{f'_c} \ldots (psi) \quad (8a)$$

$$v_c = v_b = (0.07 + 10\,\rho_w)\sqrt{f'_c} \le 0.2\sqrt{f'_c} \ldots (MPa) \quad (8b)$$

Eq. 8 is compared with the test results. Within the practical range of reinforcement ratio, $\rho_s = A_s/b_w d$, it represents more realistic values while Eq. 7 represents the minimum values. Therefore, Eq. 8 is selected for this analysis.

3.2.2.2 Shear Capacity of Stirrups (V_s)

Generally, both concrete and the web reinforcements carry the shear acting on any reinforced concrete member. Shear strength (V_s) predicted by the well-known truss analogy is used in this analysis. Axial force acting on a beam is considered small; thus, the angle between longitudinal axis of the member and the diagonal compression struts is assumed 45^0. Eq. 5 is used in this analysis to calculate shear strength contribution of web reinforcements that are perpendicular to the longitudinal axis of the member.

3.3 Development Length and Lap Splices

Ductility of structural components that are mainly designed for gravity loads is very low. One set of equations in ACI 318 [0] is for the component yielding regions with low ductility demands and outside the yielding regions. The other set of equations in ACI 318 [0] is for the detailed requirements and strength provisions of straight, hooked, and lap-spliced bars within the yielding regions of components with moderate and high ductility demands. Most of the recommendations given in Paulay and Priestley [0] are related to components with moderate or high ductility demands. Recommendations given in ACI 318 [0] and Paulay and Priestley [0] for components with moderate and high ductility demands were compared and yielded more or less similar results. Thus, in this analysis, the ACI equations are used, and all the conditions given under each equation are adopted.

In case, if the development, hook, and lap-splice length and detailing are not in compliance with ACI 318 [0], Eq. 9 recommended in ATC-40 [0] is used to calculate the maximum stress capacity, (f_s), of reinforcements.

$$f_s = (l_b/l_d) \times f_y \quad (9)$$

Where, l_b is the length provided for development, hook, or lap splice; l_d is the length required by ACI 318 [0] for development, hook, or lap splice.

4.0 Modelling of Existing Structure

The selected building represents the most common type of typical low-rise reinforced concrete commercial buildings (Figure 2). It has five stories, including a mezzanine floor. The building is rectangular in plan with an overall dimension of approximately 12 m by 36 m in the north-south and east-west directions, respectively.

(a) Front view (facing south)

Figure 2: Front and side views of the building

Infill walls are provided only in the outside frames (Figure 2 and Figure 3). However, east-west direction have doors or windows with partial infills (Figure 3 e and f). Frame B and frame C have no beams in the east-west direction at the fourth floor and the mezzanine floor levels, respectively (Figure 3).

All the column sizes and reinforcement detailing are changed at the 3rd floor level. From foundation to the 3rd floor level column size is 0.25m×0.25m, and at the 3rd floor level it changes to 0.2m×0.2m causing abrupt changes in stiffness and strength of the structure. Height measured from the first floor to the mezzanine floor, between frames A and B, is 2.6m. The mezzanine floor level between frames B and D is 0.65m higher than that at frames A and B, Figure 3. All these features cause vertical and plan irregularities of the structure. It is obvious that this building is weaker in the east-west direction than the north-south direction. Thus, the analysis is carried out only in the longitudinal direction. Mainly, there are four frames in that direction.

They are frame A, B, C, and D that carry gravity and lateral loads during earthquakes. Hence, seismic capacity of the structure and behavior of those frames under the gravity and lateral load combination and the failure mechanisms were studied.

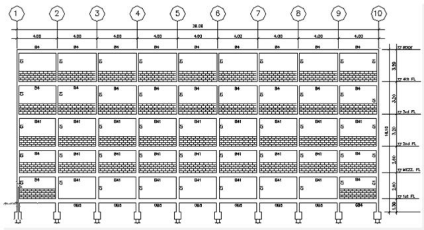
(a) Frame A (rear)

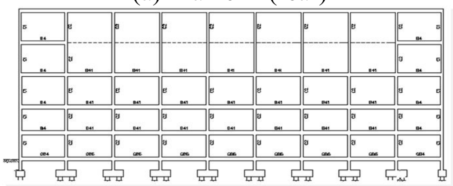
(b) Frame B (2nd interior)

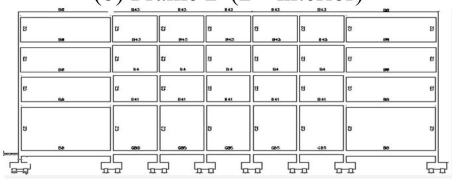
(c) Frame C (1st interior)

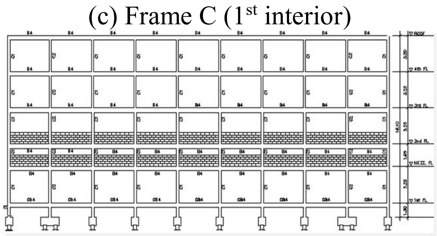
(d) Frame D (front)

Figure 3: Longitudinal frames of the building

Modeling of structural components is carried out mainly by adopting the recommendations given in ATC-40 [0] and the equations presented in section 3. For modeling of non-structural component, masonry infill panels, FEMA-273 [0] guidelines are used with necessary modifications as presented in section 4.5.2.

4.1 Computer Models

For the analysis, several different nonlinear FEM models were developed using SAP 2000 [0], two-dimensional inelastic models for frames A, B, C, and D with fixed-base, three-dimensional inelastic models with fixed-base, flexible-base (with foundations), and flexible-base with masonry infill panels. These models were constructed using as-built drawings and the best models of individual components to simulate a more realistic behavior in the nonlinear range of the structure and to accommodate all the irregularities and the other unfavorable features in the existing building.

4.2 Loads

4.2.1 Gravity Loads

Structural response to an earthquake depends on the magnitude of gravity load present at the time it hits the building. For the most reliable evaluation of the structural response, the gravity load should consists of dead load plus most likely live loads. ATC-40 [0] presents the most likely live loads for various occupancies based on a survey conducted in Washington, D. C. In this analysis, direct use of these values is not realistic. Thus, by comparing the design live loads given in Uniform Building Code (UBC) with the values in ATC-40 [0], it is necessary to find the most likely live load as a percentage of the design live load.

For this analysis, dead and most likely live loads are considered. For the dead load, the density of concrete is assumed as 2400 kg/m^3. Dead load of half and full width masonry walls are 90 kg/m^2 and 180 kg/m^2, respectively. Most likely live loads are calculated as 45% and 30% of the design live loads for residence and storage areas, respectively. As per ATC-40 [0] guidelines service loads are used.

4.2.2 Lateral Loads

For low-rise buildings, the first mode of vibration is dominant and generally the shape is idealized as an inverted triangular. If plan or vertical irregularities exist, inverted triangular load pattern assumption may not yield accurate enough results. In that case, the loading pattern according to the first mode shape is required. In this analysis, both the inverted triangular and the first mode shape load patterns are considered. The loads are applied as concentrated loads at the floor levels (at beam-column joints).

To determine mode shapes, joint masses are required. In the mass calculation, contributions of all the structural and non-structural components are considered. Building masses are simplified as lumped masses at the beam-column joints.

4.3 Load Deformation Relationship

Nonlinear load-deformation relation is used in reinforced concrete component modelling (Figure 4). This load-deformation relationship is used to represent the moment-curvature, shear force-shear angle, and axial force-axial deformation relations of the components. During the analysis, gravity load is applied prior to the lateral load. Thus, lateral loading starts at a point other than the origin of the load-deformation relation. The slope from A to B of the Figure 4 corresponds to the fully cracked stiffness of flexure-dominated components and uncracked stiffness for shear-dominated components. Point B represents the yield strength. The slope between B and C represents the strain hardening of reinforced concrete components. Point C corresponds to the ultimate strength. The sudden drop from point C to D represents the initial failure of the component. Residual strength of the component is indicated from point D to E. Total collapse that occurs by losing its gravity carrying capacity is denoted by the sudden drop at point E.

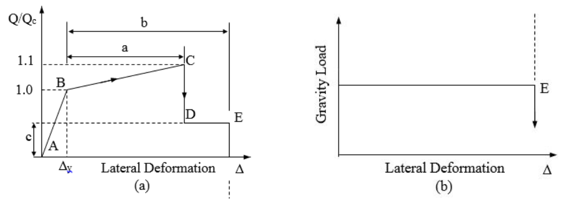

Figure 4: Generalized load-deformation relation for reinforced concrete components

4.4 Material Properties

For the evaluation of existing buildings, properties need to be determined by inspection and testing. Concrete modulus of elasticity is calculated using Eq. 10.

$$\ldots E_c = 4700\sqrt{f_c'} \ldots\ldots\ldots(MPa)\ldots \qquad (10)$$

Concrete compressive strength of 20.6 MPa for structural components and 35 MPa for piles is used. Steel used in construction sites shows larger variation between nominal yield strength and the actual yield strength [0]. Yield strength of 390 MPa and elasticity modulus of 200 GPa are used to calculate flexure and shear capacities of beams and columns. Yield strength of steel 1.62 GPa is used for piles. Compressive strength of 4 MPa and elasticity modulus of 1.275 GPa are used for masonry [0, 0].

4.5 Structural Modeling

Analytical model for the evaluation must represent all the influential components in complete three-dimensional characteristics of building behavior, including mass distribution, strength, stiffness, and deformability. The effective initial stiffness is calculated based on ATC-40 [0] recommendations.

4.5.1 Beam-Column Frames

The beam-column frame model should represent the strength, stiffness, and deformation capacity of beams, columns, and beam column joints. Beam-column joints are assumed rigid because they are monolithically cast.

4.5.1.1 *Beam*

Flexure, shear, and development length effects are the three main factors considered in modeling of beam components. In the analytical model of the beam, all the properties are concentrated at the component centerline. This analyzed building has pre-cast slabs at each floor level except at the roof. The stiffness and strength contribution of precst slabs as well as the roof slab are not considered.

Beam flexural and shear capacities vary along the length of the component. Generally, it is required to provide plastic hinges along the centerline so that the beam can develop inelastic response. In this analysis, plastic hinges are assigned only at critical sections. Following the reinforcement detailing given in the drawing, hinges are provided at both ends, midspan, and at intermediate sections based on the reinforcement cut-off details.

4.5.1.2 Column

Two main influential factors considered are shear and flexure with the axial force interaction. In the analytical model of the column, all the properties are concentrated at the component centerline. It is required to define axial force-moment interaction yield surfaces for each assigned flexural plastic hinge. During the analysis, variation of axial force is not significant. Thus, the axial force due to gravity load is selected as the effective axial force for defining necessary parameters.

The analysis option "Restart Using Secant Stiffness", which is recommended in ATC–40 [0], is selected for the pushover analysis. With this option the axial-moment (P-M-M) hinge available in SAP 2000 Nonlinear does not work properly. Therefore, the flexural hinge is assigned to the columns instead of the P-M-M hinge. The yield moment for the flexural hinge is calculated using the axial force-moment interaction diagram and the column axial load due to gravity loads.

Flexural hinges are assigned at column ends. Additional hinges are assigned at intermediate levels when beams are connected at intermediate levels of a column or partial infills are present. Whenever necessary, induced shear forces on columns are checked with the shear capacities of the relevant components.

4.5.2 Masonry Infill Panels

At low levels of an in-plane lateral force, the frame and infill panel act in a fully composite fashion; as a structural wall with boundary elements. When lateral deformations increase, the behavior becomes more complex as a result of the frame attempting to deform in a flexural mode while the panel attempting to deform in a shear mode. The result is a separation between frame and panel at the corners on the tension diagonal, and the development of a diagonal compression strut on the compression diagonal. In this analysis, infill panels are modeled with equivalent strut as per FEMA-273 [0] guidelines.

Failure of a masonry infill is complex and involves combination of bed joint sliding, corner crushing, and diagonal cracking. The exact mode of failure depends upon material properties such as compressive strength (f_m'), shear strength (τ_i), and friction coefficient (μ).

4.5.2.1 Equivalent Strut Model

The stiffness contribution of the infill is represented with an equivalent compression only strut connecting windward upper and leeward lower corners of the infilled frame. In this analytical model the thickness and the modulus of elasticity of the strut are assumed to be the same as those of the infill. The equivalent strut width (a) is determined using the recommended equation given in FEMA-273 [0].

$$a = 0.175\left[\lambda_1 h_{col}\right]^{-0.4} r_{\inf} \qquad (11)$$

$$\lambda_1 = \left[\frac{E_{me} t_{inf} Sin(2\theta)}{4 E_{fe} I_{col} h_{inf}}\right]^{1/4} \qquad (12)$$

Where h_{col} =height of column, E_{me}= modulus of elasticity of masonry infill wall, t_{inf}= thickness of infill wall, θ = aspect ratio of infill wall, E_{fe} = modulus of elasticity of reinforced concrete frame, I_{col} =moment of inertia of reinforced concrete column, and h_{inf} = height of infill wall.

Since it is difficult to give a good representation of infill panel behavior under seismic forces, the experimental studies of the unreinforced masonry shear strength may give greater shear strength than true shear strength of masonry under cyclic loading. By considering above factors and the available test results the equation proposed by Paulay and Priestley [0] for shear strength of uncracked masonry is,

$$\tau_i = \tau_o + \mu f_m \qquad (13)$$

where: f_m is the compressive stress of infill due to gravity load. For typical range of axial compression stresses,

$$\tau_0 = 0.04 f_m' \qquad (14)$$

Infill panels do not have a tight connection with the overlying beam. The vertical extension of tension column tends to separate the frame and the panel along the top edge. Hence, there is no contribution from the term μf_m in Eq. 13 [0]. The horizontal component of the force resisted by the equivalent strut should be compared with the expected shear strength of the infill panel. Hence, the expected infill shear strength is,

$$V_{ine} = A_{ni}\tau_i \qquad (15)$$

4.5.2.2 Load Deformation Relationship

FEMA-273 [0] recommends a nonlinear simplified load-deformation relations for masonry infill panels in the form of story drift ratio. In this analysis effects of partial infill panels are also considered. Since there is no well-established guidelines for modeling of perforated infills, the strut formation is assumed as shown in Figure 5. Shear strength of a panel with opening is considered in proportion to the ratio of the *infilled area/total area* of the panel. The ratio h_{inf}/l_{inf} is assumed to be one. Other modeling parameters are considered in accordance with FEMA-273 [0].

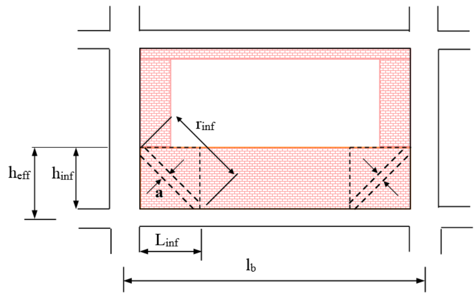

Figure 5: Infill panel with opening

4.5.3 Foundation Model

Foundation is modeled applying the Winkler model concept. This building has two types of foundations, single pile and double-pile, both of the foundation systems do not have dowels connecting the pile and the pile cap. There is no possibility to transfer any moment from column base to the pile. Thus, the foundation was modeled as pin supports. For this model, the column bases are evaluated for the resulting axial and shear forces as well as the ability to accommodate the necessary end rotations of the columns.

5.0 Summary and Conclusions

A 5-story reinforced concrete building is chosen as a representative of typical low-rise reinforced concrete commercial buildings. This building has typical irregular form of structural system found in many parts of the world. Moreover, a poor foundation system and several partial infill masonry panels are some other undesirable features found in this building system. Therefore, to make a realistic seismic evaluation of the building, a complex nonlinear FEM model was developed.

The selected building was analysed to evaluate its seismic performances during the ground motions having 2%, 10%, and 50% of probability of being exceeded in a 50-year period. It was possible to see the effects of two-dimensional and three-dimensional modeling, lateral loading pattern, foundation, and nonstructural components on failure mechanisms. Each and every influential parameter was studied and updated the model step by step to accommodate all the parameters for the seismic evaluation. Finally, three strengthening methods were proposed to overcome the deficiencies in the existing structure.

The following conclusions are derived from this study:

- Existing structure has low level of seismic capacity and may cause the most undesirable brittle failure.
- A lot of earthquake vulnerable features, such as weak/soft story, strong beam/weak column phenomena, torsion, and $P-\Delta$ effects can be found.
- There is not much effect of partial infill panels and foundation on the seismic capacity of this building.
- Though very few irregularities can be identified, they change the structural behavior significantly depending on the analysis methods, 2D or 3D. Some irregularities, which are dominant in 2D analysis, are not effective in 3D analysis.
- Since actual structural behavior is three-dimensional, the most realistic 3D nonlinear FEM model is needed for seismic performance evaluation.
- For the improvement of existing structures, it is possible to test and evaluate many strengthening schemes. Their effectiveness can be clearly seen and quantified. The most cost-effective scheme can be easily identified. For this particular building, it is found that the best way is to improve the deformability of the structure while removing other earthquake vulnerable features of the existing structure. But strengthening of the superstructure is limited by the poor foundation system.

References

[1]. Bertero, V.V. "Major issues and future directions in earthquake-resistant design", *Proceedings of the 10th WCEE*, pp. 6407-6443, 1994.

[2]. Ruiz, S.E., Diederich, R. "The Mexico Earthquake of September 19, 1985 – The Seismic Performance of Buildings with Weak First Storey", *Earthquake spectra*, Vol.5,No.1, 1989.

[3]. Miranda, E., Bertero, V.V. "The Mexico Earthquake of September 19,1985-Performance of Low-Rise Buildings in Mexico City", *Earthquake Spectra*, Vol.5, No.1, 1989.

[4]. Sheu, M. S., Tu, Y. H., Chen, Y. S., and Kuo, S. Y. "Damages of RC Buildings in Chi-Chi Earthquake, Taiwan, September 21, 1999", Department of Architecture, National Cheng-Kung University, Tainan, Taiwan, 2000.

[5]. Murty, C.V.R.. Jain, S. K. "Beneficial Influence of Masonry Infill Walls on Seismic Performance of RC Frame Buildings", *Proceedings 12th WCEE*, Paper No.1790, 2000.

[6]. McCabe, S. L., Thies-Houghton, K. M. "Assessment of Torsional Response of Low-Rise Structures", *Proceedings of 4th U.S. National Conference on Earthquake Engineering*,Palm Springs, California, Vol.2, pp.401-410, 1990.

[7]. ATC-40., Seismic Evaluation and Retrofit of Concrete Buildings. Volume 1, Applied Technology Council, Redwood City,California, 1996.

[8]. FEMA, NEHRP Guidelines for the Seismic Rehabilitation of Buildings, FEMA 273; and *NEHRP Commentary on the Guidelines for the Seismic Rehabilitation of Buildings*, FEMA 274, Federal Emergency Management Agency, Washington, D.C., 1997.

[9]. Miranda, E. "Assessment of The Seismic Vulnerability of Existing Buildings", *Proceedings of the 11th WCEE,* 1996.

[10].MacGregor, J. G., Reinforced Concrete, 3rd ed, Prentice-Hall, Inc. New Jersey, 1997.

[11].Park, R. and Paulay, T., Reinforced Concrete Structures, John Wiley & Sons Inc., 1975.

[12].ACI., ACI Manual of Concrete Practice, Part 3, American Concrete institute, P.O.Box 9094, Farmington Hills, MI 48333, 2012.

[13].Priestley, M. J. N., Verma, R., and Xiao,Y. "Seismic shear Strength of Reinforced concrete Columns", *Journal of Structural Engineering,* Vol.120, No. 8, pp.2310-2329, 1994.

[15].ASCE-ACI Task Committee 426. "The Shear Strength of Reinforced Concrete Members", *Journal of the Structural Division,* Vol.99,No. ST6, pp.1091-1187, 1973.

[16].Paulay, T., Priestley, M.J.N., Seismic Design of Reinforced Concrete and Masonry Buildings. John Wiley and Sons, 1992.

[17].SAP 2000. User Manuals, Computers and Structures, Inc., 2012.

[18].Limpsuwon, A. Reliability of Reinforced Concrete Structures in Bangkok, Research Project No. ST-00-1, Asian Institute of Technology, Thailand, 1988.

[19].Malaivongs, K., The Structural Behavior of brick Infilled Steel Frames. Master Thesis, SEATO graduate School of Engineering, Bangkok, Thailand, 1967.

[20].Tongpatanakul, S., The Structural Behavior of Brick Infilled Reinforced Concrete Frames, Thesis no. 201, Asian Institute of Technology, Thailand, 1968.

SECM/15/35

Construction of Consistent Mass Spring Model Based on Meta-Modeling Theory for Seismic Response Analysis of Large Scale Bridge Structures

J. A. S. C. Jayasinghe[1*], M. Hori[2], M. R. Riaz[1], N. Tamechika[1], M. L. L. Wijerathne[2], and T. Ichimura[2]

[1]Department of Civil Engineering, University of Tokyo, Tokyo, Japan
[2]Earthquake Research Institute, University of Tokyo, Tokyo, Japan
*E-Mail: supun0chamara@gmail.com, TP: +8180-3572-1984

Abstract: Meta-modeling theory is aimed at constructing a set of analysis models which are consistent with continuum mechanics or a solid element model. This paper presents a consistent mass spring model (CMSM) of a large scale bridge structure, which is constructed according to the meta-modeling theory to make efficient seismic response analysis. The CMSM shares the same dynamic characteristics as the solid element model and can be used to study fundamental seismic responses for a complicated large scale bridge structure that consists of piers and decks. In the numerical experiment, time history analysis is made for six different bridge structures. Full comparison is made for a CMSM and a solid element model of these six bridge structures, and it is shown that the CMSM is able to estimate the dynamic responses such as displacement and base shear for a certain class of ground motions.

Keywords: bridge structure, consistent modeling, continuum mechanics, mass spring model, structural mechanics.

1. Introduction

Construction of a few different fidelity models at the beginning of complex structure's analysis [1, 2] is a common practice among present engineers. If a numerical model of desired fidelity could be constructed for a target structure, we can choose a suitable analysis method and operate numerical simulation that uses the analysis model and the analysis method. Such model selection is very important especially for a dynamic seismic analysis of large structure which requires larger numerical computational resources as compared to a quasistatic analysis of small structure.

The fidelity of the model and accuracy of analysis are directly related which means that the highest fidelity model should have highest accuracy among a set of models which is developed for a particular structure. However, different fidelity models ought to share the fundamental dynamic characteristics such as natural frequency. It is meaningless to compare seismic responses of models which have different fundamental dynamic characters.

Mass spring model is popular on account of its simplicity and conservative response predictions, see references [3, 4, 5, 6]. For typical mass spring model, the target structure is discretized with set of beam elements. The lumped mass for each node of spring mass model is estimated from the portion of the weight of target structure, which is called "tributary area consideration". There are mainly two ways to estimate stiffness of spring in typical mass spring model, which are; static and geometric methods [3, 7]. The static method uses an arbitrary static load applied to a single layer of the full (3D) finite element model, it works as a pushover analysis [8, 9], while the geometric method considers the geometric shape of the cross-section to calculate sectional moment of inertia and shearcoefficients.

An issue with the ordinary mass spring model discussed above is that it does not consider the consistency with other more sophisticated models. It is easy to reproduce observed or synthesized dynamic response by tuning of mass spring model's parameters (mass and stiffness) for particular input motion but it may not be applicable for other input motions. However, construction of a consistent mass spring model; the one having same fundamental dynamic characteristics as more sophisticated models, is surely desirable.

The authors are proposing meta-modeling theory [10, 11, 12, 13, 14, 15], which allocates structural mechanics as mathematical approximation of solving a Lagrangian problem of continuum mechanics. The key concept of meta-modeling is that the same physical problem of continuum mechanics is solved by all modelings using distinct mathematical approximations. Therefore, it is well expected to construct a mass spring model of the same fundamental dynamic characteristics as a continuum mechanics model, according to the metamodeling theory.

This paper aims to apply meta-modeling based consistent mass spring model (CMSM) for fundamental seismic response analysis of six bridge structures with different pier arrangements. The contents of this paper are as follows. In Section 2, meta-modeling is briefly explained and in Section 3, the approximations made for deriving the governing equations of the CMSM from continuum mechanics theory are presented. In Section 4, we carry out the numerical experiment to obtain the fundamental seismic response for six multi-span bridge structures by employing CMSMs. Concluding remarks are made at the end in section 5.

2. Meta-modeling theory

In the meta-modeling theory, modeling means to create a mathematical problem for a target physical problem. There are many ways to develop a distinct mathematical problem, depending on the accuracy that is expected in solving the physical problem. The meta-modeling theory delivers a set of consistent modelings which produce an approximate solution of the original modeling. As an example in structural problems, the meta-modeling theory uses continuum mechanics modeling as the basic modeling. Some of the structure mechanics modelings are specified as consistent modelings of the continuum mechanics modeling. Then, those consistent structure mechanics modelings produce an approximate solution of the continuum mechanics modeling.

For simplicity, we assume small deformation, dynamic state, and linear isotropic elasticity. A boundary value problem of solid continuum mechanics is converted to a variational problem of using a Lagrangian,

$$\mathcal{L}[\mathbf{v},\boldsymbol{\epsilon}] = \int_V \frac{1}{2}\rho\mathbf{v}\cdot\mathbf{v} - \frac{1}{2}\boldsymbol{\epsilon}:\mathbf{c}:\boldsymbol{\epsilon}\,\mathrm{d}v \quad (1)$$

where $\mathbf{v}$ is velocity, ρ is density, $\boldsymbol{\epsilon}$ is strain tensor and $\mathbf{c}$ is elasticity tensor; for a given displacement vector, $\mathbf{u}$, $\boldsymbol{\epsilon}$ is computed as $\boldsymbol{\epsilon} = sym\{\nabla\mathbf{u}\}$ where sym stands for the symmetric part of the secondorder tensor of $\nabla\mathbf{u}$ and ∇ stands for spatial differentiation operator; and V is the analysis domain.

In structural mechanics, the integral of $\frac{1}{2}\boldsymbol{\epsilon}:\mathbf{c}:\boldsymbol{\epsilon}$, (i.e., strain energy density) is replaced by, say, $\frac{1}{2}E\epsilon^2$, for bar theory [16], where ϵ is a normal strain component and E is Young's modulus. This strain energy density corresponds to a stress-strain relation of $\sigma = E\epsilon$, where σ is normal stress component in the same direction as ϵ. However, for this stress strain relation to hold, normal strain components in the transverse directions are non-zero. Therefore, $\sigma = E\epsilon$ is often regarded as an assumption of one dimensional stress-strain relation. It is not acceptable to make an assumption which is not experimentally validated. As mentioned, $\sigma = E\epsilon$ holds when transverse normal strain components are non-zero, but the presence of these components are ignored. Meta-modeling replaces the integrand and changes the Lagrangian in the following form:

$$\mathcal{L}^*[\mathbf{v},\boldsymbol{\epsilon},\boldsymbol{\sigma}] = \int_V \frac{1}{2}\rho\mathbf{v}\cdot\mathbf{v} - \left(\boldsymbol{\sigma}:\boldsymbol{\epsilon} - \frac{1}{2}\boldsymbol{\sigma}:\mathbf{c}^{-1}:\boldsymbol{\sigma}\right)\mathrm{d}v \quad (2)$$

where $\boldsymbol{\sigma}$ is stress tensor and $\mathbf{c}^{-1}$ is the inverse of $\mathbf{c}$. By selecting σ as a unique non-zero component of $\boldsymbol{\sigma}$, without making any assumption, we can derive $\sigma = E\epsilon$ from $\delta\mathcal{L}^* = 0$ with respect to $\boldsymbol{\sigma}$ (or σ) for quasi-static state.

The use of the Lagrangian of Eq. (2) is the basic concept of meta-modeling. The governing equations of beam theory and plate theory are derived from this $\mathcal{L}^*$, just by using a suitable subset of the function space of $\{\mathbf{u},\}$, from which the arguments of $\mathcal{L}^*$, i.e., $\boldsymbol{\epsilon}$ and $\boldsymbol{\sigma}$, are computed. We have to emphasize that there is no need to make a physical assumption of $\sigma = E\epsilon$, (which is not experimentally validated), in deriving the governing equations. We regard using a subset of $\{\mathbf{u}, \boldsymbol{\sigma}\}$ to solve $\delta\mathcal{L}^* = 0$ as mathematical approximation.

3. Consistent mass spring model

A mass spring model is a set of masses and linear springs, and the direction of the mass movement is fixed. As the simplest case, we study a mass spring model which consists of two masses. We seek to construct a mass spring model which shares the same fundamental dynamic characteristics as continuum mechanics; this model is called consistent mass spring model (CMSM).
According to the meta-modeling theory, we consider an approximate displacement function of the following form:

$$(\mathbf{x}, t) = \sum_{\alpha=1}^{2} U(t)\boldsymbol{\phi}^{\alpha}(\mathbf{x}), \tag{3}$$

where U^{α} is displacement of the α-th mass point and $\boldsymbol{\phi}^{\alpha}$ is the corresponding displacement mode. By definition, the displacement is required to satisfy the following two requirements:

A1) $(\mathbf{x}^{\alpha})$ is a unit vector.

A2) $(\mathbf{x}^{\beta})$ vanishes for $\alpha \neq \beta$.

Here, $\mathbf{x}^{\alpha}$ is the location of the α-th mass point. We substitute Eq. (3) into Eq. (1), and obtain

$$\mathcal{L} = \sum_{\alpha,\beta=1}^{2} \frac{1}{2} m^{\alpha\beta} \dot{U}^{\alpha} \dot{U}^{\beta} - \frac{1}{2} k^{\alpha\beta} U^{\alpha} U^{\beta}, \tag{4}$$

where

$$m^{\alpha\beta} = \int_V \rho \boldsymbol{\phi}^{\alpha} \cdot \boldsymbol{\phi}^{\beta} \, \mathrm{d}v, \quad k^{\alpha\beta} = \int_V \nabla\boldsymbol{\phi}^{\alpha} : \mathbf{c} : \nabla\boldsymbol{\phi}^{\beta} \, \mathrm{d}v. \tag{5}$$

Since a Lagrangian of a conventional mass spring model of two masses is in the form of

$$\frac{1}{2}(\cdot)(\dot{U}^1)^2 + \frac{1}{2}(\cdot)(\dot{U}^2)^2 - \frac{1}{2}(\cdot)(U^2 - U^1)^2 - \frac{1}{2}(\cdot)(U^2)^2$$

with $(\cdot)$ being a suitable scalar, $\mathcal{L}$ of Eq. (4) becomes the above, if the following two requirements are satisfied:

B1) $m^{12} = 0$.

B2) $k^{12} + k^{22} = 0$.

It is readily seen that finding two functions $\boldsymbol{\phi}^1$ and $\boldsymbol{\phi}^2$ which satisfy the four conditions of A1, A2, B1 and B2 is generally not possible.

Now we can consider dynamic mode shapes to construct a mass spring model, so that it shares the same dynamic fundamental characteristics with a continuum model. We suppose that two dynamic modes $\{\boldsymbol{\psi}^{\alpha}, \omega^{\alpha}\}$ ($\alpha = 1$ or 2), are given; $\boldsymbol{\psi}^{\alpha}$ is a mode shape and ω^{α} is a natural frequency. Recall that the dynamic mode satisfies

$$(\omega^{\alpha})^2 \boldsymbol{\psi}^{\alpha} + \nabla \cdot (\mathbf{c} : \nabla\boldsymbol{\psi}^{\alpha}) = 0, \tag{6}$$

and

$$\int_V \rho \boldsymbol{\psi}^{\alpha} \boldsymbol{\psi}^{\beta} \, \mathrm{d}v = 0, \quad \int_V \nabla\boldsymbol{\psi}^{\alpha} : \mathbf{c} : \nabla\boldsymbol{\psi}^{\beta} \, \mathrm{d}v = 0, \tag{7}$$

for $\alpha \neq \beta$.

We can use Eq. (1) or (2) but for simplicity, we use $\mathcal{L}$ of Eq. (1), and, substituting $\mathbf{u} = \sum u^{\alpha} \boldsymbol{\psi}^{\alpha}$ into it, we obtain

$$\mathcal{L} = \sum_{\alpha,\beta=1}^{2} \frac{1}{2} m^{\alpha} (\dot{U}^{\alpha})^2 - \frac{1}{2} k^{\alpha} (U^{\alpha})^2 \tag{8}$$

where

$$m^{\alpha} = \int_V \rho \boldsymbol{\psi}^{\alpha} \cdot \boldsymbol{\psi}^{\alpha} \, \mathrm{d}v, \quad k^{\alpha} = \int_V \nabla\boldsymbol{\psi}^{\alpha} : \mathbf{c} : \nabla\boldsymbol{\psi}^{\alpha} \, \mathrm{d}v. \tag{9}$$

Due to the orthogonality, Eq. (7), $\{\boldsymbol{\psi}^{\alpha}\}$ does not produce cross terms. Furthermore, due to Eq. (6), it is readily seen that m^{α} and k^{α} of Eq. (9) satisfy

$$(\omega^{\alpha})^2 m^{\alpha} = k^{\alpha}, \tag{10}$$

for $\alpha = 1$ and 2.

Now, we seek to find suitable linear combinations of $\{\boldsymbol{\psi}^{\alpha}\}$ that satisfy the requirements A1 and A2. To this end, we consider the following combination:

$$\boldsymbol{\phi}^{\alpha} = \sum t^{\alpha\beta} \boldsymbol{\psi}^{\alpha}, \tag{11}$$

where $t^{\alpha\beta}$ is a component of two-by-two matrix. It is readily seen that this matrix can be determined when $\boldsymbol{\psi}^1$ and $\boldsymbol{\psi}^2$ do not change the direction and are parallel to each other.

4. CMSM for bridge structures

4.1 Problem setting

As a more realistic example, a CMSM is constructed for a set of multi-span curved and straight continuous bridge structures. Three curved and three straight bridge structures with different types of pier arrangement are studied; see Figure 1. The longitudinal and transverse directions are considered separately in this numerical study. The CMSM for the transverse direction includes two dynamic modes while that for the longitudinal direction uses only first mode. This is because in the longitudinal direction, the first mode has much lower natural frequency than other modes.

A schematic view of the CMSM with the third spring that connects the top mass to the ground is shown in Figure 2. The stiffness values, K_1, K_2 and K_3, are computed as follows:

$$K_1 = k_{22} + k_{12},\ K_2 = -k_{12},$$

$$\text{and}\ \ K_3 = k^{11} + k^{12}.$$

Tie connection is used for the connection between the pier and the deck in this problem. This is the simplest connection, and more sophisticated connection could be used if more detailed information is available for the connection. Table 1 shows the material properties of both the pier and the deck. Linear isotropic elasticity is assumed. The ground motion displayed in Figure 3 is employed. frequency domain.

First, we construct a solid element model, in order to obtain first two dynamic mode shapes in the transverse direction ($\boldsymbol{\psi}^1{}_z$ and $\boldsymbol{\psi}^2{}_z$) and first dynamic mode shape in the longitudinal direction ($\boldsymbol{\psi}^1_x$); see Figure 4(a) and 5(a) for $\boldsymbol{\psi}^1{}_z$ and $\boldsymbol{\psi}^2{}_z$ of cases SC_1 and CC_1 respectively. Approximate displacement functions ($\boldsymbol{\phi}^1{}_z$ and $\boldsymbol{\phi}^2{}_z$) of cases SC_1 and CC_1 for transverse direction are shown in Figure 4(b) and 5(b) respectively. Second, we determine locations of

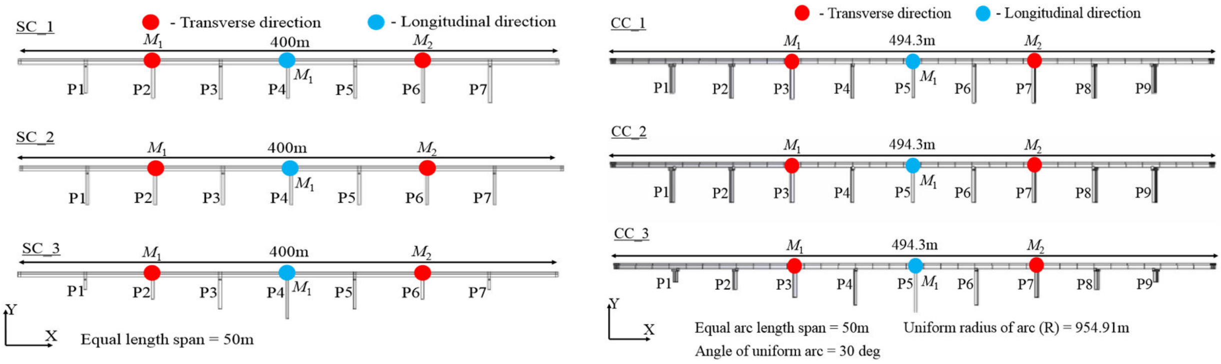

(a) (b)

Figure 1: Geometric and mass points' information about multi-span bridge structures: (a) straight continuous (SC); and (b) curved continuous (CC).

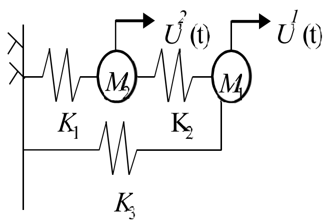

Figure 2: Schematic view of a consistent mass spring system consisting of two mass points.

Table 1: Material data of multi- span bridge structures (SC & CC).

Item	E / GPa	ρ / Kgm^{-3}	v
Pier	24	2400	0.2
Deck	200	2000	0.3

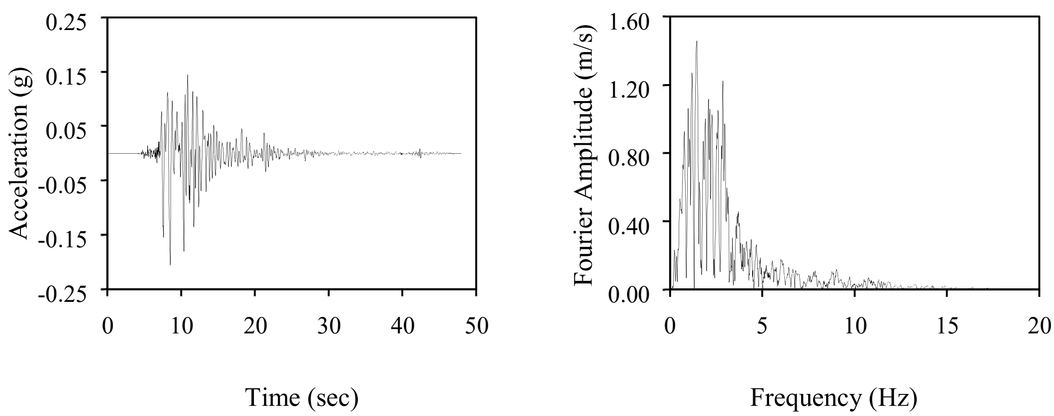

(a) (b)

Figure 3: Input ground motion for multi-span bridge structure: (a) in time domain; and (b) in frequency domain

mass points along the deck axis, considering target locations of response output from the models; see Figure 1. Third, CMSM parameters are computed from the dynamic mode shapes and the mass points' location.

4.2 Results and discussion

Natural frequencies of the CMSMs in the transverse and longitudinal directions are presented in Tables 2 and 3, respectively; the natural frequencies of the original solid element models are presented, too. As is seen, the natural frequencies of the CMSMs coincide with those of the solid element models.

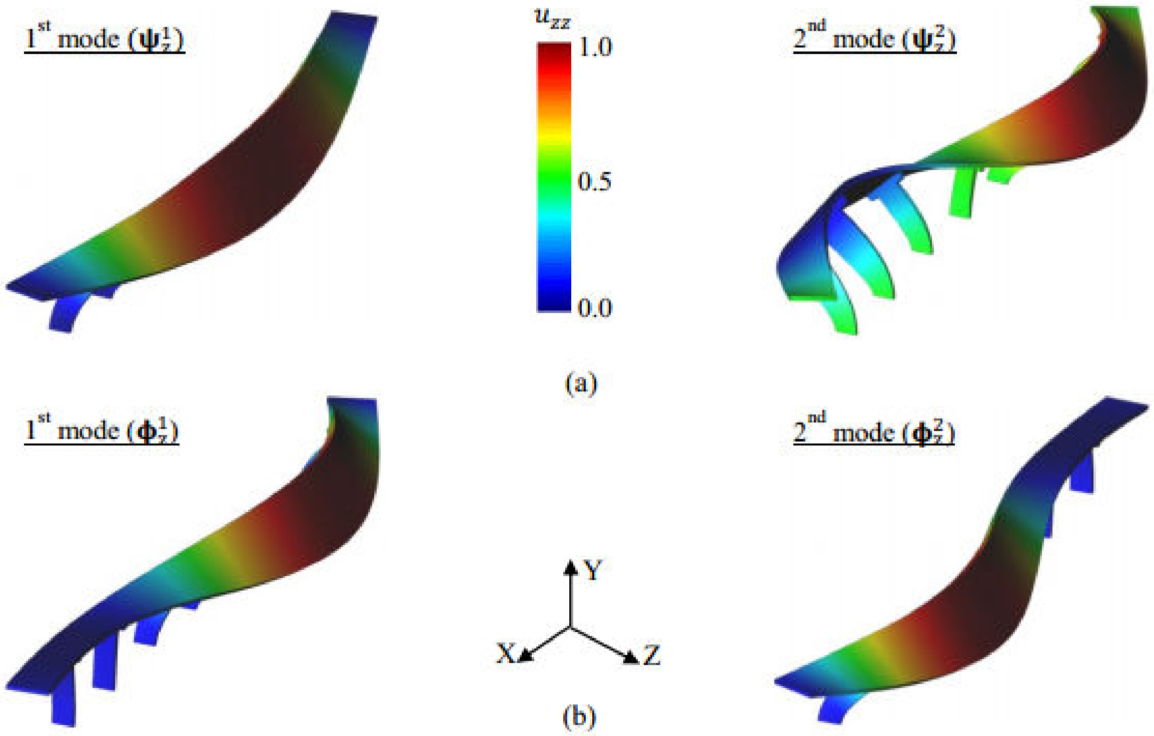

Figure 4: Solid bridge model along the transverse direction of bridge (SC_1): (a) first two dynamic modes; and (b) developed approximate displacement modes.

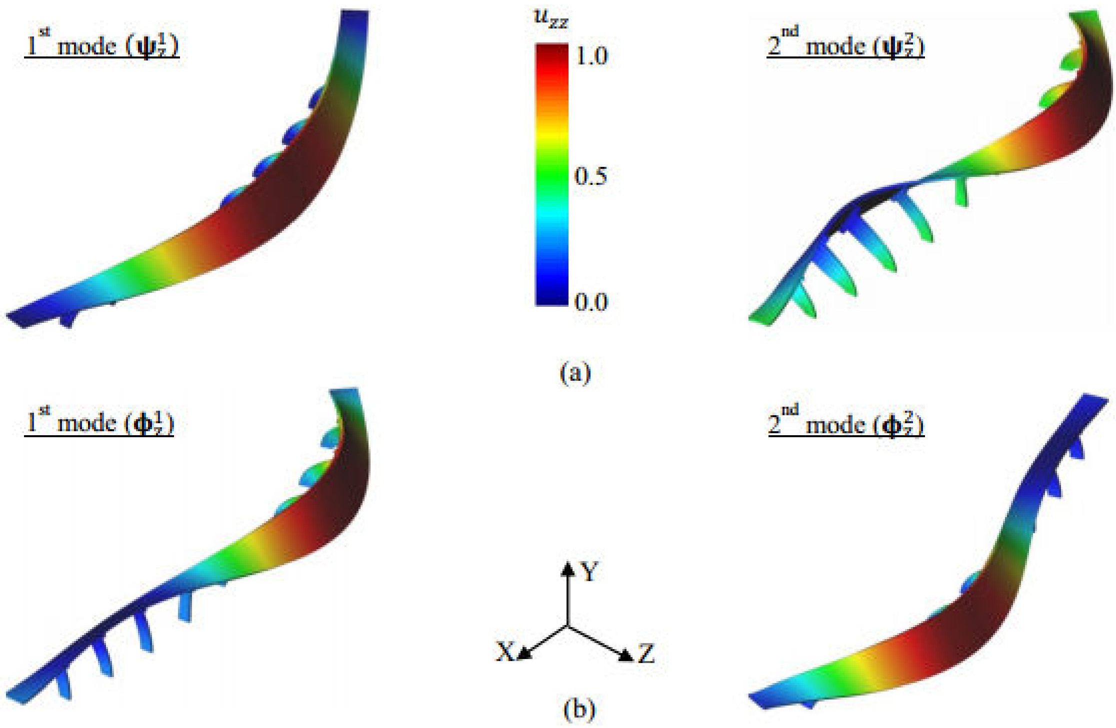

Figure 5: Solid bridge model along the transverse direction of bridge (CC_1): (a) first two dynamic modes; and (b) developed approximate displacement modes.

Table 2: Natural frequencies along the transverse direction of multi-span bridge structure (CMSM and solid element model)

Case ID	Frequency / (Hz)				Difference / (%)	
	CMSM		Solid			
	1st mode	2nd mode	1st mode	2nd mode	1st mode	2nd mode
SC_1	1.625	2.610	1.624	2.610	0.062	0.000
SC_2	1.752	2.703	1.752	2.702	0.000	0.037
SC_3	2.191	3.882	2.190	3.881	0.046	0.026
CC_1	1.541	2.152	1.540	2.151	0.065	0.046
CC_2	1.692	2.254	1.692	2.253	0.000	0.044
CC_3	1.894	3.131	1.893	3.130	0.053	0.032

Table 3: Natural frequencies along the longitudinal direction of multi-span bridge structure (CMSM and solid element model)

Case ID	Frequency / (Hz)		Difference / (%)
	CMSM	Solid (1st mode)	
SC_1	0.630	0.630	0.000
SC_2	0.680	0.680	0.000
SC_3	1.640	1.640	0.000
CC_1	0.713	0.712	0.140
CC_2	0.730	0.730	0.000
CC_3	1.624	1.623	0.062

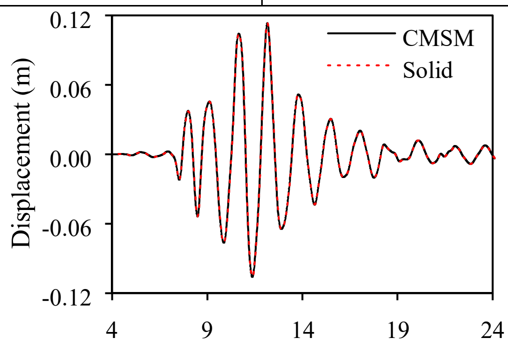

(a)

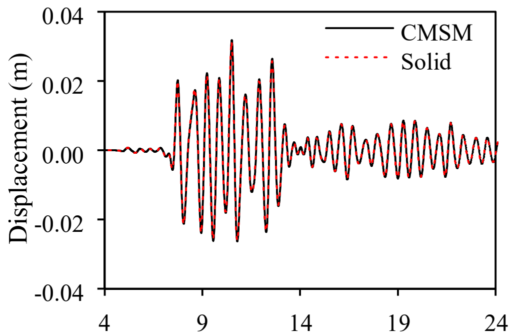

(b)

Figure 6: The displacement results of SC_1 at M_I mass point location: (a) the CMSM for the longitudinal direction (z-direction); and (b) the CMSM for the transverse direction (x-direction).

Time series of displacement responses of the CMSM is compared with that of the original solid element model; see Figure 6 for case SC_1. It is seen that the response of the CMSM matches well with that of the solid element model. Relative errors of the maximum displacement in the longitudinal and transverse directions of the CMSM are presented in Tables 4(a) and 4(b), respectively. As is seen, the maximum relative error in all the cases is 2.852%

Next, shear force values at the base of the fourth pier (P4) are estimated; see Figure 1 for the location of P4. The cross sectional shear force is computed as follows:

$$\mathsf{F}(t) = \sum u^{\alpha}(t) \int \mathbf{n} \cdot (\mathbf{c}(\mathbf{0}) \colon \nabla \boldsymbol{\psi}^{\alpha}(\mathbf{0}))\mathrm{d}s, \tag{6}$$

where $\mathbf{x} = \mathbf{0}$ corresponds to the base of the target pier, $\mathbf{n}$ is the unit normal on base, and the surface integration is made on the base. This computation is logical in the sense that the present CMSM is essentially the same as the modal analysis [5, 6, 17], and is able to compute local responses by using the approximate displacement, i.e., $\mathbf{u} = \sum u^\alpha \boldsymbol{\psi}^\alpha$.

In Figure 7, **F** is presented for the longitudinal and transverse directions. Relative errors of the maximum resultant force are summarized in Tables 5(a) and 5(b). As is seen, the maximum relative error in all the cases is 3.524%, and it is clear that the CMSM can be used to approximately estimate structural seismic responses for certain class of ground motions which cause a target bridge structure to mainly excite in its first two modes.

5. Conclusions

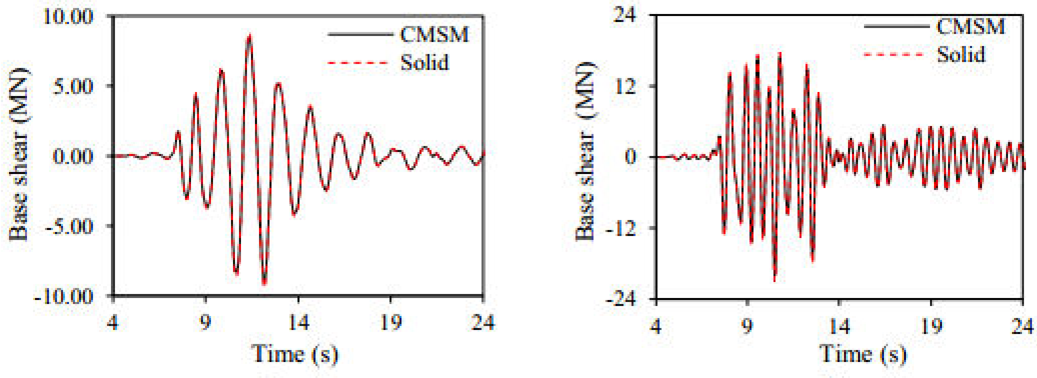

Figure 7: The resultant shear force of SC_1 at base of P4: (a) the CMSM for the longitudinal direction (z-direction); and (b) the CMSM for the transverse direction (x-direction).

Table 4: Relative error for the maximum displacement between solid element model and CMSM: (a) the CMSM for the longitudinal direction; and (b) the CMSM for the transverse direction.

(a)

Case	Location	Error / (%)
SC_1	M_1	1.027
SC_2	M_1	1.145
SC_3	M_1	1.403
CC_1	M_1	2.230
CC_2	M_1	1.313
CC_3	M_1	1.953

(b)

Case	Location	Error / (%)
SC_1	M_1	1.201
	M_2	1.206
SC_2	M_1	1.025
	M_2	1.024
SC_3	M_1	1.995
	M_2	1.992
CC_1	M_1	2.195
	M_2	2.192
CC_2	M_1	2.852
	M_2	2.799
CC_3	M_1	2.804
	M_2	2.710

Table 5: Relative error for the maximum resulting shear force at base of P4 between solid element model and CMSM: (a) the CMSM for the longitudinal direction; and (b) the CMSM for the transverse direction.

(a)

Case	Error / (%)
SC_1	2.254
SC_2	2.547
SC_3	3.210
CC_1	3.312
CC_2	3.524
CC_3	3.425

(b)

Case	Error / (%)
SC_1	2.985
SC_2	2.958
SC_3	3.058
CC_1	3.124
CC_2	3.460
CC_3	3.451

In this paper, we propose a consistent mass spring model (CMSM) for fundamental seismic response analysis of a bridge structure. While CMSM contains additional springs in comparison to conventional mass spring models, the CMSM shares fundamental dynamic characteristics and is able to yield structure seismic responses which agree well with those of original models (solid element model). Six different bridge structures are tested successfully in this study. In particular, the resultant force at a specific cross section can be estimated accurately for certain class of ground motions which cause a target bridge structure to mainly excite in its first two modes.

There is a possibility of constructing a more accurate CMSM, by extending the number of mass points. Also, there is a possibility of extending a CMSM to non-linear structure. At least, it is straightforward to apply the meta-modeling to incremental responses of a non-linear elasto-plastic structure.

References

[1]. Bose, M. K., Soni, R. S., Mahajan, S. C., and Kakodkar, A., "Strain Energy Concept for Developing Lumped Mass Stick Model of Complex Structures," in 11th World Conference on Earthquake Engineering, 1996.

[2]. Lee, H., Roh, H., Youn, J., and Lee, J. S., "Frequency Adaptive Lumped-Mass Stick Model and Its Application to Nuclear Containment Structure", in 15th World Conference on Earthquake Engineering, Lisbon, Portugal, 2012.

[3]. Varma, V., Reddy, G. R., Vaze, K. K., and Kushwaha, H. S., "Simplified approach for sesmic analysis of structures", International Journal of Structural Stability and Dynamics, Vol. 2, pp. 207-225, 2002.

[4]. Huang, Y. N., Whittaker, A. S., and Luco, N., "Seismic performance assessment of baseisolated safety-related nuclear structures", Earthquake Engineering and Structural Dynamics, Vol. 39, pp. 1421-1442, 2010.

[5]. Clough, R. W., and Penzien, J., Dynamics of structures, 2nd ed., McGraw-Hill, New York,2000.

[6]. Chopra, A. K., Dynamics of Structures (Theory and Applications to Earthquake Engineering), 3rd ed., Prentice Hall, New Jersey, 1995.

[7]. Soni, R. S., Reddy, G. R., Kushwaha, H. S., and Kakodkar, A., "A unified approach for the seismic analysis of 500 Mwe PHWR building", in Proceeding of 9th Structural Mechanics in Reactor Technology (SMIRT-9), Lausane, Switzerland, 1987.

[8]. Paraskeva, T. S., Kappos, A. J., and Sextos, A. G., "Extension of modal pushover analysis to seismic assessment of bridges", Earthquake Engineering and Structural Dynamics, Vol. 35, no 10, pp 1269–1293, 2006.

[9]. Makarios, T. K., and Salonikios, T. N., "Use of New Equivalent Nonlinear SDF System of Planar Multi-Story R/C Frames in Static Pushover Procedure", in 14th World Conference on Earthquake Engineering, 2008.

[10]. Hori, M., Maggededaera, L., Ichimura, T., and Tanaka, S., "Meta-Modeling for Constructing Model Consistent with Continuum Mechanics," Journal of Structural Mechanics and Earthquake Engineering, vol. 9, no. 4, pp. 269–275, 2014.

[11]. Jayasinghe, J. A. S. C., Tanaka, S., Wijerathne, L., Hori, M., and Ichimura, T., "Rigorous Conversion of Solid and Beam Element Solutions Based on Meta Modeling," Journal of JSCE (Applied Mechanics), vol. 70, no. 2, pp. 223–233, 2014.

[12]. Jayasinghe, J. A. S. C., Tanaka, S., Wijerathne, L., Hori, M., and Ichimura, T., "Automated Construction of Consistent Lumped Mass Model for Road Network," Journal of JSCE (Structural and Earthquake Engineering), vol. 71, 2015.

[13]. Hori, M., Tanaka, S., Wijerathne, L., Ichimura, T., and Jayasinghe, J. A. S. C., "Meta-Modeling for Consistent Seismic Response Analysis," in 5th ECCOMAS Thematic Conference on Computational Methods in Structural Dynamics and Earthquake Engineering, Crete Island, Greece, 2015.

[14]. Jayasinghe, J. A. S. C., Tanaka, S., Wijerathne, L., Hori, M., and Ichimura, T., "Conversion Between Solid and Beam Element Solutions of Finite Element Method Based on Meta-Modeling," in ICCBEI (2nd International Conference), Tokyo, Japan, 2015.

[15]. Hori, M., Ohtani, H., Jayasinghe, J. A. S. C., Maddegedara, L., Ichimura, T. and Fujita, K.: Automated Model Construction for Integrated Earthquake Simulation, CC2015, Fifteenth International Conference on Civil, Structural and Environmental Engineering Computing, Prague, Czech Republic, 2015.

[16]. Doyle, J. F., Wave Propagation in structures (Mechanical engineering series), 2nd ed., Springer, New York, 1997.

[17]. He, J., and Fu, Z. F., Modal Analysis. Butterworth-Heinemann, Boston, 2001.

SECM/15/55

Concrete Filled Steel Tubes for Performance Improvement of Steel Truss Bridges

H. M. G. U. Karunarathna[1] and K. A. S. Susantha[2*]

[1]Central Engineering Consultancy Bureau, Colombo, Sri Lanka
[2]University of Peradeniya, Kandy, Sri Lanka
*E-Mail: samans@pdn.ac.lk, TP: +94812393351

Abstract: The use of concrete-filled steel tubes (CFST) in engineering structures has become popular because of their excellent seismic resistance structural properties such as high strength, high ductility and large energy absorption capacity. In CFSTs the surrounding steel tube provides effective confinement to the filled-in concrete and in turn the concrete helps to reduce the potential local buckling of the steel tube resulting improved seismic resistant performance. This study aimed at investigating the benefit of CFST members in railway steel truss bridges susceptible to earthquake loads. Since the end frames of truss bridges are mainly subjected to compressive loads CFST is a good alternative for end raker. The steel weight of the rib can be reduced with CFST and hence the method is economically sound. The seismic behaviour of steel truss bridges with steel and CFST end rakers is discussed based on the results of nonlinear time history analyses. Five truss bridges were designed with different types of end rakers namely existing HEB end raker, square hollow end raker, three square hollow CFST end raker bridges with varying concrete grades. Time history analyses were performed for transverse direction using selected past earthquakes and natural frequencies, maximum vertical and lateral deflections, residual vertical and lateral deflections and member stresses were checked. It was found that the use of CFST in steel truss bridges can be effectively utilized to improve the seismic resisting performance.

Keywords: Concrete-filled steel tube, truss bridges, material nonlinearity, seismic resistance capacity

1. Introduction

The use of concrete-filled steel tube (CFST) is a well-recognized technique for improving strength and ductility of steel structures. It is economical as CFTS members have much higher strength than the sum of individual strengths of equivalent steel and concrete members. The CFST is essentially a composite member where, usually, thin-walled steel tube is filled with concrete. The concrete in the tube improves the stability of the thin-walled steel tube in compression and delays its local buckling while steel tube confines the inside concrete resulting triaxial compression stress state in the concrete. Therefore, CFST has higher compression capacity and ductility [1, 2, 3, 4, 5, 6]. Moreover, in construction the tube acts as the formwork for the concrete. Hence, the technique is good for the application in bridges for members with compressive force and bending moments [7, 8, 9].

The ultimate strength of CFST members highly depends on the material properties such as yield strength of steel and compressive strength of the concrete and geometrical properties such as width-to-thickness ratio or diameter-to-thickness ratio of cross section [6]. The tubes can provide good confinement when circular hollow sections are used, especially, when the diameter to thickness ratio (*D/t* ratio) is small. Local buckling of steel tube is not likely to occur when *D/t* ratio is lower than 40 [10, 11, 12].

The CFST members have been innovatively applied in various structures as bridges, roof structures, sports stadiums, multi storey frame buildings with excellent seismic resistance. For bridges, CFST is adopted for arch ribs, members of truss girders and piers of which the members induced axial compression forces and bending moments [13, 14].

In this research seismic behaviour of a railway truss bridge is investigated based on the results of series of nonlinear dynamic analyses. An existing modified warren type 47.344 m span railway truss bridge at Kalutara on Southern Railway line in Sri

Lanka was modelled using finite element analysis method with and without CFST member for end raker. End raker is the end diagonal member of main truss which create the end frame of bridge to withstand lateral loads. With the use of time-history analyses performed in transverse direction for selected past earthquakes, maximum stresses and deflections were studied in view of identifying the effects of CFST members in improvement of seismic resisting capacity of steel truss bridges.

2. Design of Steel Bridges

The end raker of the existing single track railway bridge was checked for induced maximum design forces and verified the available member has an adequate strength to withstand the loads. For that, a linear static analysis was performed for relevant railway loads specified in BS 5400 part 2 [15] and Railway track and bridge manual [16]. The member was designed according to BS 5400 part 3 code [17]. Then another four bridges were designed for the purpose of comparison of performance of the bridges by replacing the end raker member with square hollow steel section and CFST members. The CFST member was designed according to the method in BS 5400-5 code [18].

The strength of steel was 350 N/mm^2 and concrete was varied from 30 N/mm^2 to 50 N/mm^2. Square hollow sections with B/t ratio lower than 40 were used for the end raker. The bridges are of modified warren type trusses with 47.344 m long span. First bridge, namely HEB, was with a European standard wide flange H steel beam (section HEB 300). Second bridge, namely SHS, was with square hollow section (section SHS 250x250x12.5mm) and the third bridge, namely CFST-C40, was with a square hollow section (section SHS 250x250x8mm) filled with grade 40 concrete.

3. Finite Element Model

Three types of truss bridges including existing railway bridge designed as explained in the previous chapter were modelled using finite element program OpenSees [19]. The software can be employed for linear and nonlinear structural and geotechnical modelling. In addition to the designed CFST end raker bridge with C40 filled in concrete, another two bridges with CFST end rakers with grades C30 and C50 concrete were modelled for the purpose of comparison. The model created with force based beam column elements for main truss girder members, stringers, cross girders and bracings as shown in Figure 1. The cross sections of H beam, hollow and composite members were divided into number of segments (fibres). The fibre arrangements of three basic types of end raker members are shown in Figure 2. The fibre sections of components were interpreted by assigning available uniaxial stress-strain relations for steel and concrete for discretised smaller regions.

The uniaxial bilinear material model assigned for steel consists of Young's modulus, E = 205 GPa, yield strength, Fy = 355 Mpa and hardening ratio, b = 0.015. For filled-in concrete in CFST members, a uniaxial concrete model with zero tensile strength was used. The parameters used for the model are; compressive strength, fpc = 40 Mpa, strain at fpc, epsc0 = 0.002, crushing strength, fpcu = 8 MPa and strain at fpcu, epsu = 0.0037. The unconfined concrete model explained in M. K. M. Reddiar [20] was adopted here.

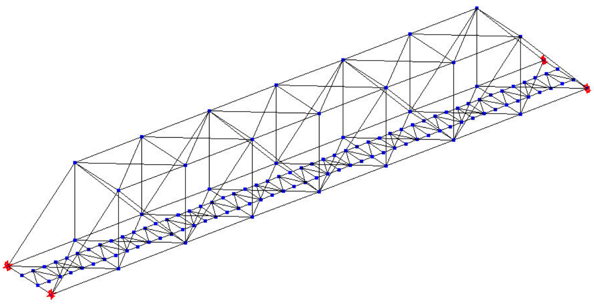

Figure 1: Finite Element Model of Bridge

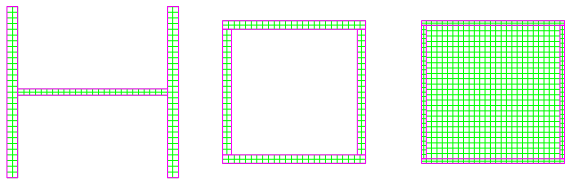

Figure 2: Fibre arrangements of end raker members

To evaluate the earthquake response characteristics, a time history analysis was performed considering the material nonlinearity. The time history analysis was carried out for each model for several past earthquakes recorded in different parts of the world. The relevant acceleration records were downloaded from PEER database [21]. The main parameter considered in selecting the earthquake records was the peak ground acceleration (PGA) even though the duration of the earthquake and local ground condition are also considered to be important in identifying behaviour of structures.

The names and PGA of the earthquake records used in this study are listed in Table 1. Each earthquake has two horizontal components. The analyses were carried out only in transverse direction of the bridge. Some selected components of these earthquake records are shown in Figure 3.

The selected earthquake records represent minor, moderate and severe earthquakes. Thus, the effects of use of CFSTs in truss bridges are investigated for different magnitudes of ground accelerations.

Table 1: Selected earthquake records and their peak ground accelerations (PGA)

Earthquake	Peak Ground Acceleration (PGA)/(g)
Cape Mendocino – 1992	0.178
Whittier Narrows – 1987	0.304
Coyote Lake – 1979	0.434
Erzincan – 1992	0.515
Victoria Mexico – 1980	0.621
Landers – 1992	0.721
Kobe – 1995	0.821

4. Results and Discussion

The results of the time history analysis of each bridge model under each earthquake which are recorded to estimate the influence of the earthquakes for the bridge are summarized here. The fundamental periods *(T)* of each bridge are listed in Table 2. It is clear from these results that fundamental periods of all three bridges do not differ much. This means that concrete-infilling does not have a great effect on fundamental periods. This will be useful in seismic design of CFST truss bridges.

The displacements of Node 1 and Node 2 which are located at the top of the end frame and mid span of the top chord consecutively are recorded for static and time history analysis. The maximum stresses induced in steel and concrete also presented separately for each type of analysis. Figure 4 shows Node 1, 2 and end raker member of which the results were obtained.

The maximum vertical deflections of the bridges from static analysis are given in Table 3. The displacements at Node 1 represents by $\delta max,z_1$ while displacement at Node 2 represent by $\delta max,z_2$. Maximum vertical displacements at two nodes have been slightly decreased when CFST member introduced and the bridge type CFST-C50 has the minimum vertical displacement among five. This is due to the fact that stiffness of the bridge increases with concrete infilling and the grade of the concrete increasing. On the other hand, the effect due to increase of self-weight would not be significant compared to the increase of stiffness. This fact was evident in fundamental periods of the bridges as well. The maximum steel and concrete stresses induced in extreme fibres of end raker member are given in Table 4. The stress in steel has been reduced when CFST end raker introduced. However, maximum concrete stress in CFST has been increased when the grade of the concrete increased.

The maximum lateral displacements of the Node 1 ($\delta max,y_1$) and Node 2 ($\delta max,y_2$) of the bridge subject to each earthquake are summarized in Table 5 and 6, respectively. It is noted that the maximum horizontal displacements at Node 1 and Node 2 have been slightly increased in most of the earthquakes when CFST members introduced. However, displacement at Node 1 in Victoria-1980 earthquake and displacement at Node 2 in Vicoria-1980 and Kobe-1995 earthquakes were slightly decreased in CFST bridges.

The lateral residual displacement of the Node 1 ($\delta res,y_1$) and Node 2 ($\delta res,y_2$) of the bridge are summarized in Table 7 and 8, respectively. The residual displacement in lateral direction at Node 1 and Node 2 have been slightly decreased in Cape Mendocino-1992, Coyote Lake-1979 and Kobe-1995 earthquakes while slightly increased in other earthquakes.

The maximum steel and concrete stresses induced in extreme fibres of end raker member are summarized in Table 9 and 10. The maximum steel stress induced in the end raker member was decreased when CFST member introduced. When the grade of the concrete increased, the stress has been further reduced. However, the maximum concrete stress in CFST has been increased when the grade of the concrete increased. These results imply that the response depends not only on PGA but also on features like period and duration of ground accelerations.

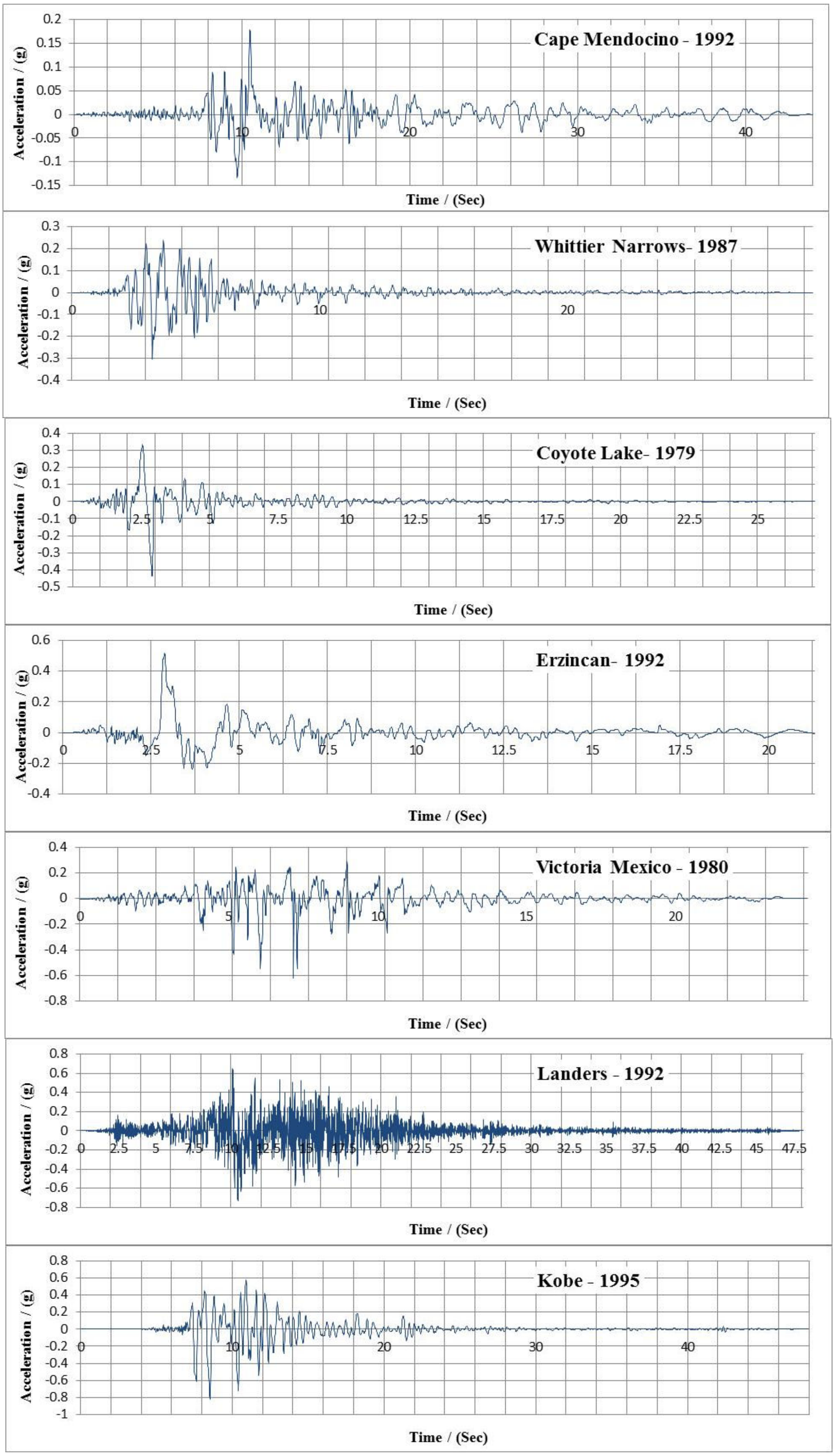

Figure 3: Selected components of earthquake records

Table 2: Fundamental periods

Bridge	T / (Sec)
HEB	1.107
SHS	1.096
CFST-C30	1.095
CFST-C40	1.096
CFST-C50	1.098

Table 3: Maximum vertical deflections (static analysis)

Bridge	$\delta max,z_1$ /(mm)	$\delta max,z_2$/(mm)
HEB	28	73
SHS	29	74
CFST-C30	28	73
CFST-C40	27	73
CFST-C50	26	72

Table 4: Maximum stresses (static analysis)

Bridge	Steel/(N/mm^2)	Concrete/(N/mm^2)
HEB	-185	-
SHS	-193	-
CFST-C30	-169	-19
CFST-C40	-153	-24
CFST-C50	-142	-28

Table 5: Maximum lateral displacement at Node 1

Earthquake	Maximum displacement / (mm)				
	HEB	SHS	CFST-C30	CFST-C40	CFST-C50
Cape	24	27	28	27	27
Whittier	50	54	55	54	54
Coyote Lake	97	109	111	110	109
Erzincan	218	254	267	263	260
Victoria	51	51	51	51	50
Landers	56	63	64	63	62
Kobe	164	173	175	174	174

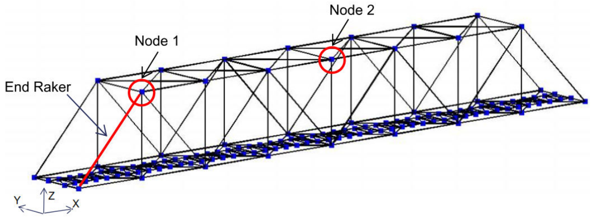

Figure 4: Node 1, Node 2 and end raker member

Table 6: Maximum lateral displacement at Node 2

Earthquake	Maximum displacement / (mm)				
	HEB	SHS	CFST-C30	CFST-C40	CFST-C50
Cape	29	31	31	31	31
Whittier	59	60	60	60	60
Coyote Lake	104	111	112	111	111
Erzincan	223	246	250	250	248
Victoria	57	54	54	54	54
Landers	61	65	66	66	65
Kobe	166	164	165	165	165

Table 7: Lateral residual displacement at Node 1

Earthquake	Maximum displacement / (mm)				
	HEB	SHS	CFST-C30	CFST-C40	CFST-C50
Cape	0	0	0	0	0
Whittier	1	2	2	2	2
Coyote Lake	5	7	6	6	6
Erzincan	15	38	54	51	45
Victoria	8	11	12	12	12
Landers	25	29	30	29	28
Kobe	8	8	7	6	6

Table 8: Lateral residual displacement at Node 2

Earthquake	Maximum displacement / (mm)				
	HEB	SHS	CFST-C30	CFST-C40	CFST-C50
Cape	1	0	0	0	0
Whittier	1	1	1	1	1
Coyote Lake	5	4	3	3	3
Erzincan	6	26	31	36	32
Victoria	9	11	11	11	11
Landers	22	24	25	24	24
Kobe	13	13	13	12	12

Table 9: Maximum stresses induced in steel

Earthquake	Maximum stress / (N/mm^2)				
	HEB	SHS	CFST-C30	CFST-C40	CFST-C50
Cape	-228	-239	-220	-204	-191
Whittier	-271	-277	-262	-246	-234
Coyote Lake	-337	-344	-337	-319	-305
Erzincan	-373	-375	-374	-373	-372
Victoria	-331	-350	-344	-325	-309
Landers	-340	-355	-355	-342	-324
Kobe	-357	-357	-357	-357	-356

Table 10: Maximum stresses induced in concrete

Earthquake	Maximum stress / (N/mm^2)				
	HEB	SHS	CFST-C30	CFST-C40	CFST-C50
Cape	-	-	-23	-29	-35
Whittier	-	-	-26	-33	-39
Coyote Lake	-	-	-29	-37	-46
Erzincan	-	-	-30	-40	-50
Victoria	-	-	-29	-38	-46
Landers	-	-	-29	-38	-47
Kobe	-	-	-30	-40	-50

5. Conclusions

The application of concrete-filled steel tubes (CFST) in truss bridges was investigated in view of identifying the seismic resisting behaviour. The effects of CFSTs on the maximum and residual displacement demands, and strength demands were checked for several past earthquake records. The main findings of the study are:

1. The fundamental natural frequencies of the bridge with H section or hollow section end raker and bridge with concrete-filled end raker do not differ much. However, this fact should be thoroughly investigated through a parametric study using different dimensions and material properties.
2. The maximum vertical displacement under static loads has significantly reduced when CFST is introduced. Therefore, CFST will be an effective technique for displacement control of railway truss bridges.
3. It is possible to reduce the thickness of steel tubes while maintaining the displacement under serviceability limit states with the use of CFSTs.
4. The behaviour of maximum and residual displacements of the bridge when subjected to a seismic event shows that the behaviour of bridges is not depending only on peak ground accelerations. Hence, further studies are needed considering other earthquake parameters such as acceleration profile, duration, frequency content and energy content for more accurate prediction of the seismic behaviour.
5. The maximum steel stresses induced in end raker member have decreased when CFSTs were introduced. Therefore, it is clear that CFST can be employed to improve the seismic performance of truss bridges.
6. Although the steel stresses were reduced, concrete stresses were increased when higher grade concrete used for composite member. Further studies are needed to find the minimum and maximum concrete grade that can be used for CFST bridge members in economical manner.

References

[1]. Chitawadagi, M. V., Narasimhan, M. C., & Kuldarni, S. M., "Axial strength of circular concrete-filled steel tube columns." Journal of Constructional Steel Research, Vol. 66, 2010, 1248-1260.

[2]. Chen, W. F. & Duan, L., "Bridge Engineering – Seismic Design," 1st ed., CRC Press, Boca Raton, London, D.C., 2003, 7-1 – 7-33.

[3]. Jai, Y. K., Choi, E. S., Chin, W. J., & Lee, J. W., "Flexural Behavior of concrete-filled steel tube members and its application." Journal of Steel Structures, 7, 2007, 319-324

[4]. Kitada, T., "Ultimate strength and ductility of state-of-the-art concrete-filled steel bridge piers in Japan" Journal of Engineering Structures, Vol. 20, 1998, Nos. 4-6, 347-354.

[5]. Morino, S., and Tsuda, K., "Design and construction of concrete-filled steel tube column system in Japan." Journal of Earthquake Engineering and Engineering Seismology, Vol. 4, 2002, No. 1, 51-73.

[6]. Susantha, K. A. S., Aoki, T., & Hattori, M., "Seismic performance improvement of circular steel columns using precompressed concrete-filled steel tube" Journal of Constructional Steel Research, Vol 64, 2008, 30-36.

[7]. Chen, B. C. and Wang, T. L., "Overview of concrete filled steel tube arch bridges in China." Journal of Practice Periodical on Structural Design and Construction, ASCE, May 2009, 70-86.

[8]. Ryall, M. J., Parke, G. A. R. & Harding, J. E., The Manual of Bridge Engineering, 1st ed., Thomas Telford, London, 2003, 449-506.

[9]. Wei, J. and Chen, B., "Estimation of dynamic response for highway CFST arch bridges." Proceedings of the 5th International Conference on Arch Bridges, Madeira, Portugal, 2007, 849-854.

[10]. Ge, H. B., Susantha, K. A. S., Satake, Y., & Usami, T., "Seismic demand predictions of concrete-filled steel box columns." Journal of Engineering Structures, 2003, 337-345.

[11]. Hu, H. T., Huang, C. S., Wu, M. H., & Wu, Y. M., "Numerical analysis of concrete-filled steel tubes subjected to axial force." Proceedings of the Twelfth (2002) International Offshore and Polar Engineering Conference, Kitakyushu, Japan, May 26-31, 2002, 73-80.

[12]. Jourley, B. C., Tort, C., Denavit, M. D., Schiller, P. H., & Hajjar, J. F., "A synopsis of studies of the monotonic and cyclic behaviour of concrete-filled steel tube members, connections and frames" *NSEL -008*, April 2008.

[13]. Fam, A., Qie, F. S., & Rizkalla, S., "Concrete-filled steel tubes subjected to axial compression and lateral cyclic loads" http://www.ce.ncsu.edu/centers/rb2c/Publications/

[14]. Huang, Y., Briseghella, B., Zordan, T., Wu, Q. & Chen, B., "Seismic analysis of a concrete filled steel tubular truss bridge", *Proceedings of the International Association for Bridge and Structural Engineering Madrid Symposium,* 2104, 364-371.

[15]. Code for Steel, Concrete and Composite Bridges, BS 5400 Part 2- Specification for loads, 1978, Board of BSI.

[16]. Manual of Specification Rules - Part 1 - Permanent way, for the guidance of the staff, Way and Works Department, Sri Lanka Railways, 2004.

[17]. Code for Steel, Concrete and Composite Bridges. BS 5400 Part 3- Code of practice for Design of steel bridges, 2000, Board of BSI.

[18]. Code for Steel, Concrete and Composite Bridges. BS 5400 Part 5- Code of practice for design of composite bridges, 1979, Board of BSI.

[19]. Mazzoni, S., McKenna, F., Scott, M. H., Fenves, G. L. & et al, "*OpenSees command Language manual*", 1st ed., 2007.

[20]. Reddiar, M. K. M., "Stress-strain model of unconfined and confined concrete and stress-block parameters", 2009, *MSc Thesis,* Texas A&M University.

[21]. Pacific Earthquake Engineering Research Centre (PEER) Database. http://peer.berkeley.edu/nga/

SECM/15/101

Behaviour of Different Bracing Systems in High Rise 3-D Benchmark Building under Seismic Loadings

D. M. Patil[1*] and K. K. Sangle[1]

[1]Structural Engineering Department, VJTI, Mumbai, India, 400019
*E-mail: patil.dhanaraj@gmail.com

Abstract: This paper presents the seismic behaviour of different bracing systems in high rise 20 storey 3-D benchmark steel building. A nonlinear static pushover analysis was carried out to on different braced 20 storey high rise 3-D benchmark steel building to capture the seismic response. In this study, five structural configurations were used: moment resisting frames (MRF), chevron braced frames (CBF), V-braced frames (VBF), X-braced frames (XBF), and zipper braced frames (ZBF). The primary goal of this study is to investigate the seismic behaviour of different bracing systems in a benchmark building under the different lateral load patterns. It is seen that the type of bracing system significantly influences the performance of high rise buildings. The seismic performance of the 20 storey benchmark building is measured in terms of the fundamental time period, capacity curve, storey displacement, and inter-storey drift ratio. It can be concluded from the study that the seismic resistance can be increased by use of the CBF, VBF, and ZBF than XBF and MRF.

Keywords: Seismic behaviour, high rise 3-D benchmark steel building, bracing systems, nonlinear pushover analysis, capacity curve.

1. Introduction

Moment resisting frames and braced frames have been commonly used as lateral load resisting structural elements in steel buildings. The different bracing systems include typical diagonal bracing, X-bracing, chevron bracing and V-bracing configurations, which connect the brace concentric to beam- column joint. Roeder and Popov proposed eccentric bracing, combining good features of moment resisting frame and concentric braced frame both [1, 2]. The seismic performance of chevron braced frames can be improved by redesigning the brace and floor beams to a weak brace and the strong beam system. This upgraded chevron braced frame result in an excellent hysteretic response [3]. Tremblay et al. studied seismic performance of concentrically braced steel frames, i.e. diagonal braced frame and X-braced frame [4]. Yang et al. proposed a design methodology for zipper braced frames to achieve good ductile behaviour [5]. The zipper braces activated buckling in all storeys except the top one [6]. Also, Nouri et al. investigated the concentric braced frames and proposed zipper braced to mitigate the vertical unbalanced force in case of chevron braced frame [7]. Similarly Patil et al. studied behaviour of different braced steel buildings of different height for symmetric plan building [8].

In this research paper, an attempt is made to investigate the seismic behaviour of different braced systems in G+20 storey high rise benchmark building. An extensive analytical investigation of the seismic behaviour of different braced buildings has been undertaken by nonlinear static pushover analysis. An attempt has been made to assess the performance of different bracing systems under application of different invariant lateral load patterns in a nonlinear static pushover analysis, by using five structural configurations: moment resisting frames (MRF), chevron braced frames (CBF), V-braced frames (VBF), X-braced frames (XBF) and zipper braced frames (ZBF).

2. Example G+20 Benchmark Building

In this study, behaviour of different bracing systems in G+20 storey high rise benchmark building for lateral loads is investigated. Total 5 different bracing systems investigated using nonlinear static pushover analysis. Results of nonlinear static pushover analysis of benchmark high rise buildings are discussed in section 4. Plan and elevation of benchmark buildings are illustrated in Fig. 1. Dimensions of benchmark buildings, basement level height is 3.65m, ground level height is 5.49m, 2nd to 20th level height is 3.96m and all bays with 6.10m width.

3. Nonlinear Static Pushover Analysis

Nonlinear static analysis is performed on benchmark buildings using different lateral load patterns to determine the effects of the lateral load on the global structural behaviour through the load-displacement curve. In this study, displacement controlled pushover analysis is carried out using SAP2000 v16 (Computer and Structures, Inc, Berkeley) software [9].

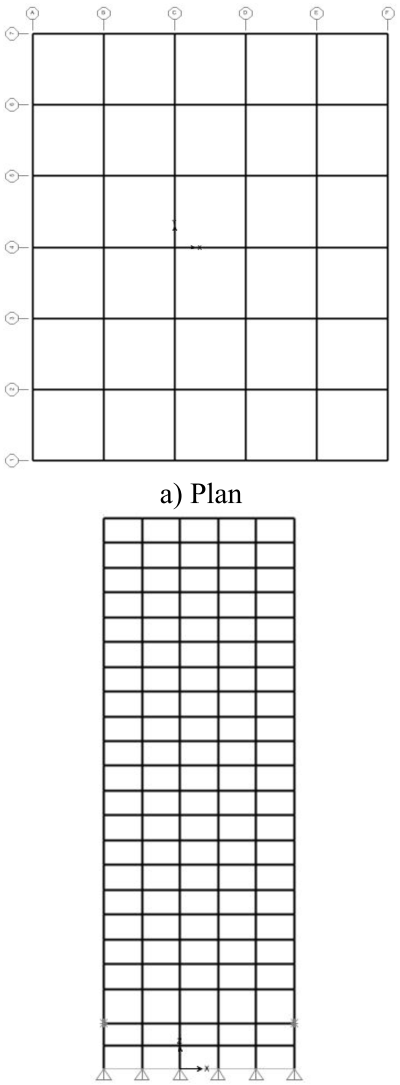

a) Plan

b) Elevation

Figure 1: Plan and Elevation of G+20 Benchmark Building

The target displacement used for each building is 4% of the total height of the building (ATC-40) [10]. Indian codes were used to calculate different parameters [11-13]. The SAP2000v16 default hinge properties based on FEMA-356 criteria are used for beams, columns and braces. Hinges are assigned at both the ends of each column, beam element and at mid-span of braces. For column, coupled (PMM) hinges, which yields based on the interaction of axial force and bi-axial bending moments at the hinge location, are used. P (axial) hinges are assigned for steel braces in tension/compression and M3 (moment) hinges are assigned to the beam elements [14].

The nonlinear static pushover analysis, as described in FEMA-273 [15] and in FEMA-356 [14], is now being used as a standard tool to estimate seismic demands for buildings. Pushover analysis has played an important role in the development of performance-based earthquake engineering concepts in guideline documents and codes (e.g. ATC-40, 1996; FEMA-356, 2000) [10, 14]. Due to the fact that the lateral force profiles in static pushover analysis influence the structural response, different lateral load patterns have been utilized to represent the distribution of inertia forces imposed on buildings. In the past few years, several researchers have discussed accuracy and limitations of pushover analysis and proposed new various methods [16-19]. Some researchers have suggested to consider higher mode effects to overcome the shortcomings of a pushover procedure [20-21]. The researchers have addressed FEMA and modal pushover analysis with inelastic response history analysis in high-rise buildings [19-21]. The objective of this investigation is to study an improved pushover analysis procedure based on the invariant force distribution of different lateral load patterns in estimating seismic demands of buildings. The different lateral load patterns used in this study are as follows:

- *Codal Lateral Load Pattern: Push 2*

The codal lateral load shape represents the forces obtained from the predominant mode of vibration. Following equation is used to calculate codal load pattern [11]:

$$V_B = A_h W \tag{1}$$

$$Q_i = V_B \frac{W_i h_i^2}{\sum_{i=1}^{n} W_i h_i^2} \tag{2}$$

Where V_B = design base shear as per IS1893 (Part-I): 2002 [11],

h_i = height of the floor *i* measured from the base,

Q_i = Lateral force at floor *i,*

W_i = seismic weight of floor *i* and

n = number of storeys in the building.

- *Elastic First mode Lateral Load Pattern: Push 3*

The first mode load pattern is related to the first displacement mode shape (Φ) of vibration. The lateral force of a storey is proportional to the product of the amplitude of the elastic first mode and mass at the storey [8,13].

$$F_i = m_i \phi_i / \Sigma\, m_i \phi_i \tag{3}$$

Where Φi = amplitude of the elastic first mode of the storey.

- *Multi-modal Lateral Load Pattern: Push 4*

This lateral load pattern considers the effects of elastic higher modes of vibrations for a long period and characteristics of the structural behaviour. The contribution of first three elastic modes of vibration is considered to calculate the multimodal lateral load pattern.

- *Uniform Lateral Load Pattern: Push 5*

In this, the lateral force at a storey is proportional to the mass of the storey [8, 13].

$$F_i = m_i / \Sigma\, m_i \tag{4}$$

where F_i = lateral force at the i^{th} floor,
m_i = the mass at i^{th} floor of the building.

4. Results and Discussion

Nonlinear static pushover analysis is performed using the calculated lateral load patterns on example different bracing systems in G+20 benchmark high rise buildings. The responses of different bracing systems are studied in terms of the fundamental period of vibration, base shear, roof displacement, storey displacement and inter-storey drift ratio. The natural period of vibration is depicted in Table 1 for benchmark buildings. In addition, modal analysis of the example buildings is carried out to find the fundamental period of vibration derived by eigenvalue method. The resulting fundamental period of vibration using eigenvalue analysis is reported in Table 1.

It is noticed from Table 1 that ZBF, and CBF shows reduced fundamental time period obtained by modal analysis. Besides this, the fundamental period obtained from the modal analysis is not close to that obtained from codal empirical equations for steel buildings.

Table 1: Period of vibration(s) of different bracing systems in G+20 Benchmark buildings

Codal Time Period	Modal analysis				
	MRF	CBF	VBF	XBF	ZBF
2.4428	3.8208	2.2296	2.2391	2.2545	2.2244

4.1 Capacity curves

The capacity curves, showing the relationship among base shear force and roof displacement, benchmark building of different invariable lateral load patterns is illustrated in Fig. 2. Table 2 depicts the base shear and roof displacement values of different bracing systems in a benchmark building for the different lateral load patterns evaluated from the nonlinear pushover analysis.

It is revealed from Table 2 that the Base shear changes with invariant lateral load patterns. ZBF and CBF show higher base shear than other structural systems in benchmark buildings. The 44% increase is observed in the base shear of ZBF than MRF for Push 2 load case. Similarly, 47%, 75%, 42% increase in base shear is seen for load case push 3, push 4, push 5 respectively.

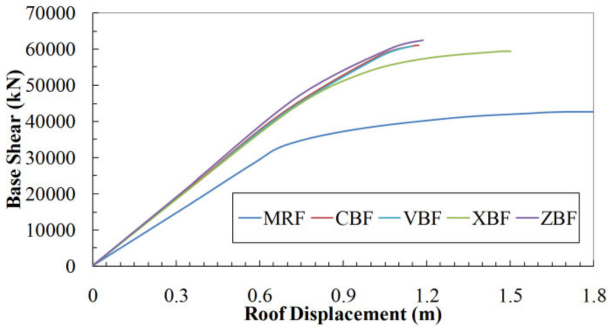

a) Push 2 load case

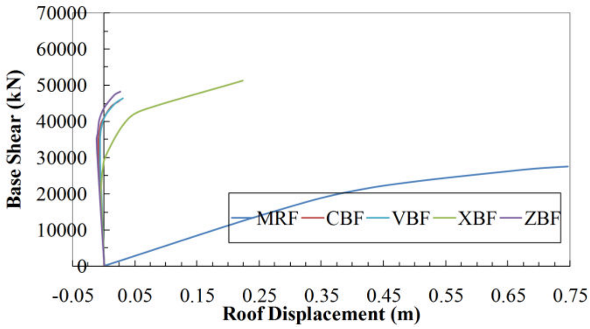

b) Push 3 load case

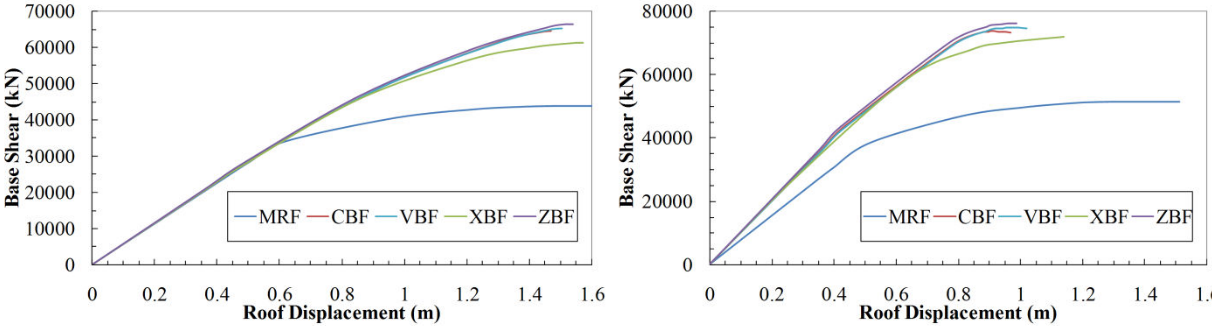

c) Push 4 load case d) Push 5 load case

Figure 2: Pushover curves of different braced benchmark buildings

Table 2: Base shear and roof displacement of different bracing systems in benchmark building

Different Bracing Systems	Push 2 load case Base Shear (kN)	Push 2 load case Roof Disp. (m)	Push 3 load case Base Shear (kN)	Push 3 load case Roof Disp. (m)	Push 4 load case Base Shear (kN)	Push 4 load case Roof Disp. (m)	Push 5 load case Base Shear (kN)	Push 5 load case Roof Disp. (m)
MRF	43425	1.9651	45007	1.9107	27505	0.7464	53695	1.5560
CBF	61123	1.1706	64693	1.4697	45741	0.0246	73711	0.9150
VBF	60829	1.1455	65356	1.5042	46386	0.0298	74839	0.9703
XBF	59470	1.5005	61362	1.5718	51411	0.2235	72320	1.2168
ZBF	62562	1.1859	66482	1.5396	48352	0.0260	76208	0.9858

4.2 Storey displacement

The storey displacements of different bracing systems in a benchmark building corresponding to different invariant lateral load patterns in pushover analysis are illustrated in Fig. 3. It is revealed from Fig. 3, trend in the similarities and/or in the variations of the different invariant lateral load patterns is reflected in the storey displacement profiles of the buildings. Storey displacement demand prediction of codal and elastic first mode load patterns is observed nearly same compared to the other lateral load patterns. The MRF buildings, as depicted in Fig. 3, show higher storey displacements than other systems as it is most ductile structural system. CBF, VBF, and ZBF show lesser storey displacement for all load cases. It is seen from Fig. 3 that XBF shows higher storey displacement than CBF, VBF, and ZBF.

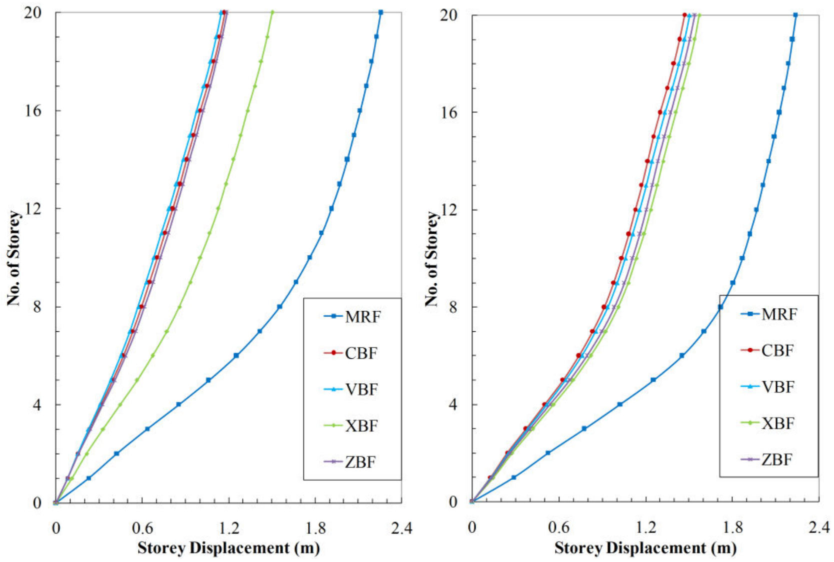

a) Push 2 load case b) Push 3 load case

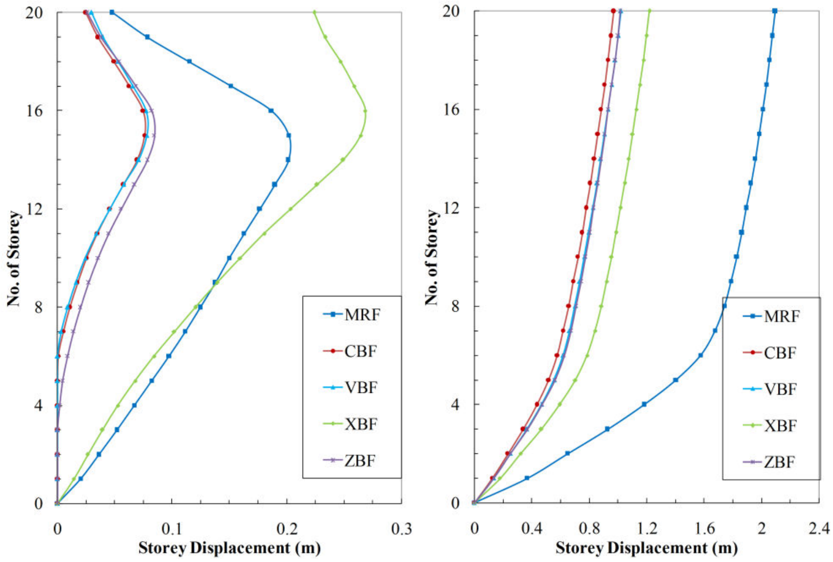

c) Push 4 load case d) Push 5 load case

Figure 3: Storey displacement of benchmark building

4.3 Inter-storey drift ratios

The inter-storey drift ratios of different bracing systems in benchmark buildings corresponding to different invariant lateral load patterns in pushover analysis are illustrated in Fig. 4. Inter-storey drift ratio is higher in MRF than CBF, VBF, XBF, and ZBF for all lateral load cases. It is observed that inter-storey drift ratio is higher at the lower storey height of buildings. CBF, VBF and ZBF show less inter-storey drift ratio for all load cases. It is observed from inter-storey drift ratio of building that CBF, VBF and ZBF are more preferred than XBF and MRF.

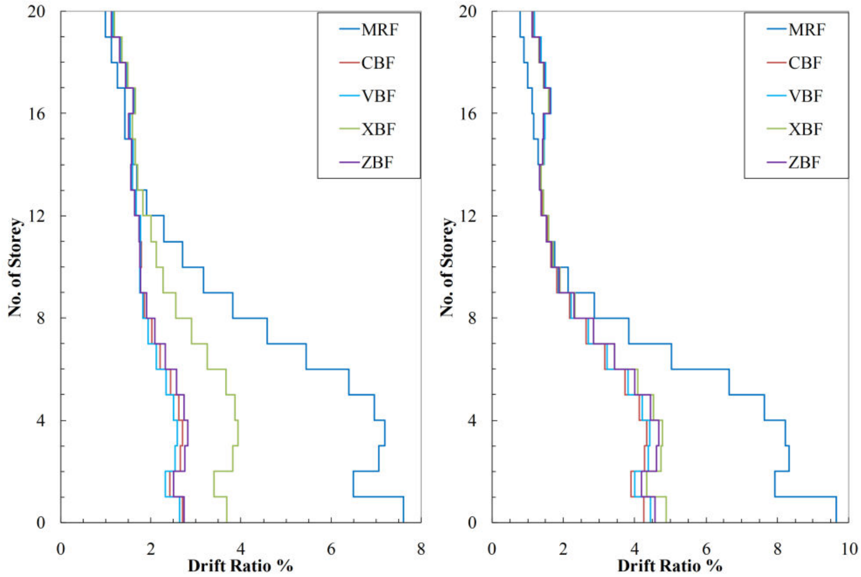

a) Push 2 load case b) Push 3 load case

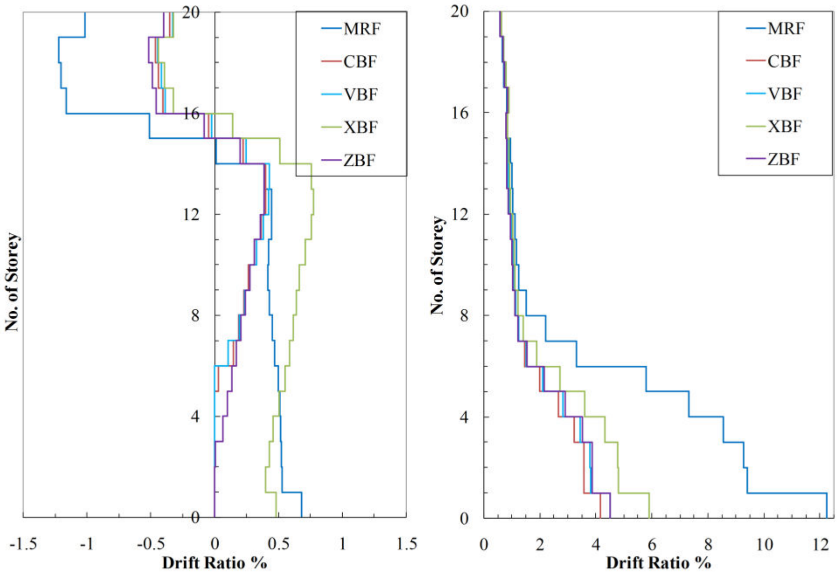

c) Push 4 load case d) Push 5 load case

Figure 4: Inter-storey drift ratio of benchmark building

5. Conclusions

In this study an attempt is made to assess the seismic response parameters of different bracing systems to examine the seismic behaviour of each system. The conclusions of this study can be summarized as follows.

1. Seismic response of CBF, VBF and ZBF benchmark building is nearly similar in terms of base shear. Seismic response of these systems is considerably higher than MRF and XBF.
2. CBF and VBF show lower storey displacement and inter-storey drift ratio indicating that these systems have strength and stiffness. ZBF also shows nearly similar storey displacement and inter-storey drift ratio.
3. The trend of the invariant lateral load patterns is reflected on seismic response of the benchmark buildings. Codal and elastic first mode lateral load patterns show similar results.
4. ZBF, VBF and CBF have higher seismic response depending on different seismic parameters such as fundamental time period, base shear, roof displacement, storey displacement, and inter-storey drift ratio than XBF and MRF.
5. CBF and VBF are most suitable bracing systems in highrise benchmark building so as to increase seismic resistance.

Acknowledgements

The fellowship granted to the first author by the V.J.T.I., Mumbai is gratefully acknowledged.

References

[1]. Roeder, C.W., Popov E.P., "Eccentric braced steel frames for earthquakes", Journal of the Structures Division, ASCE, Vol. 104, No. 3, pp. 391-411, 1978.

[2]. Hjelmstad, K..D., Popov E.P., "Characteristics of eccentrically braced frames", Journal of Structural Engineering, ASCE, Vol. 110, No. 2, pp. 340-353, 1984. http://dx.doi.org/10.1061/(ASCE)0733-9445(1984)110:2(340)

[3]. Rai, D.C., Goel, S.C., "Seismic evaluation and upgrading of chevron braced frames", Journal of Constructional Steel Research, Vol. 59, pp. 971-994, 2003. http://dx.doi.org/10.1016/S0143-974X(03)00006-3

[4]. Tremblay, R., "Inelastic seismic response of steel bracing members", Journal of Constructional Steel Research, Vol. 58, pp. 665–701, 2002. http://dx.doi.org/10.1016/S0143-974X(01)00104-3

[5]. Yang, C.S., Leon, R.T., DesRoches R., "Design and behavior of zipper braced frames", Engineering Structures, Vol. 30, pp. 1092-1100, 2008. http://dx.doi.org/10.1016/j.engstruct.2007.06.010

[6]. Yang, C.S., Leon, R.T., DesRoches R., "Pushover response of a braced frame with suspended zipper struts", Journal of Structural Engineering, ASCE, Vol. 134, No.10, pp.1619-1626, 2008. http://dx.doi.org/10.1061/(ASCE)0733-9445(2008)134:10(1619)

[7]. Nouri, G.R., Kalesar, H.I., Ameli, Z., "The applicability of the zipper strut to seismic rehabilitation of steel structures", World

Academy of Science, Engineering and Technology, Vol. 58, pp. 402-405.
[8]. Patil, D.M., Sangle, K.K., “Seismic behaviour of different bracing systems in high rise 2-D steel buildings”, Structures, Vol.3, pp. 282-305, 2015. http://dx.doi.org/10.1016/j.istruc.2015.06.004
[9]. CSI, SAP2000, Integrated finite element analysis and design of structures basic analysis reference manual. Berkeley (CA, USA): Computers and Structures; 2015
[10]. ATC-40, Seismic evaluation and Retrofit of Concrete Buildings. Applied Technical Council, 1996; 1.
[11]. IS: 1893-2002, Criteria for earthquake resistant design of structures: part–1 general provisions and buildings, Bureau of Indian Standards, New Delhi.
[12]. IS: 875 (Part 2):1987, Code of practice for design loads (other than earthquake) for buildings and structures: part 2 imposed loads, Bureau of Indian Standards, New Delhi.
[13]. IS: 800-2007, General construction in steel-code of practice, Bureau of Indian Standards, New Delhi.
[14]. FEMA 356, Prestandard and commentary for the seismic rehabilitation of buildings, FEMA 356 Federal Emergency Management Agency 2000, Washington DC.
[15]. FEMA 273, NEHRP guidelines for the seismic rehabilitation of buildings, Rep. FEMA 273 Federal Emergency Management Agency 1997, Washington DC.
[16]. Krawinkler, H., Seneviratna, G.D.P.K., “Pros and cons of a pushover analysis of seismic performance evaluation”, Engineering Structure, Vol. 20 (4-6), pp.452-464, 1998. http://dx.doi.org/10.1016/S0141-0296(97)00092-8
[17]. Elnashai, A.S., “Advanced inelastic static (pushover) analysis for earthquake applications”, Journal of Structural Engineering and Mechanics, Vol. 12, No. 1, pp. 51-69, 2001. http://dx.doi.org/10.12989/sem.2001.12.1.051
[18]. Chopra, A.K., Goel, R.K., “A modal pushover analysis procedure for estimating seismic demands for buildings”, Earthquake Engineering Structural Dynamics, Vol. 31, No. 3, pp. 561-582, 2002. http://dx.doi.org/10.1002/eqe.144
[19]. Goel, R.K., Chopra, A.K., “Evaluation of modal and FEMA pushover analyses: SAC buildings”, Earthquake Spectra, Vol. 20 No.1, pp. 225-254, 2004. http://dx.doi.org/10.1193/1.1646390
[20]. Poursha, M., Khoshnoudian, F., Reza, A., Moghadam, S., “Assessment of conventional nonlinear static procedures with FEMA load distributions and modal pushover analysis for high-rise buildings”, International Journal of Civil Engineering, Vol. 6, No.2, pp.142-157, 2008
[21]. Poursha, M., Khoshnoudian, F., Moghadam, S., “A breakthrough in estimating the seismic demands of tall buildings”, The 14th World Conference on Earthquake Engineering, Beijing, China, 2008.
[22]. http://quiver.eerc.berkeley.edu:8080/ Visited, 15 Oct. 2014.

SECM/15/120

Seismic Analysis of Guyed Mast Towers in Sri Lanka

S. Kogul[1*], A.M.L.N. Gunathilaka [2] C.S.Lewanagamage [1] and M.T.R. Jayasinghe [1]

[1]University of Moratuwa, Colombo, Sri Lanka
[2] Sri Lanka Telecom PLC
*E-Mail: kogulsk @ gmail.com, TP: +94776688345

Abstract: With the rapid development of the telecommunication sector in the country, telecommunication/broadcasting towers play a vital role in telecommunication and broadcasting sectors. There are many structural forms available for towers and guyed mast is one such type commonly seen in country sides of Sri Lanka where land is available for cheaper price. Moreover, in the case of very tall tower is needed, guyed mast is more economical solution than self-supporting towers. The failure of a guyed tower especially under a disaster situation such as earthquake is a major concern in many ways. One is the failure of communication/broadcasting may hamper the communication needs to carry out rescue and other essential operations. Further, failure of a tower may itself cause a considerable economic loss as well as damages to human life. Therefore, checking of structural performance tower under seismic and other extreme weather effects is quite vital.
Even though, Sri Lanka was believed to have no seismic threats, presently a strong argument is going on amongst the professionals regarding the seismic condition of our country with the reported earth tremors in recent times. Hence, evaluating the structural performance of existing telecommunication/ broadcasting towers under seismic loads is utmost important since almost all existing towers have not been designed considering seismic forces due to traditional belief that Sri Lanka will not be subjected to earthquakes of appreciable magnitudes.
Considering the above situation, assessment of structural performance of exiting Guyed mast towers (which were not initially designed considering earthquake loading) under possible earthquake loading was selected as the objective of this study. Accordingly, behavior of existing Guyed mast towers under seismic loading using ANSI/TIA-222-G tower design code was studied and results, observations and conclusions based on this analysis are presented.

Keywords: Guyed mast, seismic loading. Telecommunication towers

1. Introduction

Telecommunication and broadcasting sectors of the country has developed exponentially over last few decades and, a large number of telecommunication /broadcasting towers are available in the country to facilitate wireless data and signal transmissions. Guyed mast is one of the economical structural forms available for taller towers.

A failure of tower will itself cause a considerable economic loss as well as possible loss of lives. So extreme care should be given to the design of these structures especially guyed mast towers which show nonlinear response because of guy assembles. However, almost all of these towers were designed only considering wind loading since Sri Lanka was considered as a country free from earthquake. However, after Tsunami that is caused by an earthquake and with the recent tremors reported in the country, now most of the structural designers and professionals are aware of the importance of considering seismic effects for their designs. Therefore, it is worth to study performance of guy mast towers too under possible seismic effects.

2 Objective

The objective of this research is assessing the performance of exiting guy mast towers (which were not initially designed considering earthquake loading) under possible earthquake loading.
Various types of telecommunication towers with different structural forms are available in the country and this study has been limited to analysis of guyed mast towers since seismic performance on Greenfield self-supporting lattice towers, which are the most common type of telecommunication towers in this country, have been studied in the previous researches. Guyed mast is second most commonly used structural form for telecommunication towers next to self-supporting towers in Sri Lanka.

3. Methodology

For analysis of guyed towers under earthquake loading, equivalent static method given in ANSI/TIA-222-G-2005was used since there are no time history data are available for Sri Lankan context.(this is further discussed in chapter 4.2) Seismic analyses were also carried out under different seismic conditions relevant some other selected countries for comparison purpose.

Two towers having different tower heights of 35 m, and 55 m were selected for this analysis. These towers have been designed for wind speed of 50 m/s (180km/h), which is slightly above the recommended design wind speed for Zone 1 for normal structures .

ANSI/TIA-222-G-2005 Structural Standard for Antenna Supporting Structures and Antennas, which is highly appreciated and very commonly used code of practice by both local and foreign tower designers, was used for the structural analysis and design of towers under both wind and seismic loadings.

3D computer models for each tower were prepared using SAP2000 structural analysis software and analysis of towers under both wind and earthquake loads were carried out using such models. Finally, the results of analyses under wind and earthquake loads were compared.

4. Loading

4.1 Wind loads

Calculation of wind loads on towers were carried out according to ANSI/TIA-222-G-2005 for the design wind speed of 50 m/s (180 km/h) , which is close to the recommended design wind speed for Zone 1 Normal structures condition. Wind loads were also calculated for the wind speed of 33.5 m/s, which is the lowest allowable design wind speed that can be used for structural design in Sri Lanka, for the purpose of comparison of results.

4.2 Seismic loads

For the calculation of seismic loads on towers, four methods are given in the ANSI/TIA-222-G -2005. Those methods are

- Equivalent lateral force
- Equivalent modal analysis
- Modal analysis
- Time history analysis

According to the code, only equivalent static method and time history method are applicable for guyed mast towers. First method is a static method and next is a dynamic method.

4.2.1 Equivalent Static Method

For the calculation of seismic shear, Maximum considered earthquake spectral response acceleration at short period (S_S) and Maximum considered earthquake spectral response acceleration at 1.0 second (S_1) are required. These are site specific acceleration coefficients and these values for countries other than USA have not been given in ANSI/TIA-222-G-2005. Further, recommended seismic acceleration parameters are not locally available, since code of practice for seismic design is not available in Sri Lanka yet. So values used in the previous researches were considered.

It was decided to calculate S_s and S_1 using the approximate method given in USGS website[14] based on Peak Ground Acceleration of 0.1g, which is value used by Gunathilaka eta el of their study on Greenfield towers[01] . Accordingly, S_s and S_1 were calculated as 0.5 and **0.2** respectively. These two values are quite close to the recommended values for south India and cities in Australia in USGS, where similar type of seismological condition exists when compared with Sri Lanka. This would correspond to minor to moderate damage condition.

In order to compare the seismic performance of towers under higher earthquake magnitudes, another set of site-specific acceleration coefficient were also considered. Accordingly, site specific acceleration coefficients for Pakistan as S_s = 1.22 and S_1 = 0.49 given in USGS website was selected. The above values applicable to Pakistan represent severe seismic condition.

For the calculation of fundamental natural frequency of a tower, a formula has been given in ANSI/TIA-222-G-2005 [14]. However, to obtain better accuracy, natural frequencies were obtained from the modal analysis performed using SAP 2000 model and calculated fundamental natural frequencies for 35 m and 55m towers are 3.67 Hz and 2.96 Hz. The formula given in ANSI/TIA-222-G [14] gave values of 3.47 Hz and 2.48 Hz for 35m and 55m respectively and those are close range with the SAP 2000 values.

To compensate for mass of antennas and other ancillaries (such as ladders , feeder cables, platforms, etc) material density of member materials were modified by a factor individually calculated for each model based on ratio of pure weight of tower members and actual weight of tower including all ancillaries.

Consideration of masses of all ancillaries is important since mass of such items could contribute significantly for seismic force generation of a tower under an earthquake as the weight of ancillaries including antennas takes considerable portion of overall self-weight of an actual tower.

4.2.2 Time history analysis

For carrying out time history analysis of towers, guidelines given in ANSI/TIA-222-G should be adopted. There are no recorded events which represent the past earthquake occurred in Sri Lanka. So it was decided to use only the static analysis procedures for our research, as response spectrum method is not suitable for guyed mast towers according to ANSI/TIA-222-G-2005 [14].

(Whole procedure of calculations under Equivalent Static Method is described in Appendix "A".)

5. 3d modeling

3D finite element truss models were prepared for both towers (35 m & 55 m). The towers are modeled as elastic three-dimensional truss model where individual members of the mast are modeled as straight members connected at joints producing only axial forces in the members.

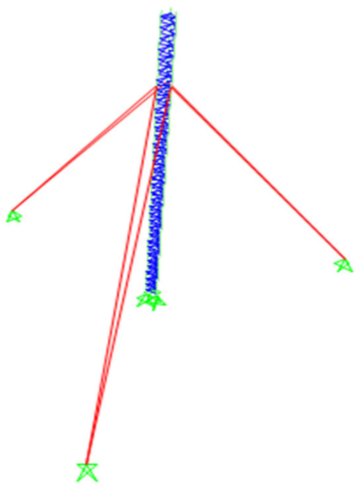

Figure 1 3D model of 35m tower

Vertical members are modeled by using sixty angle sections and cross bracing members are modeled by using L angle section.

Cable is modeled by using frame element. In addition, bending stiffness of the frame elements are reduced by scale multiplier. In addition, compression limits of those frame elements are set to zero to idealize the structural characteristics of cables.

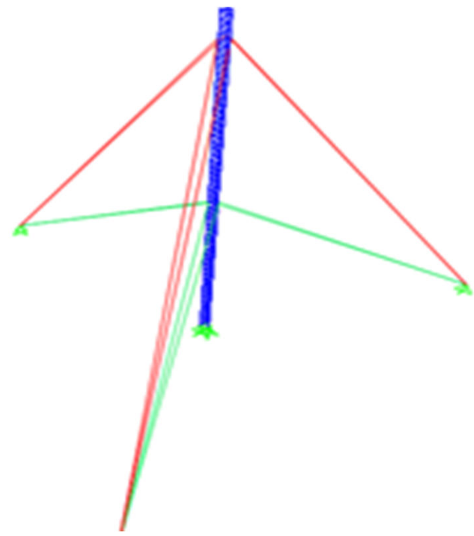

Figure 2: 3D model of 55m tower

6. Analysis and results

Each of the towers was subdivided to panels according to geometries of towers and wind and earthquake load under static equivalent analysis approach were separately calculated for each panel. The calculated wind and earthquake loads for each panel were assigned as nodal loads for respective tower models.

As per ANSI/TIA-222-G-2005 (14) specifications, following load cases given in Table 1 were considered in this study.

Supports reactions, maximum axial forces in leg members and maximum base reaction, Maximum joint displacement, Maximum guy tension of each tower for the load combinations described above were obtained from SAP 2000 analysis results of respective tower models.

As expected, maximum uplift reactions, , tension in guys and members in each and every case are observed when dead load has a factor of safety of 0.9, while maximum downward and horizontal reactions and compression forces in members are observed when dead load has a factor of safety of

1.2. Only critical load combinations in respective structural actions are shown in respective graphs.

Table 1: Considered load combinations for static analysis

Load case	Case Name	Remarks
1	0.9D+1.0Dg+1.6W33.5	Under 33.5m/s wind speed
2	0.9D+1.0Dg+1.6W50	Under 50m/s wind speed
3	1.2D+1.0Dg+1.6W33.5	Under 33.5m/s wind speed
4	1.2D+1.0Dg+1.6W50	Under 50m/s wind speed
5	0.9D +1.0Dg+ 1.0Emod.	Earthquake load under Appropriate condition for SL
6	0.9D+1.0Dg+1.0Esev.	Earthquake load under severe seismicity
7	1.2D+1.0Dg+1.0Emod	Earthquake load under Appropriate condition for SL
8`	1.2D+1.0Dg+1.0Esev.	Earthquake load under severe seismicity condition

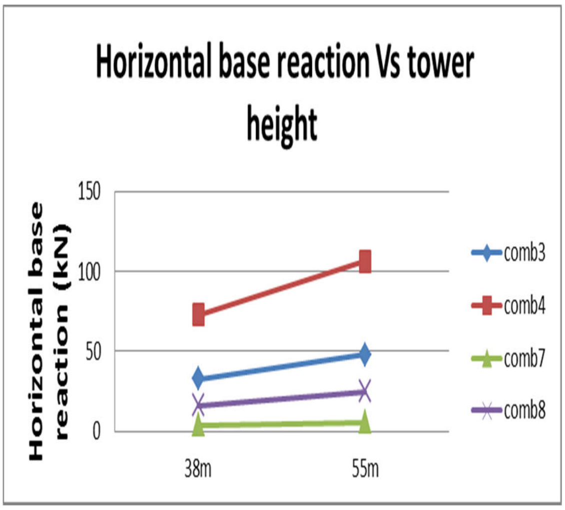

Figure 2: Variation of maximum horizontal base reaction

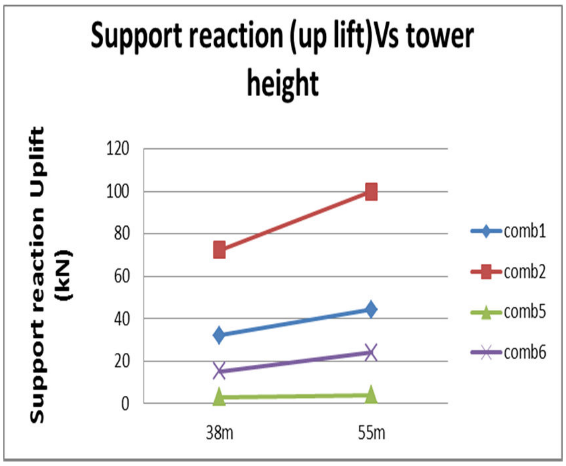

Figure 3: Variation of maximum base uplift

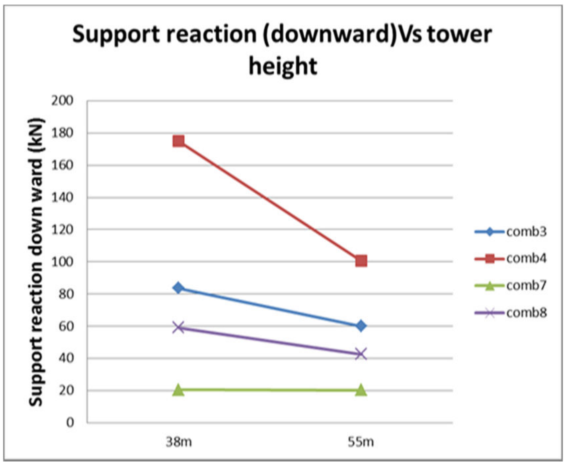

Figure 4: Variation of maximum downward base reaction

According to results of the graphs, support reactions under assumed earthquake loading condition for Sri Lanka are very much less than the support reaction under design wind loading, even if for design wind speed of 33.5m/s. The gap between reactions (uplift and horizontal) under wind loading and earthquake loading increases with the increase of the tower height. But when it considers about downward support reaction, when the tower height increases the gap reduces.

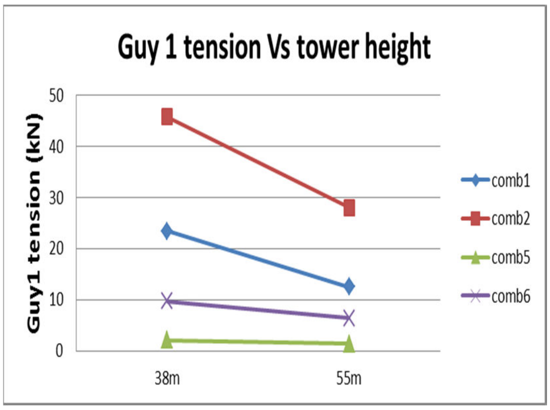

Figure 5: Variation of maximum axial tension (lower guy)

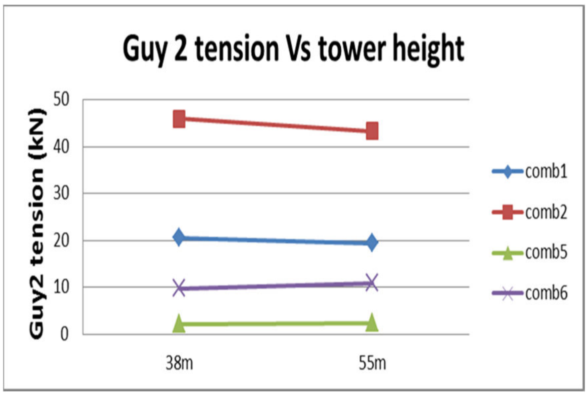

Figure 6: Variation of maximum axial tension in top guy

When it considers the results obtained for axial tension in cables (Figure 6 and 7)), they also exhibit a similar variation like support reactions (uplift and horizontal).

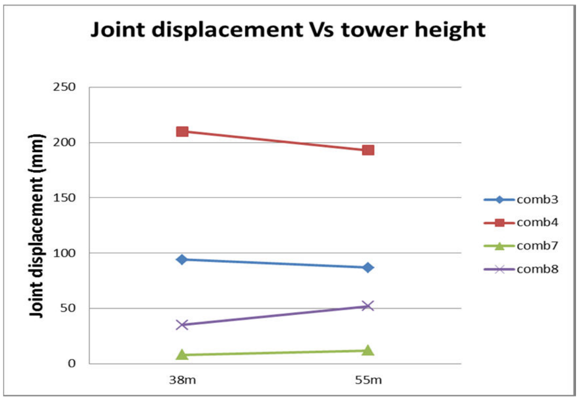

Figure 7: Variation of maximum joint displacement

Figure 8 shows the variation of maximum joint displacement of towers with respect to the considered load combinations. It is also very clear that tower deflection under assumed earthquake loading condition for Sri Lanka is far below the deflections under wind loading conditions. However, earthquakes could induce higher deflections due to dynamic nature of forces and dynamic analysis will require to verify it fully.

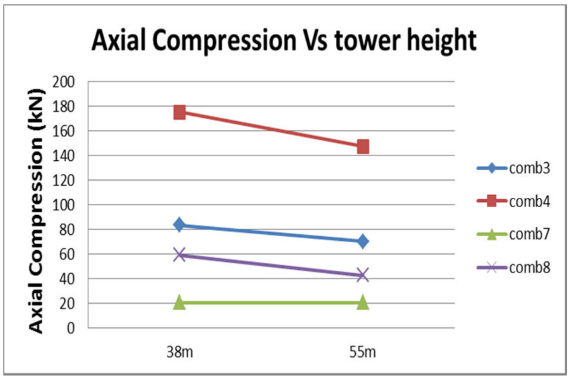

Figure 8: Variation of maximum axial compression in members

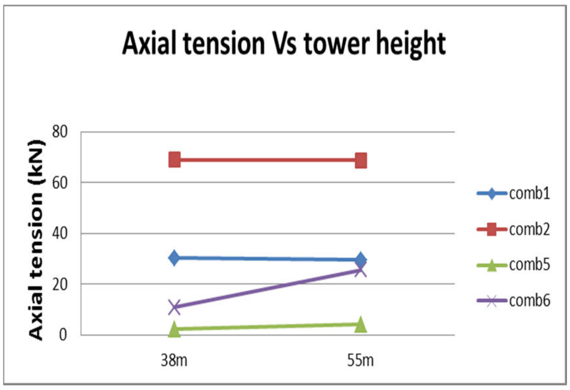

Figure 9: Variation of maximum axial tension in members

Maximum axial forces (both compression and tension) in leg members vary in same way as in support reactions. In other words this means, member stresses developed under assumed earthquake loading for Sri Lanka is not critical compared with member stresses under design wind load condition of towers. However, under earthquake loading calculated based on very severe seismicity condition, axial tension forces of leg members has almost reached the design values under 33.5m/s wind load (Figure 10). So when the height of the tower increases there is a possibility for the dominance of earthquake forces compared to wind forces.

The results obtained from this study match with the results of previous studies [1],[13] carried out in Sri Lanka for other types of towers. There are some other researches [4] done on this topic in different countries gave similar kind of results. Also, ANSI/TIA-222-G-2005[1] in itself has specified that analysis under earthquake loading for normal towers are not required if S_s is less than or equal to 1.00. This has also been proved by this analysis.

7. Conclusion

As per the objective of this study, selected guyed mast towers were analyzed using static equivalent method given in ANSI/TIA-222-G-2005 (14) to assess the structural performance of guyed mast towers under seismic loading and compared with wind load analysis. Accordingly, some interesting findings were seen as described below

• Structural actions (member forces, support reactions deflections ,etc) developed in all selected guy towers under most probable type of seismic loads relevant to Sri Lanka are very low compared with same under design wind loads when seismic analysis done as per Static Equivalent method given in ANSI/TIA-222-G-2005 (14) . Hence, it can be expected that existing towers in this height range will survive without any problem under a minor to moderate earthquake, which is the most probable type of earthquake that can be expected to a country like Sri Lanka. Further, even under a considerable major earthquake, structural actions in towers will not be greater than structural actions under design wind loads in all selected towers. Hence, it cannot expect a major problem in guy towers in this height range even under major earthquake.

• As there are no suitable time history data available for Sri Lanka, only static analysis procedure was adopted in this study. As per the ANSI/TIA-222-G-2005 (14), it cannot use other approaches as Response spectrum method too for guy mast analysis. Therefore, further studies regarding these towers using appropriate time histories obtained from other counties is recommended to verify the results obtained in this study since Static Equivalent method is only a simple conservative analytical tool for seismic analysis.

References

[1]. Earthquake performance of free standing four legged towers. Gunathilaka, A.M.L.N., Lewanagamage, C.S. and Jayasinghe, M.T.R.

[2]. The analysis of the structural behaviour of guyed antatana masts under wind and ice loading. G.J, Schott and F.R, Thurston.

[3]. P.J, Pocock. The analysis of structural behaviour of guyed antenna mast under wind and ice loading; Part 2: wind loads. 1956.

[4]. Grey, Matthew. Finite element seismic analysis of guyed masts. 2006.

[5]. Evaluation of non- linear analysis of guyed antenna towers. Wahba, Y.M.F., Madugula, M.K.S. and Monforton, G.R. s.l. : Computers and structures, 1997.

[6]. Dynamic response of guyed masts.Wahba, Y.M.F., Madugula, M.K.S. and Monfortra, G.R. s.l. : Engineering structures, 1998.

[7]. Three dimensional analysis of the seismic response of guyed masts. M.Hensley, Gregory and H.Plant, Raymond.s.l. : Science direct, 2006.

[8]. Dynamic response of guyed masts to strong motion of earthquake.Nejad, S.E. Moossavi.

[9]. Method to design a guided tower concerning dynamic behaviour. Mendonca, Cecilia and Barrros, RuiCarneiro de. 2013.

[10]. Eldhose, Bibitha K., S, Harinarayanam. andS.Usha. Linear analysis of guyed mast subjected to wind, Ice, and seismic loading. 2014.

[11]. Seismic demand prediction of eccentrically loaded steel bridge piers subjected to moderate earthquake. K.A.S.Susantha and Gunasoma, H.H.M. s.l. : IESL, 2012, Vol. 1.

[12]. Jeyasinghe, M.T.R., Hettiarachchi, D.S. and Gunawardena, D.S.R.T.N. Performance of Tall Buildings with and without Transfer Plate under Earthquake laoding.

[13]. Analysis and design of telecommunication towers for earthquake loading in Sri Lanka for sustainability.Gunathilaka, A.M.L.N., Lewanagamage, C.S. and Jeyasinghe, M.T.R. Kandy

[14]. ANSI/ TIA-222-G 2005, Structural standard for antenna supporting structures and antennas, Telecommunication industry association, U.S.A.

[15]. Pacific Earthquake engineering research centre (PEER) Data base , http:// Peer.berkeley.edu.nga/.

[16]. Seismic hazard assessment of Sri lanka and seismic risk in Colombo. L.M.N, Peiris. Risk managemntsollutions,London, U.K : s.n., 2008.

[17]. Seismic risk in colombo- Probabilitic approach.Uduweriya, S.B, Wijesundara, K.K. and Dissanayake, P.B.R. s.l. : SAITM research symposium on engineering advancement, 2013.

[18]. www..usgs.gov.

Appendix A

Calculation of equivalent static load for 35m and 55m towers

The following equation is given in ANSI/TIA-222-G [14] to calculate total seismic shear V_s under equvalant static method and it was used for the calculation of earthquake loading of towers.

$$V_s = \frac{S_{DS}\, W\, I}{R}$$

Alternatively, for ground supported structures, V_s need not be greater than

$$V_s = \frac{f_1 S_{D1}\, W\, I}{R}$$

When the alternative equation for V_s is used , V_s shall not be less than $0.044 S_{DS} WI$ and for sites where S_1 equals or exceeds 0.75 , V_s using the alternative equation shall not be less than

$$V_s = \frac{0.5 S_1\, W\, I}{R}$$

$S_{DS} = 2/3\ S_S$

$S_{D1} = 2/3\ S_1$

Where;

S_{DS}- Design spectral response acceleration at short period

S_{D1}- Design spectral response acceleration at period of 1.0 second

S_1 - Maximum considered earthquake spectral response acceleration at 1.0 second

S_s- Maximum considered earthquake spectral response acceleration at short period

f_1 - Fundamental frequency of the structure

W- Total weight of structure including appurtenances

I - Importance factor

R - Response modification coefficient equal to 3.0 for lattice self supporting structures

V_s- Total seismic shear

The vertical distribution of seismic force was done according to following formula given in ANSI/TIA-222-G[14].

$$F_{sz} = \frac{W_z h_z^{k_e}}{\sum_{i=1}^{n} W_i\, h_i^{k_e}}$$

Where;

F_{sz}= Lateral seismic force at level Z

W_z= Portion of total gravity load assigned to level under consideration

W_i= Portion of total gravity load assigned to level i

h_z = Height from the base of the structure to level under consideration

h_i = Height from the base of the structure to level i

k_e= seismic force distribution exponent (taken as 2.0 is it can set as 2.0 for any structure)

SECM/15/164

Investigation on Residual Cyclic Strength Capacity of Corroded Steel Bridge Members

W. K. N. I. Jayasundara[1*] and J.M.R.S Appuhamy[1]

[1]University of Ruhuna, Galle, Sri Lanka
*E-Mail: Nirmani.jayasundara@gmail.com, TP: +94783942140

Abstract: Steel bridges play a major role in road and railway infrastructures hence it directly influence on economy of any country. Traffic capacity reduction or even a temporary closure generates major inconveniences for the users and result in significant losses to the economy. Corrosion is one of the most significant causes of age related deterioration of steel girder bridges which affects their strength, long term mechanical performance, usability and durability. Numerous steel bridge structure collapses are associated with dynamic loadings like earthquakes and wind loading. Damaging vulnerability of steel structures due to dynamic excitations can be triggered with corrosion. Non availability of information and convenient methodology to determine the behavior of corroded steel members can lead to problematic situations for the civil engineers when evaluating the strength of deteriorated member. Therefore a comprehensive study in front of serviceability and ultimate limit states is necessary to develop efficient techniques to evaluate the structural integrity and safety. This is necessary to evaluate the feasibility of those steel structures for the current usage and to figure out the retrofitting requirement of corroded members. This research proposes a simple and reliable methodology to estimate remaining yield and ultimate cyclic strength capacities by measuring only the minimum thickness of a corroded surface based on the results of many experimental coupon tests and results of nonlinear FEM analysis of many actual corroded plates with different corrosion conditions, which can be used to make rational decisions about the maintenance management plan of steel infrastructures.

Keywords: Residual strength, cyclic loading, finite element analysis, corrosion, bridge structures.

1. Introduction

Among enormous structural edifices, bridges are a major component of any infrastructure, which facilitates day to day travel path for freights and passengers. The failure of a bridge will affect the economy of any country. When bridge structures expose to harsh environmental conditions result will be time-variant changes of their load-carrying capacity. Once the load carrying capacity reduced, the bridges' ability to safe service too violates (Appuhamy *et al,* 2009 [1]). In the future, it is evident that serious social problems will arise when the number of damaged bridges increases, as it is very difficult to retrofit or rebuild those aged bridges at the same time. Therefore, it is important to evaluate the remaining strength capacities of those bridges, in order to keep them in-service until they required necessary retrofit or rebuild in appropriate time.

Benefits of regular and proper inspections of older bridges cannot be disregarded. They not only help in planning the necessary work but also help in discovering and monitoring any problems, thereby reducing expensive maintenance, reducing operating hazards, preventing structural failures and preventing emergencies. Therefore, no negligence in inspections should be permitted as they form the essential source of information to carry out a comprehensive evaluation of its current capacity. Some researchers have already done several experimental studies in terms of estimating the remaining strength capacities under monotonic loading, and developed some durability estimation techniques which were performed with detailed investigations on corroded surfaces (Matsumoto *et al,* 1989 [2]; Muranaka *et al*, 1998 [3]; Kariya *et al,* 2003 [4]; Appuhamy *et al,* 2009 [1]).

Recent severe earthquakes worldwide have shown that steel bridges can be vulnerable. In addition, there were many collapse, buckling, fracture and cracking occurred in many steel infrastructures due to earthquakes. It is evident that, even though most of the steel bridge structures perform well with their specific energy dissipation characteristics, the failure risk associated with severe corrosion under mega earthquake events could not be underestimated.

Therefore this paper investigate the effect of corrosion damage on remaining dynamic behaviour of existing steel bridge infrastructures and presents a simple, accurate and reliable methodology to estimate residual strength capacities of corroded steel plates using both experimental and numerical analysis with the results of coupon tests and finite element modelling technique. Further validation of use of corrosion condition modelling parameters (CCM) as a more reliable methodology to model the corrosion surface in FEM modelling software in cyclic strength estimation is also considered.

2. Methodology

2.1 Experimental Analysis

2.1.1 Corroded Test Specimens

The test specimens for this experimental study were cut out from a steel girder of the Koggala Bridge in Sri Lanka on the shoreline of the Indian Ocean, which had been used for about hundred years. This bridge was constructed as a railway bridge in 1900s and this bridge was dismantled due to serious corrosion damage in year 2012.

The specimens for cyclic loading tests were taken, cutting out from the corroded members of the bridge. Four corrosion-free specimens, cut down smoothly from both sides of corroded steel plate in order to clarify the material properties. Test specimens prepared according to the JIS No.5 as shown in Figure 1 and Figure 2.

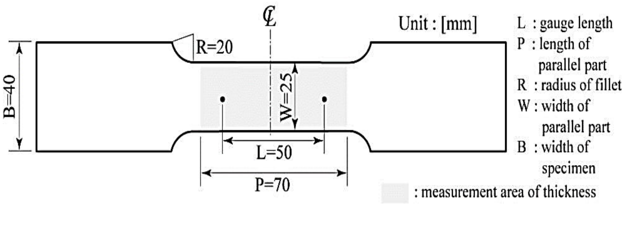

Figure 1: JIS No.5 specimen for cyclic loading test

Figure 2: Prepared test specimens according to standard shape

2.1.2 Corroded Surface Measurements and Material Properties

The rust and paint on the surface were removed by using a steel wire brush and then applying high pressure water carefully in order to not change the condition of the corrosion irregularity. Then the thicknesses of all scratched specimens were measured by using a 3D scanning of surface before the cyclic loading test and the intervals of measurement data are 2mm in X and Y directions respectively. The statistical thickness parameters such as average thickness (t_{avg}), minimum thickness (t_{min}), were calculated from the measurement results.

Table 1: Material Properties

Non Corroded Specimen no.	Elastic Modulus (GPa)	Yield Stress (MPa)	Tensile Strength (MPa)	Elongation at Breaking (%)
Sample set 1	184.4	272	431	25.59
Sample set 2	180.1	246	418.5	20.01
SS400 JIS	200	245~	400~510	-

Tensile testing was performed for the four corrosion-free specimens. The fundamental mechanical properties of the material were obtained and compared with the standard values by JIS as shown in Table 1. The material properties of actual specimens were lied within the property ranges of SS400 (JIS).

2.1.3 Cyclic Strength Determination by Cyclic Loading Test

Each specimen was tested under predetermined cyclic displacement as shown in Figure 3. It is obvious that the bridges are more vulnerable to random loading. The main focus of this research was to figure out the strength reduction percentage for a cyclic loading. Loading pattern can be random or monotonic. Particularly the loading should not be fatigue, and in addition, incremental load was selected in order to facilitate breaking point rapidly.

Applied load and the stroke displacement was recorded as shown in the Figure 4. Displacement histories were analysed to identify actual yield and ultimate cyclic strength of each specimen; shown in Table 2.

Yield point was figured out at the point where the hysteretic deviates from linear behavior and the maximum load of the hysteresis was noted as the ultimate load**.**

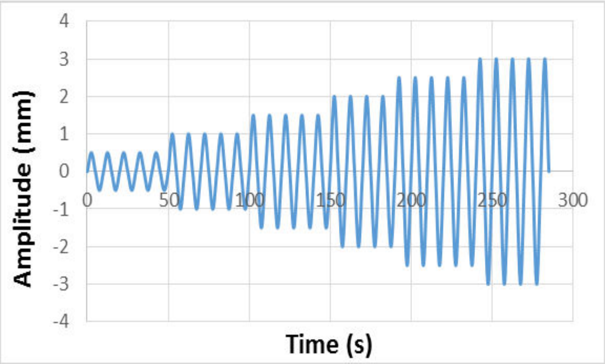

Figure 3: Graph of amplitude vs. time of applied cyclic displacement pattern

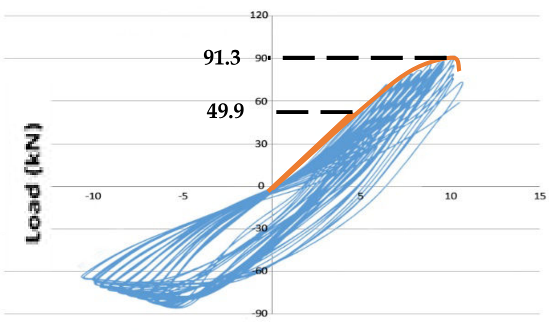

Figure 4: Load vs. displacement curve of specimen (μ = 0.359) obtained by experimental analysis

Table 2: Yield and Ultimate cyclic strength values of test specimens

Minimum Thickness Ratio ($t_{min}/ t_{initial}$)	Yielding Load - P_b (kN)	Ultimate Load - P_y (kN)
1.000	51.25	95.10
1.000	38.70	61.92
0.375	42.90	71.90
0.378	31.45	47.99
0.456	33.73	54.02
0.743	37.06	58.89
0.691	48.45	87.8
0.359	49.89	91.30
0.871	50.38	92.67
0.689	34.67	57.07
0.785	49.00	90.53

2.2 Numerical Analysis

Numerical analysis was conducted based on finite element modelling to have more reliable strength data easily. Usually, accurate predictions are based on how accurately statistical parameters are estimated and therefore mainly depend on experimental and field data. But, to develop a more reliable strength estimation technique, only experimental approach is not enough as actual corroded surfaces are different from each other. Further, due to economic constraints, it is not possible to conduct tests for each and every aged bridge structure within their bridge budgets. Therefore use of numerical analysis method could be considered to have a reliable estimation in bridge maintenance industry.

2.2.1 Numerical Procedure

In order to clarify yield and tensile strengths, non-linear finite element analyses were performed using LUSAS finite element analysis software for all specimens with different corrosion conditions. The 3D isoparametric hexahedral solid element with eight nodal points (HX8M) and updated Lagrangian method based on incremental theory were adopted in these analyses. Non-linear elastic-plastic material and Von Mises yield criterion were assumed for material properties. Further, an automatic incremental-iterative solution procedure was performed until they reached to the pre-defined termination limit.

The analytical models with length and width dimensions of 70 mm×25 mm (Figure 05) were modeled with different corrosion conditions for respective specimens. One edge of the member's translation in X, Y and Z directions were fixed and only the Y and Z direction translations of the other edge (loading edge) were fixed to simulate with the actual experimental condition. Then the predetermined displacement was applied to the loading edge. Actual material properties obtained were assigned and non-linear elasticplastic material properties obtained from the non-corroded specimen's tensile test results were assigned to all analytical models, respectively the model was compiled by assigning the same loading condition given to actual experimental specimens at the experimental analysis. Obtained results for yield and ultimate strength capacities were compared with the actually obtained strength. Models were adjusted till the results of ultimate strength of analytical models lies within close proximity with experimental results. Hence the numerical model was validated.

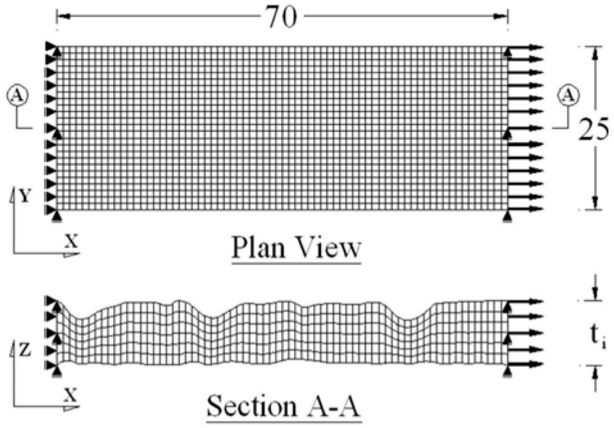

Figure 5: Analytical Model of Corroded specimen

2.2.2 Modelling of Corrosion Condition

Two corrosion condition modelling (CCM) parameters were defined to model a corroded surface considering the material loss due to corrosion and stress concentration effect (Ohga *et al,* 2011 [5]) and Appuhamy *et al,* 2011 [6]).

$$D^* = 5.2\, t_{c,max} \quad (1)$$

$$t^*_{avg} = t_0 - 0.2 t_{c,max} \quad (2)$$

Where D^* and t^*_{avg} are the representative diameter of maximum corroded pit and representative average thickness respectively. ($t_{c,max}$ = maximum corroded depth, t_0 = initial thickness)

Actual specimens were modelled using CCM parameters and analysed using validated FEM modeller and cyclic strength values were obtained. Effective stress distributions of several analytical models using CCM parameters at ultimate loads are shown in Figure 6 and Figure 7.

Comparison of experimental results with analytical results shows that there is a close relationship between strength results as shown in Table 3. The percentage error varies within negative four and positive six, which can be considered as a considerably small value. Therefore obviously the corrosion condition modelling parameters derived for tension can be effectively utilized under cyclic or seismic loading conditions.

Table 3: Ultimate cyclic strength values of test specimens under numerical analysis

Minimum Thickness Ratio ($t_{min}/t_{initial}$)	Experimental ultimate load (kN)	Numerical ultimate load (kN)	Percentage Error (%)
1.000	95.10	94.50	0.63
1.000	61.92	63.01	-1.76
0.375	71.9	70.00	2.64
0.378	47.99	45.01	6.23
0.456	54.02	55.25	-2.27
0.743	58.89	56.97	3.26
0.691	87.80	84.00	4.32
0.359	91.30	94.70	-3.72
0.871	92.67	87.08	6.032
0.689	57.07	55.54	2.68
0.785	90.53	90.53	-0.58

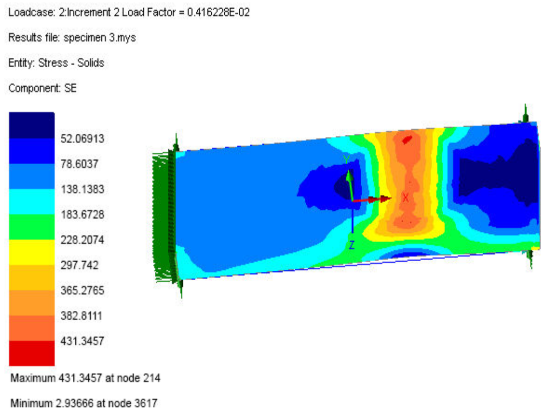

Figure 6: Stress distributions of analytical model (μ = 0.375) using CCM parameters at ultimate load

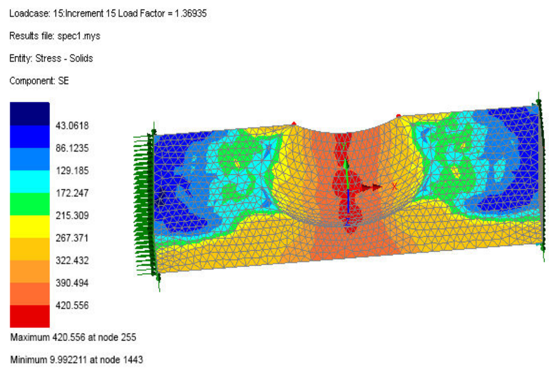

Figure 7: Stress distributions of analytical model (μ = 0.456) using CCM parameters at ultimate load

3. Results and Discussion

The percentage yield and ultimate strength reductions (%SR) were obtained by comparing the strength results of corroded specimens with non-corrosion specimen from same source according to the Equation 3. And the percentage strength reduction was plot against minimum thickness ratio of each specimen as shown in Figure 8 and Figure 9.

$$\%SR_{Yield/ultimate} = \left| \frac{P_{Y(Non-corroded\ specimen)} - P_{Y(Model\ with\ specimen)}}{P_{Y(Non-corroded\ specimen)}} \right| \times 100 \qquad (3)$$

Considering the complexity and acceptable accuracy using minimum thickness ratio, two quadratic equations were obtained as relationships, between yield and ultimate percentage strength reduction values with minimum thickness ratio of corroded specimens.

Thus $\%SR_{yield} = 25\ (1-\mu)\ (1.4-\mu)$, $\%SR_{ultimate} = 25\ (1-\mu)\ (1.7-\mu)$, can be used as a tool to estimate the residual strength of prevailing corroded bridge parts by only measuring minimum thickness.

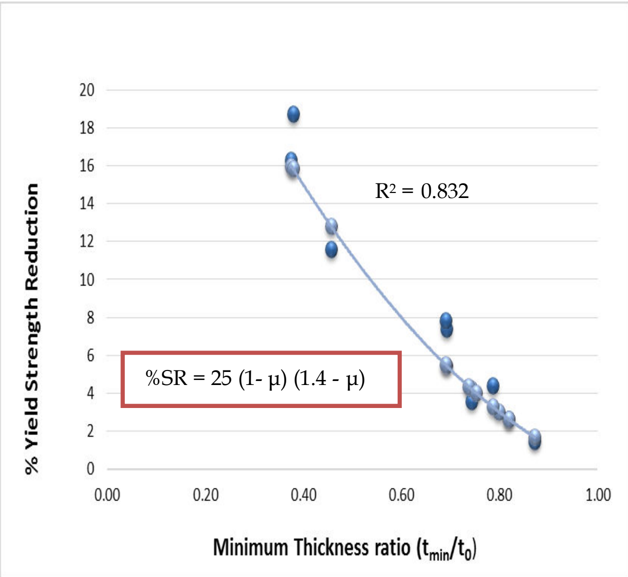

Figure 8: Relationship of percentage yield strength reduction vs. minimum thickness ratio (μ)

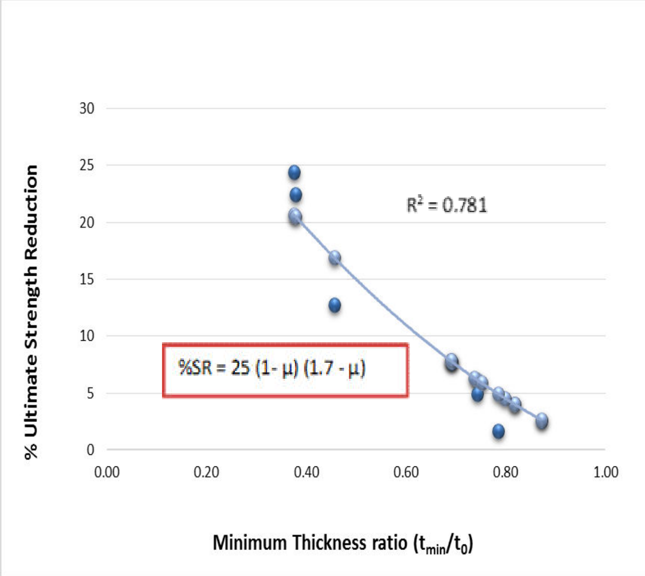

Figure 9: Relationship of percentage ultimate strength reduction vs. minimum thickness ratio (μ)

5. Conclusions and Future Directions

The yield, ultimate behaviors of steel bridge members with different corrosion conditions under cyclic loading were studied in this research. The main conclusions of this study can be summarized as follows.

It was revealed that the corrosion has a significant effect on the dynamic behavior of steel bridge infrastructures. As a reliable and efficient methodology to estimate the percentage reduction of yield/ultimate strengths due to corrosion under cyclic loading can be obtained using following Equation (4) and Equation (5).

$$\%SR_{Yield} = 25 \times (1-\mu) \times (1.4-\mu) \qquad (4)$$

$$\%SR_{Ultimate} = 25 \times (1-\mu) \times (1.7-\mu) \qquad (5)$$

As the proposed strength and energy reduction equations only requires the measurement of minimum thickness ratio μ, which is an easily measurable parameter through a quick and careful site investigation, this method can be used as a simple and reliable method to predict the cyclic, seismic behaviors of corroded steel members more easily and precisely. Furthermore, as the %SR charts give a good indication about the percentage strength reduction according to the severity of corrosion, bridge engineers would be able to decide whether the infrastructure requires any initial corrosion prevention precautions such as painting etc., retrofitting of some selected members or replacement of some critical members in order to assure the adequate safety of the existing structure.

In addition a very good agreement between experimental and nonlinear FEM results can be seen for all three classified corrosion types. Thus the adopted modelling technique can be used to predict the remaining strength capacities of actual corroded members accurately.

Usually, the accurate predictions are based on how accurately statistical parameters are estimated and therefore mainly depend on experimental and field data. But, to develop a more reliable strength estimation technique, only experimental approach is not enough as actual corroded surfaces are different from each other. Further, due to economic constraints, it is not possible to conduct tests for each and every aged bridge structure within their bridge budgets. Therefore use of numerical analysis method could be considered to have a reliable estimation in bridge maintenance industry.

Therefore adopted numerical modelling technique can be precisely used as a more reliable method to model run and retrieve the residual strength data of modelled actual bridge members.

Finally it can be concluded that this research findings have immense importance in bridge maintenance and management industry as well as the ultimate goal of this findings may safeguard human lives and property from accidental collapses in bridges all around the world.

References

[1] Appuhamy J.M.R.S, Kaita T, Ohga M & Dissanayake P.B.R (2009), *A simple and Comprehensive Estimating Method of Remaining Tensile Strength of Corroded Steel Bridge Plates*, Annual Research Journal of SLSAJ, no. 9 , pp. 6-10.

[2] Matsumoto M, Shirai Y, Nakamura I, and Shiraishi N (1989), *A proposal of effective thickness estimation method of corroded steel member*, Bridge Foundation Engineering, vol. 23(12), pp. 19-25

[3] Muranaka A, Minata O & Fujii K (1998), *Estimation of residual strength and surface irregularity of the corroded steel plates,* Journal of Structural Engineering, vol. 4A, pp. 1063-1071.

[4] Kariya A, Tagaya K, Kaita T & Fujii K (2003), Basic study on effective thickness of corroded steel plate and material property, Annual Conference of JSCE, Tokushima, Japan, pp. 967–968.

[5] Ohga M, Appuhamy J.M.R.S, Kaita T, Chun P, and Dissanayake, P.B.R (2011), *Degradation of tensile strength with the severity of corrosion condition,* World Congress on Advances in Structural Engineering and Mechanics (ASEM11plus), Seoul, Korea, pp. 5280–5297.

[6] Appuhamy J.M.R.S, Kaita T, Ohga M & Fujii K (2011), *Prediction of residual strength of corroded tensile steel plates*, International Journal of Steel Structures, vol. 11, no. 1, pp. 65–79

SECM/15/177

Probabilistic Performance-Based Earthquake Engineering: A Review

P. Rajeev[1*]

[1]Swinburne University of Technology, Hawthorn, VIC 3122, Australia
*E-Mail: prajeev@swin.edu.au, TP: +61392144942

Abstract: The next generation seismic design and assessment procedures for buildings within the performance-based framework are a radical departure from traditional seismic design practice and performance assessment. The uncertainty and randomness in the building performance and seismic hazard will be captured and quantified in each steps in design and assessment procedure, finally the performance will be measured in terms of direct and indirect economic losses and casualties. The quantification and propagation of uncertainty in every step in the procedure requires robust probabilistic methods that have been developed over the last two decades. This paper summarises the research undertaken to develop the probabilistic performance-based seismic design and assessment procedures for buildings. The analysis methods, fragility functions and seismic hazard qualification, which are key elements in procedures, are defined and discussed.

Keywords: building, intensity measure, incremental dynamic analysis, uncertainty

1. Introduction

The performance-based seismic design and assessment approach, in which the building is expected to satisfy certain performance requirements in its lifetime, make a paradigm shift from traditional design and assessment practice (Franchin, [12]). This approach allows to explicitly considering the uncertainties associated with earthquake loading, structural modelling, and structural response prediction etc. The performance-based design formulations against seismic actions specify number of performance levels that must not be exceeded under seismic actions characterised in terms of mean return periods (*fib*, [13]). The mean return periods of seismic actions can be derived and quantified through probabilistic considerations.

Numerous amount of research work has been conducted over the last two decades to develop the current state of the performance-based design procedures that are intelligently conceived and well tested. However, the procedure has serious limitation in the case of an assessment of existing buildings, where the performance requirement cannot be set on the basis of structural response without considering the damage to non-structural components as well as repair costs. In this case, the determination of performance requirements needs additional uncertain data from several sources, which makes the probabilistic approach unavoidable. On this regards, the reliability analysis to seismic design becomes an effective tool that can be used with moderated level of additional effort. As stated in *fib* [13]), "the mandatory adaptation of probabilistic performance-based design (PBD) codes may be still far away from practice, however, this time lag, should be regarded as an opportunity to familiarise with the approaches before actual application".

Thus, this paper briefly summarises the reported works on PBD and mainly provides information on main elements associated with PBD. The research on PBD can be grouped into: (1) probabilistic methods in earthquake engineering that includes fragility curves, collapse risk assessment, seismic hazard analysis with efficient simulation methods, and structural response prediction etc; and (2) seismic performance assessment of existing building that includes the treatment of epistemic uncertainty associated with structural properties and performance prediction models and effect of analysis methods on the performance prediction. However, this paper focuses on the first group of PBD. The research carried out during the last few years by the author and many co-workers also falls largely within this broad framework. Those has been briefly summarised in this paper.

2. Reliability concepts in seismic design

Der Kiureghian [11] and Pinto [19] summarise the early application on reliability concepts in seismic design. The approach can be grouped into three major categories: (1) based on the theory of random vibration with a particular attention to Rice expression for the mean rate of outcrossing of a scalar random function from a given domain, and to its generalisation to vector processes; (2) mainly based on the vast area of the simulation methods includes directional simulation (DS) and importance sampling (IS), applied either separately or in combination; and (3) represent the well-known statistical approach called response surface method to approximate the limit state function. The advantages and disadvantages of using each category have been discussed elsewhere (e.g., Pinto, [19]).

Later in 90's, the work by Bazzurro and Cornell [3] and Cornell [4] tried to compare the seismic demand and capacity of building as in the basic reliability formulation for the static case. The seismic demand was determined as the maximum response of the structure during the dynamic analysis with the specific level of seismic action. This method is called "SAC-FEMA method" which has the advantage of providing the closed-from solution to compute the probability of failure (P_f). In addition to SAC-FEMA method, the PEER method, which has several conceptual similarities with the first, is not in closed-form but it allows more flexibility and generality in the evaluation of the desired so-called "decision variable", not necessarily coinciding with P_f.

3. Performance Assessment of buildings

The probabilistic seismic performance assessment can be performed using currently available two classes of methods. The first method is more practice-oriented and widely accepted as a standard tool for performance assessment, called "conditional probabilistic approach or an IM-based approach". The second one is more advanced and requires strong knowledge in probability theory and random process, called "unconditional probabilistic approach".

3.1 Conditional probability approach (IM-based methods)

In IM-based methods, one or more ground motion intensity is used as an interface to link the seismology and structural response. Firstly, the structural response (i.e., drift demand) as function of ground motion intensity or intensities is developed and integrated with seismic hazard curve to produce a structure specific drift hazard curve, $H_D(d)$; which provides the annual probability that the drift demand D exceeds any specified value d. Then, the drift hazard curve is jointed with the drift capacity representation to estimate the annual probability of exceedance (λ_{LS}) of a specific of performance level (i.e., the probability of performance level not being met).

Using the total probability theorem (Benjamim and Cornell, [6]), the discrete form of $H_D(d)$ can be estimated as given in Cornell et al. [10]:

$$H_D(d) = P(D \geq d) = \sum_{all\ x_i} P(D \geq d \mid S_a = x_i) P(S_a = x_i) \quad (1)$$

where S_a is a spectral acceleration considered as the *IM*.

The probability of exceedance of drift is expanded by conditioning on all possible levels of the ground motion, as can be seen in Eq.(1). The likelihood of given level of spectral acceleration, $P(S_a = x)$, can be determined form the standard hazard curve $H(S_a)$. The advanced nonlinear dynamic analysis of structure can be used to estimate the $P(D \geq d \mid S_a = x)$, the likelihood that the drift exceeds d given that the value of S_a is known.

The continuous from the Eq. (1) is:

$$H_D(d) = \int P(D \geq d \mid S_a = x) \left| dH(x) \right| \quad (2)$$

where $|dH(x)|$ is the absolute value of the derivative of the site's spectral acceleration hazard curve times dx.

Using the total probability theory again, the annual probability of exceedance (λ_{LS}) of a specific level of performance can be estimated as follows:

$$\lambda_{LS} = P(C \leq D) = \sum_{all\ d_i} P(C \leq D \mid D = d_i) P(D = d_i) \quad (3)$$

The likelihood of a given displacement demand level $P(D=d)$ can be determined from the drift hazard curve derived in Eq. (1) or (2).

The IM-based methods have been the subject of a considerable body of research. Closed-form solutions of Eq. (3) have been proposed [10][23][27]. Various studies have been devoted at checking the approximation made [1][7] and reaching the conclusion that the main source of error is in the linear fit (in log-log space) of the seismic hazard curve. The latter limitation, on the other hand, is relaxed with consideration of second-order logarithm formulation [23][27][16].

While the issue of approximation of closed-form solutions is of great relevance to the adoption of the PBEE paradigm by the practicing engineers, other issues raise greater concerns. The first is the accuracy of IM-based methods in a wider sense. Eq. (3) rests on the assumption that, given S_a, the demand D is independent of all other ground motion properties, which is called the sufficiency property of the IM [23]. While it is obvious that λ_{LS} is theoretically unique, multiple studies have highlighted how estimations obtained by Eq. (3) exhibit a non-negligible dependence upon the chosen IM (Rajeev *et al.*, [22]). In order to ensure high accuracy in the assessment of structural performance via Eq. (3), the suitable IM can be selected using efficiency and sufficiency conditions (Luco [17]; Luco and Cornell [18]). An IM that exhibits these properties will tend to be structure-specific, recognising both the important modes of vibration and effects of nonlinear behaviour as well as the frequency content of the earthquake records. An efficient IM is defined as one that results in relatively small variability of structural responses for a given IM level as measured. Figure (1) shows the comparison of efficiency of two intensity measures with respect to interstory drift angle θ_{max}: on the top, elastic spectral displacement (S_{de}) and on the bottom, inelastic spectral displacement (S_{di}) as shown in Tothong [25]. The dashed vertical line represents the drift level at yielding, as determined from static pushover analysis. The circles indicate where global dynamic instability of the structure is reached. The counted-median and the 16% and 84% fractiles are shown with solid and dashed-dotted lines, respectively. Figure (1) indicates that $\sigma_{\ln IM}$ is reduced by about 50% when using S_{di} instead of S_{de}, implying that the number of records needed to achieve the same accuracy in estimating the mean $\ln\theta_{\max}|IM$ can be reduced by a factor of four. The corresponding reductions in $\sigma_{\ln\theta_{\max}|IM}$ can also be directly observed in Figure (1), by comparing the distances between the 16th and 84th fractiles of $\theta_{\max}$ for a given S_{di} with those obtained employing S_{de}.

A sufficient IM is one for which the conditional probability distribution of demand (D) given IM is independent of other ground motion parameters, such as those involved in computing the seismic hazard, i.e., the magnitude M, the distance R, and ε (the number of standard deviations by which an observed logarithmic spectral acceleration differs from the mean logarithmic spectral acceleration of an attenuation equation). A sufficient IM is desirable because it implies that any set of ground motions selected for nonlinear dynamic analysis of the structure will result in approximately the same $P(D>d|IM_1) \approx P(D>d|IM_2)$. Figure (2) shows a comparison of the sufficiency with respect to ε of elastic spectral acceleration at first-mode period of the structure (top) and inelastic spectral displacement (bottom).

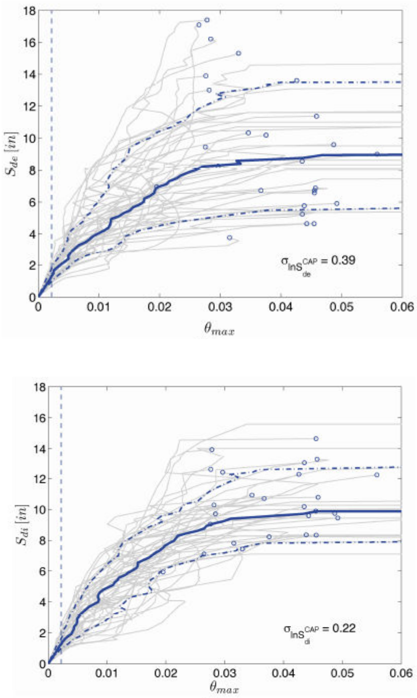

Figure 1: Comparison of the "efficiency" of the IM (adopted from Tothong [25])

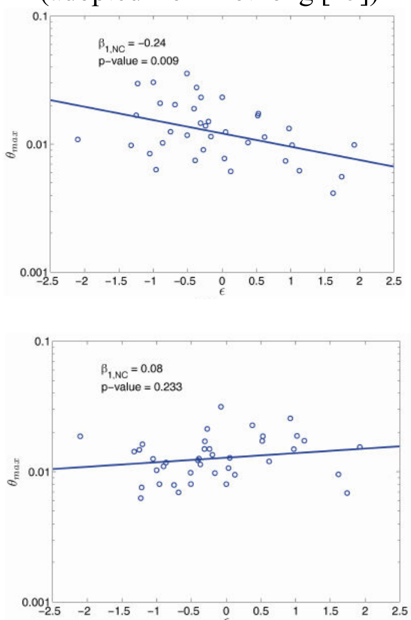

Figure 2: Comparison of the "sufficiency" of the IM (adopted from Tothong [25])

It can be seen from the figure that the response highly depends on ε, when the elastic spectral acceleration at first-mode period is considered as the *IM* (see the slope of the line $\beta_{I,NC}$ and the *p*-value). Conversely, the response negligibly depends on ε, when the inelastic spectral displacement is considered as the *IM* (see again the slope of the line $\beta_{I,NC}$ and the *p*-value). Inelastic spectral displacement is a more effective a scalar *IM* than elastic spectral acceleration at first mode period.

4. Commonly used Intensity Measures (*IM*) in probabilistic structural assessment

Selection of ground motion time-histories is an important consideration when seismic assessment of a structure is based on dynamic analysis. Careful ground motion time-history selection can achieve the same reduction in bias and variance of structural response as is gained by more advanced measures of ground motion intensity, while allowing the user to process the time-histories using simple measures of intensity such as elastic spectral acceleration (Shome and Cornell [24], Baker and Cornell [2]). This said, much efficiency (and sufficiency) can be gained by using an appropriate IM in assessing structural performance.

The peak ground acceleration of a record has been commonly used in the past. More recently, spectral response values have been used as *IM*. For example spectral acceleration at the first mode period T_1 has been shown to be more *efficient* than PGA, mostly because $S_a(T_1)$ is structure-specific. Later, the use of $S_a(T_1)$ has been shown to lead to biased estimates of response for tall and long-period structures and near-source ground motions by Shome and Cornell [24]. This is because for tall, long-period buildings, the higher modes typically contribute significantly to the seismic response (Shome and Cornell [24]). Moreover, for long-period structures $S_a(T_1)$ has been observed to be rather *insufficient* as well (i.e., given $S_a(T_1)$, response still depends on *M*). Like the observed *inefficiency*, this *insufficiency* is again due to the fact that $S_a(T_1)$ cannot reflect higher-mode spectral accelerations, which, conditional on $S_a(T_1)$, are dependent on *M*. Note, in addition, that for soft-soil or near-source ground motions with a predominant period near e.g., the second-mode period of the structure T_2, the intensity measure $S_a(T_1)$ may prove particularly inefficient. This drawback in single-valued *IM*s stimulated researchers to find alternative vector-valued IMs incorporating $S_a(T_1)$ or better scalar-valued *IM* that can more effectively predict the response of a structure.

A number of research studies have been carried out by different people [e.g., Cordova *et al.* [8], Vamvatsikos and Cornell [26], Baker and Cornell [2]] to find better scalar-valued *IM* or vector-valued *IM* that can more effectively capture important features of the ground motion. Using spectral shape ($R_{T1,T} = S_a(T)/S_a(T_1)$), magnitude (*M*), distance (*R*), or epsilon (ε), together with $S_a(T_1)$ as second component of a 2-components **IM** vector for assessment of structures has been considered in the past. Shome and Cornell [24] and Bazzuro [5] have considered a vector **IM** comprised of $S_a(T_1)$ and the ratio $S_a(T_2)/S_a(T_1)$, as well as a scalar *IM* that combines $S_a(T_1)$ and $S_a(T_2)$. The study of Cordova *et al* [8] introduced an improved intensity measure that takes into account the inelastic lengthening of the period. Luco and Cornell [18] studied several scalar-valued *IM*'s which can effectively capture the response of structures subjected to both near-source and ordinary earthquakes. The recent study by Tothong [25] explores ground motion *IM*s such as inelastic spectral displacement S_{di}, and S_{di} corrected by a higher-mode factor. The more details on the selection of *IM* and its efficiency and sufficiency can be found in Rajeev [20].

4. Prediction of Structural fragility

The structural fragility [i.e., $P(D>d|S_a=x_i)$] is equal to the probability that the performance measure *D* is larger than specified demand level as a function of the intensity measure level. This can be calculated using either numerical integration or a closed-form solution.

By making the assumption that the distribution of the demand for a given level of the *IM* is described by a lognormal distribution, the fragility function can be estimated as follows:

$$P(D > d|S_a) = 1 - \Phi\left(\frac{\ln d - \ln \eta_{D|IM}}{\beta_{D|IM}}\right) \qquad (4)$$

In the applications, however, a problem often arises with the evaluation of the parameters $\eta_{D|IM}$ and $\beta_{D|IM}$. Since structural response is evaluated by means of nonlinear time-history analyses, it is not uncommon to encounter numerical instabilities which erroneously affect the parameters estimation. In these cases, the fragility function can be calculated as follows:

$$P(D > d \mid IM) = P(D > D \mid IM, \bar{c}) \cdot (1 - P(c \mid IM)) + P(c \mid IM) \quad (5)$$

where c and $\bar{c}$ denote the collapse and non-collapse situations respectively, $P(c|IM)$ is the probability of having a collapse (identified as very large D values) for a given IM and $P(Y>1|IM, \bar{c})$ is the fragility given that no collapse has occurred, which can be again assumed to be described by a Lognormal distribution:

$$P(D > d \mid IM, \bar{c}) = 1 - \Phi\left(\frac{\ln d - \ln \eta_{D|IM,\bar{c}}}{\beta_{D|IM,\bar{c}}}\right) \quad (6)$$

where $\eta_{D|IM,\bar{c}}$ and $\beta_{D|IM,\bar{c}}$ are the median and logarithmic standard deviation of D given IM and $\bar{c}$. Use of Eq. (5) allows accounting separately for "converged" and "non-converged" values. It is important to stress, however, that the validity of Eq. (5) rests on the assumption that the "failure set" includes the "numerical non-convergence set", i.e., that all numerical non-convergence cases can be considered as failures.

The closed-form solution for structural fragility and then the mean annual frequency of limit state exceedance can be derived by making following assumptions. First, assume that the site hazard curve can be approximated as linear on a log-log plot in the region of interest

$$H(S_a) = k_0 \cdot S_a^{-k} \quad (7)$$

Typical values of the important log-log slope k are 1 to 4. The demand on the structure for a given spectral acceleration can be interpreted as:

$$D = \eta_{D|S_a} \cdot \varepsilon_{D|S_a} \quad (8)$$

where it is assumed that the median is a power-law function of spectral acceleration level ($\eta_{D|S_a} = a \cdot S_a^b$) and that $\varepsilon_{D|S_a}$ is a unit-median Lognormal variable with dispersion equal to $\beta_{D|S_a}$.

The closed form solution can be expressed as:

$$\lambda_{LS} = H(S_a)\left(1/\sqrt[b]{a}\right) \cdot e^{\frac{1}{2}\frac{k^2}{b^2}\beta^2_{Y|S_a}} \quad (9)$$

where $1/\sqrt[b]{a}$ is the spectral acceleration value that correspond to a median D value (Jalayer [14]).

The nonlinear dynamic analyses can be used to build the relationship between the demand and spectral acceleration as in Eq. (8). One procedure, also known as the "Cloud Analysis" (Jalayer *et al.* [15]), is a convenient choice (though not the most accurate). An advantage of this method is that it is based on the ground motions as they are recorded and does not require scaling. The procedure consists of applying a suite of ground motion records (in the order of 10-30 records) to the structure and to calculate the demand D. Then, by performing a simple linear regression of the logarithm of D against the logarithm of S_a, one can obtain the parameters a and b. Figure 3 shows the result Cloud Analysis and the power-law fit for the demand. However, the accuracy in the predicting the median demand depends on the selection of the ground motion that should cover the structural response from the linear to nonlinear behaviour. This may not be guaranteed in all the situations.

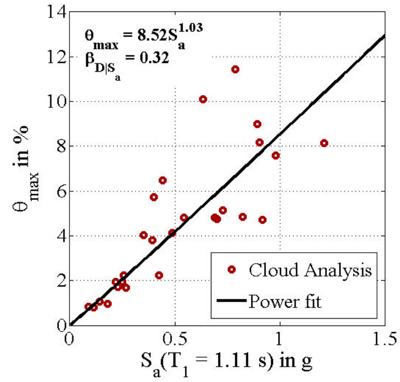

Figure 3: The power-law relationship between the interstory drift and spectral acceleration (adopted from Rajeev and Tesfamariam [21]

Another approach is to use the incremental dynamic analysis (IDA) which requires scaling of selected records at different levels of S_a's. Therefore, unlikely in the Cloud Analysis, the relationship for $\beta_{D|S_a}$ with S_a can be developed. However, the computational time is extensively high in comparison to Cloud Analysis.

In order to overcome the limitations in both Cloud Analysis and IDA, Rajeev et al., [22] proposed an alternative procedure to select record set that can cover the structural response from liner to nonlinear range and an efficient method to estimate the collapse fragilities. The approximate procedure is outlined here:

1. Estimate fractile IDA curves of the structure by means of pushover analysis, using a tool such as 'SPO2IDA' [28]. This requires a piece-wise linear fit of the pushover curve (Fig. 4, top).
2. Use these approximate IDA (Fig. 4, bottom) to get an estimate of the upper bound collapse intensity (s_C). Select records to span in an approximately uniform manner the intensity range [s=0, s=s_C]. Records should also be selected at least with reference to the causative events (magnitude and distance bins) from PSHA of each sub-interval in which [s=0, s=s_C] is divided (these need not to be large in number).
3. Perform cloud analysis and collect intensity-response data points for all responses of interest, as shown in Fig. 5.
4. Identify outliers and carry out regression analysis to fit the median model in Eq. (8) with a *constant* dispersion to non-collapse points.
5. Use the approximate IDA from step 1 to evaluate median and dispersion of the collapse intensity, $s_{C,50\%}$ and β_{sc} parameters of the approximate lognormal collapse fragility.

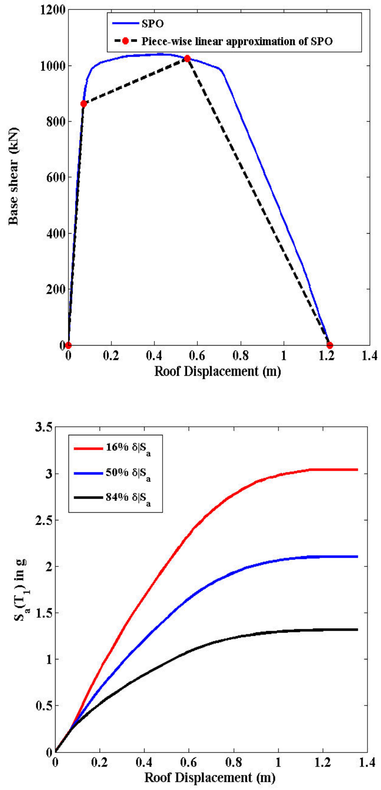

Figure 4: Pushover curves, piece-wise linear approximations and approximate IDA from SPO2IDA (adopted from Rajeev et al., 2014)

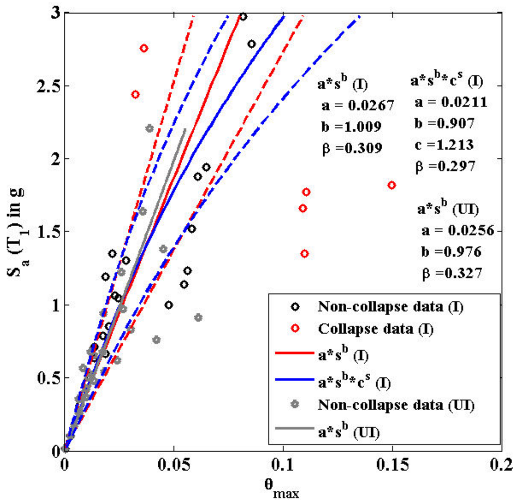

Figure 5: Cloud analysis and the median non-collapse demand model fit (solid line) together with the 16th and 84th percentile (dash line) [adopted from Rajeev et al., [22]]

The method is computationally cheaper than IDA and employs dynamic analysis as opposed to other approximate methods that rely on nonlinear static one, thus accounting for record-to-record variability and cyclic degradation, which are very important especially for non code-conforming structures.

5. Conclusions

This paper provides review on the probabilistic performance based earthquake engineering and its recent advancements. This also outlines the basic equations used in design and assessment of structures. Special consideration is given to the commonly accepted IM-based approach. Further, the methods to compute the dynamic response of structure with in the performance based framework.

References

[1]. Aslani. H. and Miranda E. (2005) Probability-based seismic response analysis. Engineering Structures, Vol. 27, pp.1151-1163.

[2]. Baker, J.W. and Cornell, C.A. (2005) "A vector-valued ground motion intensity measure consisting of spectral acceleration and epsilon," Earthquake Engineering & Structural Dynamics, Vol. 34, No. 10, pp. 1193-1217.

[3]. Bazzurro, P., and Cornell, C.A. (1994) "Seismic hazard analysis for non-linear structures I: methodology" Jnl. Struct. Eng. ASCE, Vol.120(11): 3320-3344,

[4]. Cornell, C.A. (1968) “Engineering seismic risk analysis” Bull. Seism. Soc. Am., Vol. 58: 1583-1606.

[5]. Bazzurro, P. (1998) “Probabilistic Seismic Damage Analysis,” Ph.D. Thesis, Dept. of Civil and Environmental Engineering, Stanford University, Stanford, CA.

[6]. Benjamin, J. R., and Cornell, C. A. (1970) Probability, statistics, and decision for civil engineers, McGraw-Hill, New York.

[7]. Bradley, B. A. and Dhakal, R. P. (2008) “Error estimation of closed-form solution for annual rate of structural collapse” Earthquake Engineering and Structural Dynamics, Vol. 37, pp. 1721-1737.

[8]. Cordova, P.P., Deierleni, G.G., Mehanny, S.S.F., Cornell, C.A. (2001) “Devepment of a two-parameter seismic intensity measure and probabilistic assessment procedure,” The Second U.S-Japan Workshop on Performance-Based Earthquake Engineering Methodology for Reinforced Concrete Building Structures, Sapporo, Hokkaido.

[9]. Cornell, C.A. (1996) “Calculating building seismic performance reliability: a basis for multi-level design norms” (paper 2122) Proc. 11th World Conf. Earthquake Eng., Acapulco, Mexico.

[10]. Cornell, C. A, Jalayer, F., Hamburger, R. O. and Foutch, D. A. (2002) “Probabilistic Basis for 2000 SAC Federal Emergency Management Agency Steel Moment Frame Guidelines”, Jnl of Structural Engineering, Vol. 128 (4), pp. 526-533.

[11]. Der Kiureghian, A. (1996) “Structural reliability methods for seismic safety assessment: a review” Engineering Structures, Vol. 18(6): 412-424.

[12]. Franchin, P. (2009) “Research within the framework of performance-based earthquake engineering” Earthquake Engineering by the Beach Workshop, July 2-4, 2009, Capri, Italy.

[13]. *fib* (2012) “Model Code 2010 – Final Draft” Bulletins 65 and 66, fédération internationale du béton, Lausanne, Switzerland.

[14]. Jalayer, F. (2003) “Direct probabilistic seismic analysis: Implementing non-linear dynamic assessments,” Ph.D. Thesis, Dept. of Civil and Environmental Engineering, Stanford University, Stanford, CA.

[15]. Jalayer, F., Franchin, P. and Pinto, P.E. (2007) “A scalar decision variable for seismic reliability analysis of RC frames”, Earthquake Engineering and Structural Dynamics, Vol. 36(13), pp. 2050-2079.

[16]. Kumar, R. and Gardoni, P. (2013) “Second-order Logarithmic formulation for hazard curves and closed-form approximation to annual failure probability”, Structural Safety, Vol. 45, pp. 18-23.

[17]. Luco, N. (2001) “Probabilistic seismic demand analysis, SMRF connection fractures, and near-source effects,” Ph.D Thesis, Stanford University, CA.

[18]. Luco, N., and Cornell, C.A. (2005) “Structure-specific scalar intensity measures for near-source and ordinary earthquake ground motions,” Earthquake Spectra.

[19]. Pinto, P.E. (2001) “Reliability methods in Earthquake Engineering” Progr. Struct. Eng. Materials, Vol. 3: 76-85.

[20]. Rajeev. P. (2007) “Vector-Valued Intensity Measure in Probabilistic Seismic Risk Assessment”, Research Report, ROSE School, University of Pavia, Italy.

[21] Rajeev, P. and Tesfamariam, S. (2012) Seismic Fragilities for Reinforced Concrete Buildings with Consideration of Irregularities, Structural Safety, Vol. 39, pp. 1-13.

[22]. Rajeev, P., Franchin, P. and Tesfamariam, S. (2014) “Probabilistic Seismic Demand Model for RC Frame Buildings Using Cloud analysis and Incremental Dynamic Analysis”, Proceedings of the 10th National Conference in Earthquake Engineering, Earthquake Engineering Research Institute, Anchorage, AK, US.

[23]. Romao. X., Delgado, R. and Costa, A. (2012) “Alternative closed-form solutions for the mean rate of exceedance of structural limit states” Earthq. Engng & Struct. Dyn. Vol. 42 (12), pp. 1827-1845.

[24]. Shome, N. and Cornell, C. A. (1999) “Probabilistic seismic demand analysis of nonlinear structures”. Rep. No. RMS-35, Dept.of Civil and Environmental Engineering, Stanford Univ., Stanford, Calif.

[25]. Tothong, P. (2007) “Probabilistic seismic demand analysis using advanced ground motion intensity measures, attenuation relationships, and near-fault effects”, Ph.D. Thesis, Dept. of Civil

and Environmental Engineering, Stanford University, Stanford, CA.

[26]. Vamvasikos, D., Cornell, C.A., (2005) "Developing efficient scalar and vector intensity measures for ida capacity estimation by incorporating elastic spectral shape information," Earthquake Engineering & Structural Dynamics, Vol. 34, No. 13, pp. 1573-1600.

[27]. Vamvatsikos D. (2013) "Derivation of new SAC/FEMA performance evaluation solutions with second-order hazard approximation". Earthq. Engng & Struct. Dyn., Vol. 42, pp.1171-1188.

[28]. Vamvatsikos, D. and Cornell, C. A. (2005) Direct Estimation of Seismic Demand and Capacity of Multidegree-of-Freedom Systems through Incremental Dynamic Analysis of Single Degree of Freedom Approximation. Jnl of Structural Engng; Vol. 131 (4), pp. 589-599.

SECM/15/179

Seismic Assessment of School Building in Sri Lanka Using Fragility Curves

K.A.T.M. Abeysiriwardena[1*] , R.M.A. Buddika[2] and K.K. Wijesundara[3]

[1,2,3] Department of Civil Engineering, University of Peradeniya, Sri Lanka
*E-Mail: Malingathari@gmail.com, TP: +94711919135

Abstract: Considering the occupancy of future generation and the vulnerability of their lives in school time, it is considered being a timely requirement to assess the performance levels of school buildings for different return period earthquakes which happens without any advance notification. For this purpose, Fragility curves are developed using nonlinear finite element model of three storey type plan building developed in 'OPENSEES' computer program. The damage indices based on the inter-storey drift are evaluated for immediate occupancy and collapse prevention performance levels. Corresponding inter-storey drift ratios were obtained using static pushover analysis. Since the pushover analysis is a static analysis, it cannot take into account the effects of energy content, duration and frequency content of an accelerograme while development of fragility curves a dynamic analysis of structure under input accelerograme and then the effect of those parameters to the ultimate drift can be estimated. The corresponding drift ratios for immediate occupancy and collapse prevention performance levels are developed for past 30 earthquake records with different scale increments for each earthquake using the drift ratios obtained by resultant Pushover curves. The damage index which is close to the collapse prevention performance level is observed in the school building for an earthquake with the peak ground acceleration of 0.6g and immediate occupancy performance level for an earthquake with peak ground acceleration of 0.25g highlighting the importance of designing school buildings to resist the lateral load induced by earthquakes. According to the pushover curves, this building is weaker in longitudinal direction. By introducing a section with higher moment capacity for longitudinal beams but less than the moment capacity of the column in longitudinal direction in order to increase lateral storey stiffness, the failure of the structure can be delayed and the structure will be able to withstand higher magnitudes of earthquakes.

Keywords: Earthquakes, Fragility Curves, OpenSees, Pushover Curves.

1. Introduction

Historical earthquake records in and around Sri Lanka indicate that the two major earthquakes have been occurred in Manna basin (near Colombo) in 1615 and 1938 with a moment magnitude of 6.5 and 5.9 respectively. However, vulnerability assessment of important class of structures are not performed yet to evaluate the safety against the expected seismicity in the region. Furthermore, according to the census data published in 2014, approximately 20 percent of the total population in Sri-Lanka are school children and the staff. Therefore, considering all these factors and the occupancy of school children and the vulnerability of their lives in school time in Sri Lanka, it is considered being a timely requirement to assess the safety levels of school buildings for different return period earthquakes.

2. Literature review

2.1 Damage modes

When investigating the past failure modes of reinforced concrete frame buildings due to seismic activities, failure of the plastic hinges formed either at beam and column faces, anchorage failure at the beam column joint, diagonal shear failure at beam column joint, shear failure of short columns and the failure of non-structural components such as masonry infill walls were identified. Failure of plastic hinge is due to early crushing of concrete as a result of lack of confinement in concrete and bucking of longitudinal reinforcement. Diagonal shear cracks at the beam column joints and in short columns are due to lack of transverse shear reinforcements (stirrups). (Bralie 2003 [2])

2.2 Performance objectives and pushover curve

The assessment of school building is performed based on the two performance objectives. They are immediate occupancy and collapse prevention performance levels. Immediate occupancy performance level should satisfy the objective that

the building should be used for normal services immediately after an earthquake. The collapse prevention performance level should satisfy the objective that the structure should not be collapsed due to modes of failures discussed above after an earthquake. (Vona M. 2014 [3])
However, in this study, the limits of the two performance objectives are evaluated based on the inter storey drift as a damage index parameter. The limit values of inter storey drift for the two performance objectives are obtained from the pushover curve developed for the given structure. By a static analysis, pushover curve can be developed for a building. Importance of the developing pushover curve is to identify inter story drift values for each Performance objective, immediate occupancy and collapse prevention which are important to develop the fragility curves later. When developing the pushover curves triangular force distribution was applied to each story. (Borzi at el, 2007 [1])

2.4 Fragility curve

Fragility curves are the representation of the link between the probabilities of exceedence of damage levels reached at a defined specific performance level and the expected level of earthquake. In this study the fragility curves are developed by the cumulative probability distribution curve which is drawn to probability of exceedence versus the Peak Ground Acceleration (PGA) values.
Probability of exceedence is calculated by,

$$P[dsi / I H] = \Phi\ [(1/\beta dsi) \times \ln (IH / \mu ds)] \qquad (1)$$

Where damage state is dsi, standard normal cumulative distribution function is Φ, μ is mean value for the damage state Ids , βdsi is standard deviation for the damage state and PGA(Intensity) values is I(h). (Vona M. 2014 [3])

3. Methodology

Figure 1: Selected typical school building

The selected school building is a three story reinforced concrete frame structure as shown in Figure 1: Selected typical school building, Typical gravity design school building's performance under an earthquake is assessed in this study. First all the elements were modelled using OPENSEES finite element software for analyse the structure for static pushover and time history analysis in a 3D right hand Cartesian coordinate system. In order to develop fragility curves, limit drift values of immediate occupancy and collapse prevention performance levels were obtained by pushover analysis. Next, time history analysis was performed to estimate the mean and standard deviation for different performance level. Finally, Fragility curves were developed for both performance objectives.

4. Validating section moment capacity

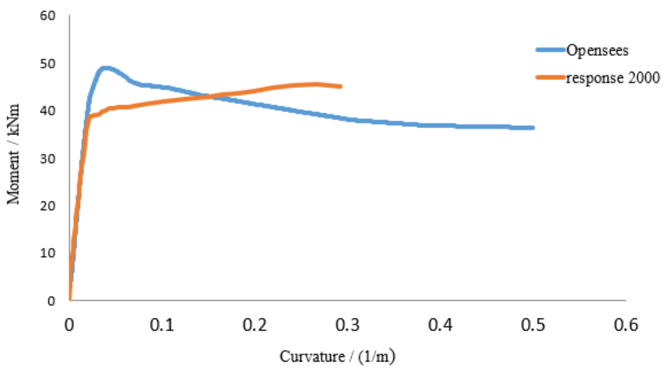

Figure 2: Moment-Curvature comparison of OpenSees and response2000 beam 39 section

Ultimate moment capacity obtained by OpenSees software and Response2000 of beam 39 is almost similar. In Response2000 software applies a fixed axial force for this analysis while in OpenSees software the beam is subjected to a variable axial force. But considering the ultimate moment capacity, the results obtained by OpenSees software is accurate.

4. Results and discussion

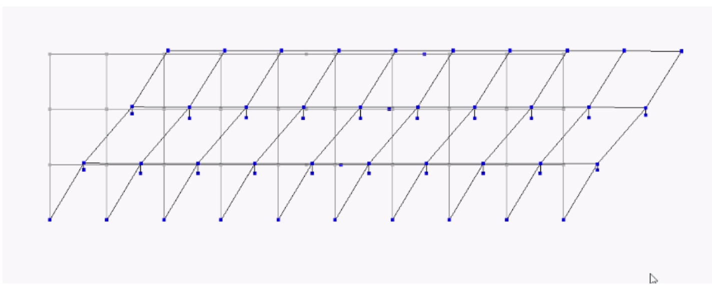

Figure 3: Deformed shape of the model due to triangular force distribution

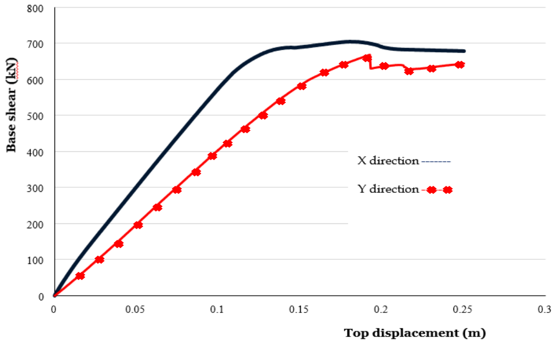

Figure 4: Pushover curves

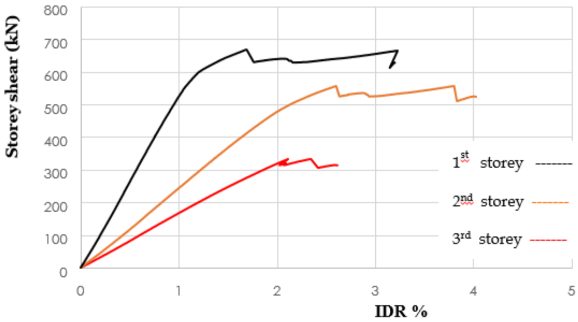

Figure 5: Story shear vs IDR% in transverse direction

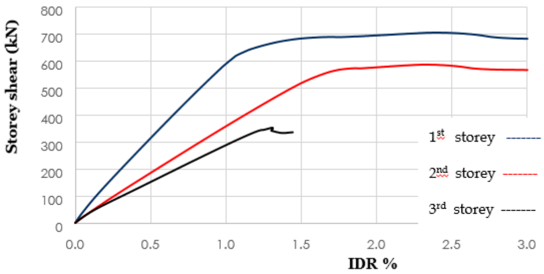

Figure 6: Story shear vs IDR% in longitudinal direction

Figure 4: Pushover curves shows that the three storey school building has base shear capacity of approximately 700 kN in both longitudinal (Y) and transverse (X) directions. However, it is observed that at the top displacement of 0.1 m in X direction, the building reaches to its elastic limit while it reaches to elastic limit at the top displacement of 0.14 m in the Y direction. Therefore, the stiffness in X direction is higher than the stiffness in Y direction. Figure 5: Story shear vs IDR% in transverse direction and Figure 6: Story shear vs IDR% in longitudinal direction shows that the three storey school building has storey shear capacities of 1st storey, 2nd storey and 3rd storey are approximately 700 kN, 600 kN, 350 kN respectively in transverse (X) direction and 670kN, 550kN, 330kN respectively in longitudinal (Y) direction. However, in X direction, it is observed that at the base, 2nd storey and in the top storey, IDR% of 1, 1.7 and 1.2 respectively the building reaches to its elastic limit while it reaches to elastic limit at the base, 2nd storey and in the top storey, IDR% of 1, 1.9 and 2 respectively in the Y direction. It can be observed that the stiffness of 1st storey and the 2nd storey are almost same for both transverse and longitudinal directions. However, the top storey in X direction compared to its Y direction.

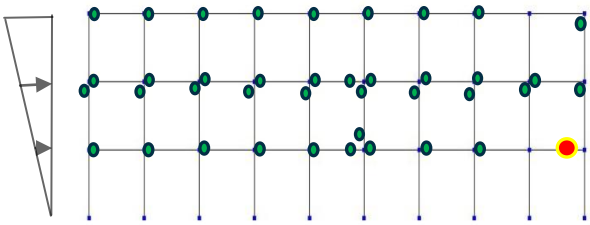

Figure 7: Plastic hinge formation in longitudinal direction

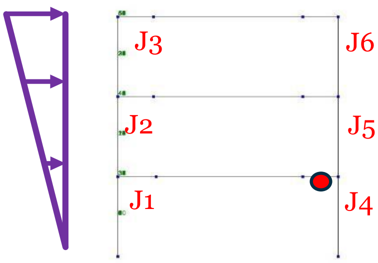

Figure 8: Plastic hinge formation in transverse direction

20% drop of moment of the member is considered as the failure of that element. Failure of one element can lead to collapse of whole building. Therefore, using the moment curvature diagrams of critical elements, load step corresponding to failure of that elements can be identify. Having found the critical load step for both x and y direction, collapse prevention performance level can be

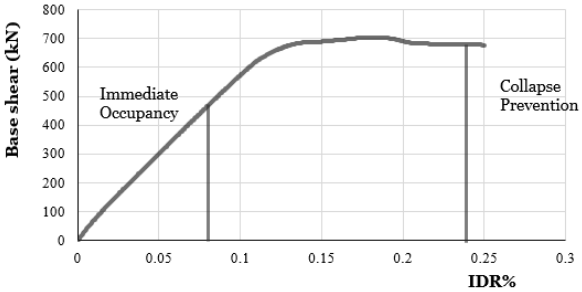

identified in the 1st storey pushover curve.
Figure 9: Performance level limits in X direction

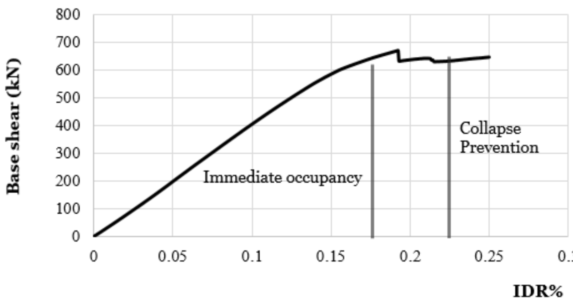

Figure 10: Performance level limits in Y direction

When a building is subjected to an earthquake, drift values of storeys are changing with the peak ground acceleration of the given earthquake. Fragility curves are drawn to show this relationship of drift values and return period/PGA values in corporate with probability. In order to develop fragility curves a data set of drift ratio percentage values are needed of the weak direction of the building which is global x direction. The building was subjected to 30 natural earthquakes consists of different PGA values and different wave forms.

5. Conclusions

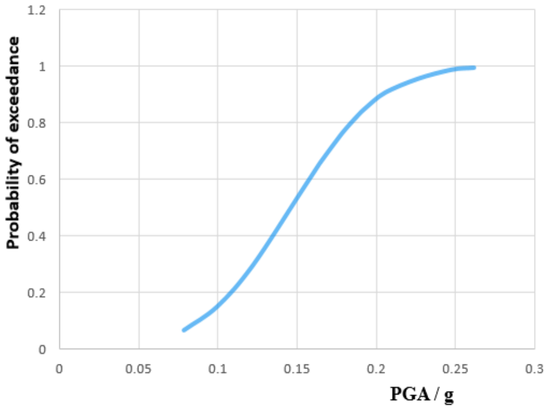

Figure 11: Fragility curve for immediate occupancy performance level

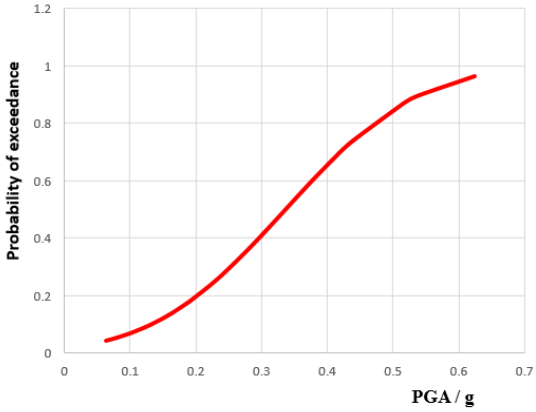

Figure 12: Fragility curve for collapse prevention performance level

According to the pushover curves, this type plan three storey school building is weak in longitudinal direction showing lower lateral storey stiffness and the moment capacity in longitudinal beams. However, the excessive rotation in the beam-column joints at the first storey level leads the failure of the longitudinal beams by forming of plastic hinges in the beam at the face of beam-column joint.
According to past studies, the expected PGA value for Sri Lanka is 0.15g. It is observed from the fragility curves that three storey 12 class room type plan school building displays 58% probability to building to get damage under an earthquake of PGA of 0.15g. And there is less than 10% of probability to get the building completely collapse under the level of PGA of 0.15g.

Figure 13: Walls with low flexural strength inside the building

Furthermore, it is important to highlight that some of the non-structural walls which have been used to separate class rooms are unconfined masonry infill walls there for it is strongly recommended that confine that masonry infill walls in order to prevent collapse due to the out of plane response of the masonry walls. By introducing a section with higher moment capacity for longitudinal beams but less than the moment capacity of the column in longitudinal direction, the failure of the structure can be delayed and it will be able to withstand higher magnitudes of earthquakes.

Acknowledgement

Deepest appreciation to all those who provided the possibility to complete this report. A very special gratitude to our final year project supervisor Dr. K.K. Wijesundara whose contribution in sharing spectacular knowledge, expertise, sincere and valuable guidance and encouragement helped to complete the project in due time and best manner.

References

[1]. Borzi B. et al., Pinho R. et al., Crowley H. et al.,2008, “Simplified pushover-based vulnerability analysis for large-scale assessment of RC buildings” Engineering Structures vol 30 pg. 804–820

[2]. Braile L., “Connections between failure modes observed in shake table testing of models in building contest and earthquake damage to actual buildings” Purdue University, October 2003

[3]. Marco Vona, “Fragility Curves of Existing RC Buildings Based on Specific Structural Performance Levels”, Open Journal of Civil Engineering , vol. 4 ,pg 120-134